Controls on lithofacies variability and organic-matter enrichment in a carbonate-dominated intrashelf basin: a multi-proxy study of the Natih-B Member (Upper Cretaceous Natih Formation, North Oman)

A thesis submitted to The University of Manchester for the degree of Doctor of Philosophy in the Faculty of Engineering and Physical Sciences

2010

Said Ali Khamis Al Balushi

School of Earth, Atmospheric and Environmental Sciences

List of Contents

Total Number of Words: 63,623

List of Figures

Total Number of Figures: 45

List of Tables

List of Appendices

Appendix A: Lithological logs from all measured sections of the Natih-B Member, **see attached CD**

Appendix B: Quantitative and semiquantitative data of all analysed Natih-B Member samples, **see attached CD**

Appendix C: Microfossil abundances chart of the Natih-B Member based on a well in the Natih field, **see attached CD**

Abstract

Intrashelf basins occurring on epeiric carbonate platforms are commonly associated with the presence of excellent carbonate source rocks, and because they often border potential carbonate reservoirs updip, they may form the core of rich petroleum systems. This is a common phenomenon of many Mesozoic hydrocarbon plays in the Middle East. Despite this fact, studies investigating intrashelf-basinal, fine-grained carbonates are rare, because it is assumed that little lithofacies variability is present in these successions as a consequence of their relatively homogeneous appearance where they are sampled in core or visited in exposures. Those that have been performed mostly lack process-detail analyses, and interpret the organic-carbon enrichment in these sediments to be simply a function of either occurrence of localised bottom-water anoxia or high primary organic production under low-energy conditions, dominated by suspension-settling events.

In order to rectify this point and conduct a process-based study on such sediments, this research focused on the source-rock-bearing, Upper Cretaceous Natih-B Member (Natih Formation, North Oman). To gather the necessary data, this study involved utilising microscopic (optical and electron-optical), mineralogical (X-ray diffraction), and geochemical (total organic-carbon [TOC] and stable-isotopic) techniques, in addition to detailed core and outcrop investigations. The generated data revealed that the predominantly fine-grained, intrashelf-basinal carbonates of this succession are very variable, even at the millimetre and less scales. The majority of the carbonate lithofacies encountered here have mudstone through to packstone textures. The individual units are variously composed of biogenic (uncompacted bioclasts) and authigenic (both replacive and pore-filling) calcite (19.9 to 97.7%, average 79.5%), and organic matter (0.3 to 13.7% TOC, average 3.3%), together with minor detrital quartz and clay, and replacive and pore-filling pyrite and dolomite, reflecting changes in primary production (both organic and inorganic), clastic input, sedimentation rate, and early diagenesis. Moreover, these units have been bioturbated to different levels, and they contain abundant evidence of in-place fauna, suggesting that persistent bottom-water anoxia did not exist during deposition of the Natih-B Member. Additionally, many of the organic-carbon-rich mudstone-wackestone lithofacies are pelleted, partially bioturbated, and exhibit inclined lenticular lamination, indicating that these sediments were mainly deposited rapidly by episodic and advective processes under relatively energetic conditions that enhanced organic-matter preservation. These units, following compaction, developed thin depositional beds that could be misidentified as depositional laminae. In contrast to these organic-carbon-rich lithofacies, the sparry-calcite-rich wackestone-packsone lithofacies, which alternate with the former in the basin centre, are uncompacted, extensively bioturbated, pervasively calcite cemented, and display scour lags and skeletal concentrations, suggesting that these lithofacies were propably associated with distal storm events, and the extensive bioturbation and cementation indicating major breaks in sediment accumulation, especially at the tops of these units where stacking patterns change. Finally, the stable-isotopic compositions obtained from whole-rock samples ($\delta^{13}C$ = −0.9 to +0.9‰, average +0.3‰; $\delta^{18}O$ = −5.6 to −3.7‰, average −4.8‰) and sparry calcite (pore-filling cement or diagenetically-replaced matrix) subsamples ($\delta^{13}C$ = −0.6 to +1.2‰, average +0.6‰; $\delta^{18}O$ = −5.7 to −3.7‰, average −4.3‰), all relative to VPDB (Vienna Pee Dee Belemnite), together with the uncompacted nature of bioclasts and evidence of bioturbation and sediment reworking, indicate that the majority of the sparry-calcite crystals in Natih-B were precipitated early, prior to compaction, derived mainly from normal-marine (open, oxic) porewaters.

Declaration

The author declares that no portion of the work referred to in the thesis has been submitted in support of an application for another degree or qualification of this or any other university or other institute of learning.

Copyright Statement

Chapter 1

Introduction

1.1. Context of the Research

Intrashelf (or intraplatform) basins are common geomorphic features on regionally-extensive epeiric carbonate platforms along passive continental margins (e.g. Markello and Read, 1981; Read, 1982; Aigner et al., 1989; Burchette and Wright, 1992; Grover, 1993; Stanton and Flügel, 1995; Sharland et al., 2001; Droste, 2003; Figure 1.1). They commonly form depocentres (< 100 m maximum water depth) for fine-grained, organic-carbon-rich carbonate sediments during major rise in relative sea level, associated with creation of accommodation (e.g. van Buchem et al., 2002a; Droste and Van Steenwinkel, 2004). Prolific petroleum systems may develop, during significant burial, in these settings where potential platform-carbonate reservoirs exist in close proximity to intrashelf-basinal carbonate source rocks (see Murris, 1980; Markello and Read, 1982; Burchette and Britton, 1985; Read, 1985; Ward et al., 1986; Droste, 1990; Alsharhan and Scott, 2000; Kuss et al., 2000; Al-Saad and Sadooni, 2001; Davies et al., 2002; van Buchem et al., 2002b; Taghavi et al., 2007).

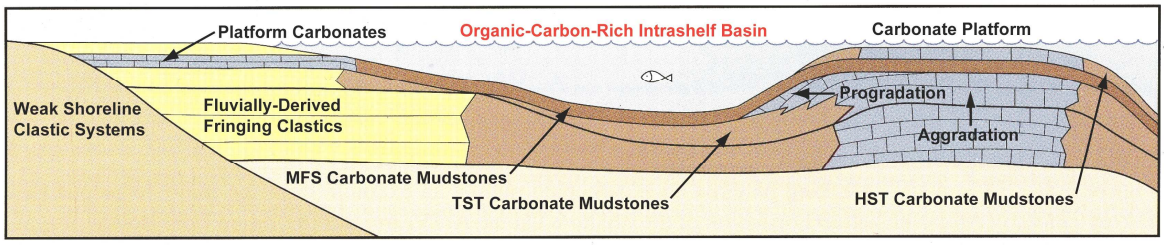

Figure 1.1. Schematic diagram illustrating intrashelf-basin environment on a carbonate platform along continental margin (modified from Sharland et al., 2001). Intrashelf basins form during major rise in relative sea level in areas with minor topographic relief as a result of differential carbonate-platform growth, which creates accommodation for organic-carbon-rich carbonate mudstones to accumulate in the basin. (TST = transgressive systems tract; MFS = maximum flooding surface; HST = highstand systems tract).

Despite their significance as excellent petroleum source rocks (e.g. Sassen et al., 1987; Summerhayes, 1987; Droste, 1990; Klemme and Ulmishek, 1991; Machhour et al., 1998;

Demirel and Guneri, 2000; Katz et al., 2000; Abdullah et al., 2005; Doyle et al., 2005; van Buchem et al., 2005), fine-grained (mudstones-wackestones), organic-carbon-rich, intrashelf-basinal carbonates have rarely been studied in great detail compared to the surrounding coarser-grained (e.g. grainstones), platform carbonates. This is probably because of their "monotonous" appearance in hand specimen, as a result of the fine-grain size and dominant dark colour (so called "black shales"), as well as their insignificance as conventional hydrocarbon reservoirs (Heydari and Wade, 2002). Therefore, exiting depositional models for intrashelf-basinal sediments are simple, suggesting little lithofacies variability in the basin centre and relating enhanced organic-matter enrichment to either high primary organic production in the water column or existence of persistent bottom-water anoxia (e.g. Demaison and Moore, 1980; Murris, 1980; Pedersen and Calvert, 1990; Scott, 1990; Burchette and Wright, 1992; Burchette, 1993; Alsharhan, 1995; Philip et al., 1995; Kuypers et al., 2002; van Buchem et al., 2002b; Droste and Van Steenwinkel, 2004; van Buchem et al., 2005; Mort et al., 2007; Homewood et al., 2008; Figure 1.2). It is, thus, assumed that the fill in these basins implemented layer-cake stacking patterns, with bull's-eye facies distributions, dominated by low-energy, suspension-settling processes. Instead, the significant role of episodic and rapid sedimentation and burial (sensu Weedon et al., 2004; Katz, 2005; Macquaker et al., 2007), associated with advective processes under relatively high-energy conditions (sensu Schieber, 1994; Macquaker and Bohacs, 2007; Schieber and Southard, 2009), in preserving organic carbon in these settings have been underestimated by many authors. Moreover, the influence of early diagenesis in causing organic-matter degradation and enhancing lithofacies cyclicity (sensu Hendry, 1993; Taylor, 1998; Westphal, 2006; Westphal et al., 2008) has also been neglected by some researchers studying such sediments.

This study, utilising high-resolution petrographic investigations (including optical and backscattered electron-optical microscopy), and geochemical and mineralogical techniques (including total organic carbon [TOC] and X-ray diffraction [XRD] analyses), seeks to determine if analogous lithofacies variability is present, at the centimetre to millimetre scales, in the predominantly fine-grained, organic-carbon-rich, intrashelf-basinal carbonates of the Upper Cretaceous Natih-B Member (North Oman; Figure 1.3) that is present elsewhere in other mudstones (e.g. Macquaker et al., 1998; Schieber, 1999; Macquaker and Jones, 2002; Macquaker and Adams, 2003; Macquaker and Keller, 2005).

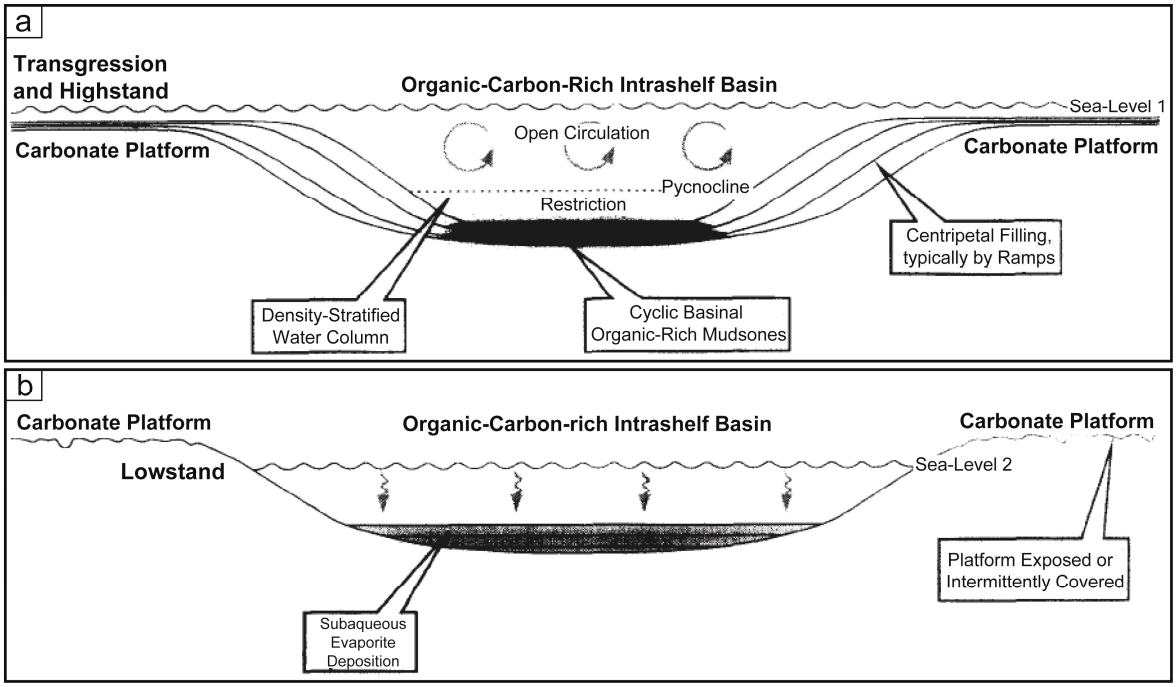

Figure 1.2. Simplified diagram illustrating "classical" depositional model for intrashelf basins (from Burchette and Wright, 1992). This model suggests that abundant organic-carbon preservation in these units is mainly, simply, driven by restriction in the basin centre, coupled with cyclic bottom-water "anoxia"; and that low-energy conditions associated with suspension-settling processes dominated in these basins. Note, in **(a)**, how ramps (platform carbonates) prograde centripetally from the basin margins during highstand, and how the basin becomes density-stratified and "anoxic" below the pycnocline. Note also, in **(b)**, how the basin becomes isolated ("silled") during lowstand, associated with deposition of subaqueous evaporites. The surrounding platform may be exposed and karsted.

This study is also designed to determine if any small sedimentary structures are preserved (e.g. scours, ripples, burrows) in the sediment that might be used to shed light upon conditions associated with sediment inputs, and subsequent modification during burial (sensu Schieber, 2003, 2009). Finally, it seeks to address how the manifest, high-frequency cyclicity exhibited by the organic-rich/carbonate-rich couplets here were formed (cf. Hallam, 1986; Ricken, 1986; Bathurst, 1987; Frank et al., 1999; Westphal et al., 2000; Westphal et al., 2004; Biernacka et al., 2005; Bádenas et al., 2009). These observations, thus, illustrate that the detailed interplay between the factors that control lithofacies variability and organic-matter enrichment in intrashelf-basinal settings is likely very complicated. This facies variability is likely controlled by a complex balance between primary production (both organic and inorganic), clastic input, rates of sediment accumulation and burial, bottom-current activity, porewater oxygen concentrations, and different styles of diagenesis associated with varying bioability of oxidants and reductants.

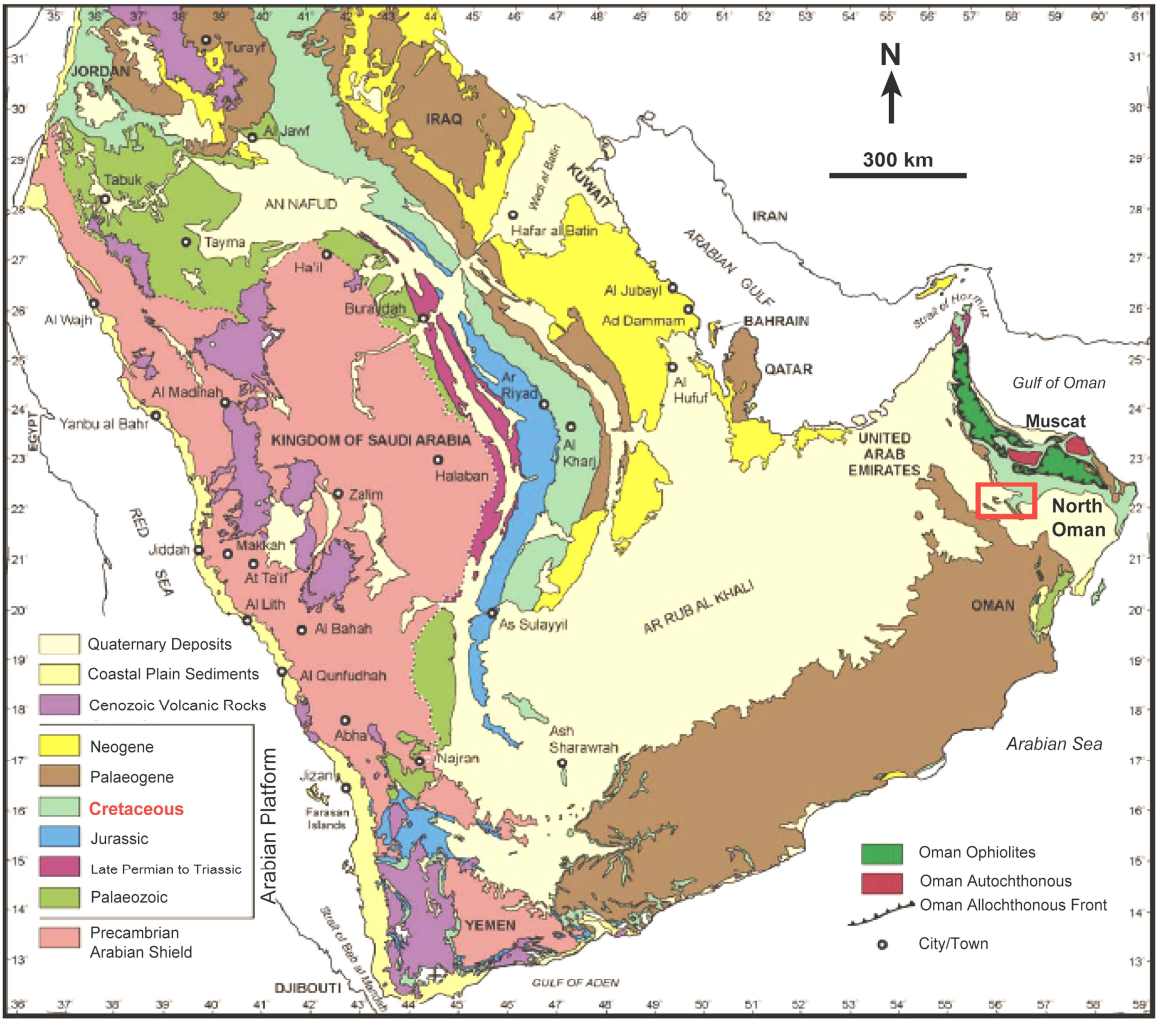

Figure 1.3. Simplified surface geology map of the Arabian Peninsula (modified from Le Nindre et al., 2003). This study is focused on the Upper Cretaceous Natih-B Member (Natih Formation, Wasia Group) of North Oman. Study area is outlined, incorporating both exposures (Adam Foothills) and wells (nearby Fahud and Natih oilfields).

1.2. Aims and Objectives of the Study

In the light of these initial observations and overaching controls, this research mainly aims to: a) demonstrate that persistent bottom-water "anoxia" could not have been the key factor controlling organic-carbon preservation during deposition of intrashelf-basinal sediments, and to discuss some of the alternative mechanisms that might have controlled organic-matter enrichment in these settings; b) investigate the degree of temporal and spatial lithofacies variability within carbonate-dominated intrashelf basins, and to discuss the main driving mechanisms responsible for this variability; c) examine the relative importance of differential early diagenesis in enhancing lithofacies cyclicity and its influence on organanic-matter degradation within carbonate-dominated, source-rock-

bearing intrashelf basins. In order to achieve these aims, the middle-late Cenomanian Natih-B Member (Upper Cretaceous Natih Formation, Wasia Group; e.g. van Buchem et al., 2002b; Figure 1.4) of North Oman (Figure 1.3) has been chosen as an ideal succession. The Natih-B Member is dominated by intrashelf-basinal (40 to 60 m maximum water depth), fine-grained carbonates with source-rock intervals (up to 13.7% TOC, average 5.4%) deposited during worldwide marine transgression, and surrounded by an epeiric carbonate-platform system (e.g. Harris and Frost, 1984; van Buchem et al., 2002b; van Buchem et al., 2005; Figure 1.5). These units are well exposed at the surface in several easily-accessible localities, and are supported by a significant volume of subsurface datasets, including cores, wireline logs, and seismic data from different parts of the basin.

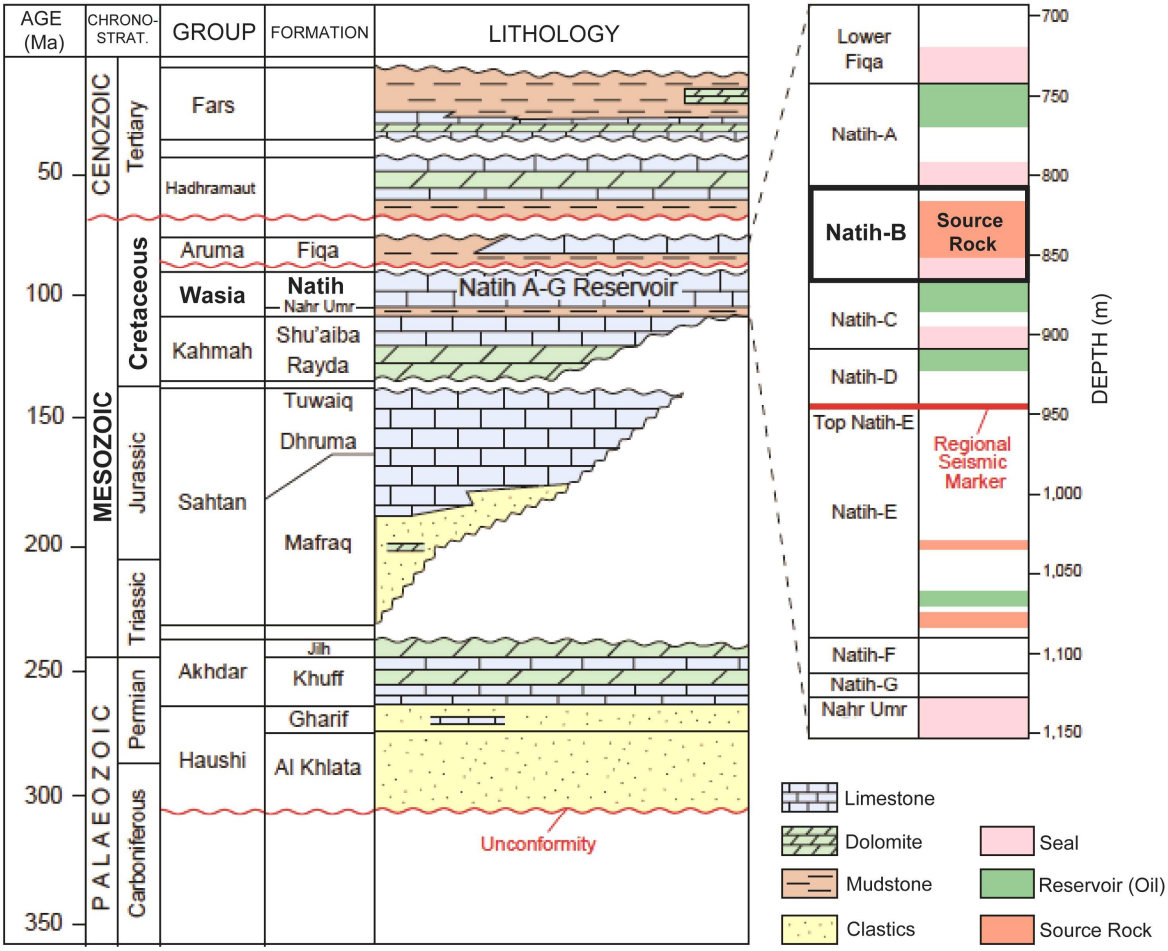

Figure 1.4. Stratigraphic column of sedimentary successions in the Natih field (North Oman) illustrating regional chronostratigraphic and lithostratigraphic framework (modified from Hitchings and Potters, 2000; original source of Natih Formation internal stratigraphy is Terken, 1999). The Natih-B Member – focus of this study- is a major carbonate source-rock interval in North Oman (up to 13.7% TOC, from this study).

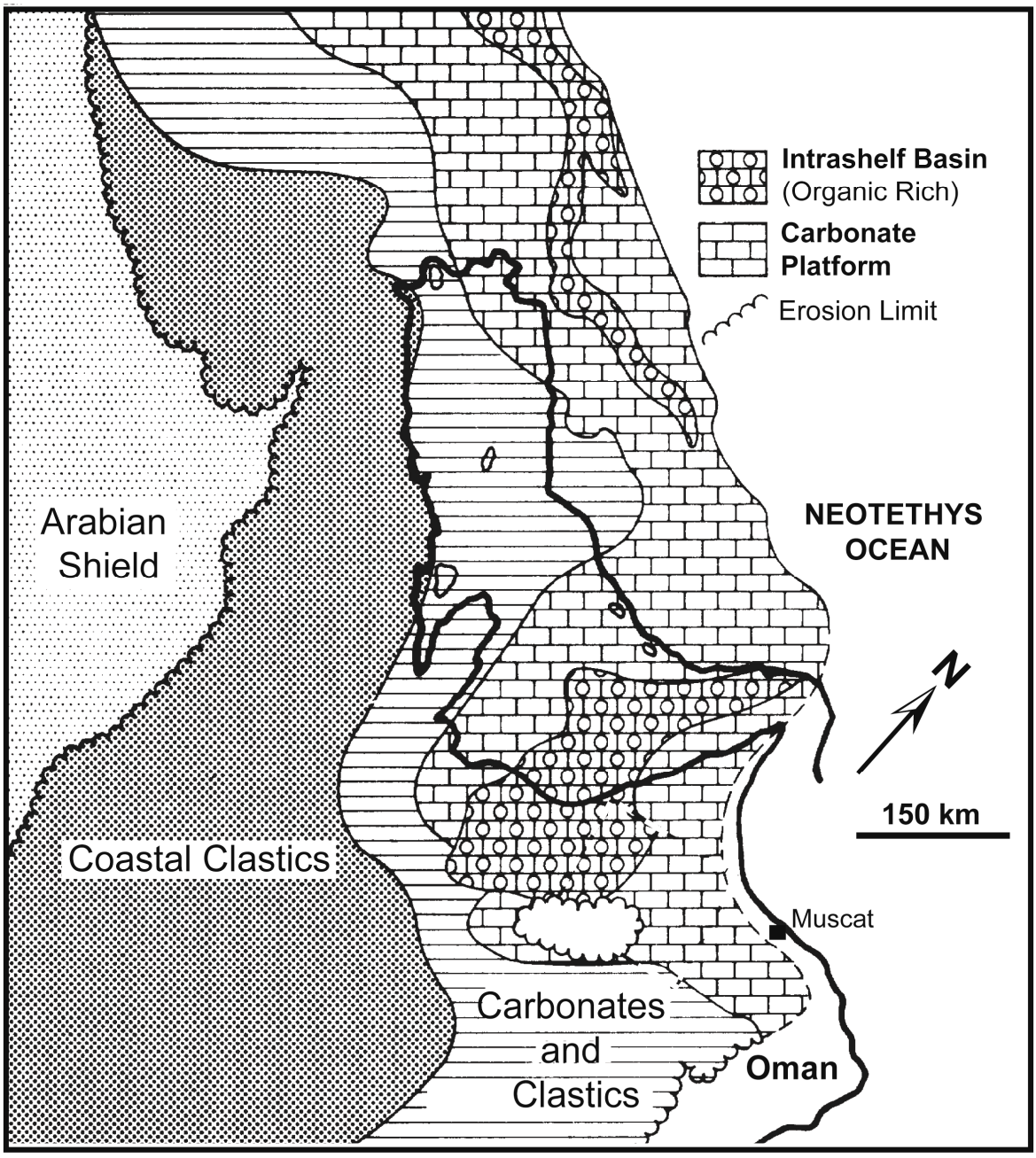

Figure 1.5. Simplified palaeogeographic map of the Gulf region during the time when Natih-B (Cenomanian-aged) intrashelf-basinal, organic-carbon-rich, fine-grained carbonates and associated lithofacies where deposited in North Oman (modified from Murris, 1980; Harris and Frost, 1984; cf. Figure 1.3). Note the distribution of these units in other parts of the region.

The area of study is located in the interior of North Oman, to the south of the Oman Mountains, mainly in the Adam Foothills and Natih oil field areas (Figures 1.3 and 1.6). The exposures in the Adam Foothills provide continuous outcrops of the Natih Formation at the kilometre-scale documenting lateral facies variability, while the cores in the nearby Natih field provide the necessary data for surface-to-subsurface correlations. The outcrop sections of the Adam Foothills are oriented perpendicular to the palaeocoastline of the Natih-B intrashelf basin, and are ideally suited to illustrate the temporal and spatial lithofacies changes when passing from a proximal carbonate platform into a more distal intrashelf basin (Schwab et al., 2005, and references therein). The Adam Foothills are structurally located to the south of the Hawasina Nappes and to the northeast of the strike-slip Maradi Fault Zone (Al-Kindi 2006, Figure 1.6). The Natih field is situated within the Fahud Salt Basin on an anticlinal structure, measuring an area of about 60 km^2. It is bounded to the north and northeast by a large, NW-SE-trending reverse fault, with a throw of about 1 km (Hitchings and Potters, 2000).

The rocks of the Adam Foothills were relatively deeply buried (≥ 8 km burial depth) as a result of major thrusting during the Upper Cretaceous (van Buchem et al., 2002b, and references therein). Faulting and uplift in the Miocene brought the Natih Formation carbonates back to the surface (van Buchem et al., 2002b), and gave them their present-day topography and overall anticlinal structure of the Adam Foothills (also know as the Salakh Arch; e.g. Al-Kindi, 2006). The Natih field area, however, was not covered by thrust sheets, and the late Albian-early Turonian carbonates were consequently much less deeply buried (van Buchem et al., 2002b). Moreover, the sedimentary rocks of the study area appear to have not been affected by the emplacement of the Oman Ophiolites and associated units, compared those of the Oman Mountains (Figure 1.3), which have been significantly squashed by this Upper Cretaceous overburden (Homewood et al., 2008).

To meet the aims of this study, representative samples of the Natih-B Member were collected both from the Adam Foothills (including Jabal Salakh East, Jabal Salakh West, Jabal Nahdah and Jabal Qusaybah) where the Natih-B succession is best exposed, and from a nearby well (Natih field) where continuous core slabs of the Natih-B Member are available (Figure 1.6), along with wireline log data. This along-dip transect, from east to west, represents the ideal transition across the Natih-B intrashelf basin – from near the margin (Jabal Salakh East) to the basin centre (Natih field). The majority of the gathered

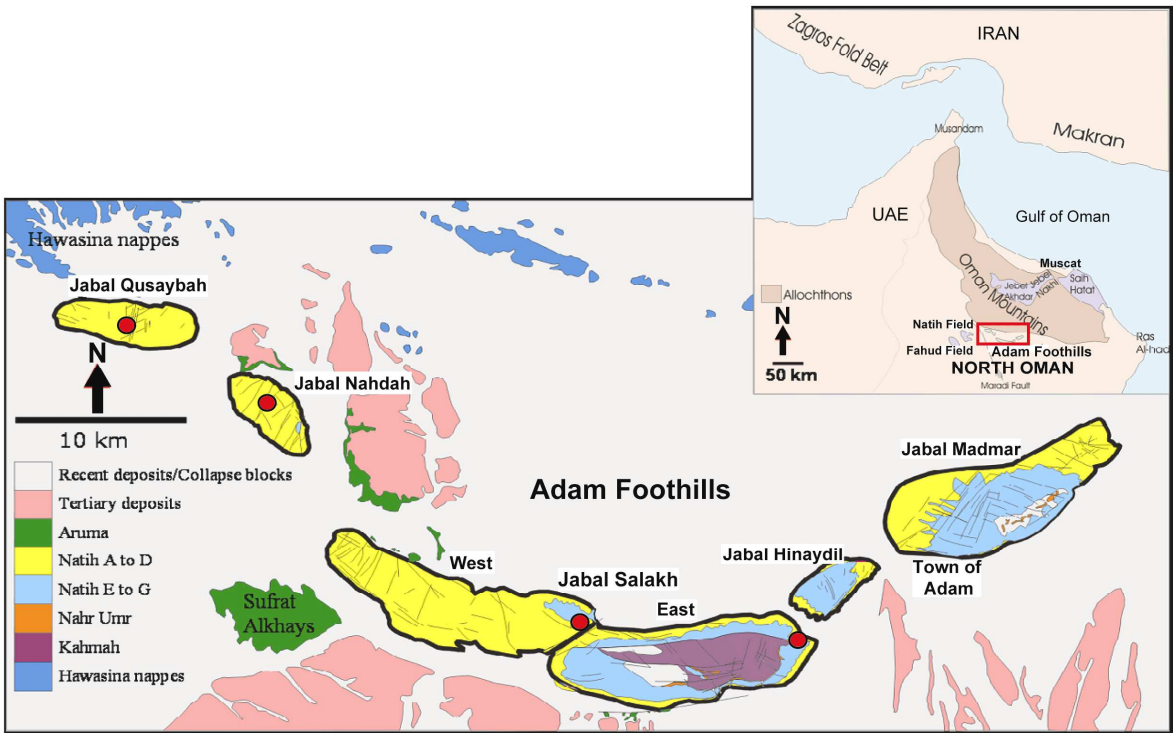

Figure 1.6. Simplified surface geology map of the study area (Adam Foothills, North Oman; modified from Al-Kindi, 2006). Refer to Figure 1.4 for details on stratigraphy. Four sections were measured and sampled from these exposures (outlined; Jabal Qusaybah, Nahdah, and Salakh West and East), in addition to cores from nearby Natih and Fahud fields. Jabal Hinaydil and Madar were not included in this study because the Natih-B Member at these exposures is poor in organic carbon and forms part of platform rather than intrashelf basin (see van Buchem et al., 2002b). Thus, the studied transect from Jabal Salakh East to Jabal Qusaybah, and further west to Natih and Fahud fields, represents gradual transition from basin margin to basin centre.

samples were made into thin sections, which were then described at a range of scales using thin-section scanning, staining, and combined transmitted-light, cathodoluminescence and backscattered scanning-electron microscopy. In addition, whole-rock mineralogical and geochemical techniques (XRD and TOC) have been employed on some of these samples, together with stable-isotopic (C and O) analyses on both whole-rock samples and carefully-selected subsamples. The application of these combined petrographic, mineralogical, and geochemical methods enabled obtaining detailed textural, palaeontological, mineralogical, and diagenetic information of these predominantly fine-grained carbonates. On the basis of these investigations, this study provides better understanding of the factors that controlled lithofacies variability and organic-matter enrichment within the Natih-B. This information also assisted in constructing a lithofacies depositional model for the Natih-B Member at the platform-to-basin scale, which may aid hydrocarbon exploitation in these settings.

1.3. Structure of the Thesis

The structure of this PhD thesis follows the alternative format, which incorporates central chapters (Chapters 3 to 5) that are in a format suitable for submission for publication in peer-reviewed journals, in addition to other chapters (Chapters 1, 2 and 6; Introduction, Methodology and Summary, respectively) that have been written as in a standard-format thesis. This structure was chosen because the data obtained during this multi-disciplinary study divide up naturally into a number of interconnected themes that make coherent, separate research contributions. Specifically, the self-contained, but interrelated, publication-style chapters allowed each of the key aims (see Section 1.2) of this study to be dealt with individually. Each of these paper-style chapters consists of the data, results, and conclusions that have been reached during this PhD programme. Since each publication-style chapter forms a self-contained unit, some overlap and repetition of the background information, methodologies, and references is inevitable.

The layout of the thesis is as follows:

- As mentioned above, Chapter 1 (Introduction) provides initial background information to the research topic and its context, bringing the major themes (the three paper-style chapters) of the study together. It also outlines the key aims and objectives of the study, as well as the structure of the thesis.

- Following this introductory chapter, Chapter 2 (Methodology) describes all the techniques that have been used in order to achieve the research aims and objectives, including field and core descriptions, sampling strategies, thin-section preparation and descriptions, as well as mineralogical and geochemical analyses.

- Chapter 3 (first manuscript, entitled “Sedimentological evidence for bottom-water oxygenation during deposition of the Natih-B intrashelf-basinal sediments: Upper Cretaceous carbonate source rock, Natih Formation, North Oman”) discusses the role of “anoxia” during the period that the Natih-B source rock was being deposited. It also provides detailed

discussion of the factors that have controlled organic-matter preservation in the Natih-B Member. This paper has been peer-reviewed and accepted for publication in *GeoArabia*, Middle East Petroleum Geosciences.

- Chapter 4 (second manuscript, entitled "High-resolution lithofacies analyses of predominantly fine-grained carbonates in and around an intrashelf basin: an example from the Upper Cretaceous Natih-B Member source rock, North Oman") deals with the physical, biological and chemical controls on both temporal and spatial lithofacies variability in intrashelf basins using the Natih-B Member as a natural laboratory, with emphasis on the role of rapid and episodic sedimentation as a controller on source-rock quality. This paper is currently in the final review stage and will be submitted to *Sedimentary Geology*.

- Chapter 5 (third manuscript, entitled "Influence of early oxic diagenesis on source potential and lithofacies cyclicity: new insight from the intrashelf-basinal carbonates of the Natih-B Member (Upper Cretaceous Natih Formation, North Oman") discusses the role of early diagenesis in the degradation of organic matter and its influence on lithofacies cyclicity. This paper will be submitted to *Petroleum Geoscience*.

- Finally, Chapter 6 (Summary) brings together all the results and conclusions reached from this multi-proxy study (specifically Chapters 3 to 5) into a comprehensible synthesis. Recommendations for areas of possible further investigation arising from this research are presented at the end of this chapter.

- In addition, the appendices, which are presented in an electronic format on a CD, include: lithological logs from all measured sections of the Natih-B Member (Appendix A), quantitative and semiquantitative data of all analysed Natih-B samples (Appendix B), and microfossil abundances chart of the Natih-B Member based on a well in the Natih field (Appendix C).

The writing of the publication-style chapters (Chapters 3 to 5) involved collaboration with one or two coauthors. I am the first author on each of the manuscripts, with Dr Joe Macquaker (my main supervisor) being the second author on all of them and Dr Cathy Hollis (my co-supervisor after Dr Macquaker moved to Canada in September 2008) being the third author on the second and third manuscripts. Both coauthors provided suggestions for information additions and modifications, as well as editing and checking the cohesion of the manuscripts. The author, from his association with both coauthors, has gained a lot of knowledge and experience in conducting high-quality research, and he is extremely grateful to their invaluable guidance and support. Any mistakes that may occur in the manuscripts or other parts of the thesis, however, are entirely the author's responsibility.

References

Abdullah, F.H., B. Carpentier, I. Kowalewski, F. van Buchem and A.Y. Huc 2005. Organic matter identification in source and reservoir carbonate in the Lower Cretaceous Mauddud Formation in Kuwait. GeoArabia, v. 10, no. 4, p. 17-34.

Aigner, T., M. Doyle, D. Lawrence, M. Epting and A. Van Vliet 1989. Quantitative modeling of carbonate platforms: some examples. In, P.D. Crevello, J.L. Wilson, J.F. Sarg and J.F. Read (Eds.), Controls on Carbonate Platform and Basin Development. SEPM (Society for Sedimentary Geology), Special Publication 44, p. 27-37.

Al-Kindi, M. 2006. Structural Evolution and Fracture Pattern of Salakh Arch. PhD Thesis, University of Leeds, United Kingdom, 261 p.

Al-Saad, H. and F.N. Sadooni 2001. A new depositional model and sequence stratigraphic interpretation for the upper Jurassic Arab "D" reservoir in Qatar. Journal of Petroleum Geology, v. 24, no. 3, p. 243-264.

Alsharhan, A.S. 1995. Facies variation, diagenesis, and exploration potential of the Cretaceous rudist-bearing carbonates of the Arabian Gulf. American Association of Petroleum Geologists, v. 79, no. 4, p. 531-550.

Alsharhan, A.S. and R.W. Scott 2000. Hydrocarbon potential of Mesozoic carbonate platform-basin systems, U.A.E. In, A.S. Alsharhan and R.W. Scott (Eds.), Middle East Models of Jurassic/Cretaceous Carbonate Systems. SEPM (Society for Sedimentary Geology), Special Publication 69, p. 335-358.

Bádenas, B., M. Aurell, J.C. García-Ramos, B. González and L. Piñuela 2009. Sedimentary vs. diagenetic control on rhythmic calcareous successions (Pliensbachian of Asturias, Spain). Terra Nova, v. 21, no. 3, p. 162-170.

Bathurst, R.G.C. 1987. Diagenetically enhanced bedding in argillaceous platform limestones; stratified cementation and selective compaction. Sedimentology, v. 34, no. 5, p. 749-778.

Biernacka, J., K. Borysiuk and P. Raczyński 2005. Zechstein (Ca1) limestone-marl alternations from the North-Sudetic Basin, Poland: depositional or diagenetic rhythms? Geological Quarterly, v. 49, no. 1, p. 1-14.

Burchette, T.P. 1993. Mishrif Formation (Cenomanian–Turonian), southern Arabian Gulf: carbonate platform growth along a cratonic basin margin. In, J.A.T. Simo, R.W. Scott and J.P. Masse (Eds.), Cretaceous Carbonate Platforms. American Association of Petroleum Geologists, Memoir 56, p. 185-200.

Burchette, T.P. and S.R. Britton 1985. Carbonate facies analysis in the exploration for hydrocarbons: a case study from the Cretaceous of the Middle East. In, P.J. Brenchley and B.P.J. Williams (Eds.), Sedimentology: Recent Developments and Applied Aspects. Geological Society, Special Publication 18, p. 311-338.

Burchette, T.P. and V.P. Wright 1992. Carbonate ramp depositional systems. Sedimentary Geology, v. 79, no. 1-4, p. 3-57.

Davies, R.B., D.M. Casey, A.D. Horbury, P.R. Sharland and M.D. Simmons 2002. Early to mid-Cretaceous mixed carbonate-clastic shelfal systems: examples, issues and models from the Arabian Plate. GeoArabia, v. 7, no. 3, p. 541-598.

Demaison, G.J. and G.T. Moore 1980. Anoxic environments and oil source bed genesis. American Association of Petroleum Geologists Bulletin, v. 64, no. 8, p. 1179-1209.

Demirel, I.H. and S. Guneri 2000. Cretaceous carbonates in the Adiyaman region, SE Turkey: an assessment of burial history and source-rock potential. Journal of Petroleum Geology, v. 23, no. 1, p. 91-106.

Doyle, P., D.G. Poire, L.A. Spalletti, D. Pirrie, P. Brenchley and S.D. Matheos 2005. Relative oxygenation of the Tithonian-Valanginian Vaca Muerta-Chachao formations of the Mendoza Shelf, Neuquen Basin, Argentina. Geological Society, Special Publications, v. 252, no. 1, p. 185-206.

Droste, H. 1990. Depositional cycles and source rock development in an epeiric intraplatform basin: the Hanifa Formation of the Arabian Peninsula. Sedimentary Geology, v. 69, p. 281-296.

Droste, H. 2003. Intra-platform basins in the Cretaceous carbonate platform of Oman (abstract), AAPG International Conference. Barcelona, Spain, American Association of Petroleum Geologists.

Droste, H. and M. Van Steenwinkel 2004. Stratal geometries and patterns of platform carbonates: the Cretaceous of Oman. In, G. Eberli, J.L. Massaferro and J.F.R. Sarg (Eds.), Seismic Imaging of Carbonate Reservoirs and Systems. American Association of Petroleum Geologists, Memoir 81, p. 185-206.

Frank, T.D., M.A. Arthur and W.E. Dean 1999. Diagenesis of lower Cretaceous pelagic carbonates, North Atlantic: paleoceanographic signals obscured. Journal of Foraminiferal Research, v. 29, no. 4, p. 340-351.

Grover, G. 1993. Intrashelf basins: a geologic model for source-bed and reservoir facies deposition within carbonate shelves (abstract), AAPG International Conference. The

Hague, Netherlands, American Association of Petroleum Geologists Bulletin, v. 77, p. 1629.

Hallam, A. 1986. Origin of minor limestone shale cycles: climatically induced or diagenetic? Geology, v. 14, no. 7, p. 609-612.

Harris, P.M. and S.H. Frost 1984. Middle Cretaceous carbonate reservoirs, Fahud field and northwestern Oman. American Association of Petroleum Geologists Bulletin, v. 68, no. 5, p. 649-658.

Hendry, J.P. 1993. Geological controls on regional subsurface carbonate cementation: an isotopic-paleohydrologic investigation of Middle Jurassic limestones in central England. Diagenesis and basin development, p. 231-260.

Heydari, E. and W.J. Wade 2002. Massive recrystallization of low-Mg calcite at high temperatures in hydrocarbon source rocks: implications for organic acids as factors in diagenesis. American Association of Petroleum Geologists Bulletin, v. 86, no. 7, p. 1285-1303.

Hitchings, V.H. and H. Potters 2000. Production and geological implications of the Natih 9C3D seismic survey. GeoArabia, v. 5, no. 4, p. 511-524.

Homewood, P., P. Razin, C. Grélaud, H. Droste, V. Vahrenkamp, M. Mettraux and J. Mattner 2008. Outcrop sedimentology of the Natih Formation, northern Oman: a field guide to selected outcrops in the Adam Foothills and Al Jabal Al Akhdar areas. GeoArabia, v. 13, no. 3, p. 39-120.

Katz, B.J. 2005. Controlling factors on source rock development - a review of productivity, preservation, and sedimentation rate. In, N.B. Harris (Ed.), The Deposition of Organic-Carbon-Rich Sediments: Models, Mechanisms, and Consequences. SEPM (Society for Sedimentary Geology), Special Publication 82, p. 7-16.

Katz, B.J., E.I. Dittmar and G.E. Ehret 2000. A geochemical review of carbonate source rocks in Italy. Journal of Petroleum Geology, v. 23, no. 4, p. 399-424.

Klemme, H.D. and G.F. Ulmishek 1991. Effective petroleum source rocks of the world: stratigraphic distribution and controlling depositional factors. American Association of Petroleum Geologists Bulletin, v. 75, no. 12, p. 1809-1851.

Kuss, J., C. Scheibner and R. Gietl 2000. Carbonate platform to basin transition along an Upper Cretaceous to Lower Tertiary Syrian Arc Uplift, Galala Plateaus, Eastern Desert of Egypt. GeoArabia, v. 5, no. 3, p. 405-424.

Kuypers, M.M.M., R.D. Pancost, I.A. Nijenhuis and J.S. Sinninghe Damste 2002. Enhanced productivity led to increased organic carbon burial in the euxinic North Atlantic basin during the late Cenomanian oceanic anoxic event. Paleoceanography, v. 17, no. 4, p. 3-1.

Le Nindre, Y.M., D. Vaslet, J. Le Metour, J. Bertrand and M. Halawani 2003. Subsidence modelling of the Arabian Platform from Permian to Paleogene outcrops. Sedimentary Geology, v. 156, no. 1, p. 263-285.

Machhour, L., J.P. Masse, J.L. Oudin, B. Lambert and P. Lapointe 1998. Petroleum potential of dysaerobic carbonate source rocks in an intra-shelf basin: the Lower Cretaceous of Provence, France. Petroleum Geoscience, v. 4, no. 2, p. 139-146.

Macquaker, J.H.S. and A.E. Adams 2003. Maximizing information from fine-grained sedimentary rocks: an inclusive nomenclature for mudstones. Journal of Sedimentary Research, v. 73, no. 5, p. 735-744.

Macquaker, J.H.S. and K.M. Bohacs 2007. On the accumulation of mud. Science, v. 318, no. 5857, p. 1734-1735.

Macquaker, J.H.S., R.L. Gawthorpe, K.G. Taylor and M.J. Oates 1998. Heterogeneity, stacking patterns and sequence stratigraphic interpretation in distal mudstone successions: examples from the Kimmeridge Clay Formation, U.K. In, J. Schieber, W. Zimmerle and P. Sethi (Eds.), Shales and Mudstones, Volume I: Basin Studies, Sedimentology, and Palaeontology. E. Schweizerbart'sche Verlagsbuchhandlung, p. 163-186.

Macquaker, J.H.S. and C.R. Jones 2002. A sequence-stratigraphic study of mudstone heterogeneity: a combined petrographic/wireline log investigation of Upper Jurassic mudstones from the North Sea (U.K.). In, M. Lovell and N. Parkinson (Eds.), Geological Applications of Well Logs. American Association of Petroleum Association, Methods in Exploration 13, p. 123-141.

Macquaker, J.H.S. and M.A. Keller 2005. Mudstone sedimentation at high latitudes: ice as a transport medium for mud and supplier of nutrients. Journal of Sedimentary Research, v. 75, no. 4, p. 696-709.

Macquaker, J.H.S., K.G. Taylor and R.L. Gawthorpe 2007. High-resolution facies analyses of mudstones: implications for palaeoenvironmental and sequence-stratigraphic interpretations of offshore ancient mud-dominated successions. Journal of Sedimentary Research, v. 77, no. 3-4, p. 324-339.

Markello, J.R. and J.F. Read 1981. Carbonate ramp-to-deeper shale shelf transitions of an Upper Cambrian intrashelf basin, Nolichucky Formation, southwest Virginia Appalachians. Sedimentology, v. 28, no. 4, p. 573-597.

Markello, J.R. and J.F. Read 1982. Upper Cambrian intrashelf basin, Nolichucky Formation, southwest Virginia Appalachians. American Association of Petroleum Geologists Bulletin, v. 66, no. 7, p. 860-878.

Mort, H., O. Jacquat, T. Adatte, P. Steinmann, K. Föllmi, V. Matera, Z. Berner and D. Stüben 2007. The Cenomanian/Turonian anoxic event at the Bonarelli Level in Italy and Spain: enhanced productivity and/or better preservation? Cretaceous Research, v. 28, no. 4, p. 597-612.

Murris, R.J. 1980. Middle East: stratigraphic evolution and oil habitat. American Association of Petroleum Geologists Bulletin, v. 64, no. 5, p. 597-618.

Pedersen, T.F. and S.E. Calvert 1990. Anoxia vs. productivity: what controls the formation of organic-carbon-rich sediments and sedimentary rocks? American Association of Petroleum Geologists Bulletin, v. 74, no. 4, p. 454-466.

Philip, J., J. Borgomano and S. Al-Maskiry 1995. Cenomanian-Early Turonian carbonate platform of northern Oman: stratigraphy and palaeoenvironments. Palaeogeography, Palaeoclimatology, Palaeoecology, v. 119, p. 77-92.

Read, J.F. 1982. Carbonate platforms of passive (extensional) continental margins: types, characteristics and evolution. Tectonophysics, v. 81, no. 3-4, p. 195-212.

Read, J.F. 1985. Carbonate platform facies models. American Association of Petroleum Geologists Bulletin, v. 69, no. 1, p. 1-21.

Ricken, W. 1986. Diagenetic Bedding: A Model for Marl-Limestone Alternations. Lecture Notes in Earth Sciences, Springer-Verlag, 210 p.

Sassen, R., C.H. Moore and F.C. Meendsen 1987. Distribution of hydrocarbon source potential in the Jurassic Smackover formation. Organic Geochemistry, v. 11, no. 5, p. 379-383.

Schieber, J. 1994. Evidence for high-energy events and shallow-water deposition in the Chattanooga Shale, Devonian, central Tennessee, USA. Sedimentary Geology, v. 93, no. 3-4, p. 193-208.

Schieber, J. 1999. Distribution and deposition of mudstone facies in the Upper Devonian Sonyea Group of New York. Journal of Sedimentary Research, v. 69, no. 4, p. 909-925.

Schieber, J. 2003. Simple gifts and buried treasures – implications of finding bioturbation and erosion surfaces in black shales. The Sedimentary Record, v. 1, no. 2, p. 4-8.

Schieber, J. 2009. Discovery of agglutinated benthic foraminifera in Devonian black shales and their relevance for the redox state of ancient seas. Palaeogeography, Palaeoclimatology, Palaeoecology, v. 271, no. 3-4, p. 292-300.

Schieber, J. and J.B. Southard 2009. Bedload transport of mud by floccule ripples - direct observation of ripple migration processes and their implications. Geology, v. 37, no. 6, p. 483-486.

Schwab, A.M., P.W. Homewood, F.S.P. van Buchem and P. Razin 2005. Seismic forward model of a Natih Formation outcrop: the Adam Foothills Transect (northern Oman). GeoArabia, v. 10, no. 1, p. 17-44.

Scott, R.W. 1990. Chronostratigraphy of Cretaceous carbonate shelf, southeastern Arabia. In, A.H.F. Robertson, M.P. Searle and A.C. Ries (Eds.), The Geology and Tectonics of the Oman Region. Geological Society, Special Publication 49, p. 89-108.

Sharland, P.R., R. Archer, D.M. Casey, R.B. Davies, S.H. Hall, A.P. Heward, A.D. Horbury and M.D. Simmons 2001. Arabian Plate Sequence Stratigraphy. GeoArabia, Special Publication 2, 371 p.

Stanton, R.J. and E. Flügel 1995. An accretionary distally steepened ramp at an intrashelf basin margin: an alternative explanation for the Upper Triassic Steinplatte "reef" (Northern Calcareous Alps, Austria). Sedimentary Geology, v. 95, no. 3-4, p. 269-286.

Summerhayes, C.P. 1987. Organic-rich Cretaceous sediments from the North Atlantic. In, A.J. Fleet and J. Brooks (Eds.), Marine Petroleum Source Rocks. Geological Society, Special Publication 26, p. 301-316.

Taghavi, A.A., A. Mørk and E. Kazemzadeh 2007. Flow unit classification for geological modelling of a heterogeneous carbonate reservoir: Cretaceous Sarvak Formation, Dehluran field, SW Iran. Journal of Petroleum Geology, v. 30, no. 2, p. 129-146.

Taylor, K.G. 1998. Spatial and temporal variations in early diagenetic organic matter oxidation pathways in Lower Jurassic mudstones of eastern England. Chemical Geology, v. 145, no. 1-2, p. 47-60.

Terken, J.M.J. 1999. The Natih petroleum system of North Oman. GeoArabia, v. 4, no. 2, p. 157-180.

van Buchem, F.S.P., A.Y. Huc, B. Pradier and M. Stefani 2005. Stratigraphic patterns in carbonate source-rock distribution: second-order to fourth-order control and sediment flux. In, N.B. Harris (Ed.), The Deposition of Organic-Carbon-Rich Sediments: Models, Mechanisms, and Consequences. SEPM (Society for Sedimentary Geology), Special Publication 82, p. 191-223.

van Buchem, F.S.P., B. Pittet, H. Hillgärtner, J. Grötsch, A.I. Al Mansouri, I.M. Billing, H.H.J. Droste, W.H. Oterdoom and M. van Steenwinkel 2002a. High-resolution sequence stratigraphic architecture of Barremian/Aptian carbonate systems in northern Oman and the United Arab Emirates (Kharaib and Shu'aiba formations). GeoArabia, v. 7, no. 3, p. 461-500.

van Buchem, F.S.P., P. Razin, P.W. Homewood, W.H. Oterdoom and J. Philip 2002b. Stratigraphic organization of carbonate ramps and organic-rich intrashelf basins: Natih Formation (middle Cretaceous) of northern Oman. American Association of Petroleum Geologists Bulletin, v. 86, no. 1, p. 21-53.

Ward, R.F., C.G.S.C. Kendall and P.M. Harris 1986. Upper Permian (Guadalupian) Facies and their Association with Hydrocarbons - Permian Basin, West Texas and New Mexico. American Association of Petroleum Geologists Bulletin, v. 70, no. 3, p. 239-262.

Weedon, G.P., A.L. Coe and R.W. Gallois 2004. Cyclostratigraphy, orbital tuning and inferred productivity for the type Kimmeridge Clay (Late Jurassic), Southern England. Journal of the Geological Society, v. 161, no. 4, p. 655-666.

Westphal, H. 2006. Limestone-marl alternations as environmental archives and the role of early diagenesis: a critical review. International Journal of Earth Sciences, v. 95, no. 6, p. 947-961.

Westphal, H., M.J. Head and A. Munnecke 2000. Differential diagenesis of rhythmic limestone alternations supported by palynological evidence. Journal of Sedimentary Research, v. 70, no. 3, p. 715-725.

Westphal, H., A. Munnecke, F. Böhm and S. Bornholdt 2008. Limestone-marl alternations in epeiric sea settings - witnesses of environmental changes or diagnesis? Special Paper - Geological Association of Canada, p. 389-406.

Westphal, H., A. Munnecke, J. Pross and J.O. Herrle 2004. Multiproxy approach to understanding the origin of Cretaceous pelagic limestone-marl alternations (DSDP site 391, Blake-Bahama Basin). Sedimentology, v. 51, no. 1, p. 109-126.

Chapter 2

Methodology

2.1. Introduction

This chapter describes the various analytical methods employed during the course of the study and outlines the rationale for conducting them. Specifically, it illustrates the outcrop/core procedures, sampling strategies and laboratory analyses (including petrographic, mineralogical and geochemical techniques) that facilitated understanding the fundamental controls on lithofacies variability and organic-matter enrichment in the Cenomanian-aged Natih-B Member (Upper Cretaceous Natih Formation, North Oman; Figures 1.4 and 1.6). Detailed outcrop and core descriptions of sedimentological and palaeontological features, as well as sampling strategies that consider the temporal and spatial variations in these features were essential for the accomplishment of high-resolution lithofacies investigations in fine-grained sediments. Laboratory methods study microscopic depositional and diagenetic features, and provide detailed petrographic, mineralogical and geochemical information, utilising optical and electron-optical microscopy, X-ray diffraction (XRD), total organic carbon (TOC) and stable isotope (C and O) analyses.

The combination of petrographic, mineralogical, and geochemical dataset, in addition to outcrop/core information, enabled detailed lithofacies descriptions of the predominantly fine-grained carbonates of the Natih-B Member. These methods allowed the textures and components of individual samples to be imaged, and the proportions of the various bioclasts and minerals (both detrital and authigenic) to be obtained (see also Macquaker and Gawthorpe, 1993; Macquaker, 1994; Macquaker and Taylor, 1996; Macquaker et al., 1998; Macquaker and Howell, 1999; Macquaker and Jones, 2002; Macquaker and Adams, 2003; Macquaker and Keller, 2005; Macquaker et al., 2007).

A brief description of the rock nomenclature scheme is also included at the end of this chapter. Specific methodology description of the techniques, classification schemes and any statistical analysis used in this study are further discussed within the related chapters.

2.2. Outcrop and Core Procedures

Excellent outcrop sections and subsurface core materials of the 50- to 60-m-thick Natih-B succession in the Adam Foothills and Al Jabal Al Akhdar and in the nearby oilfields (including Natih, Fahud, and Yibal fields) of North Oman (see Figures 1.3 to 1.6) have been used as natural laboratories for this study. The data from these locations allowed a comprehensive study on the Natih-B intrashelf-basinal sediments and detailed understanding of its source potential variations.

In order to describe the temporal stacking patterns and lateral lithofacies variability, four different outcrop sections in the Adam Foothills and one subsurface core section in the Natih field were studied in detail (see Figure 1.6). Detailed sedimentary graphic logs were measured at the scale of 1:50 (see Appendix A), and samples were collected along a 100-km-long transect from the five locations across the Natih-B intrashelf basin. These include Jabal Salakh East (intermediate to proximal location [basin margin]), Jabal Salakh West (intermediate to distal location [marginal to basinal location]), and Jabal Nahdah, Jabal Qusaybah and a well from the Natih field (distal locations [basin centre]). The logs record information on the lithology, grain size, layer thickness, sedimentary structures, macrofossil types and content and extent of bioturbation, as well as sample locations. The logs are complimented by detailed notes, diagrams, sketches and relevant exposure and core photographs. Observations of discontinuity surfaces and facies stacking patterns were also conducted in this study. Where possible, layers were traced laterally within and between the exposures to determine lateral continuity and overall lithofacies variability.

The locations of the measured outcrop sections were chosen for best accessibility to the exposure and the quality and completeness of the Natih-B succession. The rocks in the Adam Foothills are well exposed and allow direct correlation of major stratal surfaces and associated sedimentary units. Lateral correlations between these units were accomplished by a combination of physically walking the contacts in the exposure, binocular observation at outcrop, and later photomontage assessment of cliff faces. This correlation allowed the identification of lithofacies and key stratal surfaces. The lithofacies were interpreted in terms of depositional features and diagenetic overprints.

The Natih-B sediments from the well in the Natih field (Figure 1.6) are considered to be particularly suitable for this study because both core and comprehensive wireline log suites are available through thick, carbonate-mudstone-dominated succession with alternating organic-carbon-rich/sparry-calcite-rich units that are most commonly interpreted as a result of variation in primary productivity and/or bottom-water "anoxia". This well is the only well from which a complete section of the Natih-B Member has been recovered. In this well, the Natih-B was cored using a 5 ¼" diameter inner barrel that resulted in 100% recovery. When working with core material, housed at the core shed of Petroleum Development Oman (Mina Al Fahal, Muscat), the surface of the core was wetted to improve observation and measurement. These cores were also studied from high-resolution digital images. The digital images were enhanced by modifying the brightness and contrast on a specialist programme (either Adobe Photoshop CS2 or Microsoft Office Picture Manager).

Overall, the five sampled sections were used for detailed study of both temporal and spatial lithofacies distribution. Correlation between the core and outcrop sections was achieved by comparing the sedimentary logs and exposure and core photographs. All of the field and core work was carried out during four periods (January 2006, 11 days; January 2007, 14 days; January 2008, 13 days; March 2008, 12 days), totalling seven weeks.

2.3. Sampling Strategy

In order to generate detailed lithofacies descriptions and to determine the spatial and temporal lithofacies variability, a total of 318 samples were collected from the studied sections (Figure 1.6). The majority of the samples were collected from core to reduce the effects of surficial weathering. Nevertheless, the collection of weathered samples in the field was minimised by digging small trenches to excavate less weathered samples. The least-weathered samples are differentiated from the weathererd material by being more intact, darker-grey or black in colour, and contain less dusty material.

One hundred and thirty unweathered, core samples were collected systematically (every 0.1 to 0.5 m) from Natih field well over driller's-depth interval 894.0 to 950.5 m, in order to investigate the small-scale temporal lithofacies variability. One hundred and eight

samples were similarly collected from the nearby section at Jabal Qusaybah to facilitate comparison with samples deposited elsewhere in the basin. Samples from other locations were obtained from laterally-equivalent intervals, in order to assist in the investigation of the lateral lithofacies variability across the carbonate-platform margin and intrashelf basin. The location and character (at hand-specimen scale) of each gathered sample are recorded on the sedimentary logs.

From the 318 samples gathered, 286 polished, large (~ 40 × 60 mm), thin sections (≤ 30 µm thick) were prepared for petrographic investigations. Prior to thin section preparation, the samples were sliced and slabbed, and macro-sedimentary features at hand-specimen scale were documented. The thin sections were chosen to best represent the lithofacies present both in the core and exposure, and to determine the small-scale lithofacies variability.

All the prepared thin sections were scanned and investigated optically (normal transmitted-light [TL] microscopy). From these thin sections, 133 samples were examined electron-optically (backscattered scanning-electron [BSE] microscopy), 68 by cold cathodoluminescence (CL) microscopy, 34 sections half stained with Alizarin Red S and potassium ferricyanide, and 30 were investigated for detailed micropalaeontological analysis. In addition, 247 Natih-B samples had their TOC content determined, 91 representative samples were chosen for XRD analyses, and 31 samples were examined for stable isotope analyses. These methods and their rationales are described in more detail below. The results of these analyses are reported in Appendices B and C.

2.4. Petrographic Methods

All thin-section preparations and petrographic analyses for this study were performed at the Williamson Research Centre for Molecular Environmental Science in the School of Earth, Atmospheric, and Environmental Sciences (University of Manchester). Detailed descriptions of the thin-sections preparation technique and their petrographic analyses are discussed in the following subsections.

2.4.1. Thin-Section Preparation

All thin sections of the most promising Natih-B samples were prepared utilising standard procedures. Initially, a 1- to 2-mm-thick slice of the resin-impregnated sample was cut perpendicular to bedding planes from the region of interest using a nonaqueous cutting medium to minimise sample damage by hydration of clays (Adams et al., 2006). One side of the sample slice was then mechanically ground flat utilising a 100-µm particle-size (120-grade) carborundum (silicon carbide) abrasive powder. Finer grades of abrasive (60 µm to 12 µm particle size) were gradually applied to the same surface. When flat, the ground slice surface was then attached to a microscope slide with epoxy-resin adhesives (Araldite DBF resin and Araldite HY951 hardener) that possess suitable refractive index properties. The mounted slice was finally ground to the desired thickness (≤ 30 µm) utilising a 12-µm particle-size carborundum abrasive. A fine polish was applied at this stage using 0.8-µm particle-size corundum (aluminium oxide) to remove any residual surface abrasions, especially if the thin section was to be examined electron-optically.

The grinding and polishing processes were carried out in oil to avoid sample disintegration (Macquaker and Taylor, 1996). The thinner-than-normal, polished thin sections were prepared in this way to maximise textural resolution when analysed both optically and backscattered electron-optically (Macquaker, 1994; Macquaker and Keller, 2005). All the prepared thin sections were left uncovered in order to allow various petrographic and geochemical analyses (e.g. staining, CL, BSE microscopy).

Thirty four of the prepared thin sections were selectively half stained using a combined Alizarin Red S and potassium ferricyanide solution, to aid in distinguishing calcite from dolomite, and also determine whether their cements/replacements are ferroan or nonferroan (see Dickson, 1965; Adams and Mackenzie, 1998). The staining solution was prepared, firstly, by separately adding 100.0 mL of 1.5% HCl to 0.2 g of Alizarin Red S and 2.0 g of potassium ferricyanide, and then mixing the two solutions together. Then each thin section was partially immersed perpendicular to bedding in the mixture of solutions for 30 to 45 seconds and immediately washed gently in running water for a few seconds, and then left to dry naturally.

2.4.2. Thin-Section Scanning

All the 286 prepared thin sections (stained and unstained) were scanned utilising either a flatbed scanner (Epson Perfection 3170 Photo) or a Polaroid Sprintscan 35 LE 35 mm scanner to generate large images for detailed annotation and record textural details at low resolution (10^{-2} to 10^{-3} m scale), less than × 1 magnification. This simple technique of thin-section scanning permitted immediate capture of high-quality digital images of whole thin sections at a pixel resolution of 1200 pixels per inch (ppi). This is a facility that is not easily obtainable using petrographic microscopes (De Keyser, 1999; Francus et al., 2002; Soreghan and Francus, 2004). "Such images fall into the range of macrophotography and bridge the gap between standard photography and photomicrography" (De Keyser, 1999).

2.4.3. Transmitted-Light Microscopy

Following scanning, the thin sections were then examined optically at low to medium resolution under transmitted light (both plane polarised and cross polarised) using a binocular petrographic microscope (Nikon Optiphot2-Pol), attached to a digital camera (Jenoptik Jena D-07739). A set of photomicrographs were captured from 142 selected thin sections at magnifications of × 2, × 4, × 10, and × 20. This standard petrographic investigation helped to obtain lithological, textural, compositional, and diagenetic information at 10^{-3} to 10^{-4} m.

In addition to this optical photomicrography, 30 selected thin sections of the cored interval form Natih field were analysed under plane-polarised light at × 10 magnification, in order to provide microfossil abundances chart of the Natih-B Member (see Appendix C). Absolute abundances of microfossils (planktonic foraminifera, benthic foraminifera [both agglutinated and calcareous forms], algal and shell fragments, fish debris, calcispheres, and ostracods) were determined in each thin section by counting 100 specimens every 200 mm (10 fields of view at × 10 magnification). Because the thin sections prepared for this study are large (see above), the microfossils counting process used here differs slightly from the commonly-used method (e.g. Eshet and Moshkovitz, 1995, and references therein), which involves counting 200 specimens per (normal-sized) slide. In this process and where possible, individual species of planktonic and benthic foraminifera, calcispheres, and ostracods were recorded and counted as individual specimens (see Appendix C). No major

difficulty was encountered during the process of species identification and counting, as the microfossils are generally well preserved in the subsurface samples. Broken specimens that were not identifiable, however, were not counted. The microfossil abundances chart constructed from these thin-section analyses provides statistical information on the Natih-B microfossil assemblages and distribution in the stratigraphic column, which aids in providing rigorous lithofacies descriptions and palaeoenvironmental interpretations (see Chapter 4).

2.4.4. Cold-Cathode Cathodoluminescence Microscopy

Out of the 142 optically-photomicrographed sections, 68 were investigated by cold-cathode cathodoluminescence (CL) microscopy, utilising a CITL Cathodoluminescence Unit (Model CCL 8200 mk3) that is in connection with an Olympus BH-2 binocular petrographic microscope. The CL unit was operated at approximately 20.0 kV electron-gun potential, 300.0 μA electron-beam current, and 0.2 Torr vacuum. The petrographic microscope was also equipped with a digital camera (Jenoptik Jena D-07739), and photomicrographs (both under plane-polarised light and CL) were obtained from each thin section at × 4 and × 10 magnifications.

During each analysis, the polished, uncovered thin-section was placed in a vacuum chamber and the surface of the sample was bombarded with electrons using a focused electron beam (~ 0.5 mm diameter), which resulted in 'exciting' the surface and the emission of light (luminescence). The resultant low-intensity luminescence observed using the petrographic microscope can reveal details of carbonate cements, replacements, growth fabrics, mineral zonation and diagenetic phases (see Marshall, 1988; Barker and Kopp, 1991 for further detail).

2.4.5. Backscattered Scanning Electron Microscopy

At even higher resolution (10^{-4} to 10^{-5} m scale), 133 samples of the already optically-analysed thin sections were examined electron-optically utilising a JEOL 6400 scanning electron microscope (SEM), equipped with a Link 4-Quadrant, solid-state, backscattered electron detector. A number of backscattered electron (BSE) images from each thin section were captured at a set of scales (× 20, × 100, × 250, × 500, × 1000 and × 2500

magnifications) using a Semafore digital framestore that is in connection with the SEM. With this high-power imaging technique, minerals were identified in the produced electron images based on their backscatter coefficients (η), and also sometimes with the aid of a PGT semiquantitative, energy-dispersive, X-ray spectrometer that is in connection with the JEOL instrument. Microtextures and other micro- and nano-components were also investigated using this technique. The microscope was operated at 20 kV and 2 nA, with 15 mm working distance.

Before each SEM analysis, the uncovered, polished thin section was coated with a 100- to 150-Å layer of carbon to warrant sufficient conductivity and prevent sample charging, as sedimentary rocks are characterised by being poorly-conductive (Soreghan and Francus, 2004). Then, the thin section was transferred into its customised sample holder, and drops of silver 'dag' were added at either end of the holder making a good electrical leakage track between the sample and metal of sample holder in order to improve image quality by ensuring an equal distribution of conductivity throughout the surface of the sample.

In addition to TOC and XRD data (see below for descriptions of these techniques), component abundances in each sample were quantified by visual estimation from the optical and electron-optical photomicrographs, taken at a range of magnifications (× 2 to × 2500), and with reference to standard comparison charts (see Flügel, 2004). All data from these analyses are reported in Appendix B.

2.5. Mineralogical and Geochemical Techniques

The mineralogical and geochemical techniques described in this section included XRD, TOC, and stable isotope analyses (see the following subsections). All XRD and TOC analyses and some of the isotope analyses were performed on crushed, finely-ground (< 5 μm), powdered, whole-rock samples. Sample crushing was achieved using a powered jaw-crusher and grinding was achieved using a vibro-mill in the Williamson Research Centre, University of Manchester.

2.5.1. XRD Analyses

The XRD analyses were employed in this study for the determinations of bulk-rock mineralogy of some selected samples throughout the Natih-B Member (91 samples from all studied sections but mostly from Natih field well). A Philips PW1730 X-ray diffractometer was used at the Williamson Research Centre operated at 40 kV and 20 mA, utilising a copper Kα radiation with a step size and time constant of 0.01º and 2.00 s. For each XRD analysis, a thin smear was prepared by mixing approximately 0.5 g of the powdered sample with a small volume (few drops) of amyl acetate and then left to dry on a small glass slide (e.g. half a standard microscope slide) before being inserted into the diffractometer.

2.5.2. TOC Analyses

TOC analyses were performed on 247 samples in order to judge the hydrocarbon source-rock potential of the Natih-B Member. TOC data are also useful to understand the temporal and spatial distribution of organic-carbon-rich lithofacies. It is worth mentioning here that the Natih-B source rock, based on Rock-Eval analyses (van Buchem et al., 2002), is immature, with low hydrogen index (HI) values (< 110), in the cores from Natih field, and is overmature (HI values up to 650) in the adjacent exposures of the Adam Foothills.

The TOC contents for this study were obtained utilising a LECO carbon and nitrogen analyser (TruSpec CN) at the Department of Environmental and Geographical Sciences, Manchester Metropolitan University. Prior to each measurement, approximately 0.2 g of each powdered sample was reacted with 10.0 mL of hydrochloric (HCl) solution (1.0 M molar concentration) and left overnight to dissolve all carbonate present. Then, both the dried acid-digested sample and undigested (natural) sample had their total carbon (TC) contents measured using an induction furnace within the LECO instrument that burned the samples to about 950˚C. The TOC contents here are considered to be the same as the TC contents obtained from the acid-digested samples, assuming that all the carbonate carbon had been removed from each acid-digested sample, and that the carbon content obtained was of organic carbon. The total carbonate carbon (TCC) contents were also recorded, determined by calculating the difference between the TC contents of the undigested

samples and TC contents of the acid-digested samples (i.e. TOC contents). The reproducibility of these measurements is better than or equal to 0.1%.

2.5.3. Stable Isotope Analyses

Carbon and oxygen stable isotope analyses were conducted in order to obtain diagenetic information on the predominantly fine-grained carbonates of the Natih-B Member, which comprise mixtures of authigenic and biogenic materials. Specifically, these analyses were performed to determine whether the early-precipitated calcite spar, which occupies significant proportions of both intergranular pore-space and fine-grained matrix of the Natih-B lithofacies (especially in the sparry-calcite-rich units; see Chapters 3 and 4), was primarily derived from seawater and skeletal calcite in open oxic environment or from organic-matter oxidation (degradation by oxic respiration, bacterial sulphate reduction or methanogenesis; see Curtis and Coleman, 1988). In addition to sparry-calcite subsamples, calcite powders were extracted from diagenetically-unaltered shells to determine the original seawater isotopic composition during time of deposition, as well as whole-rock samples, in order to compare the diagenetically-altered isotopic values to both original composition and values from the mixture of components (see Chapter 5).

Twenty eight powdered subsamples were collected from ten polished core slabs (Natih field well) throughout Natih-B, together with three subsamples from a single exposure hand-specimen (Jabal Salakh West). For each stable isotope analysis, at least 3.0 mg of powdered calcite was extracted with a steel needle from identified portions of cut rock faces. These portions included unaltered oyster and pecten shells (7 subsamples), sparry-calcite-cemented shell fragments (3 subsamples), sparry-calcite-cemented microfractures (2 subsamples), and sparry-calcite-dominated, fine-grained matrix (8 subsamples), in addition to 11 homogenised bulk samples. Dolomitised samples were not collected for stable isotope analyses because they are rare in Natih-B; and also it is very difficult to separate dolomite from calcite and other components due to the fine-grain size.

As the majority of samples from this study are predominantly fine grained and contain a mixture of constituents (including authigenic, biogenic and detrital materials), great care was taken when extracting the subsamples from specific components to avoid contamination from other materials in the rock. It is hoped that this method would lead to

the most accurate determination of the isotopic signature of calcite (both original and diagenetic), even though mixing between the different rock components was likely. Bulk samples, however, comprise a mixture of all rock components that comprise mineral mixtures of biogenic carbonates from bivalve, brachiopod, echinoderm, gastropod, ostracod, foraminifer and coccolith tests, in addition to the crucial authingenic-carbonate components present in the shelter porosity of these mixed tests, as well as in the rock matrix and microfractures. Accordingly, a great deal of information was obtained about the chosen samples for stable-isotopic analyses from a combination of geochemical (TOC), mineralogical (XRD) and petrographic (thin-section staining, TL, CL and BSE microscopy) investigations. CL and TL microscopy, in particular, was used to establish the unaltered nature of the mollusc shells (oyster and pecten bivalves). The diagenetically-unaltered, texturally-pristine, foliated, nonferroan bivalve-shell calcite here is characterised by being nonluminescent under CL (see also Hendry and Kalin, 1997).

Before performing the stable-isotopic analyses, all the samples were treated in a low-temperature (25°C) oxygen-plasma furnace, at a pressure of 0.2 mbar, and left over night to remove any organic matter. Then, around 3.0 mg of each sample was reacted to completion with approximately 2.0 mL of 100% anhydrous phosphoric acid (H_3PO_4) in an online-automated preparation system at 25ºC, in order to release CO_2 (see McCrea, 1950). Librated CO_2 was collected cryogenically (−200°C) at regular intervals and analysed on an automated VG Isogas SIRA-12 triple-collector micromass spectrometer in the University of Liverpool Stable Isotope laboratory where $^{13}C/^{12}C$ and $^{18}O/^{16}O$ ratios (i.e. $\delta^{13}C$ and $\delta^{18}O$, respectively) were measured. C and O isotopic ratios were corrected for ^{17}O effects following the standard procedures (sensu Craig, 1957). The data are expressed in the usual δ (delta) and ‰ (permil) notations, relative to the VPDB (Vienna Pee Dee Belemnite) international standard (Coplen, 1994). The analytical precision of both $\delta^{13}C$ and $\delta^{18}O$ results is better than or equal to 0.1‰.

2.6. Nomenclature Used to Describe the Natih-B Sediments

In order to generate detailed descriptions of temporal and lateral lithofacies variability, and interpret genetic features and depositional environments in terms of fundamental sedimentological processes that lead to the construction of a generalised lithofacies

depositional model, the predominantly fine-grained carbonates of the Natih-B Member were broadly classified according to the scheme outlined in Dunham (1962) and its modification by Embry and Klovan (1971), together with the terminology of Macquaker and Adams (2003). The carbonate-rocks classification schemes of both Dunham and Embry-Klovan were used to describe rocks based on their depositional texture and grain size, which varied in the Natih-B samples between carbonate mudstone, wackestone, packstone and floatstone, with the majority of sediments being mud-supported (i.e. mudstones and wackestones).

The fine-grained sedimentary-rocks classification scheme of Macquaker-Adams was used to describe rocks based on their sedimentary structures and the relative abundance of all components (autochthonous, allochthonous and diagenetic), with each component making at least 10% of total rock volume in each sample. According to this nomenclature, a rock including between 10 and 50% of a particular constituent is classified as being "bearing" that constituent, a rock containing between 50 and 90% is described as being "rich" in that constituent, and one comprising more than 90% is said to be "dominated" by that constituent. These terms are then prefaced by adjectives that describe the principal sedimentary fabrics present (e.g. "extensively-bioturbated", "nodular") to give an instantly-recognisable name that expresses in a few words the essence of a particular sediment. Therefore, a strongly burrow-mottled wackestone containing 70% sparry-calcite crystals, 20% shell fragments and 10% planktonic foraminifera can be described as an ''extensively-bioturbated, planktonic-foraminifera- and shell-fragments-bearing, sparry-calcite-rich wackestone''.

This attempt of the Natih-B sediments classification has been designed to produce a systematic description of all lithofacies present according to their depositional textures and major constituents (e.g. grain size, grain origin and grain type). Although this nomenclature is mainly based on petrographic investigations, hand-specimen scale features together with mineralogical (XRD) and geochemical (TOC) data have also been considered. This classification scheme is particularly useful because it describes both the depositional and diagenetic characteristics of carbonate sediments, even when some impurity exists as a result of mixing with a few siliciclastic components (see Chapter 4; Mount, 1985; Macquaker and Adams, 2003).

One major problem involved with this scheme of classification, however, is the difficulty associated with the estimation of calcite spar and bioclasts in each lithofacies. Because calcite spar exists both as pore-filling cement and diagenetically-replaced, microcrystalline matrix (i.e. "microspar"; sensu Flügel, 2004) it can be tricky to separately estimate the abundance of the calcite spar and predominantly sparry-calcite-cemented bioclasts (e.g. bivalves, gastropods, planktonic foraminifera). Consequently, as sparry calcite occurs frequently in the Natih-B samples, the majority of the lithofacies present are described as being either sparry-calcite rich or sparry-calcite bearing (see Appendix B; Chapter 4). Flügel (2004) also emphasised the impact of diagenesis on such sediments, and concluded that carbonates revealing mudstone, wackestone and packstone textures could as well be products of diagenetic modifications (e.g. matrix cryptocrystalline-calcite replacement, micritisation, neomorphism), rather than being predomiantly depositional in character (cf. Dunham, 1962; Embry and Klovan, 1971).

Another problem that could arise from the use of Dunham and Embry-Klovan classification is the distinction between mud-supported carbonates (mudstones and wackestones) and grain-supported carbonates (packstones). For instance, some muddy carbonates that were originally deposited as wackestones were probably converted into packstones as a result of mechanical compaction, caused by dewatering of the sediment (Shinn and Robbin, 1983; Tucker and Wright, 1990). Moreover, it is sometimes impossible to find out whether carbonate matrix in a mudstone, wackestone or packstone was initially produced during deposition or subsequently infiltrated a primary grainy sediment (Adams and Mackenzie, 1998). Also, because of compaction and associated pressure-solution processes, many carbonate rocks have altered their original texture. Thus, care was taken when classifying these rocks to account for subsequent sediment modification and diagenetic overprinting.

References

Adams, A.E. and W.S. Mackenzie 1998. A Colour Atlas of Carbonate Sediments and Rocks Under the Microscope. Manson Publishing, 180 p.

Adams, L.K., J.H.S. Macquaker and J.D. Marshall 2006. Iron(III)-reduction in a low-organic-carbon brackish-marine system. Journal of Sedimentary Research, v. 76, no. 6, p. 919-925.

Barker, C.A. and O.C. Kopp 1991. Luminescence Microscopy and Spectroscopy: Qualitative and Quantitative Applications. SEPM (Society for Sedimentary Geology), Short Course 25, 195 p.

Coplen, T.B. 1994. Reporting of stable hydrogen, carbon and oxygen isotope abundances. Pure and Applied Chemistry, v. 66, no. 2, p. 273-276.

Craig, H. 1957. Isotopic standards for carbon and oxygen and correction factors for mass-spectrometric analysis of carbon dioxide. Geochimica et Cosmochimica Acta, v. 12, no. 1-2, p. 133-149.

De Keyser, T.L. 1999. Digital scanning of thin sections and peels. Journal of Sedimentary Research, v. 69, no. 4, p. 962-964.

Dickson, J.A.D. 1965. A Modified staining technique for carbonates in thin section. Nature, v. 205, no. 4971, p. 587.

Dunham, R.J. 1962. Classification of carbonate rocks according to depositional texture. In, W.E. Ham (Ed.), Classification of carbonate rocks, A symposium. American Association of Petroleum Geologists, Memoir 1, p. 108-171.

Embry, A.F. and J.E. Klovan 1971. A late Devonian reef tract on northeastern Banks Island Nordwest Territories. Bulletin of Canadian Petroleum Geology, v. 19, p. 730-781.

Eshet, Y. and S. Moshkovitz 1995. New nannofossil biostratigraphy for Upper Cretaceous organic-rich carbonates in Israel. Micropaleontology, v. 41, no. 4, p. 321-341.

Flügel, E. 2004. Microfacies of Carbonate Rocks: Analysis, Interpretation and Application. Springer, 976 p.

Francus, P., F. Keimig and M. Besonen 2002. An algorithm to aid varve counting and measurement from thin-sections. Journal of Paleolimnology, v. 28, no. 2, p. 283-286.

Hendry, J.P. and R.M. Kalin 1997. Are oxygen and carbon isotopes of mollusc shells reliable palaeosalinity indicators in marginal marine environments? A case study from the Middle Jurassic of England. Journal of the Geological Society, v. 154, no. 2, p. 321-333.

Macquaker, J.H.S. 1994. A lithofacies study of the Peterborough Member, Oxford Clay Formation (Jurassic), UK: an example of sediment bypass in a mudstone succession. Journal of the Geological Society, v. 151, no. 1, p. 161-172.

Macquaker, J.H.S. and A.E. Adams 2003. Maximizing information from fine-grained sedimentary rocks: an inclusive nomenclature for mudstones. Journal of Sedimentary Research, v. 73, no. 5, p. 735-744.

Macquaker, J.H.S. and R.L. Gawthorpe 1993. Mudstone lithofacies in the Kimmeridge Clay Formation, Wessex Basin, southern England: implications for the origin and controls of the distribution of mudstones. Journal of Sedimentary Research, v. 63, no. 6, p. 1129-1143.

Macquaker, J.H.S., R.L. Gawthorpe, K.G. Taylor and M.J. Oates 1998. Heterogeneity, stacking patterns and sequence stratigraphic interpretation in distal mudstone successions:

examples from the Kimmeridge Clay Formation, U.K. In, J. Schieber, W. Zimmerle and P. Sethi (Eds.), Shales and Mudstones, Volume I: Basin Studies, Sedimentology, and Palaeontology. E. Schweizerbart'sche Verlagsbuchhandlung, p. 163-186.

Macquaker, J.H.S. and J.K. Howell 1999. Small-scale (< 5.0 m) vertical heterogeneity in mudstones: implications for high-resolution stratigraphy in siliciclastic mudstone successions. Journal of the Geological Society, v. 156, no. 1, p. 105-112.

Macquaker, J.H.S. and C.R. Jones 2002. A sequence-stratigraphic study of mudstone heterogeneity: a combined petrographic/wireline log investigation of Upper Jurassic mudstones from the North Sea (U.K.). In, M. Lovell and N. Parkinson (Eds.), Geological Applications of Well Logs. American Association of Petroleum Association, Methods in Exploration 13, p. 123-141.

Macquaker, J.H.S. and M.A. Keller 2005. Mudstone sedimentation at high latitudes: ice as a transport medium for mud and supplier of nutrients. Journal of Sedimentary Research, v. 75, no. 4, p. 696-709.

Macquaker, J.H.S. and K.G. Taylor 1996. A sequence-stratigraphic interpretation of a mudstone-dominated succession: the Lower Jurassic Cleveland Ironstone Formation, UK. Journal of the Geological Society, v. 153, no. 5, p. 759-770.

Macquaker, J.H.S., K.G. Taylor and R.L. Gawthorpe 2007. High-resolution facies analyses of mudstones: implications for palaeoenvironmental and sequence-stratigraphic interpretations of offshore ancient mud-dominated successions. Journal of Sedimentary Research, v. 77, no. 3-4, p. 324-339.

Marshall, D.J. 1988. Cathodoluminescence of Geological Materials. Winchester, MA, Allen & Unwin, 128 p.

Mount, J. 1985. Mixed siliciclastic and carbonate sediments: a proposed first-order textural and compositional classification. Sedimentology, v. 32, no. 3, p. 435-442.

Shinn, E.A. and D.M. Robbin 1983. Mechanical and chemical compaction in fine-grained shallow-water limestones. Journal of Sedimentary Petrology, v. 53, no. 2, p. 595-618.

Soreghan, M.J. and P. Francus 2004. Processing backscattered electron digital images of thin sections. In, P. Francus (Ed.), Image Analysis, Sediments and Paleoenvironments. Springer, p. 203-225.

Tucker, M.E. and V.P. Wright 1990. Carbonate Sedimentology. Blackwell Science, 482 p.

van Buchem, F.S.P., P. Razin, P.W. Homewood, W.H. Oterdoom and J. Philip 2002. Stratigraphic organization of carbonate ramps and organic-rich intrashelf basins: Natih Formation (middle Cretaceous) of northern Oman. American Association of Petroleum Geologists Bulletin, v. 86, no. 1, p. 21-53.

Chapter 3

Sedimentological evidence for bottom-water oxygenation during deposition of the Natih-B intrashelf-basinal sediments: Upper Cretaceous carbonate source rock, Natih Formation, North Oman

Said A.K. Al Balushi and Joe H.S. Macquaker

3.1. Abstract

Geologists commonly assume that the deposition of excellent carbonate source rocks (up to 13.7% total organic carbon) in the Upper Cretaceous Natih-B intrashelf basin (water depth circa 50 m) was mainly controlled by the presence of bottom-water "anoxia" in the basin centre. Some authors have even linked the formation of the Natih-B organic-carbon-rich sediments to the development of "oceanic anoxia", related to high organic productivity as a result of an increased nutrient flux to the ocean during sea-level transgressions. Recent research suggests that the mechanisms that underpin organic-carbon enrichment in intrashelf-basinal settings, however, are complicated; being controlled by a complex balance between primary (both organic and inorganic) production, clastic dilution, bottom-water anoxia, early diagenesis and rates of sedimentation. In this study, the requirement for persistent bottom-water anoxic conditions for the preservation of organic matter in this setting is assessed, evidence for oxic/dysoxic bottom-water conditions during deposition of the Natih-B organic-carbon-rich sediments is presented, and alternative models to explain organic-matter enrichment are considered.

Natih-B sediments (collected both spatially and temporally from both core and outcrop in North Oman) have been investigated using a combination of optical and electron-optical (backscattered electron imagery) techniques, which provide additional data to those gathered by traditional field and geochemical methods. Natih-B lithofacies alternate between two main types: organic-carbon-rich carbonate mudstones and sparry-calcite-rich

wackestones. The organic-rich mudstones are typically, fine grained, dark grey, exhibit remnant parallel lamina, and are partially burrowed (average about 5.4%, up to 13.7% total organic carbon). These units commonly contain planktonic foraminifera, coccoliths, and organic matter. In addition, in-place bivalves (including thick-shelled oysters and flattened pectens) are present. The sparry-calcite-rich wackestones are lighter in colour and extensively bioturbated (in most cases < 1.5% total organic carbon). This lithofacies comprises a mix of reworked skeletal fragments (including bivalves, gastropods, echinoderms, brachiopods and corals), ostracods, calcispheres, and both benthic and planktonic foraminifera that are pervasively cemented by sparry calcite.

Given the above observations, bottom waters during deposition of the Natih-B intrashelf-basinal sediments must have contained at least some oxygen and, therefore, it is very unlikely that they were persistently anoxic. Instead, it is likely that short-term enhanced organic productivity, rapid delivery of organic components to the sediment/water interface, optimal rates of sediment accumulation and episodic burial were the fundamental parameters that controlled organic-carbon production and preservation. Organic-matter enrichment was, therefore, not restricted to basinal anoxic settings, and exploration strategies need to be revised in outer-shelf depositional settings.

3.2. Introduction and Aims

The fine-grained, carbonate-dominated, middle-late Cenomanian sediments of the Natih-B Member (Natih Formation, North Oman; Figures 3.1 and 3.2) were deposited in a sediment-starved intrashelf basin (40 to 60 m deep) during a marine transgression, surrounded by a shallow-water carbonate-ramp system (Murris, 1980; Harris and Frost, 1984; Philip et al., 1995; van Buchem et al., 1996; Immenhauser et al., 2000; van Buchem et al., 2002; Homewood et al., 2008; Figure 3.1b). Their deposition was intimately associated with abundant accumulation of organic carbon (average 3.2%, range 0.3 to 13.7% total organic carbon [TOC], based on samples from a well in Natih field), making this interval a prolific source rock (e.g. Grantham et al., 1987; Terken, 1999; van Buchem et al., 2005). Here organic-matter accumulation is commonly interpreted as having occurred within a “silled basin” (sensu Demaison and Moore, 1980) within this intrashelf environment. As a consequence, this interpretation has led many authors (e.g.

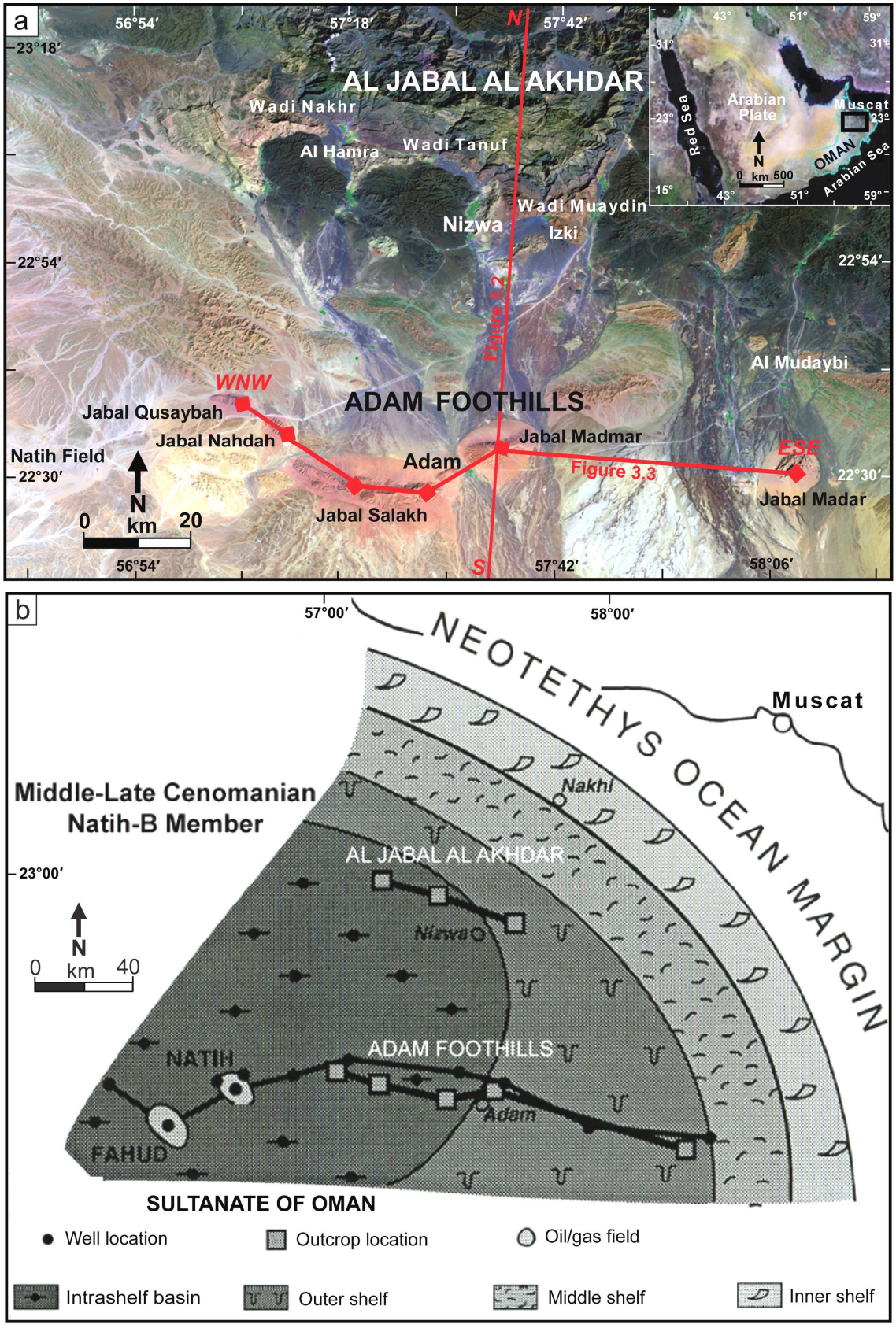

Figure 3.1. (a) Satellite images (source: Petroleum Development Oman [PDO]) showing the area of study in North Oman, mainly at the Adam Foothills. **(b)** Palaeogeographic map illustrating the outline of the middle-late Cenomanian Natih-B intrashelf basin and the surrounding carbonate-platform system (from van Buchem et al., 2002).

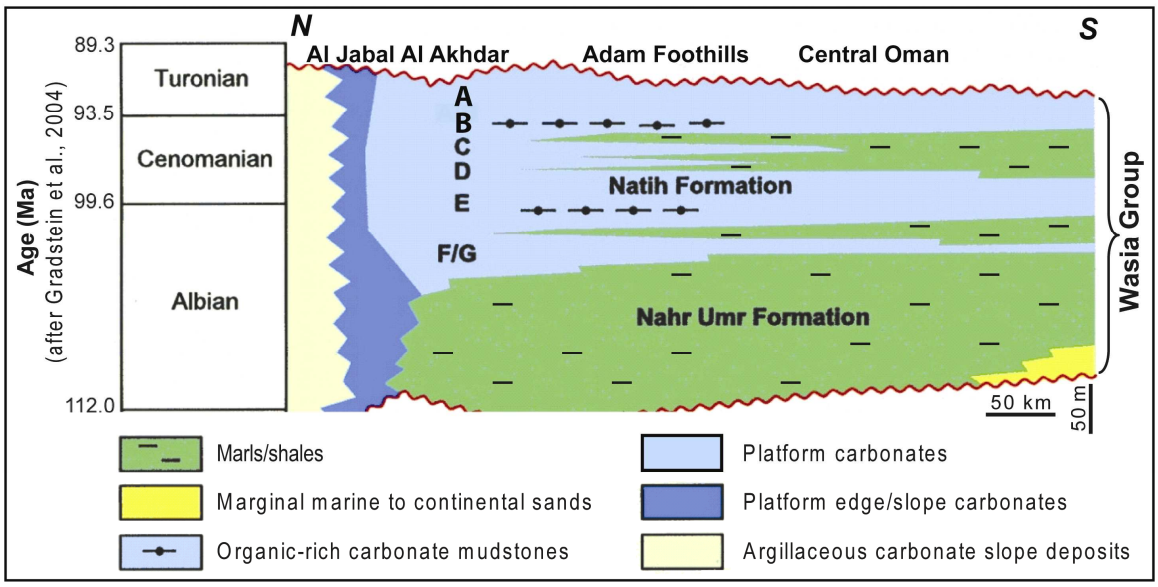

Figure 3.2. N-S schematic geological cross section (see Figure 3.1a for location) illustrating the Middle-Upper Cretaceous chronostratigraphy of Oman (from Droste and Van Steenwinkel, 2004).

Murris, 1980; Scott, 1990; Burchette, 1993; Alsharhan, 1995; Philip et al., 1995; Droste and Van Steenwinkel, 2004; Homewood et al., 2008; Vahrenkamp, in review) to suggest that bottom-water "anoxia" was the fundamental factor controlling enhanced organic-matter preservation in the Natih Formation.

Sedimentary successions deposited on continental shelves and within intrashelf basins commonly exhibit cyclical and repeated lithofacies motifs. For instance, Mesozoic-aged sediments preserved over much of the globe comprise alternating lithofacies of clay- and organic-matter-rich and carbonate-rich facies (e.g. Arthur et al., 1984; Weedon, 1986; Hallam, 1987; Droste, 1990; Jenkyns, 1991; Burchette, 1993; Macquaker and Taylor, 1996; Kuhnt et al., 1997; Damholt and Surlyk, 2004; van Buchem et al., 2005; Macquaker et al., 2007; Varban and Plint, 2008). These patterns are commonly interpreted as being either products of: a) varying clastic dilution of primary production-derived components in hemipelagic settings, b) varying accommodation availability and resulting energy available at the sediment/water interface during periods of shallow water (usually manifested by the presence of storm layers and changes in grain size), c) development of anoxia when the basin was deeper, or d) preferential diagenesis of particular strata, particularly during early burial.

Typically, most authors assume that the overarching control on these factors is long-term changes in climate, usually driven by a Milankovitch mechanism (e.g. Weedon et al., 2004). In spite of the superficial simplicity of the controlling factors of these systems, the detailed interplay between the factors that control lithofacies variability and organic-matter preservation in intrashelf-basinal settings is very complicated. These factors are linked to subtle changes in primary production (both organic and inorganic), rates of sediment accumulation and burial, porewater oxygen concentrations, and early diagenesis (Pedersen and Calvert, 1990; Macquaker and Gawthorpe, 1993; Macquaker, 1994; Bohacs et al., 2005; Katz, 2005; Tyson, 2005).

In the Natih-B Member, the carbonate (derived from both primary production and diagenetic processes) content varies from 80 to 100%, clay (both detrital and authigenic) content from 0 to 10% (van Buchem et al., 2005), TOC content from 0.3 to 13.7%, quartz content from 0 to 10%, with pyrite and phosphate (fish debris) each varying from 0 to 5%. The Natih-B facies variability has traditionally, broadly, been interpreted in terms of variations in primary production or alternating oxic/anoxic cycles, following the research of van Buchem et al. (2005) and Homewood et al. (2008), and the logic of Pedersen and Calvert (1990) and Demaison and Moore (1980).

Existing models used to explain organic-matter preservation in the distal parts of the Natih-B intrashelf basin are, however, simple and rely on occurrences of “anoxic” bottom-water conditions. In these settings, the importance of changes in primary organic production, coupled with episodic and relatively rapid burial – not sufficiently rapid to cause dilution – has likely been underestimated. Overall, existing published sedimentologic and stratigraphic work on the Natih Formation (e.g. Philip et al., 1995; van Buchem et al., 2002; Droste and Van Steenwinkel, 2004; Schwab et al., 2005; van Buchem et al., 2005; Grélaud et al., 2006; Homewood et al., 2008) seems reasonable, although it lacks process-detail analyses on the more distal facies (source-rock intervals and their associated units).

The main aim of this paper, based on more in-depth study of process-detail analysis, is to illustrate that persistent bottom-water “anoxia” is unlikely to have been the key factor controlling organic-carbon preservation during deposition of the Natih-B intrashelf-basinal sediments, and to discuss some of the alternative mechanisms that might have controlled: a) organic-matter enrichment and b) lithofacies variability.

3.3. Objectives

To meet the aims of this paper, the Natih-B Member has been sampled both from the Adam Foothills where it is best exposed, and from the continuous core slabs of a Natih well in the subsurface. Polished thin sections were prepared from each sample. The constituent components of each lithofacies were then described, utilising optical, electron-optical, mineralogical (X-ray diffraction [XRD]) and geochemical (TOC) methods, in order to obtain textural and mineralogical data at spatial scales ranging from 10^{-5} to 10^{4} m, and at temporal scales that likely range from the time taken for individual depositional events to deposit beds to 10^{5} years. New data gathered were then integrated with existing information, and the controls on organic-matter preservation and lithofacies variability were investigated.

3.4. Samples and Methods

Excellent outcrop sections and core slabs of the 50- to 60-m-thick Natih-B unit in the Adam Foothills and Al Jabal Al Akhdar regions and in nearby oilfields of North Oman have been used as natural laboratories for this study (Figure 3.1). Detailed sedimentary logs were measured at the scale of 1:50, and samples were gathered systematically from five locations: Natih well, Jabal Qusaybah, Jabal Nahdah (distal locations), Jabal Salakh West (distal to intermediate location), and Jabal Salakh East (intermediate to proximal location) (see Figure 3.1b). Overall, around three hundred samples were obtained from these locations at vertical intervals, 0.5 to 3.0 m apart.

Unusually thin (≤ 0.03 mm), polished, large (~ 40 x 60 mm) thin sections were prepared from each sample, in order to acquire information on sediment textures and mineral constituents at different scales of magnification. At first, each thin section was scanned using a flatbed scanner (Epson Perfection 3170) to record textural details at 50 to 10 mm scales. The thin sections were then analysed optically (first under transmitted light (both plane polarised and cross polarised) and then by cold-cathode cathodoluminescence) using a binocular Nikon petrographic microscope, attached to a digital camera (Jenoptik Jena D-07739), to obtain textural, compositional and diagenetic information at 10.0 to 0.1 mm scales. The cold-cathode cathodoluminescence petrography was performed using a CITL

Cathodoluminescence Unit (Model CCL 8200 MK3), operated at approximately 20 kV, 300 µA. Finally, at even higher resolution (100 to 1 µm scales), the thin sections were investigated electron-optically using JEOL 6400 scanning-electron microscope (SEM), equipped with a backscattered electron detector. With this high-power imaging technique, minerals were identified in the produced images based on their backscatter coefficients (η), and also sometimes with the aid of a semiquantitative, energy-dispersive spectrometer that is in connection with JEOL 6400. The SEM was operated at 15 mm working distance, and at approximately 2 nA and 20 kV.

XRD analyses were also performed on selected samples to determine bulk-rock mineralogy, utilising a Philips PW1730 X-ray diffractometer. Before each analysis, approximately 0.5 g of each powdered sample was treated with a few drops of amyl acetate and left to dry on a flat piece of glass, which is then inserted into the diffractometer. The XRD was operated using copper Kα radiation at 40 kV and 20 mA.

Finally, the TOC contents of the majority of samples were obtained using a LECO C and N analyser (TruSpec CN). In order to determine the TOC contents, approximately 0.2 g of each powdered sample was reacted with 10.0 mL of HCl solution (1.0 M molar concentration), and left overnight to dissolve all carbonate present. Then, both the acid-treated sample and untreated (natural) sample had the total carbon (TC) contents measured using an induction furnace within the LECO instrument that heated the samples to approximately 950°C. The TOC contents here are considered to be the same as the TC contents obtained from the acid-treated samples, assuming that all the inorganic carbon has been removed from each acid-treated sample, and that the carbon being measured is organic carbon. The total carbonate carbon (TCC) contents were also recorded, determined by calculating the difference between the TC contents of the untreated samples and TC contents of the acid-treated samples (i.e. TOC contents). The reproducibility of these analyses is better than or equal to 0.1%.

The application of the thin-section scanning, optical, and backscattered electron-optical imaging techniques, in addition to the conventional field (logging and photomontages) and mineralogical (XRD) and geochemical (TOC) methods, have facilitated making detailed lithofacies descriptions of the predominantly fine-grained, organic-carbon-rich Natih-B sediments. These combined techniques have enabled us to provide details of the various

sediment textures, grain size, faunal assemblages, bioturbation processes, mineralogy, organic-matter contents, and transport mechanisms, giving also accounts on how these components change in space and time (see also Macquaker and Howell, 1999; Macquaker and Adams, 2003; Macquaker et al., 2007).

3.5. Geological Setting

During the time from Lower Jurassic to Upper Cretaceous, Oman was located on the northeastern margin of the Arabian Plate and was a site for an extensive carbonate-platform deposition, which also covered most of the Arabian Peninsula and Gulf (Murris, 1980; Droste and Van Steenwinkel, 2004). This major Mesozoic deposition took place following the breakup of Gondwana and opening of the Neotethys Ocean (Loosveld, 1996). In the interior of North Oman, a peripheral foreland bulge formed as a result of the building of the Oman Mountains during the Upper Cretaceous (Robertson, 1987; Boote et al., 1990; Warburton et al., 1990; Terken, 1999).

The Cretaceous carbonate-platform succession of Oman is up to 1.2 km thick and 1,000 km wide (Droste and Van Steenwinkel, 2004). This large-scale succession started to grow in Central Oman during the late Berriasian, after a major marine transgression that had facilitated the deposition of shallow-water carbonates over tilted, uplifted, and eroded Jurassic and older strata, following the rifting between the African-Arabian Plate and Greater India (Droste and Van Steenwinkel, 2004; Razin et al., 2005). Droste and Van Steenwinkel (2004) pointed out that the carbonate deposition during Berriasian to Turonian times was associated with regular subaerial exposures and influxes of terrigenous material from the Arabian Plate hinterland. The late Aptian, large-scale, relative sea-level fall recorded a major regional unconformity, and is related to extensive karstification and erosion in Oman. This major tectonic and eustatic event (Sharief et al., 1989) terminated the deposition of the Shu'aiba Formation platform carbonates, enabling the prevalent distribution of siliciclastics of the latest Aptian-late Albian Nahr Umr Formation. During the late Albian, Cenomanian, and early Turonian times, platform carbonates of the Natih Formation were deposited over the Nahr Umr mudstones (e.g. van Buchem et al., 2002; Figure 3.2). In the Turonian, a regional phase of uplift and erosion concluded the progression of the Cretaceous platform-carbonate succession at the end of the Natih

Formation deposition (e.g. Hughes Clarke, 1988; Droste and Van Steenwinkel, 2004). This emergent period was then followed by the influx of the Fiqa/Muti mudstones, which unconformably overlie the Natih Formation carbonates.

3.6. Stratigraphy and Previous Work

The Natih-B Member – the unit chosen for this study – occurs within the late Albian-early Turonian Natih Formation, which forms the upper part of the Wasia Group (Smith et al., 1990; Philip et al., 1995; van Buchem et al., 2002; Figure 3.2). Lateral age-equivalent units to the Natih in the Arabian Gulf region are the shallow-water carbonates of the Mauddud and Mishrif formations, and intrashelf-basinal carbonates of the Shilaif/Khatiyah Formation (also known as Rumaila Formation in Kuwait and Iraq) (e.g. Harris and Frost, 1984; Alsharhan and Nairn, 1988; Burchette, 1993; Aqrawi et al., 1998; Ehrenberg et al., 2008). The Natih Formation includes intrashelf-basinal carbonate source rocks and adjacent, time-equivalent shallow-water carbonate reservoirs (e.g. Figure 3.1b). The carbonate petroleum system of the Natih Formation is well known in the subsurface of interior Oman (e.g. Harris and Frost, 1984; Grantham et al., 1987; Terken, 1999; Droste and Van Steenwinkel, 2004; Morettini et al., 2005) and in the excellent outcrops in the Oman Mountains (Al Jabal Al Akhdar) and Adam Foothills (e.g. van Buchem et al., 1996; van Buchem et al., 2002; Schwab et al., 2005; Homewood et al., 2008).

The Natih Formation is approximately 400 m thick, and it is informally subdivided in the subsurface into seven members: Natih-A to Natih-G, top to bottom (sensu Hughes Clarke, 1988; Figure 3.2). It mostly comprises mud-supported and some grain-supported limestones, with local rudist growth, alternating with calcareous mudstones. The shallow-water, rudist-bearing platform carbonates are prolific hydrocarbon reservoirs for the Cretaceous petroleum system in the Middle East (e.g. Harris and Frost, 1984; Burchette and Britton, 1985; Alsharhan, 1995; van Buchem et al., 1996). The Natih Formation is considered as a significant carbonate source rock because it includes at least two organic-carbon-rich levels deposited in intrashelf basins (lower Natih-E and Natih-B; Figure 3.2) during transgressive phases (e.g. Grantham et al., 1987; Scott, 1990; Terken, 1999; van Buchem et al., 2002; Droste and Van Steenwinkel, 2004). A thick shale succession of the

overlying Fiqa Formation (Aruma Group) provides a major regional seal for the Natih reservoirs.

In order to be more predictive with regard to the distribution of reservoir and source-rock facies, and to the geometrical and genetic relationships between intrashelf basins and adjacent carbonate platforms of the Natih Formation, high-resolution sequence-stratigraphic studies have been carried out by van Buchem et al. (1996), van Buchem et al. (2002) and Schwab et al. (2005) on outcrops in the Adam Foothills and Al Jabal Al Akhdar; see also Grélaud et al. (2006) and Homewood et al. (2008). Generally, these researchers subdivide the Natih Formation into three major depositional units, Sequences I, II and III from base to top. These sequences are regarded as larger-scale accommodation cycles that were subject to third-order (0.5 to 3.0 my) eustatic sea-level variations, each recording scenarios of transgressive/regressive patterns.

Van Buchem et al. (2002) interpret the deposition of Sequence I (late Albian–earliest Cenomanian Natih-G, F and E members; Figure 3.2) as being mainly controlled by eustatic sea-level fluctuations and that it developed intrashelf basins at lower Natih-E. A sequence boundary at the top of Natih-E is recognised, which was associated with the development of hardgrounds and incisions along emergence surfaces (see Grélaud et al., 2006). Sequence II (middle Cenomanian Natih-D and C members; Figures 3.2 and 3.3) did not develop an intrashelf basin and was dominated by clay deposition, which – as Homewood et al. (2008) have stated – inhibited the *carbonate factory*. Sequence III (middle-late Cenomanian–early Turonian Natih-B and A members; Figures 3.2 and 3.3) is very similar to Sequence I in that it records another development of an intrashelf basin during a major transgression, and that it experienced extensive subaerial exposures at its top (see Homewood et al., 2008; Figures 3.1b and 3.3) during subsequent relative sea-level fall. However, van Buchem et al. (2002) argued that facies variability in the lower part of Sequence III was controlled by a more rapid relative sea-level rise, enhanced by a slight differential subsidence, which both enabled the creation of the relatively broader and more organic-carbon-rich Natih-B intraplatform basin. Many researchers (e.g. Murris, 1980; Scott, 1990; Philip et al., 1995; Homewood et al., 2008; Vahrenkamp, in review) have linked the development of bottom-water "anoxia" in the Natih-B intrashelf basin to this rapid rise in relative sea level. More specifically, Homewood et al. (2008) and Vahrenkamp (in review) claim that stratification of the water column developed during this

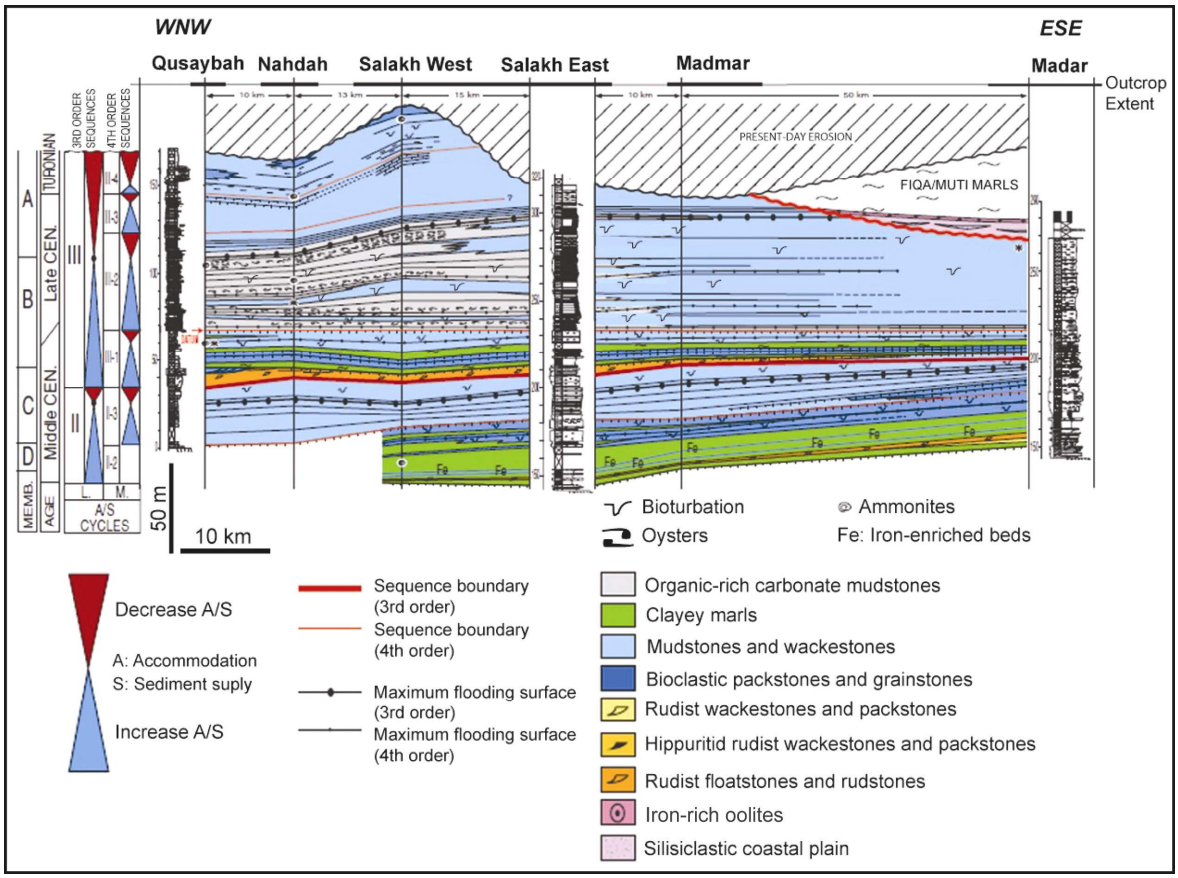

Figure 3.3. WNW-ESE high-resolution sequence-stratigraphic cross section (see Figure 3.1 for location) of the upper half of the Natih Formation (members D-A, sequences II and III) in the Adam Foothills (from van Buchem et al., 2002). Note the abundant development of the Natih-B organic-rich carbonate mudstones in an intrashelf basin environment at Jabal Qusaybah, Nahdah and Salakh, and how this depositional environment changes laterally into a shallow-water carbonate platform to the ESE at Jabal Madmar and Jabal Madar.

transgression, which also – according to these authors – increased the clay and nutrient flux to the intrashelf basin, causing "organic bloom" and "oceanic anoxia". Considering the biostratigraphically-constrained age (middle-late Cenomanian; van Buchem et al., 2005) of the Natih-B Member, Homewood et al. (2008) and Vahrenkamp (in review), however, found it difficult to tie the deposition of the excellent Natih-B source rocks (characterised by relatively light $\delta^{13}C$ values; Vahrenkamp, 2010) to a specific global Oceanic Anoxic Event (cf. Jenkyns et al., 1994; Paul et al., 1994; Rodriguez-Lázaroet al., 1998; Jarvis et al., 2006), and concluded that their occurrence might represent a unique local "expanded anoxia".

Van Buchem et al. (2002) and Droste and Van Steenwinkel (2004) have generally characterised the development of intrashelf basins on the extensive Cretaceous carbonate

platform of North Oman as being mostly driven by relative changes in sedimentation rates as a result of high-frequency fluctuations in relative sea level. They suggest that tectonism only played a trivial role in the formation of basin topography, probably through the development of slight initial relief (local depression) during differential drowning of platform-interior areas. Moreover, the lack of obvious clinoform geometries in the Natih-B unit also implies a shallow and broad intrashelf basin.

The carbonate-source-rock intervals of the Natih-E and Natih-B members are identified in outcrops in the Adam Foothills and Al Jabal Al Akhdar, and on well logs and core slabs from nearby oilfields in North Oman. It is likely that these intervals were the sources of the hydrocarbons in the Natih reservoirs of many fields, including the giant Fahud and Natih fields (Grantham et al., 1987; van Buchem et al., 1996; Terken, 1999; Homewood et al., 2008). Grantham et al. (1987) and Terken (1999) have described both source-rock levels as being geochemically similar. However, the Natih-B unit, that is the focus of this study, is the more important source rock in the Natih Formation, simply because it is thicker (up to 40 m thick) and excellent in quality (up to 13.7% TOC). According to Terken (1999), the TOC content of the Natih-E source rock rarely exceeds 5%.

3.7. General Observations

The transgressive, dm- to m-thick bedded, greyish Natih-B sediments overlie an iron-enriched (brownish/reddish coloured), bored, extensively-bioturbated hardground at top of Natih-C Member, and conformably underlie relatively thicker, shallower-marine, whitish carbonate beds of the Natih-A Member (Figure 3.4). In outcrops of Jabal Qusaybah, Jabal Nahdah and Jabal Salakh, the Natih-B Member can informally be subdivided into five units, based on their weathering and lithological characteristics: Natih-B1 (NB1) to Natih-B5 (NB5), base to top (Figure 3.4). It is worth mentioning here that the lower units (NB1 to NB3) are the outcrop equivalent to unit B4 of Natih-B in the subsurface; NB4 is the equivalent to B3; and NB5 is the equivalent to B2 and B1 (cf. Homewood et al., 2008).

The deposition of the inner-platform facies – abundant evidence of mixed benthic foraminifera (including calcareous forms of miliolids, miliolinid alveolinids, *[Praealveolina* spp. and *Cisalveolina* spp.], *Aeolisaccus* spp., *Nezzazata conica, N.*

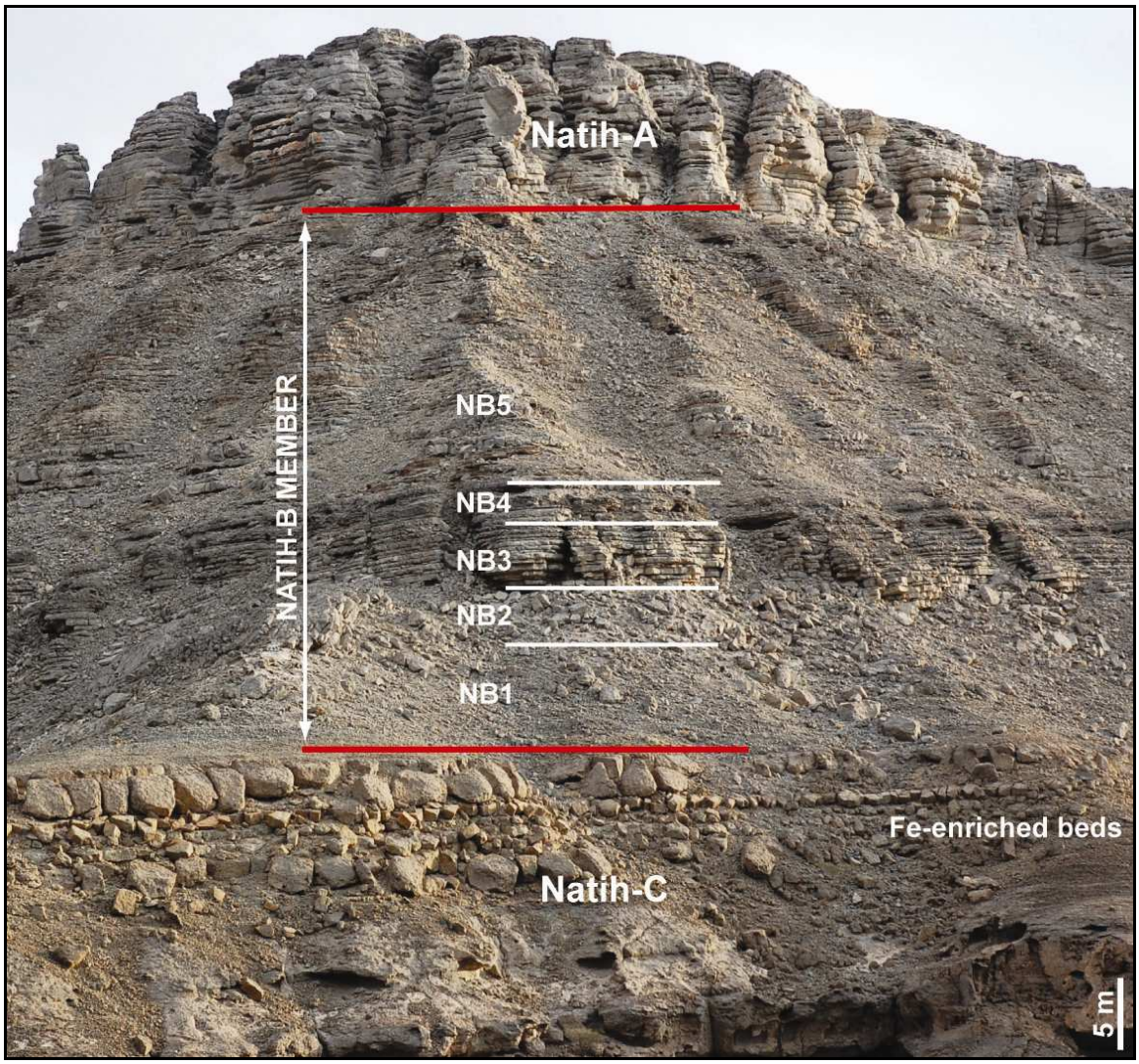

Figure 3.4. Looking SSE; outcrop section in Jabal Nahdah displaying the upper members (C to A) of the Natih Formation. The Natih-B Member overlies an extensively bioturbated, iron-enriched beds (note brownish/reddish colour) at the top of the Natih-C Member, and underlies whitish, well-bedded unit of the Natih-A Member, with an eroded top. Note also the subdivision of the Natih-B Member here into five units: NB1 to NB5, from base to top; with NB1 and NB2 being poorly exposed and structurally deformed; NB3 and NB4 being better exposed, thinly bedded and laterally continuous; and NB5 composed of the organic-carbon-rich carbonate mudstone and sparry-calcite-rich wackestone units alternating with one another.

simplex, *Idalina* spp. and *Nummolofallotia apula*, and agglutinated forms of *Chrysalidina* spp., *Dicyclina* spp., *Nautiloculina* spp. and *Pseudolituonella reicheli*) – of NB1 over the Natih-C hardground (Figure 3.5a) marks a significant deepening and transgressive shift of facies. This dramatic change in the depositional environment happened as a response to a major mid-Cenomanian transgression, the culmination of the longer-term cycle recorded by deposition of the predominantly shallow-marine carbonates of the Natih-G, F, E, D and

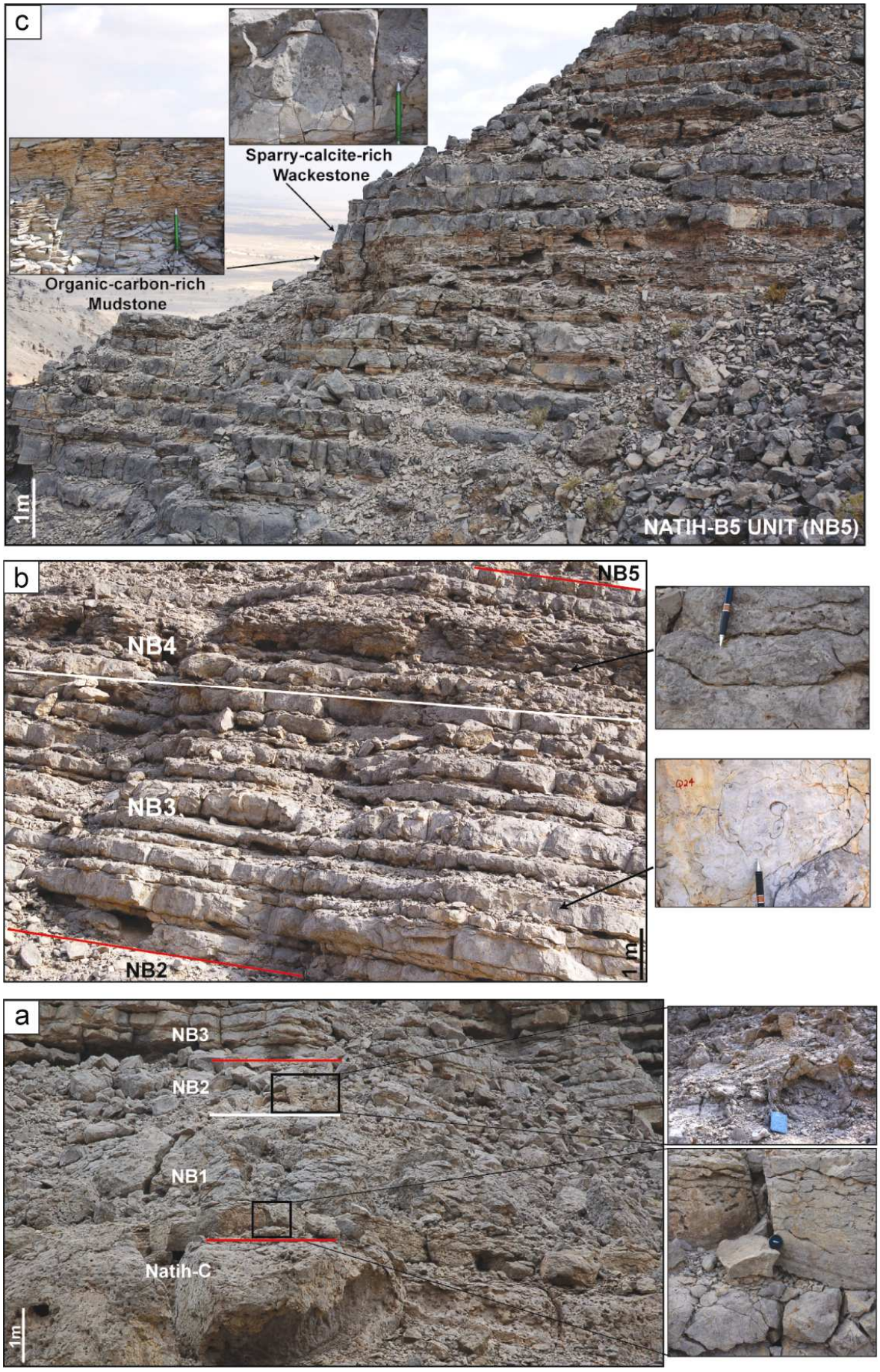

Figure 3.5. (see caption next page)

Figure 3.5. (see previous page): **(a)** Close-up view (Jabal Nahdah) of the lower units of the Natih-B Member (NB1 and NB2) that overlie an iron-enriched hardground (extensively bioturbated, bored and cemented) at top Natih-C. Note the light-grey, m-thick, nodular, laterally-discontinuous beds of NB1, and poorly-exposed, structurally-deformed beds of NB2. **(b)** Close-up view (Jabal Qusaybah) of the middle units of Natih-B (NB3 and NB4) with well-exposed, laterally-continuous thin beds. Note the light-grey, bioturbated beds of NB3 overlain by dark-grey, very nodular, bioclast-rich beds of NB4. **(c)** Close-up view (Jabal Nahdah) of the upper unit of Natih-B (NB5), illustrating the two main lithofacies alternating with one another: i) fissile, strongly-weathered (weak), organic-carbon-rich carbonate mudstone and ii) less-weathered (competent), sparry-calcite-rich wackestone.

C members of the Natih Formation. In exposures, the NB1 and NB2 units are poorly exposed and composed of 0.3- to 0.9-m-thick, nodular, extensively bioturbated strata (Figures 3.4 and 3.5a). The NB2 unit is different from the NB1 unit because it is poorly exposed, structurally deformed, and brecciated (Figure 3.5a).

Natih-B3 (NB3) and Natih-B4 (NB4) contain slightly darker-grey strata that are well exposed and laterally continuous (Figures 3.4). Both units are bioturbated and bioclastic, but NB4 appears more nodular, bioclast-rich, and with even darker-grey beds than NB3 (Figure 3.5b).

The NB5 unit, on which this study is focused, covers the upper half of the Natih-B Member (up to 40 m thick; Figure 43.), comprising the intrashelf-basinal organic-carbon-rich sediment, interbedded with (relatively) shallower sparry-calcite-rich sediment. In these broad terms, the NB5 lithofacies can be divided into two main lithofacies types, alternating with one another (Figure 3.5c): a) organic-carbon-rich carbonate mudstone and b) sparry-calcite-rich wackestone, both are described below (see Table 3.1 for a summary of both lithofacies).

3.8. Detailed Facies Analyses: Organic-Carbon-Rich Carbonate Mudstone

3.8.1. Description

The organic-carbon-rich carbonate mudstone lithofacies varies in thickness from about 1.5 to 165.0 cm (average 17.5 cm; Figure 3.5c). It is typically fine-grained, grey to very dark

Table 3.1. Summary of the characteristic features of the two main lithofacies described in this study. These lithofacies are found alternating with one another in the intrashelf basin of the Natih-B Member, the upper NB5 unit.

Lithofacies	Organic-Carbon-Rich Carbonate Mudstones	Sparry-Calcite-Rich Wackestones
Colour (Fresh Surface)	Grey to very dark grey	Whitish to dark grey
Thickness (cm)	1.5 to 165.0, average 17.5	2.0 to 185.0, average 20.5
Texture	Partially-bioturbated mudstone, with relict very thin beds (3 to 30 mm thick)	Extensively-bioturbated wackestone, commonly with erosive bases and amalgamated thin beds (5 to 50 mm thick)
Ichnofossils	Common *Planolites* isp.; less common *Phycosiphon* isp. and *Thalassinoides* isp.	Very common *Thalassinoides* isp; less common *Planolites* isp., and rare *Phycosiphon* isp.
Macrofossils	Frequent in-place thick-shelled oysters and flattened pectens	Reworked skeletal fragments of bivalves, gastropods, echinoderms, and brachiopods
Microfossils and Nannofossils	Abundant planktonic foraminifera and coccoliths	Common benthic foraminifera, ostracods, calcispheres; less common planktonic foraminifera
Mineralogy (%)	Calcite (80 to 90), quartz (5 to 10), dolomite (< 1 to 6), pyrite (< 1 to 5), clay (< 1 to 5) and phosphate (<1 to 4)	Calcite (90 to 100), quartz (0 to 6), dolomite (0 to 5), pyrite (0 to 4), clay (0 to 1) and phosphate (0 to 1)
TOC (%)	2.0 to 13.7, average 5.4	0.3 to 1.9, average 1.1
Total Gamma-Ray Values (API units)	25 to 135, average 55	10 to 25, average 15

grey in fresh surface and in the exposures, exhibits a well-developed fissility (Figure 3.6a and b).

These mudstone units commonly contain well-preserved, in-place bivalves (including thick-shelled oysters (Figure 3.6a to c), as well as thin-walled pectens (Figures 3.6f and 3.7a to f) and brachiopods. Here the oysters (*Exogyra* and *Amphidonte*) are mostly

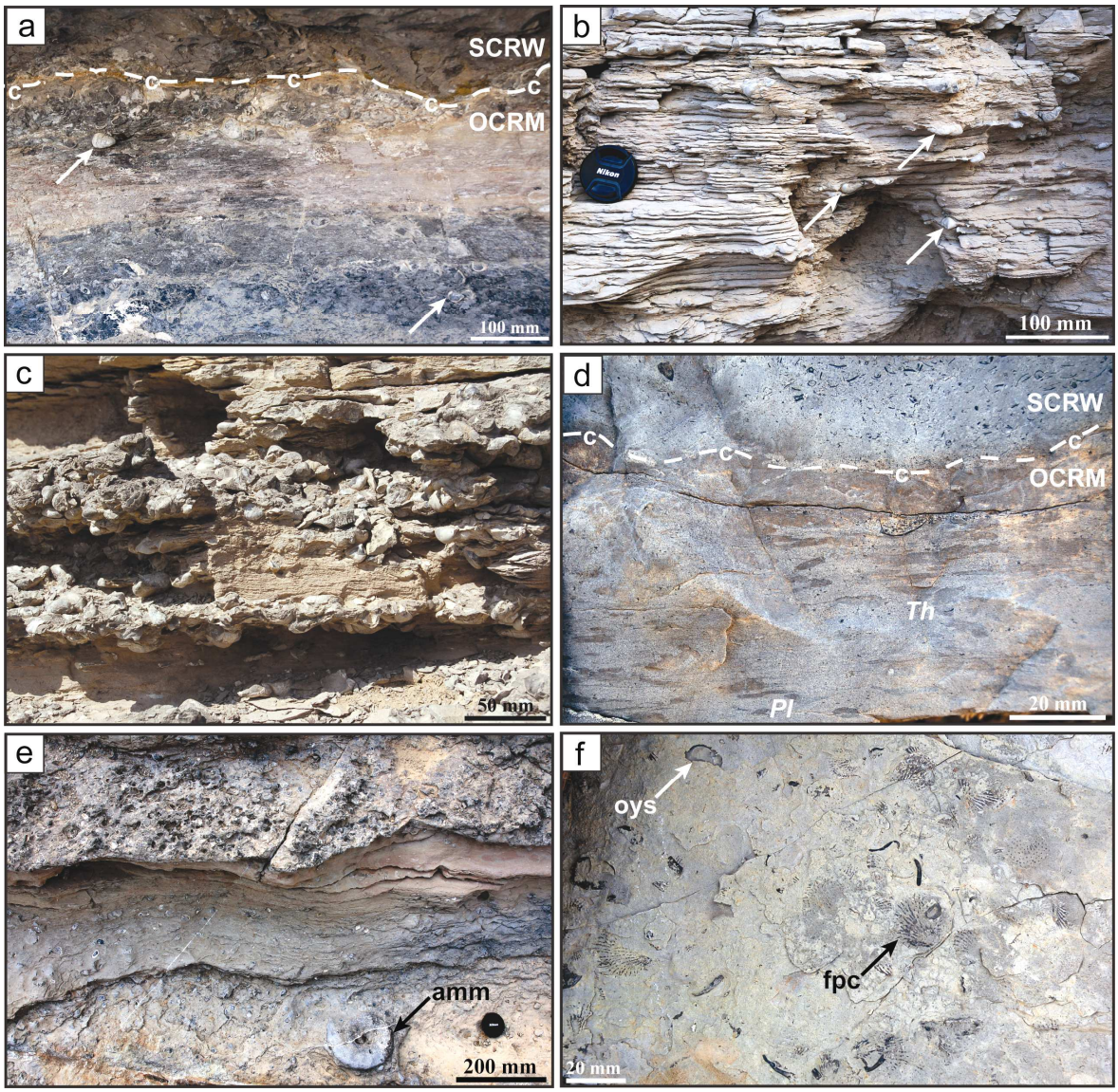

Figure 3.6. Outcrop photographs of the organic-carbon-rich carbonate mudstone lithofacies. **(a)** At Jabal Nahdah, displaying both fresh, very dark-grey surface and weathered, fissile texture of the organic-carbon-rich mudstone (OCRM), overlain by sparry-calcite-rich wackestone (SCRW). Note the in-place, thick-shelled oysters (arrowed) in the OCRM and erosive base of the SCRW. **(b)** At Jabal Salakh West, showing a well-developed fissility in the OCRM with abundant evidence of in-place fauna (e.g. oysters, arrowed). **(c)** At Jabal Qusaybah, illustrating a fissile unit with oyster shell pavements. **(d)** At Jabal Qusaybah; note the burrow fabrics of *Thalassinoides* isp. (*Th*) and *Planolites* isp. (*Pl*) in the OCRM, and the erosive base of the SCRW with a mixture of reworked shell fragments. **(e)** At Jabal Salakh West, illustrating the development of shell plasters on a hardground. Note an ammonite (amm) present here in association with articulated oysters. **(f)** At Jabal Nahdah, showing oysters (oys) and flattened pectens (fpc) on a bedding surface of the OCRM unit.

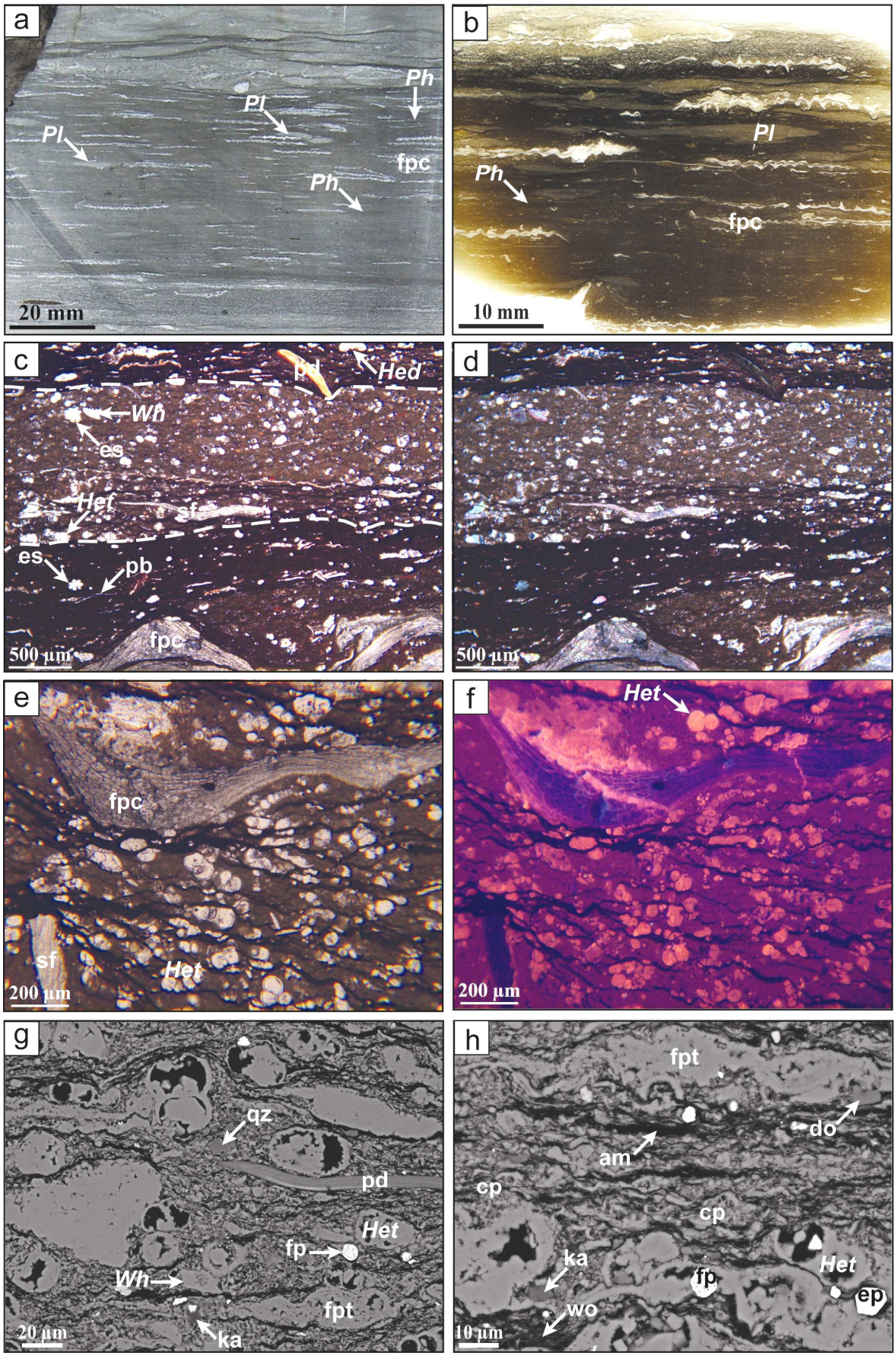

Figure 3.7. (see caption next page)

Figure 3.7. (see previous page): Detailed facies analyses of a representative partially-bioturbated, organic-carbon-rich carbonate mudstone (sample S11 from core of a Natih well, 915.2 m depth [914.0 m driller's depth]). This mudstone has a high TOC content of 9.3%. (Abbreviations: *Pl = Planolites* isp.; *Ph = Phycosiphon* isp.; fpc = flattened pectens; *Het = Heterohelix* spp.; *Hed = Hedbergella* spp.; *Wh = Whiteinella* spp.; pb = planktonic bivalve; es = echinoid spine; sf = shell fragment; pd = phosphatic debris; fpt = faecal pellet; qz = quartz; ka = kaolinite; do = dolomite; cp = coccolith plates; am = amorphous organic matter; wo = woody organic matter; fp = framboidal pyrite; ep = euhedral pyrite). **(a)** Core photograph and **(b)** thin-section scan illustrating a coarsening-upward mudstone unit, exhibiting remnant parallel lamination in the lower part of the photograph and stronger bioturbation towards the top. Note also the irregular and laterally-discontinuous laminae of organic matter throughout the sample. Trace fossils here are horizontal and highly compacted, attributed to *Planolites* isp. (infilled with light-grey material) and *Phycosiphon* isp. (infilled with dark-grey material). Note also the abundant, in-place bivalves (flattened pectens) present at disrupted and laterally-discontinuous bedding surfaces that bound relict thin beds. **(c)** Low-power optical micrograph under plane-polarised light (PPL) and **(d)** under cross-polarised light (XPL), both displaying the same area. Note the outlined (dashed lines) burrow fabric in (c), attributed to *Planolites* isp. that is abundantly infilled with planktonic foraminifers (mostly as *Heterohelix* spp. with rare *Whiteinella* spp.) and some bioclastic debris and echinoid spines. Organic matter (black material) is abundant in the areas of the sample that are not burrowed, associated with planktonic foraminifera, planktonic bivalves, echinoid spines, and phosphatic debris. Note also a rare *Hedbergella* spp. at the top right-hand corner of the micrographs. **(e)** Low-power optical micrograph under PPL and **(f)** under cold-cathode cathodoluminescence (CL), both displaying the same area in a *Planolites* isp. fabric. Note the abundance of *Heterohelix* spp. with their tests being infilled with sparry-calcite cement, and also the pressure-solution seams that cut through them. The sparry-calcite-cemented foraminifers display relatively bright luminescence in (f), whereas the diagenetically-unaltered bivalve shells are nonluminescent. **(g), (h)** High-power, backscattered, electron-optical micrographs illustrating the matrix components of this mudstone unit. These include disarticulated planktonic foraminifers (mostly as *Heterohelix* spp.) and coccoliths, organic matter (both amorphous and woody), pyrite (both framboidal and euhedral), phosphate, and rare quartz, clay (authigenic kaolinite) and dolomite. Note also the presence of faecal pellets and some shelly fragments.

articulated, frequently concentrated on bedding planes forming shell pavements (Figure 3.6a, c and e). Ammonites, including *Acanthoceras rhotomagense* (sensu Philip et al., 1995), have also been found in association with some of these oyster shell pavements (Figure 3.6e).

The organic-carbon-rich mudstone is partially bioturbated, attributed mainly to horizontal and compressed burrows (Figures 3.6d and 3.7a, b) that are predominantly infilled with detrital carbonate mud (including coccoliths, planktonic and benthic foraminifera, and shell debris; Figure 3.7c and d). A variety of small and intermediate trace-fossil taxa including *Planolites* isp., *Phycosiphon* isp., and *Thalassinoides* isp. have been recognised.

Burrowing, commonly, becomes increasingly more intense towards the unit tops (Figures 3.6d and 3.7a, b).

The partial bioturbation of sediment here has disrupted most of the primary sedimentary structures in the rock. Textural analyses of hand specimens and thin sections, however, enabled us to observe some relict internal bedding structures in a number of samples (e.g. Figures 3.6a to c and 3.7a to b). These relict beds are described here as very thin (3 to 30 mm thick) depositional units, "thin beds" representing individual depositional events (sensu Ingram, 1954; Campbell, 1967; Macquaker et al., 2007). They are commonly bounded from above and below by laterally-discontinuous bedding surfaces, which are commonly marked by either shell pavements (Figures 3.6a to c and 3.7a to b) or concentrations of planktonic foraminifera.

Planktonic foraminifera frequently dominate this lithofacies. The dominant species present are *Heterohelix* spp. (some of which showing bimodal distribution) with rare *Whiteinella* spp. and *Hedbergella* spp. (Figure 3.7c to h). Theses species range in size from 50 to 250 µm. The shelter porosity within some of the foraminifer tests is partly infilled with carbonate cements, together with organic matter, clay (kaolinite) and/or pyrite (Figure 3.7g and h). The sediment enclosing the planktonic foraminifera is typically compacted around the tests. The matrix also contains pressure-solution seams (Figure 3.7e and f), which mostly display concentrations of organic- and/or clay-rich material.

The rock matrix comprises fragmented foraminifer tests, disarticulated coccolith plates, organic matter (both amorphous and woody), authigenic clay (mostly as kaolinite), fine-grained calcite replacement ("microspar"), and infrequent pyrite (framboidal and euhedral) (Figure 3.7g and h; Table 3.1). The foraminifer tests, coccolith plates, and organic matter are commonly contained in faecal pellets. Other minor components that are present in the rock include rare bioclastic debris (bivalve fragments and echinoid spines), thin-walled planktonic bivalves, phosphatic debris (mostly as fish vertebrae), quartz, and rare dolomite (Figure 3.7c to h; Table 3.1). This lithofacies is described as being a partially-bioturbated, organic-matter-, calcareous microplankton- (planktonic foraminifera) and calcareous nannoplankton- (coccoliths) bearing carbonate mudstone.

The TOC content of this lithofacies can reach up to 13.7% but averages 5.4%, based on our TOC analyses on samples gathered from a well in the Natih field (North Oman). In well logs, the organic richness of these carbonate mudstones is reflected by relatively high total gamma-ray readings, which roughly range from 25 to 135, average about 55 API units.

Standard geochemical techniques and maceral observations suggest that the organic matter of the mainly oil-prone Natih-B source rock is hydrogen-rich and consists of a mixture of both algal and bacterial, predominantly structureless, mostly load-bearing organic matter (Kharusi, 1984; Terken, 1999). In addition, both maceral observations and pyrolysis flame ionization detector (FID) results (Rutten, 1985), together with the high hydrogen index (HI) values (range from 400 to 650; van Buchem et al., 2002) indicate that the Natih-B source rock in the well of Natih field is immature for any hydrocarbon generation.

3.8.2. Interpretation

The fine-grained texture and common occurrences of planktonic foraminifera and coccoliths in these organic-carbon-rich mudstone lithofacies suggest that a relatively low-energy depositional environment dominated during the deposition of these units (little evidence of erosion and redeposition – the oysters are mostly preserved as living assemblages, rarely winnowed), with their constituents being deposited predominantly from suspension settling (pelagic components) close to storm wave base (e.g. Markello and Read, 1982; Burchette and Britton, 1985; Droste, 1990; Philip et al., 1995; van Buchem et al., 1996; Kuhnt et al., 1997).

The lack of preserved lamina, presence of burrows and frequent occurrence of in-place benthic fauna suggest that, at the time of deposition, the conditions at the sediment/water interface were oxic-dysoxic, rather than anoxic (cf. Hudson and Martill, 1991; Wetzel and Uchmann, 1998; Macquaker et al., 2007). Moreover, the presence of in-place oysters as shell pavements (colonisation surfaces) and moderate bioturbation in these units suggest that the sediment was firm (rather than “soupy”), and that there were prolonged breaks between sediment supply events (see Kenig et al., 2004; Macquaker et al., 2007), in order to allow sediment colonisation both by the oysters and burrowing organisms.

The predominance of planktonic foraminifera and coccoliths, together with the abundantly preserved organic matter, in this lithofacies also implies that there were episodically high rates of both inorganic and organic primary production during deposition of this sediment. Photosynthesising micro-organisms (mainly phytoplankton) living in the upper part of the water column were probably the major contributors to organic-matter production here (e.g. Killops and Killops, 1993; Arthur and Sageman, 1994). Inevitably, primary inorganic production from pelagic organisms (including planktonic foraminifers, coccoliths and planktonic bivalves) within the surface waters contributed in reducing some of the organic-carbon contents in this lithofacies through the dilution of organic components by the carbonate tests (i.e. organic-matter autodilution).

From the abundance of predominantly structureless organic matter associated with coccoliths and planktonic foraminifera, it may, therefore, be speculated that the origin of the source-rock organic matter is mainly from surface phytoplankton (algal bloom) deposited in an open, relatively deeper-marine environment, and transformed by bacteria into structureless organic matter (Kharusi, 1984). Here, however, persistent anoxia cannot be the main cause of organic-matter preservation. Given the presence of hiatal surfaces, associated with oyster colonisation events and evidence of high primary production in the matrix components, it is likely that the sediment was supplied episodically to the basin as phytoplankton blooms and then buried rapidly. In this way organic matter could have been buried prior to it being mineralised (e.g. Arthur and Sageman, 1994). This means that the reoccurrence frequency of sediment delivery events was more rapid than the rate at which organic matter was being decayed. This was most likely a function of phytoplankton blooms occurring in close successions.

The carbonate cements infilling the planktonic foraminifer tests in these units may be related to very early diagenetic processes, as the tests are uncompacted. The presence of a calcite-pyrite cement assemblage might suggest that this early diagenesis was linked to microbial decay of organic matter (cf. Irwin, 1980; Taylor and Macquaker, 2000). Specifically, it is likely that sulphate-reducing bacteria living in the sediment porewaters at a depth of less than 0.2 m below the sediment/water interface were using sulphate as an oxidant to oxidise organic matter, producing hydrogen sulphide (e.g. Berner, 1981; Canfield, 1994) and liberating bicarbonate into the porewaters. It is also possible that associated iron reduction was contributing alkalinity to the porewaters (e.g. Coleman et al.,

1993; Macquaker et al., 1997), causing a proportion of the organic matter to be mineralised and converted into carbonate cement (e.g. Sansone et al., 1990; Machent et al., 2007).

The presence of compacted sediment around the foraminifer tests and development of pressure-solution seams suggest that both physical and chemical compaction processes dominated part of the diagenetic history of this lithofacies. Pressure solution in these organic-rich mudstones caused the sediment to develop thin partings (fissility). These partings may have been mistaken for genetic laminae (sensu Campbell, 1967) by previous workers.

3.9. Detailed Facies Analyses: Sparry-Calcite-Rich Wackestone

3.9.1. Description

The sparry-calcite-rich wackestone lithofacies is slightly coarser grained and lighter coloured, compared to the more organic-rich units (Figures 3.8 and 3.9). Additionally, it is both extensively bioturbated (Figures 3.8a to c and 3.9a) and pervasively cemented by sparry calcite (Figure 3.9e to h). Units dominated by this facies vary in thickness from 2.0 to 185.0 cm (average 20.5 cm; Figure 3.5c). Extensive bioturbation has destroyed most of the primary sedimentary structures, and this, coupled with the pervasive cementation, causes these units to exhibit both mottled and recrystallised appearance (Figures 3.8a to c and 3.9a). Burrowing in this lithofacies is mostly attributed to *Thalassinoides* isp. (Figures 3.8a, c and 3.9a), and rarely to *Planolites* isp. and *Phycosiphon* isp.

In most cases, the bases of these units are sharp and erosive, and internally their grain sizes fine upward (Figures 3.6a, d and 3.8b to c). They may exhibit cm-scale scouring features (Figure 3.8c), and amalgamation of several thin (5 to 50 mm thick), normally-graded, individual beds is frequent (e.g. Figure 3.8d and e). Moreover, these units commonly contain a mix of predominantly uncompacted, disarticulated shelly material, including reworked bivalves, brachiopods, gastropods, patchy echinoderm debris, corals, and occasional rudist fragments (Figures 3.8c to e and 3.9b to d).

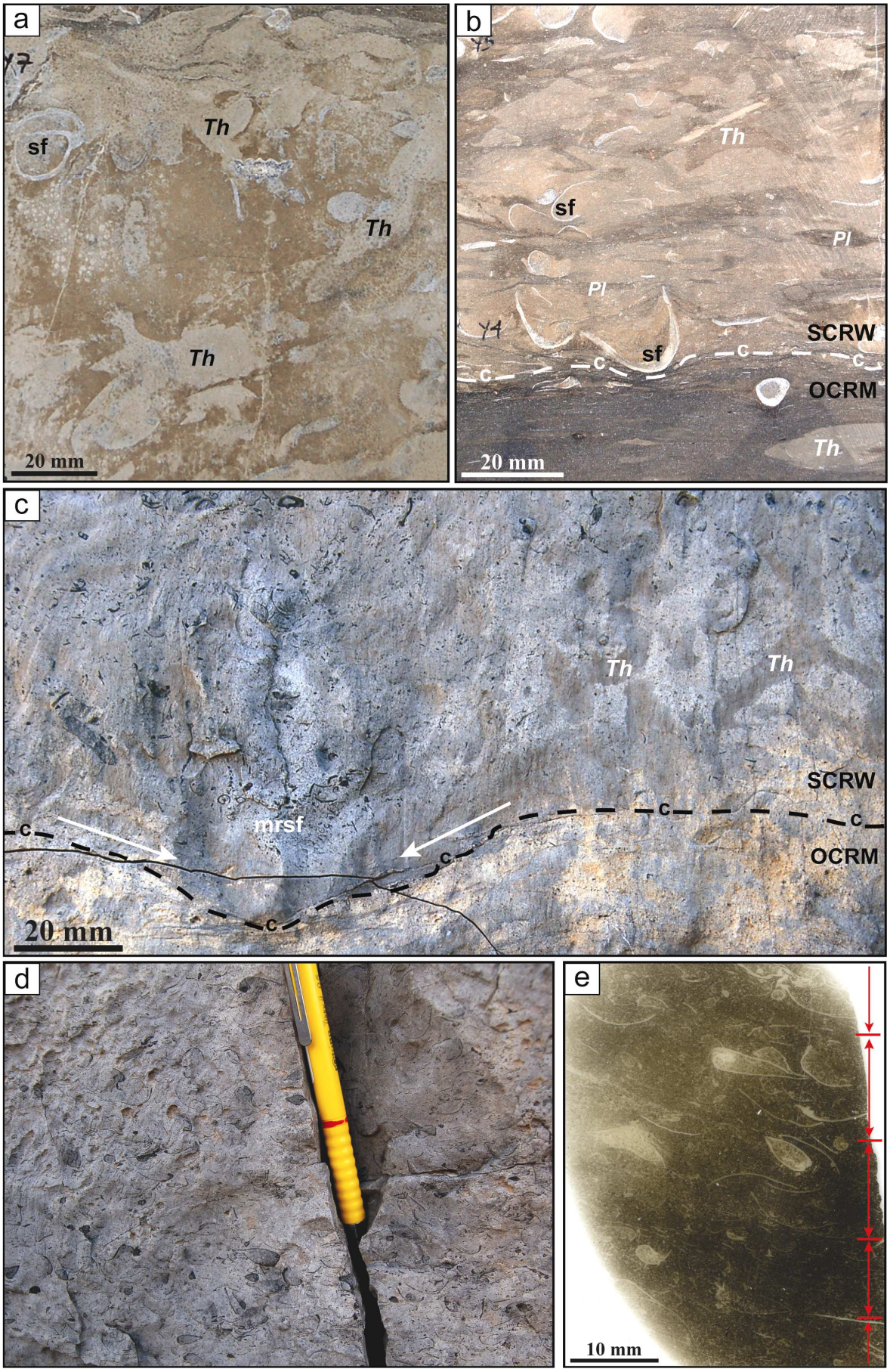

Figure 3.8. (see caption next page)

Figure 3.8. (see previous page): Core and outcrop photographs of the sparry-calcite-rich wackestone lithofacies. **(a)** Core photograph (Natih field well, ~ 929.3 m depth [~ 928.1 driller's depth]) illustrating extensive bioturbation, attributed to mainly *Thalassinoides* isp. (*Th*), which destroyed the primary structures in this unit and resulted in a mottled appearance. Note also the presence of reworked shell fragments (sf). **(b)** Core photograph (Natih field well, ~ 929.5 m depth [~ 928.3 m driller's depth]) showing the sparry-calcite-rich wackestone (SCRW) with abundant *Thalassinoides* isp. (*Th*) and *Planolites isp.* (*Pl*) burrow fabrics and reworked shell fragments (sf). Note the irregular (erosive) contact between the SCRW and OCRM (organic-carbon-rich mudstone). **(c)** Outcrop photograph (Jabal Qusaybah) illustrating cm-scale scouring (arrowed) at the base of the SCRW unit, with a mixture of reworked shell fragments (mrsf). Note also the common *Thalassinoides* isp. (*Th*) in this unit. **(d)** Outcrop photograph (Jabal Qusaybah) displaying abundantly reworked shells in the wackestone unit. **(e)** Thin-section scan, close-up from (d), illustrating amalgamated, 10- to 20-mm-thick beds in the same unit.

Figure 3.9. (see next page): Detailed facies analyses of a representative extensively-bioturbated, sparry-calcite-rich wackestone (sample S9 from core of Natih field well, 926.85 m depth [925.65 m driller's depth]). This sample has a low TOC content of 0.5%. (Abbreviations: *Th* = *Thalassinoides* isp.; rf = rudist fragment; pb = planktonic bivalve; bf = bivalve fragment; ef = echinoid fragment; cf = coral fragment; pd = phosphatic debris; af = agglutinated foraminifer; *Le* = *Lenticulina* spp.; *Het* = *Heterohelix* spp.; *Hed* = *Hedbergella* spp.; os = ostracod; cs = calcispheres; do = dolomite; ep = euhedral pyrite). **(a)** Core photograph showing intensely-burrowed, sparry-calcite-rich wackestone unit, giving a mottled fabric. Trace fossils here are mostly attributed to *Thalassinoides* isp., some are roughly outlined with dashed lines. Note also the sparry-calcite-cemented shell fragments and vertical microfractures. **(b)** Thin-section scan, close-up from (a), illustrating a matrix-supported wackestone with a mix of reworked and broken shells of bivalves, brachiopods, gastropods, echinoderms, and a larger rudist fragment at the top of the photograph. **(c)** Low-power optical micrograph under PPL and **(d)** under XPL of the same area, illustrating a diversity of uncompacted, predominantly sparry-calcite-cemented macrofossils (including fragmented bivalves and gastropods) and microfossils (including agglutinated foraminifers, *Lenticulina* spp., *Heterohelix* spp., calcispheres and ostracods). Note also the presence of phosphatic debris and thin-walled planktonic bivalves. **(e)** Low-power optical micrograph under PPL and **(f)** under cold-cathode CL of the same area, showing sparry-calcite-cemented shells, microfractures and matrix with varying degrees of luminosity. Note also the occurrence of a coral fragment, planktonic bivalves, agglutinated foraminifera, *Lenticulina* spp., *Hedbergella* spp. and calcispheres. **(g)**, **(h)** High-power, backscattered, electron-optical micrographs illustrating the matrix components of this organic-poor wackestone unit, as being extensively diageneatically altered. Note the abundance of calcite microspar, and the pervasive sparry-calcite cementation in the tests of the foraminifers and other shells. Other rare components present in the matrix include, phosphatic debris, organic matter (material with low η), euhedral pyrite and dolomite.

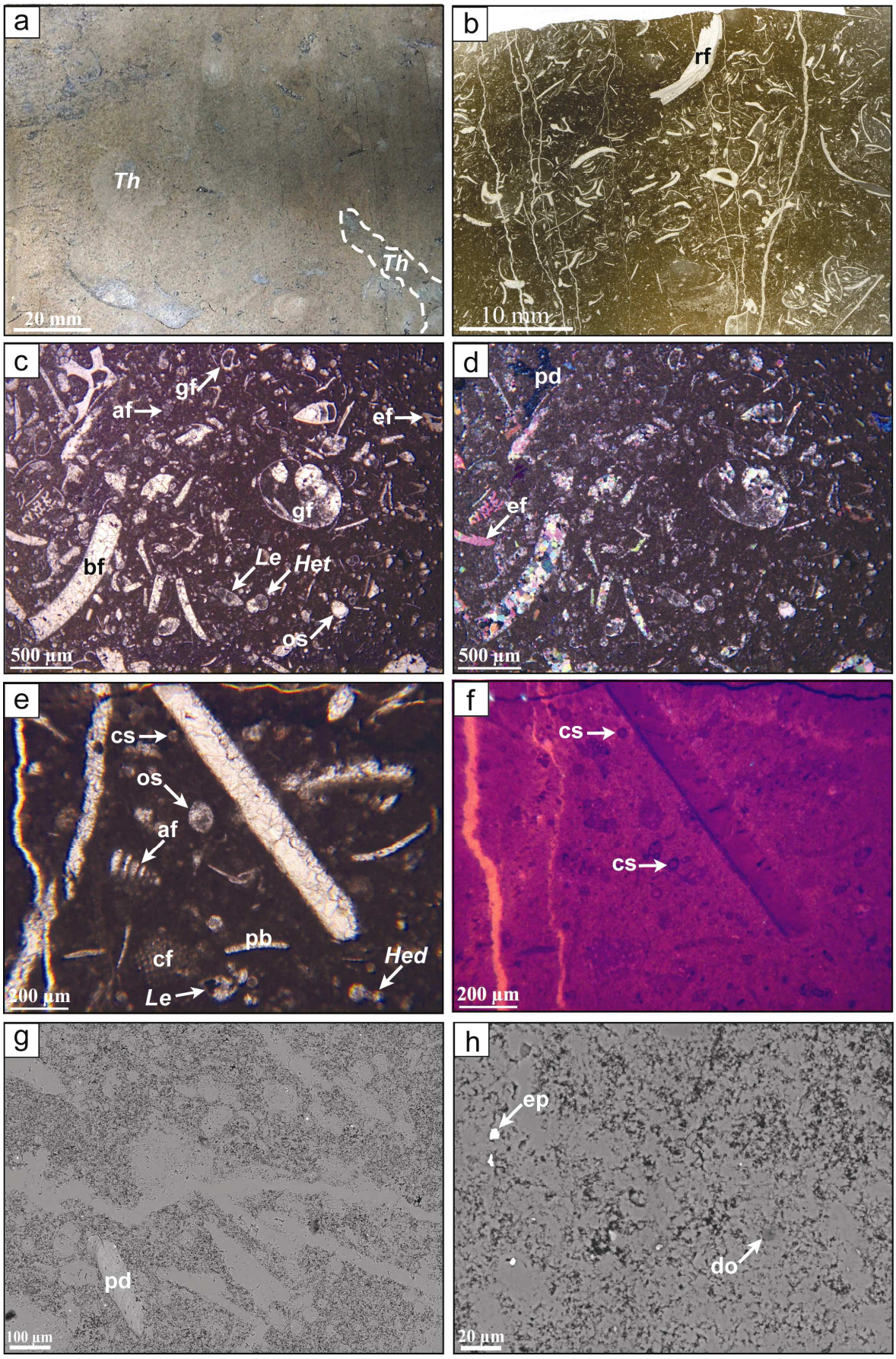

Figure 3.9. (see caption in previous page)

Benthic foraminifera (mostly as *Lenticulina* spp.) commonly occur in the background, with some planktonic foraminifera (including *Heterohelix* spp. and *Hedbergella* spp.), ostracods, and calcispheres, cemented by sparry calcite (Figure 3.8c to f). The sparry-calcite cement and replacement appear to dominate this unit, cementing pore-spaces of the bioclasts and replacing depositional micrite mud in the rock matrix (Figure 3.8e to h). Other minor components in this lithofacies include quartz, dolomite (mostly as scattered rhombs) and euhedral pyrite, with scarce clay, phosphate and organic matter, occurring mostly in the matrix of the rock (Figure 3.8g and h; Table 3.1). The composition and texture exhibited by this unit cause us to describe it as being an extensively-bioturbated, shell-fragments-bearing, sparry-calcite-rich wackestone.

The diagenetic history of this lithofacies is dominated by calcite precipitation. There is little evidence of mechanical compaction or pressure solution; only rare sutured pressure-solution stylolites are present. Some microfracturing is present and may be cemented by calcite (Figure 3.9e and f), dolomite, or quartz.

The TOC content in these sparry-calcite-rich intervals can be as low as 0.3% (mostly < 1.5%, average 1.1%). On well logs, these organic-carbon-poor wackestones exhibit relatively low total gamma-ray response, with values ranging roughly from 10 to 25, average approximately 15 API units.

3.9.2. Interpretation

The slightly coarser grain size, common occurrence of scour surfaces, benthic foraminifera and ostracods, with diverse reworked shell fragments and extensive bioturbation in these units, all indicate that this lithofacies was deposited in a relatively shallower-marine, higher-energy, well-oxygenated environment, above storm wave base (e.g. Brett and Allison, 1998; Wetzel and Uchmann, 1998; Hallam et al., 2000). The reworked shell fragments and the erosive bases of these units, coupled with normal grading textures suggest that sediments in these interbeds were swept by waning flow currents (likely distal storms) from the surrounding shallower carbonate platform down into the basin (cf. Droste, 1990; Hudson and Martill, 1991; Osleger, 1991; Osleger and Read, 1991; Burchette, 1993). In addition, it is likely that these interbeds were formed by the amalgamation and winnowing of individual, thinner storm-generated beds, resulting from the reworking of

sediment during major storm events (Myrow and Southard, 1996; Varban and Plint, 2008). Particular offshore-directed and geostrophic currents produced by storms may have been responsible for erosion, sediment mixing, and both shore-parallel and offshore sediment transport (Aigner, 1982; Leckie and Krystinik, 1989; Duke, 1990; Duke et al., 1991).

The abundance of early-marine calcite cement and replacement (predating compaction), low preserved organic-matter content, and degree of bioturbation in these wackestone lithofacies indicate that there was sufficient time for solutes to be diffused to the sites of precipitation, and for the sediment to be extensively burrowed. These data also imply that overall sediment accumulation rates in these units were rather slower than that of the organic-carbon-rich mudstone units (cf. Fisher and Hudson, 1987; Ekdale and Bromley, 1991; Damholt and Surlyk, 2004). Moreover, the abundance of *Thalassinoides* isp. here indicates that between storm events the depositional environment was reasonably quiet, and that overall rates of sediment accumulation were relatively slow. This also suggests that the substrate was fairly firm and stable, as these burrows were kept open (unlined) at the seafloor for a prolonged period of time.

3.10. Discussion

The large-scale, spatial context of the Natih-B sediments indicates that deposition occurred within a basin surrounded by a shallow-water carbonate platform (Markello and Read, 1981; Droste, 1990; Burchette, 1993; Philip et al., 1995; van Buchem et al., 2002; Droste and Van Steenwinkel, 2004; Figure 3.10). The faunal assemblages in both alternating facies overall indicate a relatively shallow-marine environment, up to 60 m maximum water depth (see also Harris and Frost, 1984; Immenhauser et al., 2000; van Buchem et al., 2005; Homewood et al., 2008). This implies that there were significant differences in accommodation availability, as a result of relative sea-level change, during deposition of the two main alternating facies; with the partially-bioturbated, organic-matter-, microplankton- and nannoplankton-bearing mudstones being deposited during increase of accommodation, compared to the extensively-bioturbated, shell-fragments-bearing, sparry-calcite-rich wackestones, which were deposited during decrease of accommodation (see discussion in Mettraux et al., 1999).

In spite of the relatively similar absolute water depths, the faunal assemblages present suggest that suspension settling contributed most of the sediment during deposition of the mudstone lithofacies, whereas a greater proportion of sediment in the wackestone lithofacies was supplied either by advective processes transporting sediment from the surrounding carbonate platform or by in-place production of biogenic material (Figure 3.10). There is no doubt that the supply of carbonate debris caused some organic-matter autodilution in the Natih-B Member (sensu van Buchem et al., 2005). Additionally, organic-matter mineralisation by biogenic degradation processes probably also lowered the organic-matter content of this unit.

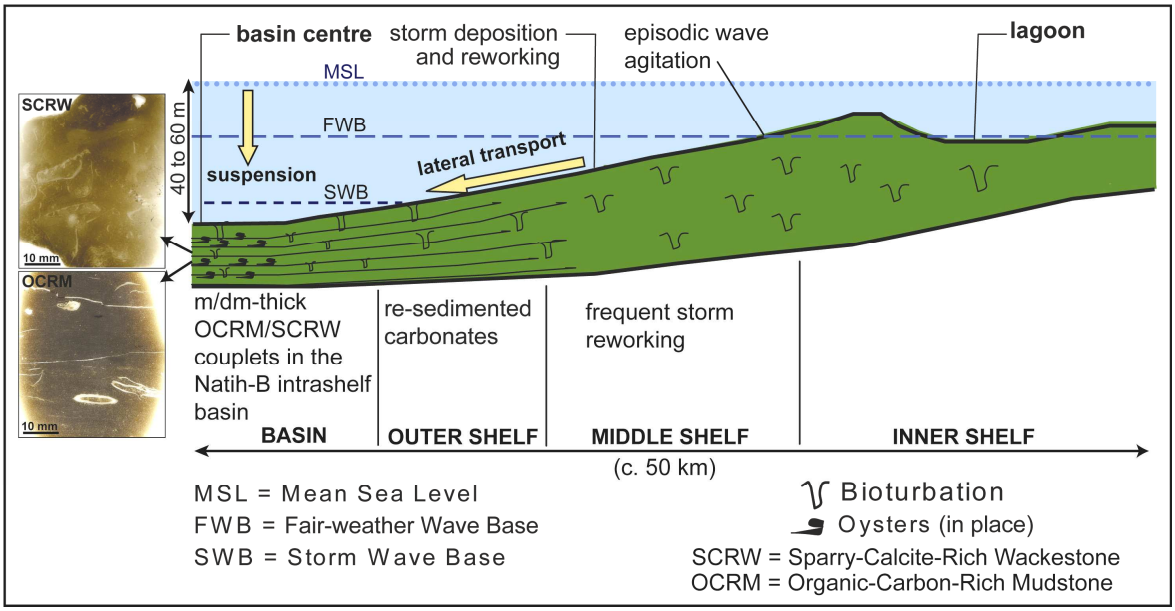

Figure 3.10. Schematic depositional model (modified from van Buchem et al., 1996) for the Natih-B intrashelf-basinal sediments (NB5 unit in particular) illustrating the two main lithofacies alternating with one another in the basin centre; namely the organic-carbon-rich mudstone (OCRM) and sparry-calcite-rich wackestone (SCRW). Note that sediments deposited through suspension settling dominate the mudstone lithofacies, and sediments supplied by lateral transport and storm-reworking dominate the wackestone lithofacies.

3.10.1. Sources of Organic Matter

Taking into consideration the relatively shallow-marine setting and the fact that some of the organic matter is derived from woody material, it is likely that there was some offshore-directed sediment transport component (e.g. Tyson, 1995). While this woody material may have a land source, it is also possible that it was derived from seagrasses (e.g. Suchanek et al., 1985; Kenig et al., 1990; De Leeuw et al., 1995). Seagrasses are marine-

flowering, vascular higher plants that are capable of growing whilst completely submerged in the shallow-water environment, typically at less than 10 m water depth but sometimes down to 30 m because they lack accessory photosynthesising pigments (De Leeuw et al., 1995; Tyson, 1995; Orth et al., 2006; Short et al., 2007). Their evolutionary history might be as long ago as 100 million years, and there is evidence of their existence during Upper Cretaceous times (Pomar, 2001; Pomar et al., 2005; Short et al., 2007).

Phytoplankton (and to lesser extent zooplankton and bacteria) were likely the major contributors to the production of the abundant amorphous (structureless) organic matter in the Natih-B Member (e.g. Killops and Killops, 1993; Tyson, 1995). The presence of faecal pellets composed of planktonic foraminifer tests, coccolith plates, and organic matter suggests that this amorphous matter was predominantly produced in the upper part of the water column, before being transported to the seafloor relatively rapidly within faecal pellets (McCave, 1985; Alldredge and Silver, 1988; Tyson, 1995; Kuhnt et al., 1997; Damholt and Surlyk, 2004). It is very likely that these faecal pellets were produced by filter-feeding organisms (including zooplankton and other animal sources), which bundled much of the microscopic components in the water column into organominerallic aggregates (Alldredge and Silver, 1988).

High hydrogen index (HI) values ranging from 400 to 650 of subsurface source rocks, reported by van Buchem et al. (2002), provide further evidence for the presence of the amorphous organic matter in Natih-B. However, interpretation of Type-II organic-matter composition, based on palynofacies analysis (van Buchem et al., 2005), may support the coexistence of both amorphous and woody organic-matter types in the Natih-B source-rock interval (see also Killops and Killops, 1993; Tyson, 1995; Terken, 1999).

3.10.2. Organic-Matter Enrichment in the Organic-Carbon-Rich Carbonate-Mudstone Units

The very high TOC values in the intrashelf-basinal organic-carbon-rich mudstone units can be interpreted as a result of increased primary productivity of organic matter, both in the water column (phytoplankton bloom) and in the shallow shelf (woody matter), that was episodically delivered to the sediment/water interface at relatively higher rates, and buried

rapidly. Evidence for the latter factor is also provided by the abundant preservation of articulated shells of bivalves (cf. Brett and Allison, 1998) in this lithofacies (see above).

Apparently, higher (local) sedimentation or burial rates decrease the exposure time of organic matter at the sediment/water interface (e.g. Arthur and Sageman, 1994; Weedon et al., 2004; Katz, 2005), giving it less chance to be degraded by benthos at the oxic-dysoxic bottom waters, where large benthic organisms (abundant evidence of in-place fauna and bioturbation in both lithofacies here) frequently agitate the sediment (see also Damholt and Surlyk, 2004). However, sedimentation rate should not be persistently too high, in order to reduce the dilution of organic matter by carbonates (shelly material) and/or clastics (detrital clays) (e.g. Bohacs et al., 2005; Tyson, 2005; van Buchem et al., 2005).

Given this, we suggest that the enhanced organic-matter enrichment in this lithofacies was controlled by high primary organic productivity at the surface waters, and accompanied by rapid but episodic rates of sediment accumulation and burial (cf. Hudson and Martill, 1991). The rapid and episodic input of sediments does, in fact, enhance organic-matter preservation in these units by quickly burying the organic matter and transporting it into the methanogenic zone, out of the zone of substantially and relatively organic-matter degradation (e.g. Tyson, 1995). Moreover, there is no indication of sufficient clastic flux (rare detrital clay and quartz) into the intrashelf basin to significantly dilute the organic-matter constituent during relatively higher sedimentation rates. Burchette (1993) also suggested that changes in sedimentation rates could have controlled the high-frequency cyclic pattern of the carbonate-rich units, interbedded at 200 to 300 mm scale with the organic-rich facies, in the intrashelf basin of the Shilaif/Khatiyah Formation of the United Arab Emirates (age-equivalent to the Natih-B Member in Oman).

3.10.3. Organic-Matter Reduction in the Sparry-Calcite-Rich Wackestone Units

The reduced organic-matter content in the sparry-calcite-rich interbeds likely result from a combination of organic-matter autodilution (high carbonate influx during storm events for instance), and more importantly by organic-matter degradation during early aerobic (oxic) and anaerobic (sulphate reduction) diagenesis.

Given the well-oxygenated bottom-water conditions and the relatively lower sedimentation rates during the deposition of these units, it is likely that a high proportion of the original organic matter present at the sediment/water interface was degraded by the abundant benthic fauna living on top or within the sediment (e.g. Tyson, 1995) respiring with oxygen. Once the residual organic component has been overall buried slowly to depths where free oxygen is no longer available (i.e. sulphate-reduction zone), in-place anaerobic bacteria also caused significant amount of organic-matter degradation (e.g. Machent et al., 2007). During their metabolism, these micro-organisms converted the organic matter present to carbon dioxide and bicarbonate, which ultimately become incorporated in the sediment as calcite cement/replacement.

This interpretation of organic-matter mineralisation by oxic respiration and anoxic sulphate reduction is also supported by the recent chemostratigraphic work of Vahrenkamp (2010) on the Albian-Turonian Natih Formation sediments. His whole-rock, stable-isotopic analyses of carbonate carbon on cores from Fahud field (North Oman; Figure 3.1b) show relatively light $\delta^{13}C$ values in the Natih-B Member source-rock interval (NB5), in the range from +0.1 to +1.8‰ (average +0.1‰ VPDB [Vienna Pee Dee Belemnite]; cf. Allison et al., 2008). This is compared to a range of $\delta^{13}C$ values (about +1.5 to about +5.5‰ VPDB) for other Natih Formation members, average around +3.5‰ VPDB (Vahrenkamp, in review). However, because the $\delta^{13}C$ values of the Natih-B sediments are overall near 0.0‰, and given the relatively shallow setting and oxic-dysoxic depositional environment of the Natih-B intrashelf basin (interpretations from this study), it is likely that the majority of the calcite spar in the Natih-B source-rock interval was derived from normal (open, oxic) marine porewaters (e.g. Marshall and Ashton, 1980; Dickson, 1985). Moreover, the $\delta^{13}C$ depletion (negative shift) in the Natih-B Member suggests that the excellent source rock within this succession does not tie to any global Oceanic Anoxic Event (see Homewood et al., 2008; Vahrenkamp 2010, in review), providing further evidence that "expanded anoxia" probably did not exist during deposition of Natih-B (cf. Jenkyns et al., 1994; Rodriguez-Lázaroet al., 1998; Voigt, 2000; Jarvis et al., 2006).

Although these stable-isotopic analyses were performed on whole-rock samples, rather than individual components of the Natih-B fine-grained sediments, relying on such data, however, makes it impossible to be specific about the processes controlling either the preservation or degradation of organic matter, as these sediments comprise mineral

mixtures of biogenic carbonates from bivalve, brachiopod, echinoderm, gastropod, ostracod, foraminifer and coccolith tests, in addition to the crucial authigenic-carbonate components present in the shelter porosity of these mixed tests, as well as in the rock matrix and microfractures.

3.10.4. Shell Pavements and Facies Stacking Pattern

The observation of shell pavements (organism colonisation surfaces) within the organic-carbon-rich mudstone lithofacies can be interpreted as bedding planes (or depositional surfaces) that bound individual beds (e.g. Kidwell, 1985; Beckvar and Kidwell, 1988; Banerjee and Kidwell, 1991). These surfaces also represent periods of nondeposition or rapid change in depositional settings (e.g. Campbell, 1967; Brett et al., 2006). These bedding planes are well pronounced in the context of the Natih-B intrashelf basin. They frequently separate the two interbedded lithofacies described here, appearing at the top of the sparry-calcite-rich wackestone beds, but formed as the depositional surfaces for the overlying organic-carbon-rich mudstone beds (see Campbell, 1967; Figure 3.11a and b), following a shallowing-up sequence (cf. Macquaker and Howell, 1999; Figure 3.11c and d).

The early calcite precipitation (predating compaction), which dominates the tops of the extensively-bioturbated, shell-fragments-bearing, sparry-calcite-rich units (Figure 3.11a and d), is interpreted to be explicitly related to breaks in sedimentation (see Macquaker and Howell, 1999; Kenig et al., 2004). Therefore, the in-place oysters that form shell plasters, where present, were probably developed on hardgrounds (e.g. McLaughlin and Brett, 2007). This also suggests that the deposition of the oyster pavements was probably coincident with marine flooding surfaces at the tops of bed sets, formed during periods when sediment supply rates were reduced. These surfaces usually cap thin (average 400 mm thick), upward-coarsening units (parasequences) of the organic-rich mudstone and spar-rich wackestone couplets (cf. Morettini et al., 2005; Figure 3.11c and d). Genetic beds here are typically less than 30 mm thick (sensu Ingram, 1954; Campbell, 1967; see above). These genetic thin beds are commonly exhibited in the organic-carbon-rich mudstone units as a well-developed fissility (described above); whereas in the sparry-calcite-rich wackestone interbeds they are frequently displayed as amalgamated, storm-deposited thin beds (mentioned above), resulting in a series of vertically-stacked units.

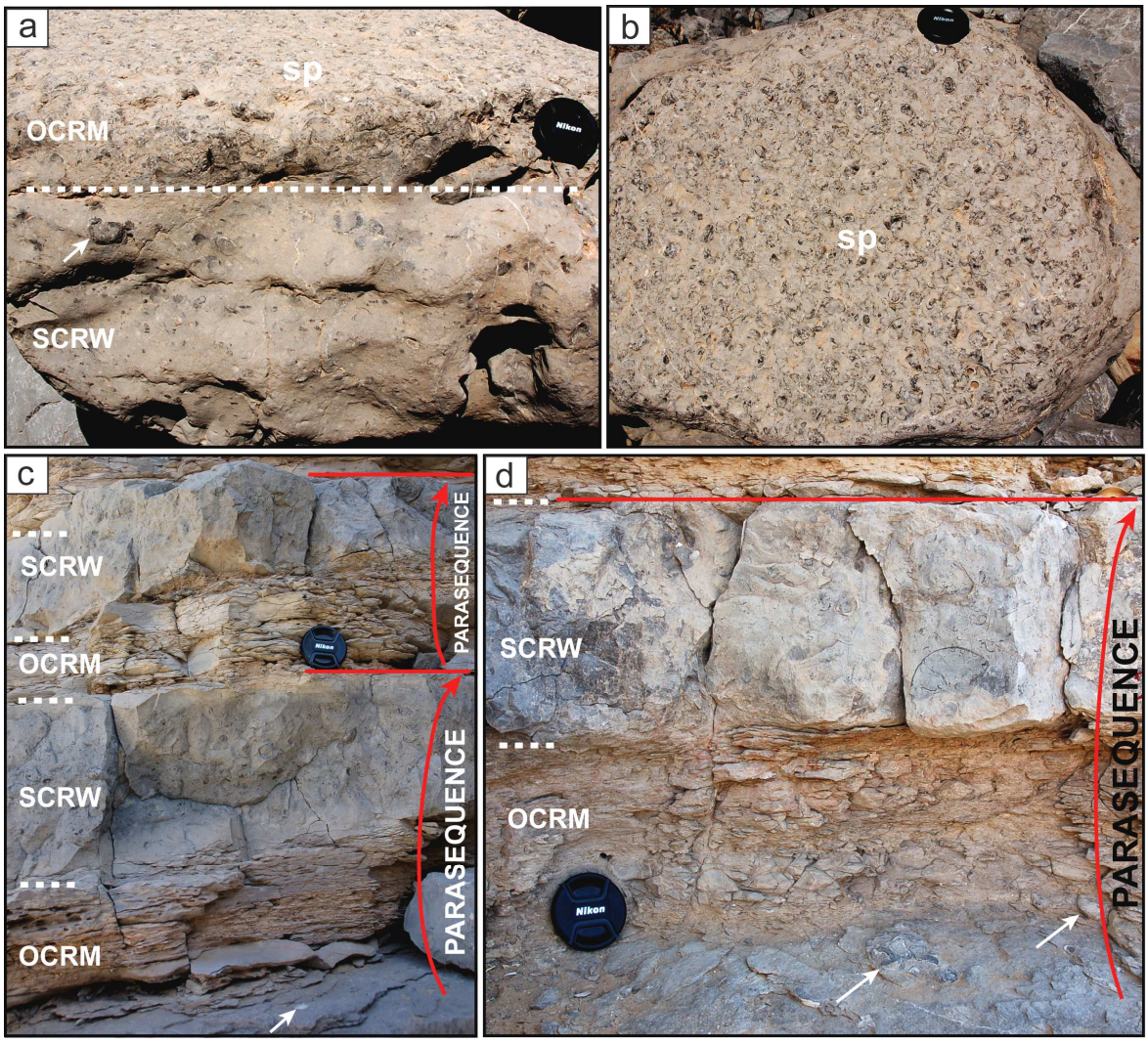

Figure 3.11. Outcrop photographs (Jabal Salakh West) illustrating shell pavements and stacking pattern of the two alternating lithofacies in NB5: organic-carbon-rich mudstone (OCRM) and sparry-calcite-rich wackestone (SCRW). (The cap of camera's lens is 60 mm in diameter). **(a)** Illustration of the upper part of the SCRW and base of the OCRM; note the extensive cementation near the top of the SCRW unit (arrow indicates a cemented oyster shell), capped with a shell plaster developed on a hardground at the base of the OCRM unit. **(b)** Plan view from (a) illustrating a shell pavement (sp), which is colonised by articulated oysters. **(c)** Illustration of facies stacking pattern in parasequences; arrow indicates cemented oyster at the base of the OCRM unit. **(d)** Close-up view from (c) illustrating characteristic features of a parasequence in the context of the NB5 sequence, where the OCRM (transgressive unit) being deposited initially at a flooding surface (arrows indicate cemented shells), capped with the SCRW (regressive unit).

A parasequence in this context includes both lithofacies as one transgressive-regressive cycle (Figure 3.11d), with the organic-carbon-rich mudstone (transgressive hemicycle) deposited initially (during marine flooding) and subsequently overlain by the relatively-shallower sparry-calcite-rich wackestone (regressive hemicycle) that displays colonised and cemented surfaces at top (see also Mettraux et al., 1999; Morettini et al., 2005). At

larger scales parasequences stack into parasequence sets and systems tracts – sequence boundaries may be marked here by shell beds with robust fauna.

3.11. Conclusions

On the basis of detailed analyses, two main lithofacies types are described from the Natih-B intrashelf basin, interbedding with one another, namely: a) partially-bioturbated, organic-matter-, calcareous microplankton- and nannoplankton-bearing mudstone with in-place thick-shelled oysters and flattened pectens, and b) extensively-bioturbated, shell-fragments-bearing, sparry-calcite-rich wackestone. These observations suggest that the existing models used to explain lithofacies variability and organic-matter preservation in the Natih-B succession, which rely upon changing bottom-water anoxia or styles of carbonate productivity, are incorrect. Instead, these data suggest that the need for bottom-water anoxia to preserve organic matter has been overestimated, and that the mineralisation of organic matter to carbonate precipitates during early diagenesis was probably very important in controlling lithofacies variability. Therefore, the main factors underpinning organic-matter enrichment under the oxic-dysoxic conditions of this depositional setting might have required abundant nutrients to fuel the short-term high primary organic productivity, rapid delivery of organic components to the sediment/water interface, coupled with rapid and episodic burial of organic material.

Finally, the generally shallow-water depth (40 to 60 m) of the intrashelf basin, rare evidence of clinoform stratification within the Natih-B Member, lacking a shelf-slope break, and the sedimentological and palaeontological data from this study suggest that it is very unlikely that persistent “anoxia” existed during the deposition of the Natih-B sediments, even in the most organic-carbon-rich facies. Therefore, appreciation of these critical observations will instrumentally improve our understanding of the fundamental controls underpinning source-rock development and distribution in intrashelf depositional basins, and ultimately enhance our hydrocarbon exploration and production strategies in such setting.

Acknowledgements

This project was kindly supported by grants from Petroleum Development Oman (PDO), which also provided substantial logistic support in the field, and supplied necessary satellite images, maps, reports, and subsurface core material. We also wish to thank Peter Homewood who initiated and recommended this study; Henk Droste, Cathy Hollis, and Carine Grélaud for useful discussions on the sedimentology and stratigraphy of the Natih Formation; Mohammed Al-Kindy for some assistance in locating the best outcrop sections of the Natih-B Member; Volker Vahrenkamp for providing his stable-isotopic data on the Natih Formation; Stephen Packer for his help with microfossil analyses; Thomas Heard for some comments on the trace fossils; Harry Williams and Stephen Stockley for thin-section preparations; Steve Caldwell and David Plant for some aid when using the SEM; Kevin Taylor for suggesting the method to run the TOC analyses; David McKendry for assistance in using the LECO instrument; and John Waters for aid in XRD analyses. Thanks also to both anonymous reviewers for thorough and thought-provoking comments. Finally, the authors would like to express gratitude to PDO and the Ministry of Oil and Gas (Sultanate of Oman) for permission to publish the subsurface data referred to in this paper.

References

Aigner, T. 1982. Calcareous tempestites: storm-dominated stratification in Upper Muschelkalk limestones (Middle Trias, SW Germany). In, G. Einsele and A. Seilacher (Eds.), Cyclic and Event Stratification. Springer-Verlag, p. 180-198.

Alldredge, A.L. and M.W. Silver 1988. Characteristics, dynamics and significance of marine snow. Progress in Oceanography, v. 20, no. 1, p. 41-82.

Allison, P.A., S.P. Hesselbo and C.E. Brett 2008. Methane seeps on an Early Jurassic dysoxic seafloor. Palaeogeography, Palaeoclimatology, Palaeoecology, v. 270, no. 3-4, p. 230-238.

Alsharhan, A.S. 1995. Facies variation, diagenesis, and exploration potential of the Cretaceous rudist-bearing carbonates of the Arabian Gulf. American Association of Petroleum Geologists, v. 79, no. 4, p. 531-550.

Alsharhan, A.S. and A.E.M. Nairn 1988. A review of the Cretaceous formations in the Arabian Peninsula and Gulf: Part II. Mid-Cretaceous (Wasia Group) stratigraphy and palaeogeography. Journal of Petroleum Geology, v. 11, no. 1, p. 89-112.

Aqrawi, A.A.M., G.A. Thehni, G.H. Sherwani and B.M.A. Kareem 1998. Mid-Cretaceous rudist-bearing carbonates of the Mishrif Formation: an important reservoir sequence in the Mesopotamian Basin, Iraq. Journal of Petroleum Geology, v. 21, no. 2, p. 57-82.

Arthur, M.A., W.E. Dean and D.A.V. Stow 1984. The Cenomanian-Turonian oceanic anoxic event II: palaeoceanographic controls on organic-matter production and preservation. In, D.A.V. Stow and D.J.W. Piper (Eds.), Fine-grained Sediments: Deep-Water Processes and Facies. Geological Society, Special Publication 15, p. 527-560.

Arthur, M.A. and B.B. Sageman 1994. Marine black shales: depositional mechanisms and environments of ancient deposits. Annual Review of Earth and Planatary Sciences, v. 22, p. 499-551.

Banerjee, I. and S.M. Kidwell 1991. Significance of molluscan shell beds in sequence stratigraphy: an example from the Lower Cretaceous Mannville Group of Canada. Sedimentology, v. 38, no. 5, p. 913-934.

Beckvar, N. and S.M. Kidwell 1988. Hiatal shell concentrations, sequence analysis, and sea-level history of a Pleistocene coastal alluvial fan, Punta Chueca, Sonora. Lethaia, v. 21, no. 3, p. 257-270.

Berner, R.A. 1981. A new geochemical classification of sedimentary environments. Journal of Sedimentary Research v. 51, no. 2, p. 359-365.

Bohacs, K.V., G.J. Grabowski, A.R. Carroll, P.J. Mankiewicz, K.J. Miskell-Gerhardt, J.R. Schwalbach, M.B. Wegner and J.A.T. Simo 2005. Production, destruction, and dilution – the many pathways to source-rock development. In, N.B. Harris (Ed.), The Deposition of Organic-Carbon-Rich Sediments: Models, Mechanisms, and Consequences. SEPM (Society for Sedimentary Geology), Special Publication 82, p. 61-101.

Boote, D.R.D., D. Mou and R.I. Waite 1990. Structural evolution of the Suneinah foreland, central Oman Mountains. In, A.H.F. Robertson, M.P. Searle and A.C. Ries (Eds.), The Geology and Tectonics of the Oman Region. Geological Society, Special Publication 49, p. 397-418.

Brett, C.E. and P.A. Allison 1998. Palaeontological approaches to the environmental interpretation of marine mudrocks. In, J. Schieber, W. Zimmerle and P. Sethi (Eds.), Shales and Mudstones I: Basin Studies, Sedimentology, and Palaeontology. E. Schweizerbart'sche Verlagsbuchhandlung, p. 384.

Brett, C.E., P.A. Allison, C.J. Tsujita, D. Soldani and H.A. Moffat 2006. Sedimentology, taphonomy, and palaeoecology of metre-scale cycles from the Upper Ordovician of Ontario. Palaios, v. 21, no. 6, p. 530-547.

Burchette, T.P. 1993. Mishrif Formation (Cenomanian–Turonian), southern Arabian Gulf: carbonate platform growth along a cratonic basin margin. In, J.A.T. Simo, R.W. Scott and J.P. Masse (Eds.), Cretaceous Carbonate Platforms. American Association of Petroleum Geologists, Memoir 56, p. 185-200.

Burchette, T.P. and S.R. Britton 1985. Carbonate facies analysis in the exploration for hydrocarbons: a case study from the Cretaceous of the Middle East. In, P.J. Brenchley and

B.P.J. Williams (Eds.), Sedimentology: Recent Developments and Applied Aspects. Geological Society, Special Publication 18, p. 311-338.

Campbell, C.V. 1967. Lamina, laminaset, bed and bedset. Sedimentology, v. 8, no. 1, p. 7-26.

Canfield, D.E. 1994. Factors influencing organic-carbon preservation in marine sediments. Chemical Geology, v. 114, no. 3-4, p. 315-329.

Coleman, M.L., D.B. Hedrick, D.R. Lovley, D.C. White and K. Pye 1993. Reduction of Fe(III) in sediments by sulphate-reducing bacteria. Nature, v. 361, no. 6411, p. 436-438.

Damholt, T. and F. Surlyk 2004. Laminated-bioturbated cycles in Maastrichtian chalk of the North Sea: oxygenation fluctuations within the Milankovitch frequency band. Sedimentology, v. 51, no. 6, p. 1323-1342.

De Leeuw, J.W., N.L. Frewin, P.F. Van Bergen, J.S. Sinninghe Damste and M.E. Collinson 1995. Organic carbon as a palaeoenvironmental indicator in the marine realm. Geological Society, Special Publications, v. 83, no. 1, p. 43-71.

Demaison, G.J. and G.T. Moore 1980. Anoxic environments and oil source bed genesis. American Association of Petroleum Geologists Bulletin, v. 64, no. 8, p. 1179-1209.

Dickson, J.A.D. 1985. Diagenesis of shallow-marine carbonates. Geological Society Special Publications, v. 18, no. 1, p. 173-188.

Droste, H. 1990. Depositional cycles and source rock development in an epeiric intraplatform basin: the Hanifa Formation of the Arabian Peninsula. Sedimentary Geology, v. 69, p. 281-296.

Droste, H. and M. Van Steenwinkel 2004. Stratal geometries and patterns of platform carbonates: the Cretaceous of Oman. In, G. Eberli, J.L. Massaferro and J.F.R. Sarg (Eds.), Seismic Imaging of Carbonate Reservoirs and Systems. American Association of Petroleum Geologists, Memoir 81, p. 185-206.

Duke, W.L. 1990. Geostrophic circulation or shallow-marine turbidity currents? The dilemma of paleoflow patterns in storm-influenced prograding shoreline systems. Journal of Sedimentary Research, v. 60, no. 6, p. 870-883.

Duke, W.L., R.W.C. Arnott and R.J. Cheel 1991. Shelf sandstones and hummocky cross-stratification: new insights on a stormy debate. Geology, v. 19, no. 6, p. 625-628.

Ehrenberg, S.N., A.A.M. Aqrawi and P.H. Nadeau 2008. An overview of reservoir quality in producing Cretaceous strata of the Middle East. Petroleum Geoscience, v. 14, no. 4, p. 307-318.

Ekdale, A.A. and R.G. Bromley 1991. Analysis of composite ichnofabrics; an example in Uppermost Cretaceous chalk of Denmark. Palaios, v. 6, no. 3, p. 232-249.

Fisher, I.S. and J.D. Hudson 1987. Pyrite formation in Jurassic shales of contrasting biofacies. In, A.J. Fleet and J. Brooks (Eds.), Marine Petroleum Source Rocks. Geological Society, Special Publication 26, p. 69-78.

Gradstein, F.M., J.G. Ogg and A.G. Smith 2004. A Geologic Time Scale 2004. Cambridge University Press, 589 p.

Grantham, P.J., G.W.M. Lijmbach, J. Posthuma, M.W. Hughes Clarke and R.J. Willink 1987. Origin of crude oils in Oman. Journal of Petroleum Geology, v. 11, no. 1, p. 61-80.

Grélaud, C., P. Razin, P.W. Homewood and A.M. Schwab 2006. Development of incisions on a periodically emergent carbonate platform (Natih Formation, Late Cretaceous, Oman). Journal of Sedimentary Research, v. 76, no. 4, p. 647-669.

Hallam, A. 1987. Mesozoic marine organic-rich shales. In, A.J. Fleet and J. Brooks (Eds.), Marine Petroleum Source Rocks. Geological Society, Special Publication 26, p. 251-261.

Hallam, A., P.B. Wignall, J. Yin and J.B. Riding 2000. An investigation into possible facies changes across the Triassic-Jurassic boundary in southern Tibet. Sedimentary Geology, v. 137, no. 3-4, p. 101-106.

Harris, P.M. and S.H. Frost 1984. Middle Cretaceous carbonate reservoirs, Fahud field and northwestern Oman. American Association of Petroleum Geologists Bulletin, v. 68, no. 5, p. 649-658.

Homewood, P., P. Razin, C. Grélaud, H. Droste, V. Vahrenkamp, M. Mettraux and J. Mattner 2008. Outcrop sedimentology of the Natih Formation, northern Oman: a field guide to selected outcrops in the Adam Foothills and Al Jabal Al Akhdar areas. GeoArabia, v. 13, no. 3, p. 39-120.

Hudson, J.D. and D.M. Martill 1991. The Lower Oxford Clay: production and preservation of organic matter in the Callovian (Jurassic) of central England. In, R.V. Tyson and T.H. Pearson (Eds.), Modern and Ancient Continental Shelf Anoxia. Geological Society, Special Publication 58, p. 363-379.

Hughes Clarke, M.W. 1988. Stratigraphy and rock units nomenclature in the oil-producing area of interior Oman. Journal of Petroleum Geology, v. 11, no. 1, p. 5-60.

Immenhauser, A., A. Creusen, M. Esteban and H.B. Vonhof 2000. Recognition and interpretation of polygenic discontinuity surfaces in the Middle Cretaceous Shu'aiba, Nahr Umr, and Natih formations of northern Oman. GeoArabia, v. 5, no. 2, p. 299-322.

Ingram, R.L. 1954. Terminology for the thickness of stratification and parting units in sedimentary rocks. Bulletin of the Geological Society of America, v. 65, no. 9, p. 937-938.

Irwin, H. 1980. Early diagenetic carbonate precipitation and pore-fluid migration in the Kimmeridge Clay of Dorset, England. Sedimentology, v. 27, no. 5, p. 577-591.

Jarvis, I., A.S. Gale, H.C. Jenkyns and M.A. Pearce 2006. Secular variation in Late Cretaceous carbon isotopes: a new $\delta^{13}C$ carbonate reference curve for the Cenomanian-Campanian (99.6-70.6 Ma). Geological Magazine, v. 143, no. 5, p. 561-608.

Jenkyns, H.C. 1991. Impact of Cretaceous sea-level rise and anoxic events on the Mesozoic carbonate platform of Yugoslavia. American Association of Petroleum Geologists Bulletin, v. 75, no. 6, p. 1007-1017.

Jenkyns, H.C., A.S. Gale and R.M. Corfield 1994. Carbon- and oxygen-isotope stratigraphy of the English Chalk and Italian Scaglia and its palaeoclimatic significance. Geological Magazine, v. 131, no. 1, p. 1-34.

Katz, B.J. 2005. Controlling factors on source rock development - a review of productivity, preservation, and sedimentation rate. In, N.B. Harris (Ed.), The Deposition of Organic-Carbon-Rich Sediments: Models, Mechanisms, and Consequences. SEPM (Society for Sedimentary Geology), Special Publication 82, p. 7-16.

Kenig, F., A.Y. Huc, B.H. Purser and J.L. Oudin 1990. Sedimentation, distribution and diagenesis of organic matter in a recent carbonate environment, Abu Dhabi, U.A.E. Organic Geochemistry, v. 16, no. 4-6, p. 735-747.

Kenig, F., J.D. Hudson, J.S.S. Damste and B.N. Popp 2004. Intermittent euxinia: reconciliation of a Jurassic black shale with its biofacies. Geology, v. 32, no. 5, p. 421-424.

Kharusi, N.S. 1984. The study of the organic matter of the source rocks of the Natih Formation in northern Oman, Unpublished Work. Petroleum Development Oman, Exploration Department, Report 84/1, 17 p.

Kidwell, S.M. 1985. Palaeobiological and sedimentological implications of fossil concentrations. Nature, v. 318, no. 6045, p. 457-460.

Killops, S.D. and V.J. Killops 1993. An Introduction to Organic Geochemistry. Longman Scientific and Technical, 265 p.

Kuhnt, W., A. Nederbragt and L. Leine 1997. Cyclicity of Cenomanian-Turonian organic-carbon-rich sediments in the Tarfaya Atlantic Coastal Basin (Morocco). Cretaceous Research, v. 18, no. 4, p. 587-601.

Leckie, D.A. and L.F. Krystinik 1989. Is there evidence for geostrophic currents preserved in the sedimentary record of inner- to middle-shelf deposits? Journal of Sedimentary Research, v. 59, no. 5, p. 862-870.

Loosveld, R.J.H., A. Bell and J.J.M. Terken 1996. The tectonic evolution of Interior Oman. GeoArabia, v. 1, no. 1, p. 28-51.

Machent, P.G., K.G. Taylor, J.H.S. Macquaker and J.D. Marshall 2007. Patterns of early post-depositional and burial cementation in distal shallow-marine sandstones: Upper Cretaceous Kenilworth Member, Book Cliffs, Utah, USA. Sedimentary Geology, v. 198, no. 1-2, p. 125-145.

Macquaker, J.H.S. 1994. A lithofacies study of the Peterborough Member, Oxford Clay Formation (Jurassic), UK: an example of sediment bypass in a mudstone succession. Journal of the Geological Society, v. 151, no. 1, p. 161-172.

Macquaker, J.H.S. and A.E. Adams 2003. Maximizing information from fine-grained sedimentary rocks: an inclusive nomenclature for mudstones. Journal of Sedimentary Research, v. 73, no. 5, p. 735-744.

Macquaker, J.H.S., C.D. Curtis and M.L. Coleman 1997. The role of iron in mudstone diagenesis: comparison of Kimmeridge Clay Formation mudstones from onshore and offshore (UKCS) localities. Journal of Sedimentary Research, v. 67, no. 5, p. 871-878.

Macquaker, J.H.S. and R.L. Gawthorpe 1993. Mudstone lithofacies in the Kimmeridge Clay Formation, Wessex Basin, southern England: implications for the origin and controls of the distribution of mudstones. Journal of Sedimentary Research, v. 63, no. 6, p. 1129-1143.

Macquaker, J.H.S. and J.K. Howell 1999. Small-scale (< 5.0 m) vertical heterogeneity in mudstones: implications for high-resolution stratigraphy in siliciclastic mudstone successions. Journal of the Geological Society, v. 156, no. 1, p. 105-112.

Macquaker, J.H.S. and K.G. Taylor 1996. A sequence-stratigraphic interpretation of a mudstone-dominated succession: the Lower Jurassic Cleveland Ironstone Formation, UK. Journal of the Geological Society, v. 153, no. 5, p. 759-770.

Macquaker, J.H.S., K.G. Taylor and R.L. Gawthorpe 2007. High-resolution facies analyses of mudstones: implications for palaeoenvironmental and sequence-stratigraphic interpretations of offshore ancient mud-dominated successions. Journal of Sedimentary Research, v. 77, no. 3-4, p. 324-339.

Markello, J.R. and J.F. Read 1981. Carbonate ramp-to-deeper shale shelf transitions of an Upper Cambrian intrashelf basin, Nolichucky Formation, southwest Virginia Appalachians. Sedimentology, v. 28, no. 4, p. 573-597.

Markello, J.R. and J.F. Read 1982. Upper Cambrian intrashelf basin, Nolichucky Formation, southwest Virginia Appalachians. American Association of Petroleum Geologists Bulletin, v. 66, no. 7, p. 860-878.

Marshall, J.D. and M. Ashton 1980. Isotopic and trace element evidence for submarine lithification of hardgrounds in the Jurassic of eastern England (Lincolnshire Limestone). Sedimentology, v. 27, no. 3, p. 271-289.

McCave, I.N. 1985. Properties of suspended sediment over the HEBBLE area on the Nova Scotian Rise. Marine Geology, v. 66, no. 1-4, p. 169-188.

McLaughlin, P.I. and C.E. Brett 2007. Signatures of sea-level rise on the carbonate margin of a Late Ordovician foreland basin: a case study from the Cincinnati Arch, USA. Palaios, v. 22, no. 3, p. 245-267.

Mettraux, M., P. Homewood, A.M. Schwab and F. Guillocheau 1999. Sedimentology and accommodation cycles of Paris Basin Campanian Chalk: the key to high-resolution stratigraphy and seismic signature. In, P.M. Harris, A.H. Saller and J.A. Simo (Eds.), Advances in Carbonate Sequence Stratigraphy: Application to Reservoirs, Outcrops and Models. SEPM (Society for Sedimentary Geology), Special Publication 63, p. 317-334.

Morettini, E., A. Thompson, G. Eberli, K. Rawnsley, R. Roeterdink, W. Asyee, P. Christman, A. Cortis, K. Foster, V. Hitchings, W. Kolkman and J.H. van Konijnenburg 2005. Combining high-resolution sequence stratigraphy and mechanical stratigraphy for improved reservoir characterisation in the Fahud field of Oman. GeoArabia, v. 10, no. 3, p. 17-44.

Murris, R.J. 1980. Middle East: stratigraphic evolution and oil habitat. American Association of Petroleum Geologists Bulletin, v. 64, no. 5, p. 597-618.

Myrow, P.M. and J.B. Southard 1996. Tempestite deposition. Journal of Sedimentary Research, v. 66, no. 5, p. 875-887.

Orth, R.J., T.J.B. Carruthers, W.C. Dennison, C.M. Duarte, J.W. Fourqurean, K.L. Heck Jr, A.R. Hughes, G.A. Kendrick, W.J. Kenworthy, S. Olyarnik, F.T. Short, M. Waycott and S.L. Williams 2006. A global crisis for seagrass ecosystems. BioScience, v. 56, no. 12, p. 987-996.

Osleger, D. 1991. Subtidal carbonate cycles: implications for allocyclic vs. autocyclic controls. Geology, v. 19, no. 9, p. 917-920.

Osleger, D. and J.F. Read 1991. Relation of eustasy to stacking patterns of metre-scale carbonate cycles, late Cambrian, USA. Journal of Sedimentary Research, v. 61, no. 7, p. 1225-1252.

Paul, C.R.C., S.F. Mitchell, J.D. Marshall, P.N. Leafy, A.S. Gale, A.M. Duane and P.W. Ditchfield 1994. Palaeoceanographic events in the Middle Cenomanian of Northwest Europe. Cretaceous Research, v. 15, no. 6, p. 707-738.

Pedersen, T.F. and S.E. Calvert 1990. Anoxia vs. productivity: what controls the formation of organic-carbon-rich sediments and sedimentary rocks? American Association of Petroleum Geologists Bulletin, v. 74, no. 4, p. 454-466.

Philip, J., J. Borgomano and S. Al-Maskiry 1995. Cenomanian-Early Turonian carbonate platform of northern Oman: stratigraphy and palaeoenvironments. Palaeogeography, Palaeoclimatology, Palaeoecology, v. 119, p. 77-92.

Pomar, L. 2001. Types of carbonate platforms: a genetic approach. Basin Research, v. 13, no. 3, p. 313-334.

Pomar, L., E. Gili, A. Obrador and W.C. Ward 2005. Facies architecture and high-resolution sequence stratigraphy of an Upper Cretaceous platform margin succession, southern central Pyrenees, Spain. Sedimentary Geology, v. 175, no. 1-4, p. 339-365.

Razin, P., F.S.P. van Buchem, A. Lebec, C. Grélaud, H. Hillgartner, P.W. Homewood, A.M. Schwab and H. Droste 2005. The Cretaceous carbonate platform in Oman: sequence stratigraphy, stratal geometries and controlling factors (abstract). IAS 24th Meeting of Sedimentology, Muscat, Oman. International Association of Sedimentologists.

Robertson, A.H.F. 1987. Upper Cretaceous Muti Formation: transition of a Mesozoic carbonate platform to a foreland basin in the Oman Mountains. Sedimentology, v. 34, no. 6, p. 1123-1142.

Rodriguez-Lázaro, J., A. Pascual and J. Elorza 1998. Cenomanian events in the deep western Basque Basin: the Leioa section. Cretaceous Research, v. 19, no. 6, p. 673-700.

Rutten, R.F.X. 1985. Geological, geochemical and petrophysical study of the production potential of the Natih-B Member (Natih field, northern Oman), Unpublished Work. Petroleum Development Oman, Exploration Department, Report RKTR 85.271, 115 p.

Sansone, F.J., G.W. Tribble, C.C. Andrews and J.P. Chanton 1990. Anaerobic diagenesis within Recent, Pleistocene, and Eocene marine carbonate frameworks. Sedimentology, v. 37, no. 6, p. 997-1009.

Schwab, A.M., P.W. Homewood, F.S.P. van Buchem and P. Razin 2005. Seismic forward model of a Natih Formation outcrop: the Adam Foothills Transect (northern Oman). GeoArabia, v. 10, no. 1, p. 17-44.

Scott, R.W. 1990. Chronostratigraphy of Cretaceous carbonate shelf, southeastern Arabia. In, A.H.F. Robertson, M.P. Searle and A.C. Ries (Eds.), The Geology and Tectonics of the Oman Region. Geological Society, Special Publication 49, p. 89-108.

Sharief, F.A., K. Magara and H.M. Abdulla 1989. Depositional system and reservoir potential of the Middle Cretaceous Wasia Formation in central-eastern Arabia. Marine and Petroleum Geology, v. 6, no. 4, p. 303-315.

Short, F., T. Carruthers, W. Dennison and M. Waycott 2007. Global seagrass distribution and diversity: a bioregional model. Journal of Experimental Marine Biology and Ecology, v. 350, no. 1-2, p. 3-20.

Smith, A.B., M.D. Simmons and A. Racey 1990. Cenomanian echinoids, larger foraminifera and calcareous algae from the Natih Formation, central Oman Mountains. Cretaceous Research, v. 11, no. 1, p. 29-69.

Suchanek, T.H., S.L. Williams, J.C. Ogden, D.K. Hubbard and I.P. Gill 1985. Utilization of shallow-water seagrass detritus by Carribbean deep-sea macrofauna: $\delta^{13}C$ evidence. Deep Sea Research Part A, Oceanographic Research Papers, v. 32, no. 2, p. 201-214.

Taylor, K.G. and J.H.S. Macquaker 2000. Early diagenetic pyrite morphology in a mudstone-dominated succession: the Lower Jurassic Cleveland Ironstone Formation, eastern England. Sedimentary Geology, v. 131, no. 1-2, p. 77-86.

Terken, J.M.J. 1999. The Natih petroleum system of North Oman. GeoArabia, v. 4, no. 2, p. 157-180.

Tyson, R.V. 1995. Sedimentary Organic Matter: Organic Facies and Palynofacies. Chapman & Hall, 615 p.

Tyson, R.V. 2005. The "productivity versus preservation" controversy: cause, flaws, and resolution. In, N.B. Harris (Ed.), The Deposition of Organic-Carbon-Rich Sediments: Models, Mechanisms, and Consequences. SEPM (Society for Sedimentary Geology), Special Publication 82, p. 17-33.

Vahrenkamp, V. 2010. Albian to Turonian chemostratigraphy of the Eastern Arabian Plate (abstract). EAGE 2nd Arabian Plate Geology Workshop: Albian/Cenomanian/Turonian Carbonate-Siliciclastic Systems of the Arabian Plate. Abu Dhabi, United Arab Emirates, European Association of Geoscientists & Engineers.

Vahrenkamp, V. (in review). Carbon isotope signatures of Cretaceous shallow-water carbonates from Oman: improved stratigraphic resolution and key for regional correlations.

van Buchem, F.S.P., A.Y. Huc, B. Pradier and M. Stefani 2005. Stratigraphic patterns in carbonate source-rock distribution: second-order to fourth-order control and sediment flux. In, N.B. Harris (Ed.), The Deposition of Organic-Carbon-Rich Sediments: Models, Mechanisms, and Consequences. SEPM (Society for Sedimentary Geology), Special Publication 82, p. 191-223.

van Buchem, F.S.P., P. Razin, P.W. Homewood, W.H. Oterdoom and J. Philip 2002. Stratigraphic organization of carbonate ramps and organic-rich intrashelf basins: Natih Formation (middle Cretaceous) of northern Oman. American Association of Petroleum Geologists Bulletin, v. 86, no. 1, p. 21-53.

van Buchem, F.S.P., P. Razin, P.W. Homewood, J.M. Philip, G.P. Eberli, J.P. Platel, J. Roger, R. Eschard, G.M.J. Desaubliaux, T. Boisseau, J.P. Leduc, R. Labourdette and S. Cantaloube 1996. High-resolution sequence stratigraphy of the Natih Formation (Cenomanian/Turonian) in northern Oman: distribution of source rocks and reservoir facies. GeoArabia, v. 1, no. 1, p. 65-91.

Varban, B.L. and A.G. Plint 2008. Palaeoenvironments, palaeogeography, and physiography of a large, shallow, muddy ramp: Late Cenomanian-Turonian Kaskapau Formation, western Canada foreland basin. Sedimentology, v. 55, no. 1, p. 201-233.

Voigt, S. 2000. Cenomanian-Turonian composite $\delta^{13}C$ curve for Western and Central Europe: the role of organic and inorganic carbon fluxes. Palaeogeography, Palaeoclimatology, Palaeoecology, v. 160, no. 1-2, p. 91-104.

Warburton, J., T.J. Burnhill, R.H. Graham and K.P. Isaac 1990. The evolution of the Oman Mountains foreland basin. In, A.H.F. Robertson, M.P. Searle and A.C. Ries (Eds.), The Geology and Tectonics of the Oman Region. Geological Society, Special Publication 49, p. 419-427.

Weedon, G.P. 1986. Hemipelagic shelf sedimentation and climatic cycles: the basal Jurassic (Blue Lias) of South Britain. Earth and Planetary Science Letters, v. 76, no. 3-4, p. 321-335.

Weedon, G.P., A.L. Coe and R.W. Gallois 2004. Cyclostratigraphy, orbital tuning and inferred productivity for the type Kimmeridge Clay (Late Jurassic), Southern England. Journal of the Geological Society, v. 161, no. 4, p. 655-666.

Wetzel, A. and A. Uchmann 1998. Biogenic sedimentary structures in mudstones - an overview. In, J. Schieber, W. Zimmerle and P. Sethi (Eds.), Shales and Mudstones, Volume I: Basin Studies, Sedimentology, and Palaeontology. E. Schweizerbart'sche Verlagsbuchhandlung, p. 351-369.

Chapter 4

High-resolution lithofacies analyses of predominantly fine-grained carbonates in and around an intrashelf basin: an example from the Upper Cretaceous Natih-B Member source rock, North Oman

Said A.K. Al Balushi, Joe H.S. Macquaker, and Cathy Hollis

4.1. Abstract

Intrashelf basins occur on epeiric carbonate platforms and are commonly filled with fine-grained, organic-carbon-rich carbonate sediments and may form the heart of prolific petroleum systems. Most researchers assume that organic-carbon enrichment in these units is a function of high primary production linked to the presence of persistent bottom-water anoxia and low-energy suspension-settling processes. It is, thus, assumed that the fill in these basins adopts a layer-cake stacking pattern controlled by variations in primary production, existence of bottom-water anoxia, and changing rates of sediment accumulation. This study focuses on the processes that underpin organic-carbon enrichment in the Cenomanian-aged Natih-B Member (up to 40-m thick source-rock interval, average about 4% total organic carbon [TOC]) that have sourced hydrocarbons to the adjacent Natih Formation reservoirs.

Over 300 samples from the Natih-B succession in North Oman (Natih field and Adam Foothills) have been analysed by combined optical and electron-optical petrography, in addition to whole-rock geochemistry (TOC and X-ray diffraction [XRD]) and hand-specimen descriptions. The majority of the carbonate sediments encountered in this succession have mudstone through to packstone textures, and are composed predominantly of biogenic-calcite test debris and replacive and pore-filling calcite, together with a subordinate fraction composed of organic matter (amorphous and woody), detrital quartz, detrital clay, authigenic pyrite, authigenic dolomite and phosphatic debris. Nine lithofacies

were recognised in the Natih-B succession. These facies preserve the transition from proximal lagoon and inner-ramp sediments (deposited in < 10 m of water depth) to distal outer-ramp and intrashelf-basin sediments (deposited in 40 to 60 m maximum water depth), with the latter being the most abundant.

Detailed descriptions of the sedimentary structures and constituents of these sediments, especially organic-matter-bearing pelagic mudstones-wackestones (commonly described as "monotonous black shales") uncovered significant textural and mineralogical variability at centimetre to sub-millimetre scales. In particular, inclined lenticular laminae, faecal pellets, burrow fabrics, reworked shell fragments, fragmented planktonic foraminifera and disarticulated coccolith plates indicates that many of these pelagic sediments were in fact emplaced, at least partially, by episodic and advective processes, instead of being deposited directly from suspension settling under low-energy conditions. These sediments were then subsequently reworked locally by bottom currents and disrupted by diminutive burrowing organisms living at the sediment/water interface. Bioturbation, although subtle, is common in most of units, which also contain evidence of in-place fauna suggesting that during deposition, bottom-water conditions were probably oxic to dysoxic. These sediments, following compaction, developed thin depositional beds (partings) that could be mistakenly identified as depositional laminae.

Given these observations, the preservation of organic matter (up to 13.7% TOC) in these sediments was mainly a result of high primary organic production coupled with episodic and rapid sedimentation and burial, rather than existence of bottom-water anoxia. In contrast, extensively-bioturbated, pervasively-cemented horizons, typically present at the tops of shallowing-upward sequences, are interpreted to occur when local rates of sedimentation and burial rates were very slow, allowing bacterial organogenic processes to operate and provide solutes for calcite cementation in uncompacted pore-space. The common occurrence of assemblages of reworked shell fragments associated with units that exhibit a normally-graded motif and bioturbated tops indicates that these units are likely distal tempestites. Furthermore, comparisons between Natih-B samples from different locations indicate that there is considerable lateral lithofacies variability reflecting changes in sediment supply and absolute bathymetry, in addition to local changes in primary production (both organic and inorganic), sediment accumulation rates and early diagenesis. Therefore, the paradigm for organic-matter preservation needs to be significantly modified.

4.2. Background and Introduction

Intrashelf (or intraplatform) basins are relatively shallow depressions (< 100 m maximum water depth), frequently developed within regionally-extensive epeiric carbonate platforms along passive continental margins (Markello and Read, 1982; Read, 1982; Read, 1985; Aigner et al., 1989; Burchette and Wright, 1992; Grover, 1993; Droste, 2003). They commonly form during major rises in relative sea level, with their vertical relief being enhanced by varying rates of biogenic productivity and carbonate sedimentation (Read, 1982; Read, 1985; van Buchem et al., 2002b; Droste and Van Steenwinkel, 2004), and perhaps differential compaction (Hunt et al., 1996; Saller, 1996), rather than strong tectonic subsidence. These basins are generally short-lived (in the order of 3 to 10 my) and are predominantly filled with carbonate mudstones (Markello and Read, 1982; Droste, 1990; Burchette and Wright, 1992; Grover, 1993; van Buchem et al., 2002a; Droste and Van Steenwinkel, 2004). They reflect the effects of surface-water production and early diagenesis within an offshore setting exposed to episodic influxes of coarser-grained carbonate debris that were washed from the surrounding platform by episodic storms (Al Balushi and Macquaker, in press).

Intrashelf basins are known throughout the Phanerozoic sedimentological record; examples occur in the Precambrian of Canada (Grotzinger, 1989), Cambrian of USA (Markello and Read, 1982), Devonian of Canada (van Buchem et al., 2005), and Mesozoic of the Middle East (e.g. Murris, 1980; Droste, 1990; Alsharhan, 1995; Al-Saad and Sadooni, 2001; van Buchem et al., 2002b; Sadooni and Alsharhan, 2004). The Holocene carbonate shelf of southern Belize (Grover, 1993; Purdy et al., 2003; Mazzullo, 2006) may provide a modern analogue to ancient intrashelf basins.

The carbonate mudstones in these basins are often enriched in organic carbon, and during burial may act as significant source rocks for hydrocarbon plays in associated facies, particularly shoal/reefal deposits updip (e.g. Murris, 1980; Markello and Read, 1982; Read, 1985; Ward et al., 1986; Droste, 1990; Burchette and Wright, 1992; Alsharhan and Scott, 2000; Al-Saad and Sadooni, 2001; van Buchem et al., 2002a; van Buchem et al., 2005; Taghavi et al., 2007; Homewood et al., 2008). Most authors have argued that the major controls on organic-carbon sequestration in these settings have been the development of

localised and persistent bottom-water anoxia in these restricted, predominantly low-energy depositional environments. These assumptions have been reinforced by the occurrence of apparently "unbioturbated, monotonous shales" preserved in these settings.

Recent investigations utilising high-resolution petrographic and geochemical methods, however, have revealed that many fine-grained sediments contain a great deal of previously unrecognised lithofacies variability, developed at centimetre to sub-millimetre scales (Macquaker et al., 1998; Schieber, 1999; Macquaker and Jones, 2002; Macquaker and Adams, 2003; Schieber, 2003; Macquaker et al., 2007; Al Balushi and Macquaker, in press). Detailed analyses of the textures (e.g. relict thin beds, burrow mottles, faecal pellets, lenticular laminae and scoured surfaces) and their skeletal and mineralogical components, present at these small scales, suggest genetic bed-scale processes (sensu Campbell, 1967). Moreover, it indicates that many of these sediments, rather than being deposited in low-energy settings as a result of a continuous rain of detritus to the sediment/water interface, were actually deposited at least in part by episodic and advective events that, following compaction, generated thin beds (sensu Campbell, 1967) and then were subsequently burrowed by a diminutive infauna. Furthermore, analyses of successive samples within any individual succession and laterally between related successions suggest that there were significant temporal and spatial changes in sediment supply and accommodation.

In the light of these observations, this study aims to investigate the degree of temporal and spatial lithofacies variability within a carbonate intrashelf basin, the controls on organic-carbon preservation in this type of setting, and the main driving mechanisms responsible for lithofacies variability. This study aims to perform high-resolution lithofacies analyses on predominantly fine-grained carbonates in and around an intrashelf basin of a broad and shallow carbonate platform. The Upper Cretaceous (Cenomanian) Natih-B Member of North Oman is used as an ideal example of a natural laboratory as it is both exposed at the surface and supported by a significant volume of subsurface data, including core from other parts of basin (Figure 4.1). To meet these aims, detailed descriptions of all lithofacies present in the Natih-B Member have been generated. The variability present within these samples has then been interpreted within a sequence-stratigraphic/environmental framework.

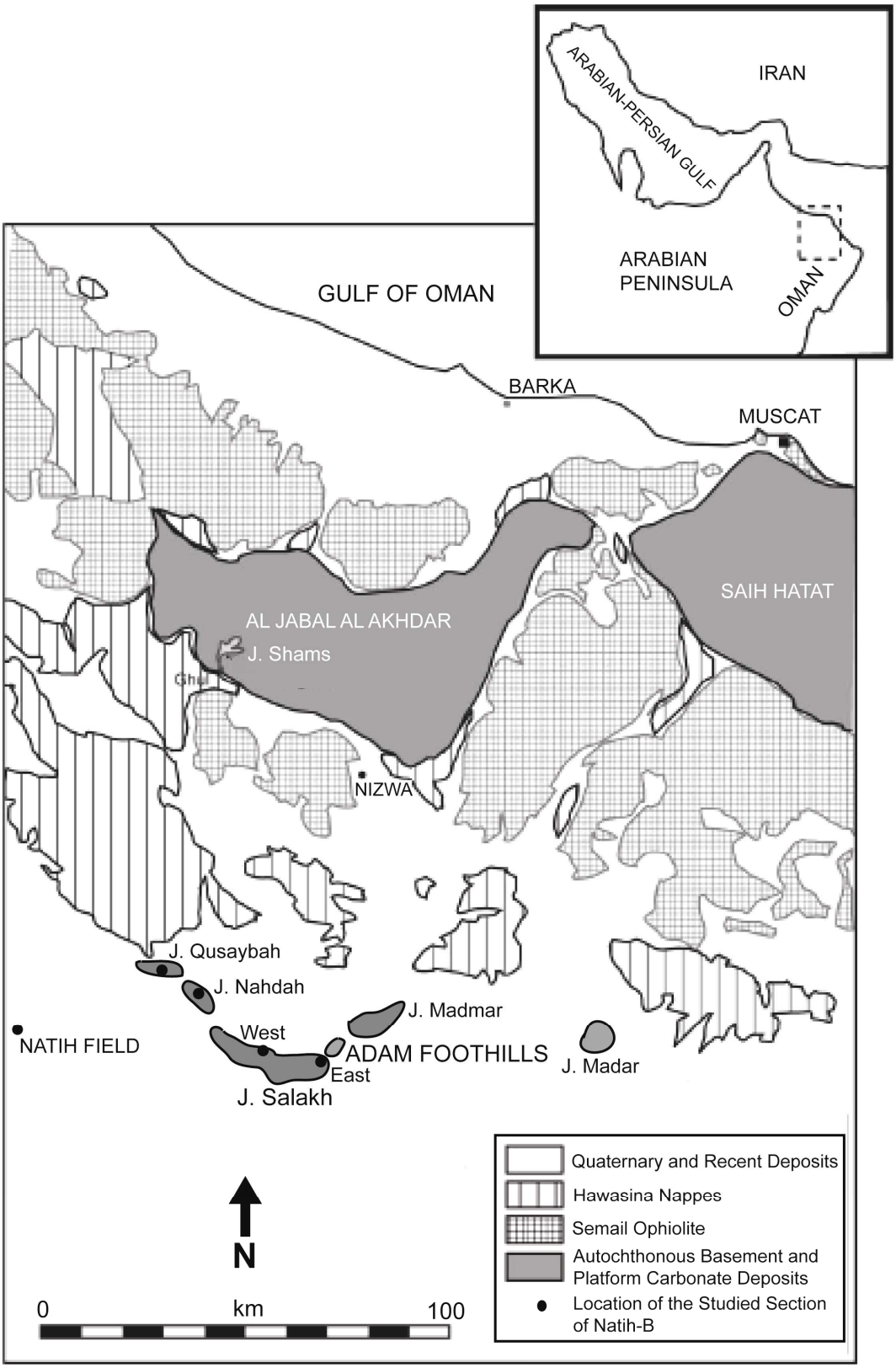

Figure 4.1. Simplified geological map of North Oman (modified from Grélaud et al., 2006). Natih-B Member outcrops are located in the southern flank of the Al Jabal Al Akhdar and in the Adam Foothills. Four outcrop locations in the Adam Foothills (Jabal Salakh East, Jabal Salakh West, Jabal Nahdah, and Jabal Qusaybah) and subsurface core from a well in the nearby Natih field were part of this study, where Natih-B sections were measured and samples werer gathered.

To perform this investigation, 318 samples were collected from an integrated outcrop to core investigation of Natih-B sections in six separate locations, along a dip transect across the basin. The majority of these samples were described using detailed thin-section (including optical and electron-optical), mineralogical (XRD) and geochemical (TOC) techniques. Using this information, a lithofacies depositional model for the Natih-B Member has been constructed at the platform-to-basin scale.

This paper builds upon the previous work by Al Balushi and Macquaker (in press), which focused on the upper part of the Natih-B Member that provided a detailed discussion of the fundamental controls on organic-carbon preservation in carbonate depositional settings.

4.3. Geologic and Stratigraphic Setting of the Natih-B Member

Throughout the Cretaceous, sedimentation on the southern Arabian Plate was dominated by an epeiric carbonate platform in a tectonically-quiescent setting, with only episodic incursions of siliciclastic material (e.g. Murris, 1980; Alsharhan and Scott, 2000; Droste and Van Steenwinkel, 2004; Figure 4.2). A major marine transgression initiated carbonate deposition in the Lower Cretaceous (late Berriasian-Aptian Kahmah Group; Hughes Clarke, 1988) over uplifted, tilted, and subaerially-exposed Jurassic and older strata in North and Central Oman. This large-scale event took place following the separation of South America, Afro-Arabia and Greater India from Gondwana, and the opening of the South Atlantic and Indian oceans (Glennie, 2000; Droste and Van Steenwinkel, 2004).

By the late Aptian, a major drop in relative sea level caused widespread karstification and erosion at the top of the Kahmah Group (Shu'aiba Formation), resulting in the formation of a prominent regional unconformity (Figure 4.2; Hughes Clarke, 1988; Scott, 1990; Droste and Van Steenwinkel, 2004). This change in relative sea level, coupled with local tectonism (Sharief et al., 1989; Droste and Van Steenwinkel, 2004), ended platform-carbonate deposition and facilitated an extensive accumulation of argillaceous/calcareous mudstones of the late Aptian-late Albian Nahr Umr Formation (lower unit of the Wasia Group; Immenhauser et al., 1999).

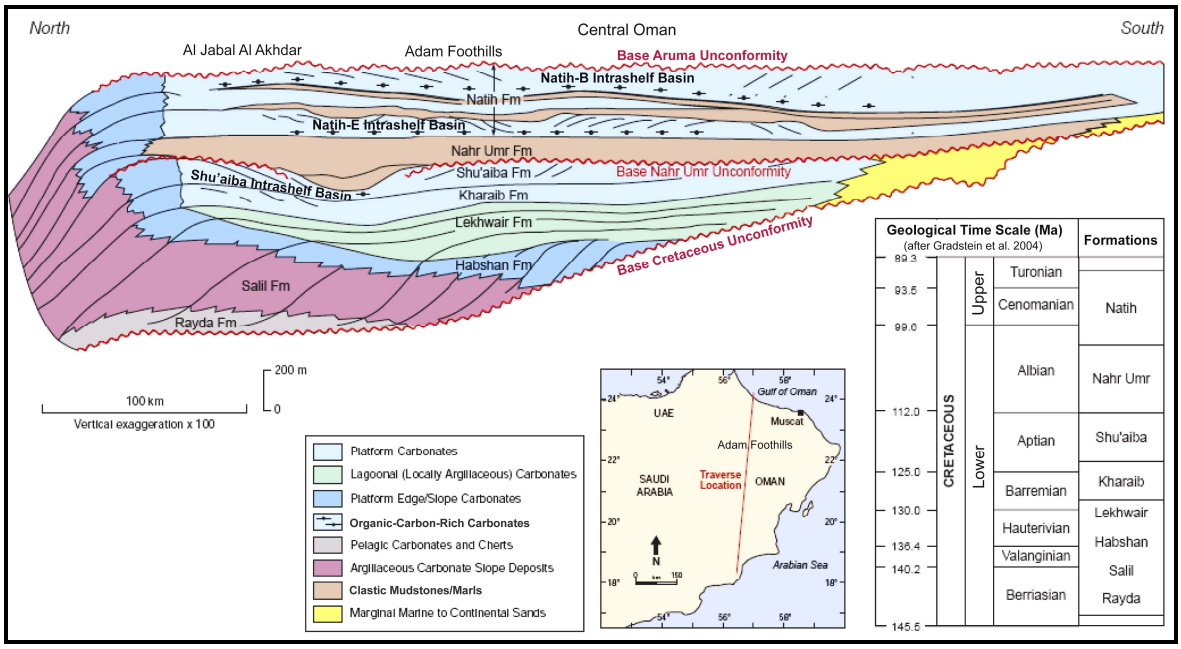

Figure 4.2. Schematic cross section showing the stratigraphy of the Cretaceous carbonate platform in Oman (modified from Homewood et al., 2008; original source: Droste and Van Steenwinkel, 2004). Note the development of three organic-carbon-rich intrashelf basins in the lower Shu'aiba Formation, lower Natih-E and upper Natih-B members (Natih Formation).

From the late Albian to early Turonian, another phase of carbonate-platform growth took place, associated with the deposition of the Natih Formation (upper unit of the Wasia Group) (Scott, 1990; Smith et al., 1990; van Buchem et al., 1996; Droste and Van Steenwinkel, 2004; Homewood et al., 2008; Figure 4.2). Based on wireline-log responses, the Natih Formation is subdivided into seven lithostratigraphic units (members A to G downward, Figure 4.3, Harris and Frost, 1984; Hughes Clarke, 1988; Terken, 1999; Droste and Van Steenwinkel, 2004; among other references). The Natih Formation has also been interpreted in terms of a high-resolution sequence-stratigraphic framework (3 third-order and 14 fourth-order depositional sequences; Grélaud et al., 2006; Figure 4.3), based on the outcrop successions in the southern flank of the Al Jabal Al Akhdar and in the Adam Foothills of North Oman (cf. Philip et al., 1995; van Buchem et al., 1996; van Buchem et al., 2002b). Uplift and erosion in the Turonian stopped the advancement of the 1.2-km thick, 1000-km wide Cretaceous carbonate-platform succession in Oman (van Buchem et al., 1996; Droste and Van Steenwinkel, 2004), enabling the influx of fine-grained clastics of the Fiqa Formation (Aruma Group; Hughes Clarke, 1988) from the Arabian craton.

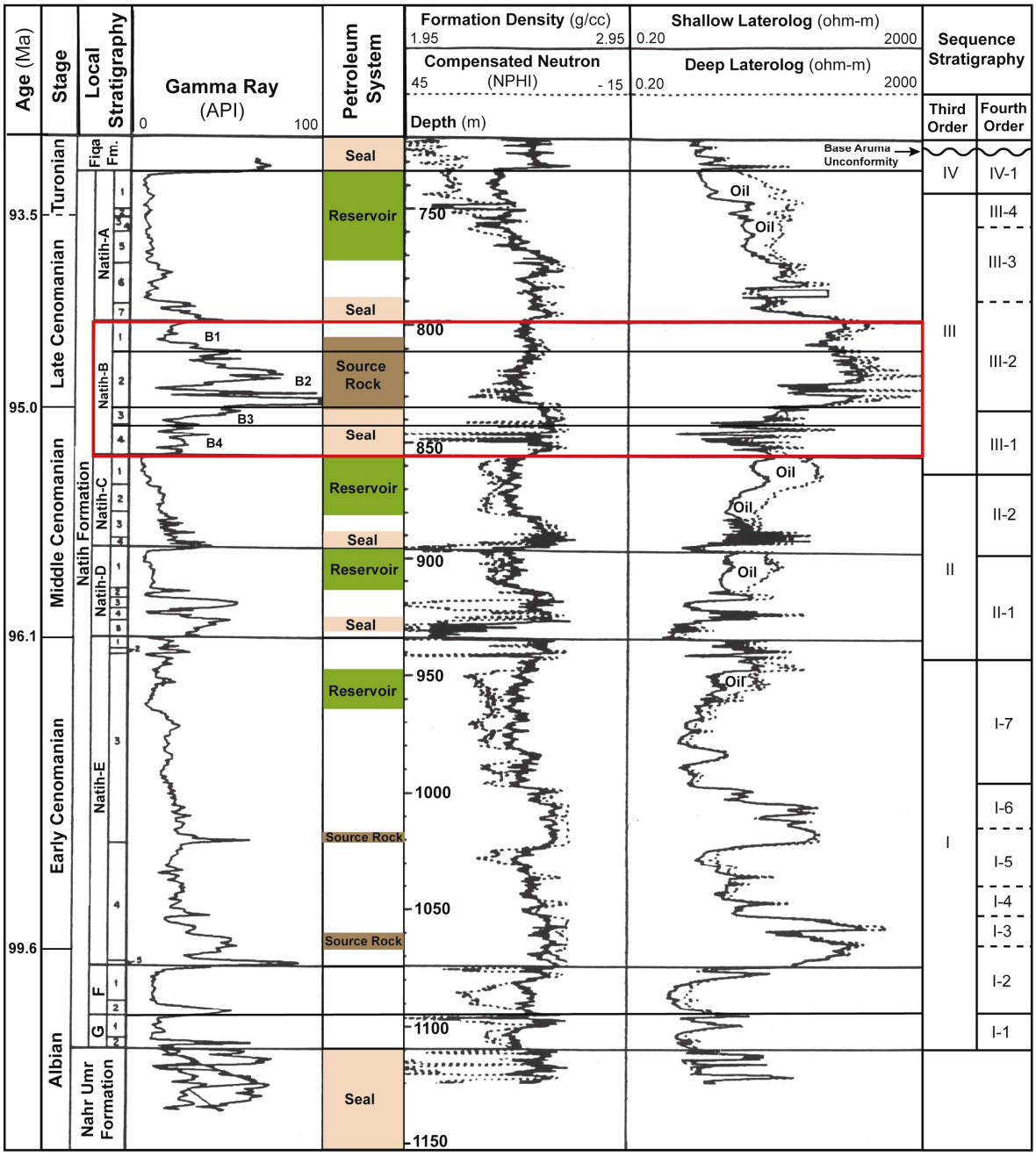

Figure 4.3. Natih Formation type log from a well in the Natih field showing seven lithostratigraphic members (Natih-G to Natih-A) and their subdivisions into lithostratigraphic units based on wireline-log signature. Age determination is based on ammonites (see van Buchem et al., 2005), and absolute ages are after Gradstein et al. (2004). Sequence-stratigraphic interpretation is after Grélaud et al. (2006). Note the distribution of the petroleum-system elements. The Natih-B Member is a major source-rock interval in the Natih Formation, and is subdivided into four lithostratigraphic units (B4 to B1).

Three major clastic-starved, intrashelf depositional basins (40 to 60 m water depth) developed in North Oman during the Cretaceous. These include the early Aptian intrashelf basin of the lower Shu'aiba Formation and the late Albian (lower Natih-E) and late Cenomanian (upper Natih-B) intrashelf basins of the Natih Formation (Figure 4.2; van Buchem et al., 2002a; Droste and Van Steenwinkel, 2004; van Buchem et al., 2005; Homewood et al., 2008). These basins, characterised by significant and widespread accumulations of carbonate source rocks with high values of total organic carbon (TOC; reaching 13.7% in Natih-B), record the outpacing of organic-matter production and accumulation by the creation of accommodation in response to major transgressions. They developed during periods of high relative sea level, in areas with minor topographic depressions and relatively low rates of carbonate-platform growth, which enhanced the accommodation availability (van Buchem et al., 2002a; van Buchem et al., 2002b; Droste and Van Steenwinkel, 2004). Although clinoform geometries for the lower Shu'aiba and lower Natih-E intrashelf basins are well interpreted in seismic lines (see Droste and Van Steenwinkel, 2004; Grélaud et al., 2006; Figure 4.2), these margin geometries are less obvious in the Natih-B; and, therefore, its intrashelf-basin extent is defined by the distribution of the distal, micro- and nanoplankton-rich facies within the carbonate platform. However, the upper Natih-B intrashelf-basinal unit is more important as a source-rock interval because it is more laterally extensive, thicker, and more organic-carbon rich (average about 3.6% TOC and 40 m thickness; Figures 4.2 and 4.3) in comparison to source-rock intervals in the lower Shu'aiba and lower Natih-E intrashelf basins. It is very likely that the Natih Formation reservoirs in the giant Fahud and Natih fields have been sourced by the contiguous carbonate source rocks of the upper Natih-B Member (Grantham et al., 1987; Terken, 1999; Homewood et al., 2008). Examples of time-equivalent (Cenomanian-aged) intrashelf-basinal carbonates to the Natih-B Member in the Middle East region include the Shilaif/Khatiah Formation of UAE, Rumaila Formation of eastern Saudi Arabia, Kuwait and southern Iraq, and upper Sarvak Formation of southwestern Iran (Alsharhan and Nairn, 1988; Burchette, 1993; Aqrawi et al., 1998; van Buchem et al., 2002b; Taghavi et al., 2007).

The Natih-B Member is subdivided in the subsurface into four main lithostratigraphic units (B4 to B1, bottom to top; Figure 4.3), based on gamma-ray readings from wells located in more distal parts of the Natih-B intrashelf basin. The lower and upper units (B4 and B1, respectively) both show relatively low gamma-ray values, varying from 12 to 56 API Units

(average about 25). The B3 unit shows gradually-increasing gamma-ray values from as low as 12 API Units to as high as 70 API Units. The B2 unit is the thickest (up to 30 m thick) and characterised by fluctuating but generally higher gamma-ray readings that can reach up to 140 API Units, and can be as low as 12 API Units (average about 100 API Units). The high gamma-ray values in B2 are generally correspondent to high TOC contents, which can reach up to 13.7%. In this paper, we follow this lithostratigraphic subdivision of the Natih-B Member for both subsurface (Figure 4.3) and outcrop successions, but we further subdivide the B4 into two units (B4-II and B4-I) and the B2 into two units (B2-II and B2-I), based on some lithological characteristics (Figure 4.4).

The outcrop-based sequence-stratigraphic model of van Buchem et al. (2002) illustrates both the Natih-B and Natih-A members to represent one complete third-order cycle (Sequence III; Figure 4.3), with the Natih-B succession comprising the lowstand and transgressive systems tracts, and the Natih-A succession comprising the highstand systems tract. The maximum flooding surface is placed near the top of the Natih-B Member, at the time of maximum transgression and lateral extent of the intrashelf basin (cf. Philip et al., 1995; Sharland et al., 2001; Homewood et al., 2008). At a higher resolution, van Buchem et al. (2002) interpreted two fourth-order cycles, Sequence III-1 (comprising units B4 and B3) and Sequence III-2 (comprising units B2 and B1; Figure 4.3).

4.4. Sampling and Analytical Procedures

4.4.1. Sample Collection Rationale

In order to generate detailed lithofacies descriptions and to determine the spatial and temporal lithofacies variability, a total of 318 Natih-B samples were gathered. These samples were obtained from two distal wells (in the Natih and Yibal fields), two distal outcrop sections (Jabal Qusaybah and Jabal Nahdah), and two marginal outcrop sections (Jabal Salakh West and Jabal Salakh East), forming a dip-oriented transect (roughly west-east direction) in North Oman, to the south of the Al Jabal Al Akhdar (see Figure 4.1). One hundred and twenty eight unweathered samples were collected systematically (every 0.1 to 0.5 m) from a complete subsurface section of a well in the Natih filed, in order investigate the small-scale temporal lithofacies variability. One hundred and eight samples were

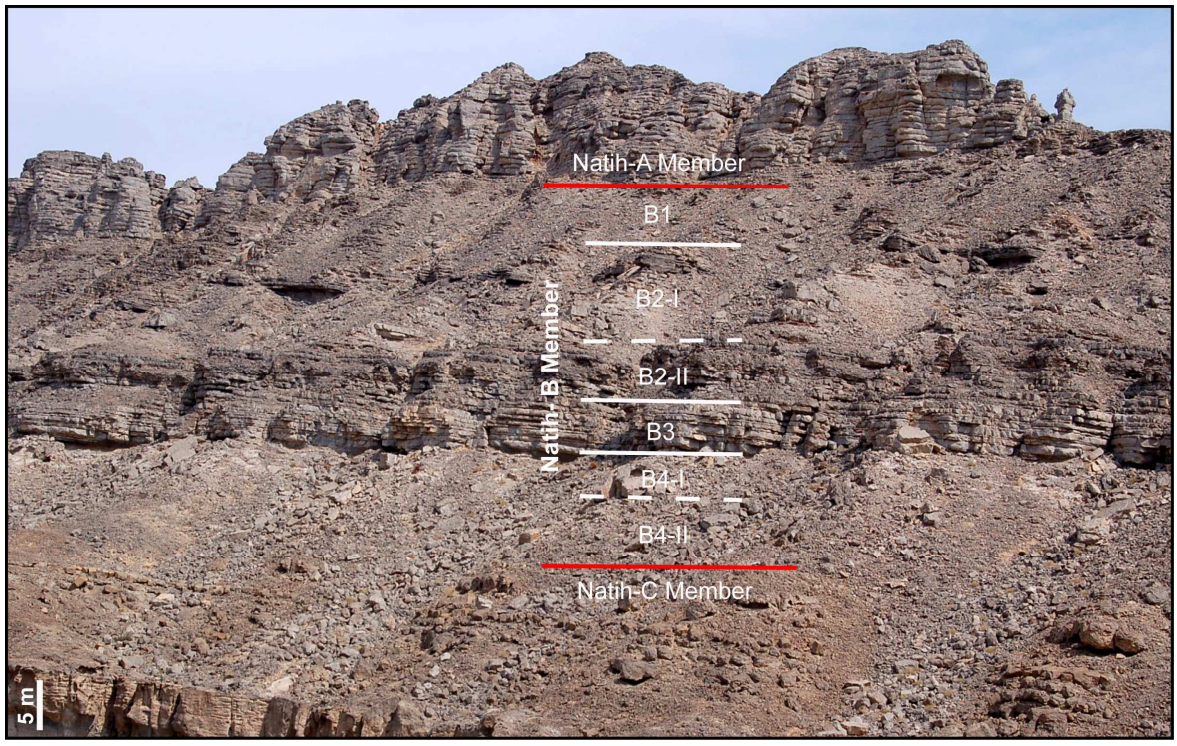

Figure 4.4. Looking NE; outcrop section in Jabal Qusaybah showing the upper half of the Natih Formation (members C to A). The Natih-B Member overlies an extensively-bioturbated, iron-enriched hardground at top Natih-C, and conformably underlies whitish, well-bedded unit of Natih-A. Note also the subdivision of the Natih-B Member here into six units: B4-II and B4-I are poorly exposed; B3 and B2-I are better exposed, thinly bedded and laterally continuous; and B2-I and B1 composed of alternating organic-matter-bearing carbonate mudstone-wackestone and sparry-calcite-rich wackestone-packstone (intrashelf-basinal deposits).

similarly collected from exposures at Jabal Qusaybah (distal location) to facilitate comparison with samples deposited elsewhere in the basin. Samples from the other locations were obtained from laterally-equivalent intervals, in order to assist in the investigation of the lateral lithofacies variability across the carbonate-platform margin and intrashelf basin.

Four graphic sedimentary logs of the 50- to 60-m thick Natih-B Member in the Natih field, Jabal Qusaybah, Jabal Nahdah and Jabal Salakh were constructed at the scale of 1:50 (see Appendix A), complimented by detailed field notes, photographs and sketches. The logs record information on the lithology, grain size, sedimentary structures, and macrofossils and trace fossils (see Figure 4.5). The location and character (at hand-specimen scale) of each sample gathered are also recorded on the logs.

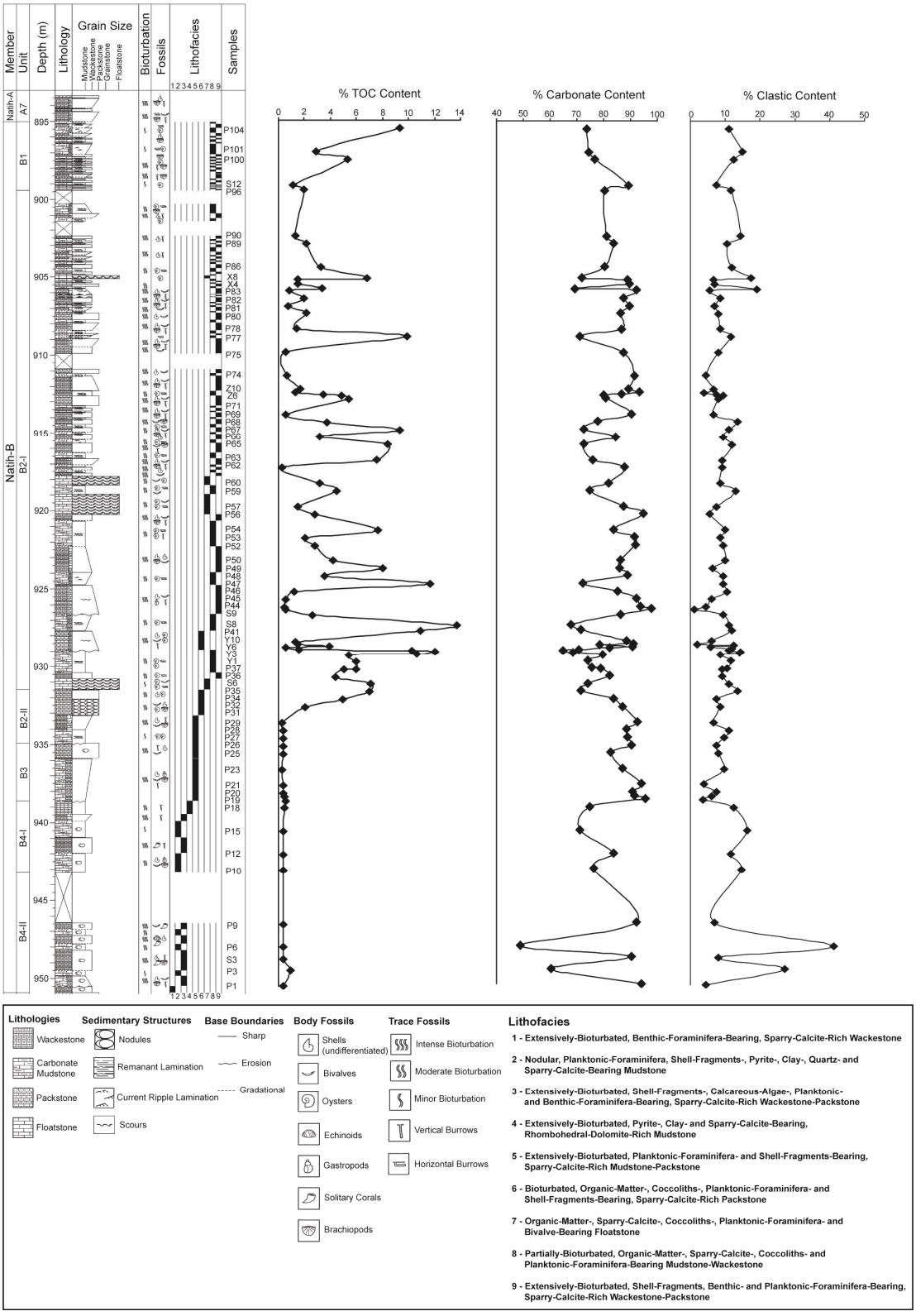

Figure 4.5. Measured section of the Natih-B Member core from a well in Natih field (see Figure 4.1 for location) illustrating the local lithostratigraphy and temporal lithofacies variability, with indication of some sample locations and their TOC (total organic carbon), carbonate (calcite and dolomite) and clastic (quartz and clay) contents. The carbonate and clastic contents were estimated using both XRD data and high-power thin-section micrographs of each sample. Note that the depth referred to here is driller's depth. See also Appendices B and C for more detailed attributes of samples.

From the 318 samples gathered, 286 polished, unusually thin (≤ 30 µm thick) thin sections were prepared. Two hundred and forty seven samples had their TOC (total organic carbon) content determined, and 91 representative samples were chosen for XRD (X-ray diffraction) analyses.

4.4.2. Petrographic Analyses

In order to provide high-resolution lithofacies analyses, all the prepared thin sections were first analysed optically, at low resolution (10^{-2} to 10^{-3} m scale) by scanning each one of them in an Epson Perfection 3170 flatbed scanner to obtain details of textures present. The majority of the thin sections were then analysed petrographically under transmitted light (both plane polarised and cross polarised) and by cold-cathode cathodoluminescence (CL), utilising a Nikon Labophot pol petrographic microscope equipped with a digital camera, to investigate the mineralogical, faunal and floral assemblages, and depositional and diagenetic features at the scale of 10^{-3} to 10^{-4} m. A CITL Cathodoluminescence Unit (Model CCL 8200 MK3) was used to perform the cold-cathode CL, operated at approximately 20 kV and 300 µA. At last, high-resolution (10^{-4} to 10^{-5} m scale), backscattered electron imagery were performed on 133 thin sections, utilising a JOEL 6400 SEM (scanning electron microscope) equipped with a Link 4-Quadrant, solid-state, backscattered electron detector and PGT energy-dispersive, semiquantitative, X-ray spectrometer, which helped in confirming mineral identity. Operating conditions were at 20 kV and 2 nA, with 15 mm working distance. A number of images from each thin section were captured at a set of scales using a Semafore digital framestore that is in connection with the SEM. The components present in each sample were semiquantified with reference to grain size abundance charts (e.g. Flügel, 2004).

In addition, 34 uncovered thin sections were chemically stained with a combined Alizarin Red S and potassium ferricyanide solution, to help distinguish calcite cements/replacements from dolomite cements/replacements, and also to determine proportions of Fe substitution of Ca in the carbonate cement/replacement lattice (see Dickson, 1965; Adams and Mackenzie, 1998). The solution was prepared, firstly, by separately adding 100.0 mL of 1.5% HCl to 0.2 g of Alizarin Red S and 2 g of potassium ferricyanide, and then mixing the two solutions together. Then each thin section was immersed in the mixture of solutions for 30 to 45 seconds and then washed gently in

running water for a few seconds.

4.4.3. TOC Analyses

The TOC measurements were performed at Manchester Metropolitan University (UK). Prior to each analysis, the powdered bulk samples were reacted with 1.0 M HCl to remove all carbonate. After that, the total carbon (TC) contents of the acid-treated samples were obtained utilising a LECO TruSpec CN analyser, equipped with an induction furnace that burned the samples at 950˚C. The TC contents of these acid-treated samples are considered to represent the TOC contents, assuming that all the carbonate carbon has been removed and carbon contents obtained are of organic carbon. The results of these analyses have a precision of ±0.1%.

4.4.4. XRD Analyses

The XRD analyses were performed in order to determine the bulk-rock mineralogy of some samples. A Philips PW1730 X-ray diffractometer was used during these analyses, operated at 40 kV and 20 mA, utilising a copper Kα radiation.

The data utilising these techniques are integrated below (see also Appendices B and C).

4.5. Lithofacies Present

The initial rock descriptions obtained from the 286 thin sections allowed nine lithofacies to be identified in the studied succession. These predominantly fine-grained carbonates were described using the terminology broadly outlined in Dunham (1962), Embry and Klovan (1971), and Macquaker and Adams (2003). The detailed attributes of each lithofacies are described and interpreted below.

It is also worth mentioning here that these lithofacies are more or less pervasively replaced and cemented by carbonate. It is beyond the scope of this paper to discuss in detail the processes controlling the diagenesis in the Natih-B Member. However, as mentioned in

this study, there is enough material (e.g. body and trace fossils) being preserved in the Natih-B sediments that can enable their depositional-environment interpretations.

4.5.1. LF1: Extensively-Bioturbated, Benthic-Foraminifera-Bearing, Sparry-Calcite-Rich Wackestone

4.5.1.1. Description

LF1 is mainly developed at the base of the Natih-B Member (base of B4 unit; Figures 4.4 and 4.5). The contact between the Natih-C and Natih-B is sharp and planar, with local iron staining (Figure 4.4) and bivalve borings. LF1 forms light-grey, nodular, extensively-bioturbated wackestone horizon (Figure 4.6a and b), up to 0.4 m thick. Burrowing here is predominantly attributed to *Thalassinoides* isp (Figure 4.6a). Bedding is indistinct in this lithofacies and no other sedimentary structures are apparent (Figure 4.6a to d). The rock is mainly composed of calcite spar (~ 88.6%, both ferroan and nonferroan, occurring both in the shelter and intergranular porosity) and fairly-diverse, uncompacted benthic foraminifera (Figure 4.6c and d), together with some peloids and calcareous algal fragments (including gymnocodiacean algae), minor fine-grained detrital quartz (~ 4.5%) and rare shell fragments (including rudist and other indeterminate bivalve fragments that were bored and abraded (Figure 4.6d), as well as disarticulated ostracods and echinoderm debris), in addition to very rare pyrite (~ 1.0%; mostly framboidal) and amorphous organic matter with up to 0.4% TOC (Figure 4.6c to f).

Identified species of the benthic foraminifera include both calcareous forms (miliolids [Figure 4.6c and d], miliolinid alveolinids [*Praealveolina* spp. and *Cisalveolina* spp.; Figure 4.6d], *Aeolisaccus* spp., *Nezzazata conica, N. simplex*, *Idalina* spp., *Nummolofallotia apula* and other indeterminate calcareous benthics) and agglutinated forms (*Chrysalidina* spp., *Dicyclina* spp., *Marssonella* spp. *Nautiloculina* spp. and *Pseudolituonella reicheli*). Peloids are mainly composed of silt-sized, ovoid micritic lumps (Figure 4.6c and d), which may be derived from reworking of lime muds or from micritisation of shell material.

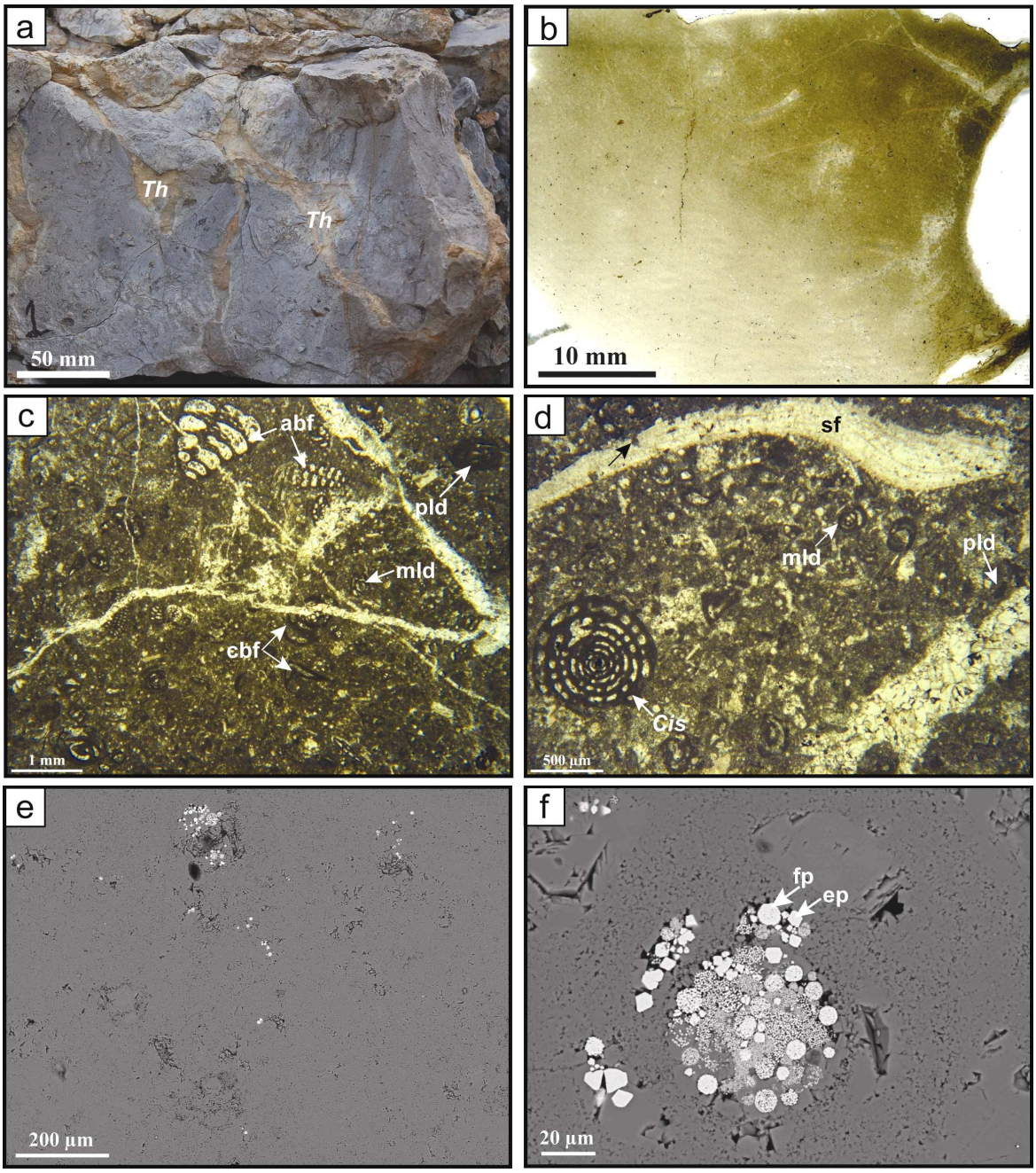

Figure 4.6. (a) Outcrop photograph of LF1 from Jabal Nahdah illustrating extensively-bioturbated (predominantly attributed to *Thalassinoides* isp. [*Th*]), well-cemented and replaced wackestone with reworked shell fragments. **(b)** Thin-section scan of the same lithofacies from a well in Natih field (sample P1; see Figure 4.5 for sample location). Note the homogenous texture of this lithofacies, with some sparry-calcite-cemented microfractures and shell fragments. **(c), (d)** Low-power optical micrographs, both under plane-polarised light (PPL), illustrating some of the microfossil components of LF1 that include both calcareous (cbf) and agglutinated (abf) benthic foraminifera, and calcareous algal fragments, together with peloids (pld). Note the common occurrence of miliolids (mld, in both [c] and [d]) and presence of *Cisalveolina* sp. (*Cis*) in (d). Note also the bored (arrowed) and abraded shell fragment (sf) in (d). **(e), (f)** High-power, backscattered, electron-optical micrographs illustrating the matrix components of LF1, dominated by sparry and finely-crystalline ("microspar") calcite. Note the presence of pyrite (both framboidal [fp] and euhedral [ep]).

LF1 exhibits some microfractures (Figure 4.6b and c) that are pervasively filled with sparry ferroan calcite cement. The matrix of this lithofacies is dominated by both ferroan and nonferroan microcrystalline calcite ("microspar").

4.5.1.2. Interpretation

The sharp surface with iron staining and borings at the top of the Natih-C Member suggests a submarine hardground that formed during a dynamic bypass (Connally and Scott, 1985; Immenhauser et al., 2000), and indicates that the contact between Natih-C and Natih-B is unconformable, consistent with its interpretation as a sequence boundary (e.g. van Buchem et al., 1996). The frequent occurrence of mixed agglutinated and calcareous benthic foraminifera (including miliolids and *Nezzazata* spp.), together with peloids and calcareous algae, and the lack of microplankton and nanoplankton in LF1 suggest that deposition occurred in a proximal, inner-platform environment, within the photic zone (above fair-weather wave base, < 20 m water depth). This is probably indicative of an inner-platform, subtidal lagoon setting (sensu Burchette and Britton, 1985; Robertson, 1998; van Buchem et al., 2002a; van Buchem et al., 2002b; Flügel, 2004) with high enough energy conditions to rework some of the algal and shell fragments.

The extensive bioturbation and occurrence of bored shells indicate that sedimentation rate was very slow during deposition of LF1, which prolonged the residence time at the sediment/water interface allowing these shells to be bored and sediment to be bioturbated extensively. This slow sedimentation rate also enhanced the early calcite cementation (evidence from uncompacted, pervasively-cemented shells and presence of pyrite) in this unit.

4.5.2. LF2: Nodular, Planktonic-Foraminifera, Shell-Fragments-, Pyrite-, Clay-, Quartz- and Sparry-Calcite-Bearing Mudstone

4.5.2.1. Description

LF2 is developed in the B4 unit, in alternation with LF3 (Figure 4.3). Horizons that comprise LF2 are easily distinguished in the core by their predominantly green colour and

argillaceous carbonate mudstone texture, with some whitish, carbonate-cemented nodules (Figure 4.7a). These horizons vary in thickness from 0.35 to 1.05 m, average about 0.56 m. At the exposures, LF2 is hardly recognised, probably due to weathering and erosion of these soft, muddy horizons. Bioturbation by locally-sparse *Thalassinoides* isp. and *Chondrites* isp. is present within certain horizons. Microtexturally, the rock is characterised by the development of solution seams, with clay minerals concentrated along them, showing some sort of wispy lamination ('horse tail' structures; Figure 4.7a, b and e).

The rock is mainly composed of nonferroan sparry calcite (average 49.8%), fine-grained detrital quartz (up to 29.9%, average 13.0%), detrital clay and mica (average 11.8%, including kaolinite and muscovite), pyrite (average 10.0%, both framboidal and euhedral), shell fragments and nonkeeled planktonic foraminifera, together with minor algal fragments, nonferroan dolomite rhombs (average 4.4%), benthic foraminifera (Figure 4.7) and K-feldspar (albite), in addition to very rare fish debris (average 0.6%), organic matter (average 0.5% TOC, predominantly woody type), pyritised wood fragments and calcispheres.

The nonferroan sparry calcite occurs mostly as cement in the shelter porosity and microfractures, and as microspar replacement in the rock matrix (Figure 4.7e and f). The shell fragments assemblage in LF2 is mainly from bivalves (oysters and other indeterminate bivalves) with rare echinoderms (including echinoid spines and plates), ostracods (mostly disarticulated), and brachiopods. The planktonic foraminifera include mainly *Hedbergella* spp. (including *H. planispira*) and *Heterohelix* spp., with rare *Praeglobotruncana* spp. The benthic foraminiferal assemblage includes both calcareous forms (miliolinid alveolinids, *Gavelinella* spp. and scarce miliolids) and agglutinated forms (*Ammobaculites* spp., *Arenobulimina* spp., *Buccicrenata hedbergi*, *Chrysalidina* spp. and *Dicyclina* spp.). The calcareous algal fragments are mostly of gymnocodiacean algae.

4.5.2.2. Interpretation

LF2, lacking extensive bioturbation and comprising some shell fragments and nonkeeled planktonic foraminifera, together with a few mixed benthic foraminifera and calcareous algae, was probably deposited in a proximal inner-platform environment, above fair-

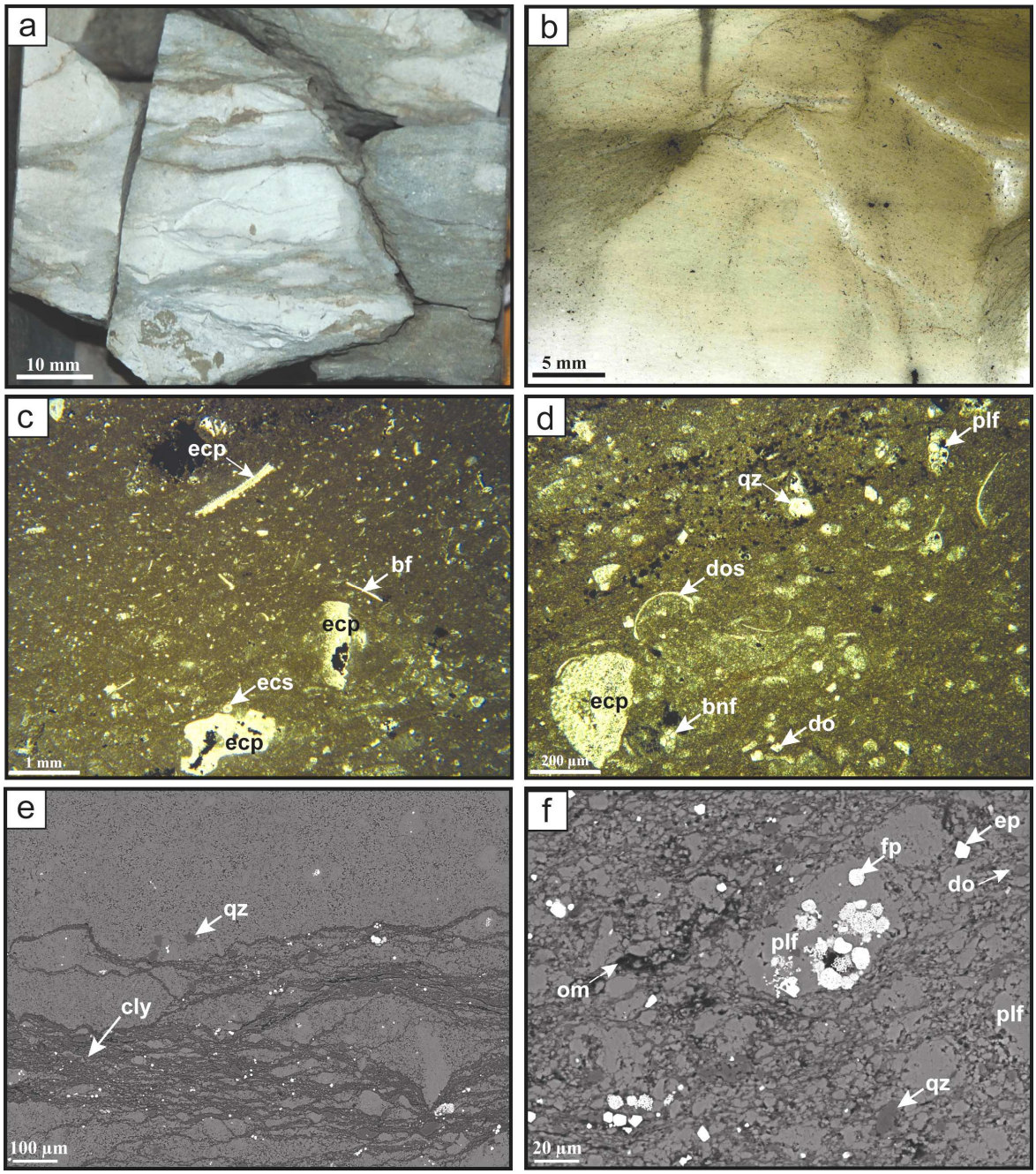

Figure 4.7. (a) Core photograph of LF2 (sample P6; see Figure 4.5. for sample location and other characteristics) showing nodular, greenish, argillaceous carbonate mudstone. Note the wispy lamination from clay concentration. **(b)** Thin-section scan, close-up from (a), illustrating homogenous texture with some solution seams and sparry-calcite-cemented fractures. **(c)**, **(d)** Low-power optical micrographs, both under PPL, illustrating some microfossil components, including both planktonic (plf) and benthic (bnf) foraminifera, calcareous algal and shell fragments (including bivalve fragments [bf], disarticulated ostracods (dos), echinoid plates [ecp] and echinoid spines [ecs]). Note the common occurrence of pyrite (black material), and the presence of rhombohedral dolomite (do) and detrital quartz (qz). **(e)**, **(f)** High-power, backscattered, electron-optical micrographs illustrating the matrix components of LF2, comprising nonferroan microcrystalline calcite ("microspar"), together with detrital clay (cly) and quartz (qz), framboidal pyrite (fp), euhedral pyrite (ep), dolomite (do) and organic matter (om). Note also the pervasively sparry-calcite-cemented planktonic forams, associated in places with pyrite.

weather wave base, under relatively less-energetic, less-oxygenated conditions (during episodically-subduded wave activity). The abundance of siliciclasitc detritus (quartz and clay), together with the production-derived components (including shell and algal fragments) in this lithofacies might suggest lengthening of the sediment transport path.

This lithofacies is considered to represent the first phase of minor marine transgression in the Natih-B4 unit. The relatively high concentrations of pyrite (average 10.0%) might indicate that LF2 was probably developed as part of a condensed section of an early transgressive systems tract.

The common occurrence of nonferroan carbonate precipitates (including calcite microspar and rhombohedral dolomite) in association with pyrite (both framboidal and euhedral) might indicate that these authigenic carbonates were precipitated during early digenesis as a result of organic-matter degredation ("organodiagenesis", sensu Compton, 1988; Mazzullo, 2000) by bacterial sulphate reduction (e.g., Compton, 1988; Machent et al., 2007). The presence of pyrite as the only early-diagenetic iron mineral in this lithofacies provides further evidence that the process of organodiagenesis was dominated by sulphate reduction (Berner, 1978; Taylor and Macquaker, 2000b).

4.5.3. LF3: Extensively-Bioturbated, Shell-Fragments-, Calcareous-Algae-, Planktonic- and Benthic-Foraminifera-Bearing, Sparry-Calcite-Rich Wackestone-Packstone

4.5.3.1. Description

LF3 is developed throughout the B4 unit (Figure 4.5), interbedded with green argillaceous carbonate mudstone (LF2). It contains whitish and greenish-grey wackestone-packstone horizons, with nodular fabric and intense burrowing (Figure 4.8a and b). These horizons vary in thickness from 0.40 to 1.30 m, average about 0.73 m. Trace fossils here are represented by *Thalassinoides* isp., and their fabric is mostly infilled with fine-grained, greenish, argillaceous carbonate mud (Figure 4.8a and b). Bioturbation becomes increasingly more intense towards the unit tops. Microtexturally, this facies is homogenous (Figure 4.8b), apart from some stylolite fabrics associated with organic matter that cut through some parts of the rock, and few solution seams with clay material (Figure 4.8a).

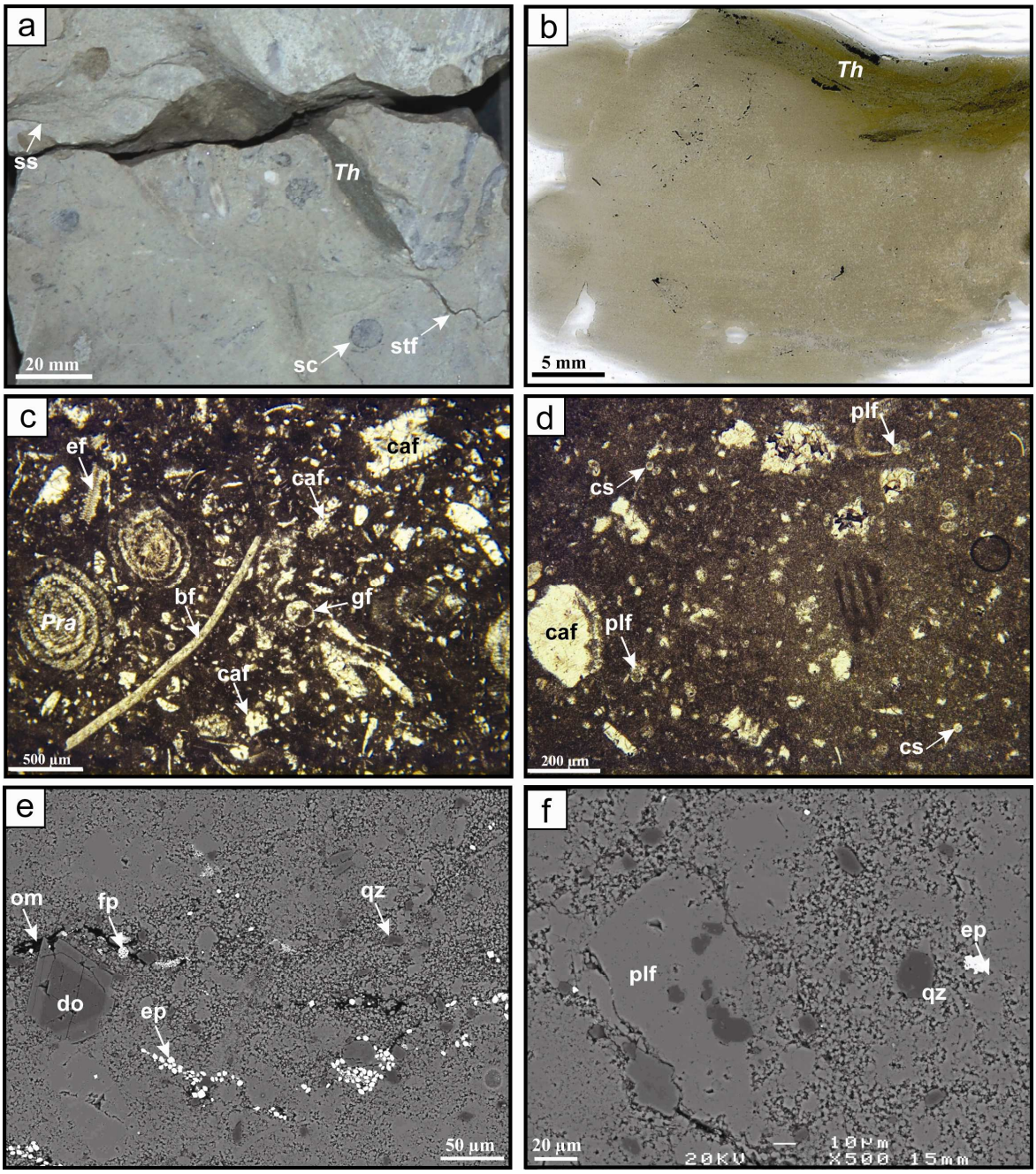

Figure 4.8. (a) Core photograph of LF3 (sample P9; see Figure 4.5 for sample location) showing extensively-bioturbated wackestone-packstone with *Thalassinoides* isp. (*Th*) burrowing, solitary corals (sc), stylolite fabrics (stf), and solution seams (ss) associated with clay. **(b)** Thin-section scan of the same lithofacies illustrating homogenous microtexture. Note the *Thalassinoides* (*Th*) burrow fabric infilled with argillaceous carbonate mud. **(c)**, **(d)** Low-power optical micrographs, both under PPL, illustrating some of the microfossil components of LF3 (sample P9) that include fragments of bivalves (bf), echinoderms (ef), gastropods (gf) and calcareous algae (caf), as well as well as *Praealveolina* spp. (*Pra*), planktonic forams (plf) and calcispheres (cs). **(e)**, **(f)** High-power, backscattered, electron-optical micrographs showing the matrix components of LF3, comprising nonferroan sparry and finely-crystalline ("microspar") calcite, together with detrital quartz (qz), framboidal pyrite (fp), euhedral pyrite (ep), zoned rhombohedral dolomite (do) and organic matter (om). Note the pervasively sparry-calcite-cemented planktonic forams.

LF3 is predominantly composed of nonferroan sparry calcite (average 70.1%), benthic foraminifera, winnowed calcareous algae, reworked shell fragments and nonkeeled planktonic foraminifera, with minor fine-grained quartz (average 7.3%), pyrite (average 2.2%), nonferroan dolomite rhombs (average 2.0%) and clay (average 1.5%), in addition to very rare organic matter (average 0.4% TOC, probably woody type), calcispheres (including *Calcisphaerula innominata*), solitary corals (average 0.5%), fish debris and pyritised wood fragments.

The nonferroan sparry calcite occurs in the shelter and intergranular porosity (predating compaction) and microfractures as sparry cement, as well as in the rock matrix as microspar replacement (Figure 4.8c to f). The benthic foraminifera in this lithofacies are predominantly calcareous (including *Praealveolina* spp. [Figure 4.8c], *Gavelinella* spp. and *Trocholina lenticularis*) and rarely agglutinated (*Textularia* spp.). The planktonic foraminifera occur in the matrix (Figure 4.8c to f), represented mainly by *Heterohelix* spp. and rarely by *Hedbergella* spp. (including *H. planispira*) and *Macroglobigerinelloides bentonensis*. The algal fragments observed in this lithofacies include both gymnocodiacean (*Permocalculus*) and dasycladacean green algae. The shell fragments present include those of bivalves (mostly of oysters with rare incoceramus and rudist fragments), echinoderms, gastropods (Figure 4.8c), and brachiopods, in addition to predominantly disarticulated ostracods.

4.5.3.2. Interpretation

The wackestone-packstone depositional texture and the frequent occurrence of benthic (including *Praealveolina* spp.) and planktonic foraminifera, together with the winnowed algal and shell fragments, and disarticulated ostracods and solitary corals in LF3 all suggest deposition in a proximal inner-platform setting (e.g. Connally and Scott, 1985; Flügel, 2004), just above fair-weather wave base. In this setting, energy conditions were probably moderate to moderately-high, where waves and/or currents were episodically strong enough to concentrate the bioclastic debris, and to possibly enhance internal precipitiation of microcryatalline calcite (e.g. Reid et al., 1990; Reid and Macintyre, 1998).

The common occurrence of large benthic foraminifera and calcareous green and red algae indicates that the sediment/water interface during deposition of LF3 was located in the photic zone. The presence of planktonic foraminifera suggests that the environment was not restricted (i.e. not a lagoon), with high-enough energy conditions to fragment the shells and algae. Furthermore, bioturbated (*Thalassinoides* isp.) surfaces suggest breaks in sediment accumulation and oxic bottom-water conditions (e.g. Philip et al., 1995). The increasing level of bioturbation towards the unit tops indicates a progressive increase of oxygenation throughout individual beds, and that the bed tops are associated with calcite-repalced and cemented hardgrounds (e.g. Ekdale and Bromley, 1991).

4.5.4. LF4: Extensively-Bioturbated, Pyrite-, Clay- and Sparry-Calcite-Bearing, Rhombohedral-Dolomite-Rich Mudstone

4.5.4.1. Description

LF4 is restricted to the uppermost part of the B4 unit (Figure 4.5), making a 0.85-m thick, extensively-bioturbated, greenish, argillaceous, partially-dolomitised, carbonate mudstone horizon (Figure 4.9a), capped by a firmground. Burrowing in this lithofacies may be attributed to *Planolites* isp. (Figure 4.9a and b) and *Thalassinoides* isp. The rock is mainly composed of nonferroan dolomite rhombs (~ 55.0%), together with nonferroan calcite microspar (~ 17.9%), detrital clay and mica (~ 11.0%, including kaolinite and muscovite), and pyrite (~ 10.7%, both framboidal and euhedral). In addition to these major components, LF4 contains very rare shell fragments (including indeterminate bivalves, echinoderms [Figure 4.9c] and disarticulated ostracods debris), fish debris, algal fragments (indeterminate gymnocodiacean algae), indeterminate planktonic foraminifera, and organic matter (0.4% TOC) of indeterminate origin (Figure 4.9e and f).

Dolomitisation, together with bioturbation, in this lithofacies has obliterated all traces of the original rock features (Figure 4.9a and b), especially in its uppermost part. The intensity of this dolomitisation decreases gradually downwards within the B4-I subunit. LF4 characteristically displays a sharp upper contact (partially erosional) and a slightly diffused lower contact. The dolomite rhombs are replacive, nonferroan, nonmimic (fabric-

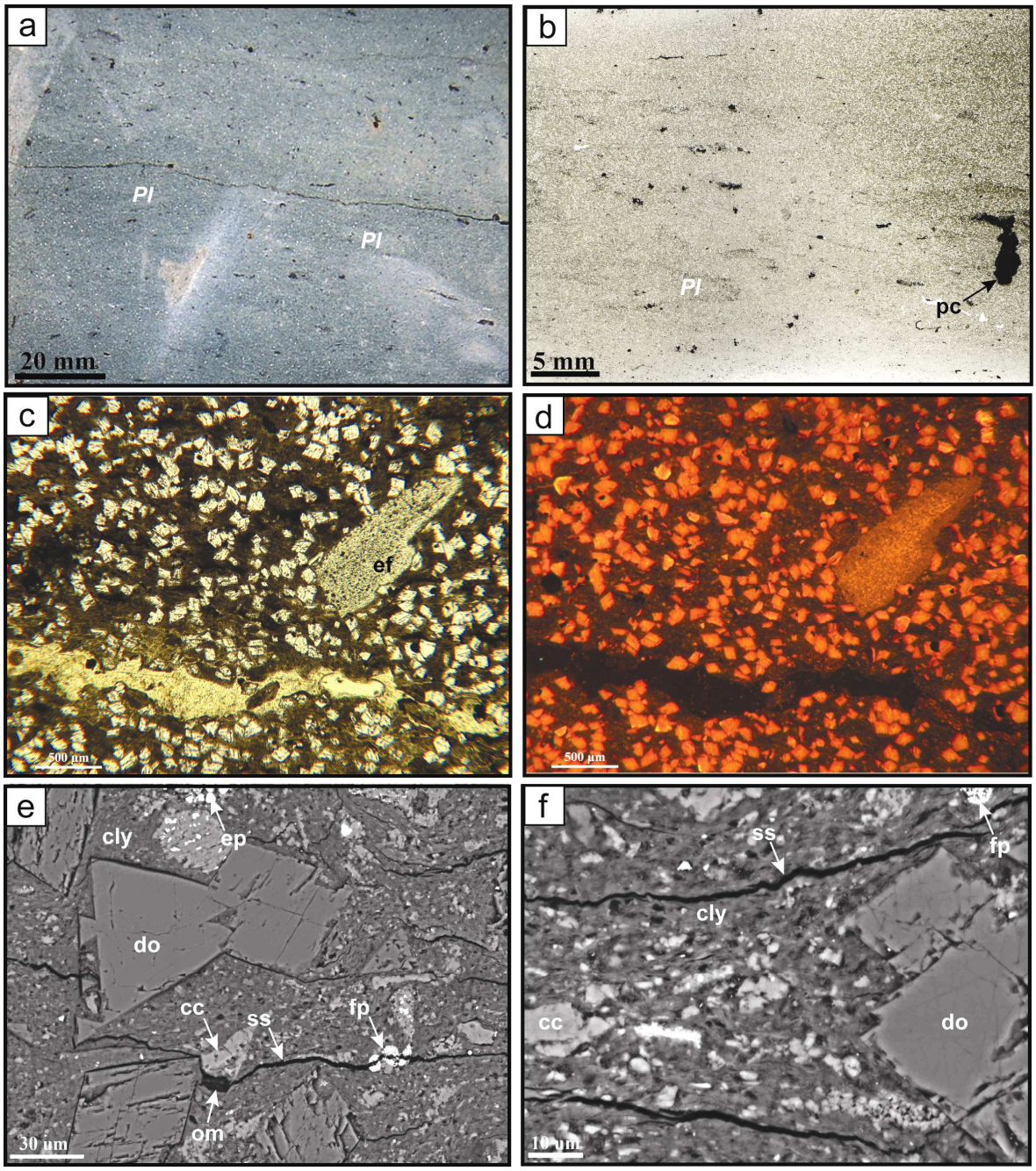

Figure 4.9. (a) Core photograph of LF4 (sample P18; see Figure 4.5 for sample location and other characteristics) displaying greenish, extensively-bioturbated, argillaceous carbonate mudstone. Note the presence of *Planolites* isp. (*Pl*). **(b)** Thin-section scan, close-up from (a), showing the homogenous microtexture of LF4. Note the common occurrence of pyrite concretions (pc). **(c)**, **(d)** Low-power optical micrographs, with (c) under PPL and (d) under CL, illustrating characteristic features of LF4 that include replacive, nonmimic, euhedral, zoned dolomite rhombs (do). Note that some of the dolomite rhombs are being partially replaced by overgrowing pyrite (black material). Note also the unreplaced echinoderm fragment (ef). **(e)**, **(f)** High-power, backscattered, electron-optical micrographs illustrating the matrix of LF4, which in addition to dolomite (do), comprises nonferroan calcite microspar (cc), together with detrital clay (cly; including kaolinite), framboidal pyrite (fp), euhedral pyrite (ep) and organic matter (om). Note how some of the dolomite rhombs and framboidal pyrite are being corss-cut by pressure-solution seams (ss).

destructive), euhedral (planar-e type; sensu Sibley and Gregg, 1987), clear crystals, 50 to 150 µm in size (Figure 4.9c to f). Many were nucleated upon or overgrew and replaced microfossils and matrix components. They show very pale-pink staining colour, suggesting inclusions of precursor nonferroan calcite, in addition to relicts of detrital clays. Some of the dolomite rhombs are partially or completely replaced by overgrowing pyrite (Figure 4.9c and d). Under CL, dolomite rhombs are commonly zoned (dull-luminescent and slightly-luminescent shades of red and orange for the outer zones, with the cores displaying brighter-orange CL; Figure 4.9d). The backscattered electron-optical images show some dolomite rhombs are crosscut by pressure-solution seams (e.g. Figure 4.9e and f).

4.5.4.2. Interpretation

The presence of fine- to medium-crystalline, euhedral, replacive, nonferroan dolomite rhombs, crosscut by solution seams, suggests that dolomitisation occurred during early-stage, shallow-burial (precompaction) diagenesis, at temperatures below 50° to 60 °C (e.g. Friedman, 1964; Dunham and Olson, 1980; Gregg and Sibley, 1984; Kastner, 1984; Taylor and Sibley, 1986; Sibley and Gregg, 1987; Aqrawi et al., 1998; Warren, 2000; Yoo et al., 2000; Scasso et al., 2005; Azmy et al., 2008; Kirmaci, 2008; Rameil, 2008). The zonation revealed by CL indicates that the chemistry of the diagenetic porefluids varied during the dolomitisation process (Azmy et al., 2008). These petrographic features, together with the common occurrence of framboidal pyrite and the depositional context of LF4, suggest that dolomitisation occurred during early burial, close to the sediment/water interface, where dissolved sulphate concentrations were low in the bacterial sulphate reduction zone (e.g. Baker and Kastner, 1981; Wiggins and Harris, 1985; Lee and Friedman, 1987; Compton, 1988; Holail et al., 1988; Purser et al., 1994; Mazzullo, 2000; Teal et al., 2000; Swart et al., 2005; Rameil, 2008). Dolomitisation in this setting is not unknown because the porewaters are sulphate depleted and the surface poisoning effect of sulphate is removed (e.g. Warren, 2000; Whitaker and Smart, 2007).

The process of dolomite formation by bacterial sulphate reduction is very important in a depositional and early-diagenetic setting such that of LF4 as it is responsible for increasing both total alkalinity and pH of porewaters (making them extremely supersaturated), and hence helping provide appropriate geochemical conditions for dolomite to precipitate (Baker and Kastner, 1981; Compton, 1988; Purser et al., 1994; Mazzullo et al., 1995;

Gingras et al., 2004). At the same time, this process is also responsible for the removal of free SO_4^{2-} ions, which potentially inhibit dolomite precipitation by combining these ions with Mg^{2+} ions (Baker and Kastner, 1981; Compton, 1988; Van Lith et al., 2003; Rameil, 2008).

The presence of extensive bioturbation in LF4, associated with early dolomitisation, complicates the interpretations of this unit. However, bioturbation coupled with extensive carbonate precipitation does suggest formation at a stratal surface. Its stratigraphic context, in association with an interval over which the sediment rapidly fines, suggests the presence of a sequence boundary and a capping transgressive flooding surface (sensu Taylor et al., 1995; Taylor et al., 2000; Swart et al., 2005; Macquaker et al., 2007). Under these conditions the uppermost part of the B4 unit was bioturbated in the oxic zone as part of a stratigraphic interval capping a shallowing-upward sequence ("dolomite cap"; sensu Rameil, 2008), and dolomitisation and the change in porewater chemistries were a response to subsequent flooding.

4.5.5. LF5: Extensively-Bioturbated, Planktonic-Foraminifera- and Shell-Fragments-Bearing, Sparry-Calcite-Rich Mudstone-Packstone

4.5.5.1. Description

LF5 is developed in the B3 unit and lower B2-II subunit (Figure 4.5), forming sub-metre thick, whitish- to light-grey horizons (Figure 4.10a). The lower horizons of this lithofacies are predominantly fine-grained with mudstone textures, and the upper horizons are coarser grained with packstone textures (Figure 4.10).

This lithofacies has been extensively bioturbated, with burrowing attributed mostly to *Thalassinoides* isp. and rarely to *Chondrites* isp. and *Planolites* isp. Extensive bioturbation has obliterated all primary sedimentary structures in the rock (Figure 4.10a and b). Moreover, some horizons explicitly show some stylolite fabrics that are associated with organic matter.

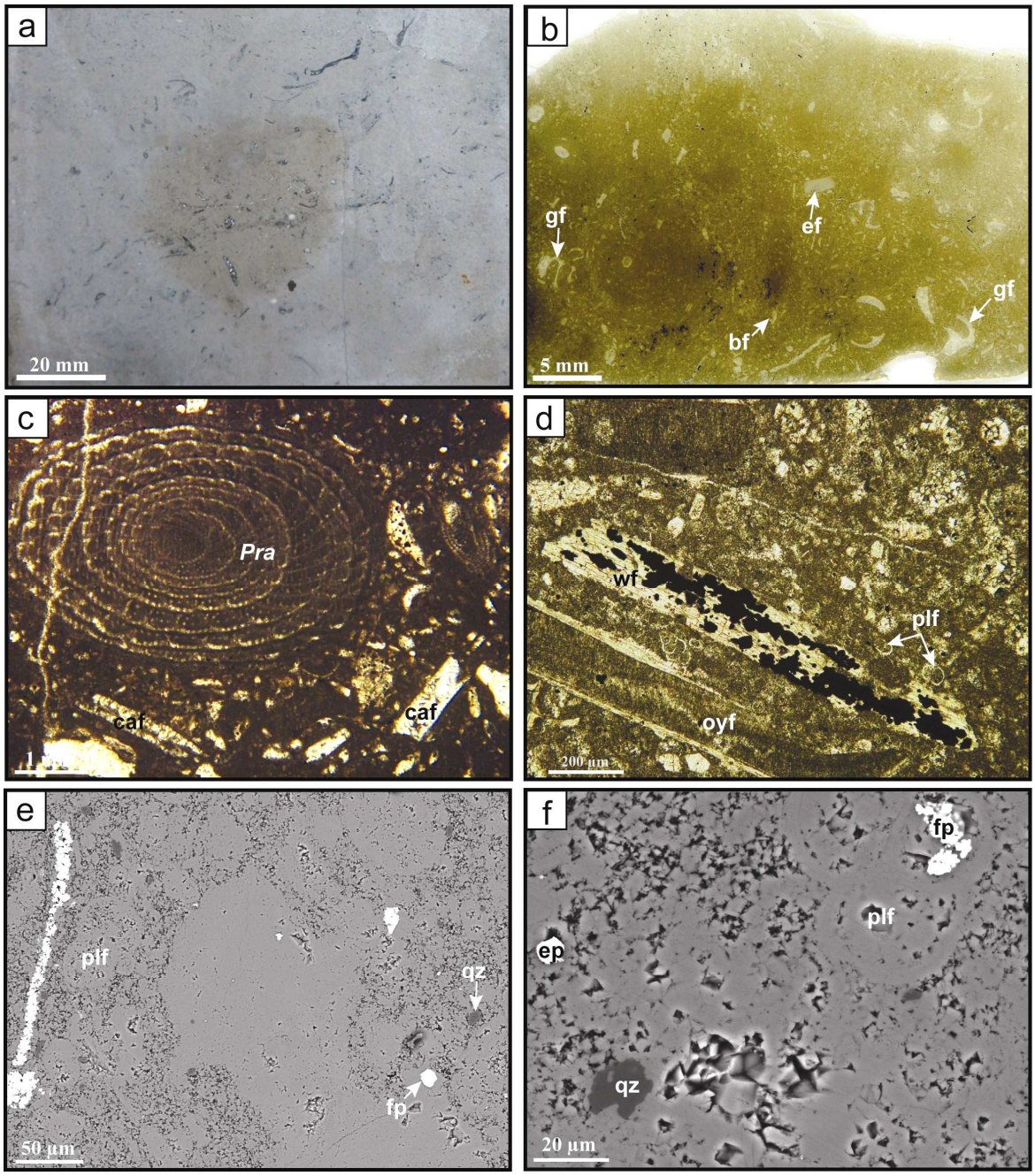

Figure 4.10 (a) Core photograph of LF5 (sample P23; see Figure 4.5 for sample location and other characteristics) illustrating extensively-bioturbated, sparry-calcite-rich packstone with abundant reworked shell fragments **(b)** Thin-section scan showing a close-up from (a). Note the circular swirls and twisted structures of skeletal debris (including gastropod [gf], bivalve [bf] and echinoderm [ef] fragments), formed by strong bioturbation (note also distinct burrow mottles) that resulted in the destruction of primary sedimentary structures. **(c)**, **(d)** Low-power optical micrographs, both under PPL, illustrating some of the microfossil components of LF5 (samples P23 and P25 respectively) that include calcareous algal fragments (caf), *Praealveolina* spp. (*Pra*), planktonic forams (plf), oyster (oyf) and pyritised wood (wf) fragments. **(e)**, **(f)** High-power, backscattered, electron-optical micrographs showing the matrix components of LF5, which include nonferroan sparry and finely-crystalline ("microspar") calcite, together with quartz (qz), framboidal pyrite (fp), euhedral pyrite (ep). Note the pervasively sparry-calcite-cemented planktonic forams, some of which are partially infilled with pyrite.

LF5 is predominantly composed of nonferroan sparry calcite (average 79.1%) that dominates the rock matrix (Figure 4.10c to f), with recrystallised, nonkeeled planktonic foraminifera (including *Heterohelix* spp., *Hedbergella* spp., *Rotalipora* spp. and *Whiteinella* baltica) and some uncompacted, predominantly sparry-calcite-cemented, reworked shell fragments (Figure 4.10c and d) of bivalves (including oysters and rudists), echinoderms (including echinoid spines and plates), gastropods (both low- and high-spired) and disarticulated ostracods. In addition to these components, LF5 contains minor benthic foraminifera (including *Praealveolina cretacea* [Figure 4.10c], *Lenticulina* spp., *Hemicyclammina* spp., *Marssonella* spp., *Textularia* spp. and other indeterminate calcareous and agglutinated benthics), fine-grained quartz (average 5.2%), algal fragments (predominantly gymnocodiacean algae; Figure 4.10c), calcispheres (including *Stomiosphaera sphaerica*) and pyrite (average 2.3%, predominantly euhedral), together with very rare clay and mica (average 1.9%, including kaolinite and muscovite), rhombohedral dolomite (average 0.8%), disarticulated coccoliths, wood fragments (Figure 4.10d), organic matter (average 0.4%, both amorphous and woody), fish debris (average 0.2%) and solitary corals.

4.5.5.2. Interpretation

The presence of nonkeeled planktonic foraminifera, calcispheres, and disarticulated coccoliths in LF5 may suggest deposition in an open-marine environment. The occurrence of mixed benthic foraminifera, calcareous algae, shell and wood fragments and solitary corals, in association with the above mentioned trace fossils, may indicate that LF5 was deposited in a distal inner-platform setting, just below fair-weather wave base under relatively high-energy conditions and well-oxygenated bottom waters. This depositional setting was probably associated with energetic bottom currents, which were able to rework and agitate fine-grained sediments from the substrate (sensu Reid et al., 1990).

The extensive burrowing of this lithofacies indicates that the rates of sediment accumulation were relatively low. Moreover, the predominance of sparry calcite, pervasively cementing uncompacted pore-space and replacing primary matrix components, together with the presence of pyrite and rhombohedral dolomite, suggest that the pervasive carbonate precipitation took place during early diagenesis, probably in association with bacterial sulphate reduction linked to organic-matter decay (Berner, 1981; Reid et al.,

1990; Reid and Macintyre, 1998). Furthermore, Reid et al. (1990) demonstrated that microcrystalline calcite ("microspar") precipitation can be very common within fine-grained, high-energy deposits. Under these circumstances, the presence of fine-grained carbonate having an authigenic origin is significant, as interpretations based on uncritical use of carbonate classification schemes, assuming primary deposition of fine-grained carbonate in a low-energy environment, are misleading (sensu Reid et al., 1990).

4.5.6. LF6: Bioturbated, Organic-Matter-, Coccoliths-, Planktonic Foraminifera- and Shell-Fragments-Bearing, Sparry-Calcite-Rich Packstone

4.5.6.1. Description

LF6 is mainly developed in the upper part of the B2-II subunit (Figure 4.5). It is characterised by its grey and very-dark grey colour, pervasively sparry-calcite-cemented, uncompacted shell fragments and predominant packstone texture (Figure 4.11a to c). Horizons formed by this lithofacies vary in thickness from 0.25 to 0.35 m, and in places exhibit scoured bases. In addition, these horizons are moderately bioturbated (attributed to *Planolites* isp. and *Thalassinoides* isp.). Rare in-place oysters have also been recognised in these units. Moreover, wispy pressure-solution seams associated with organic matter and clay occur sporadically in these packstones (Figure 4.11b and e).

LF6 is mainly composed of nonferroan sparry calcite (average 57.7%), occurring predominantly as cement in the tests of uncompacted shell fragments (including gastropods, bivalves and ostracods) and as finely-crystalline (microspar) replacement in the rock matrix (Figure 4.11b to f). In addition, nonkeeled planktonic foraminifera (mainly *Heterohelix* spp. with minor *Hedbergella* spp. [Figure 4.11d], *Macroglobigerinelloides bentonensis* and *Whiteinella baltica*), disarticulated coccoliths (Figure 4.11e and f) and thin-shelled planktonic bivalves (Figure 4.11c and d) are common in this lithofacies, together with some benthic foraminifera (including *Lenticulina* spp.; Figure 4.11c), echinoderm fragments (Figure 4.11c and d), fine-grained detrital quartz (Figure 4.11e and f; average 6.2%), clay (average 3.3%), pyrite (average 3.0%, both framboidal and euhedral; Figure 4.11f), calcispheres (including *Stomiosphaera sphaerica*; Figure 4.11c) and very rare rhombohedral dolomite (average 1.5%), fish debris and wood fragments. Many of the

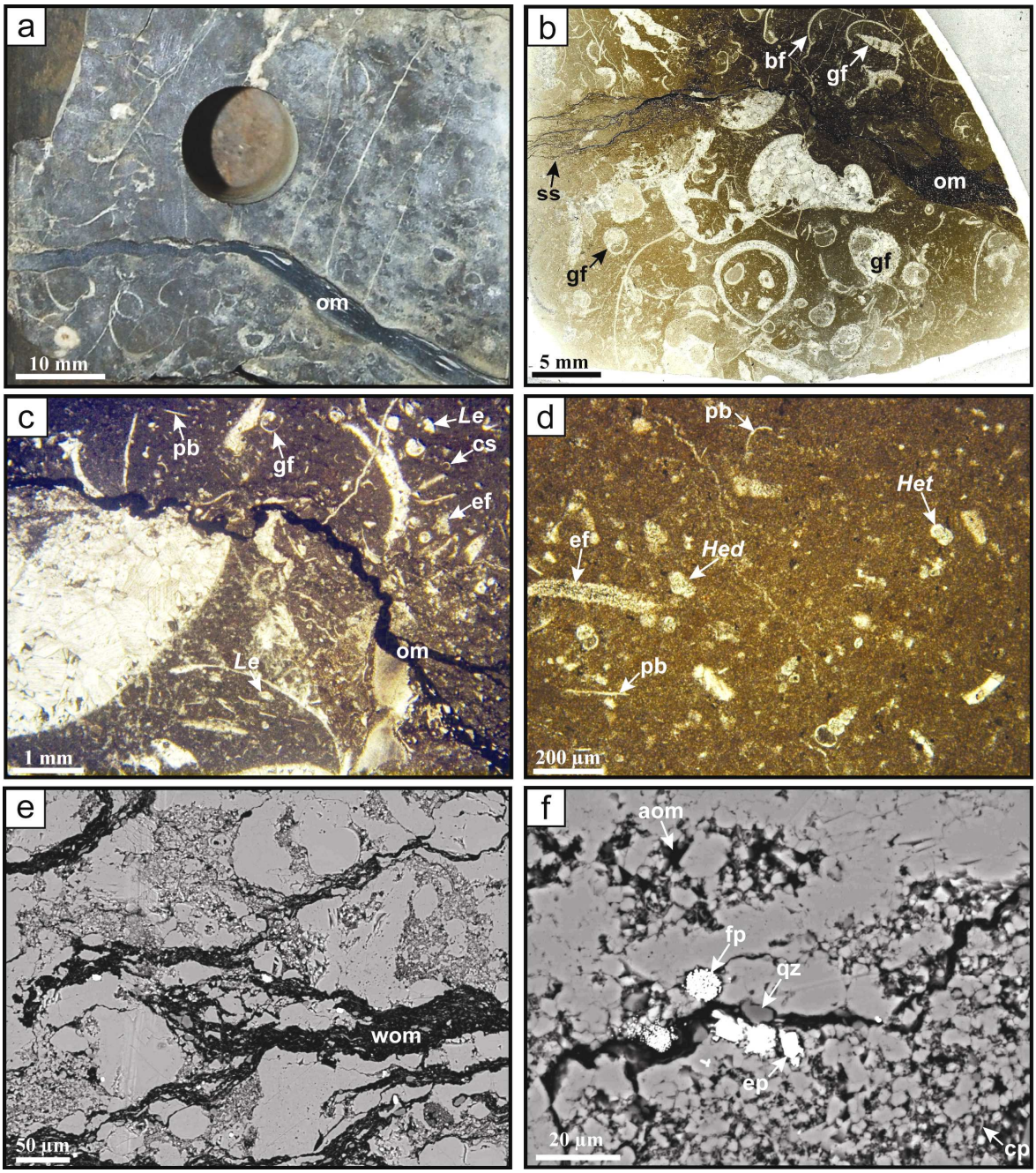

Figure 4.11. (a) Core photograph of LF6 (sample P31; see Figure 4.5 for sample location) illustrating dark-grey, bioturbated, sparry-calcite-rich packstone with abundant reworked shell fragments. Note thin black band composed predominantly of organic matter (om). **(b)** Thin-section scan showing close-up from (a). Note frequent occurrence of uncompacted, sparry-calcite-cemented shell fragments of mainly gastropods (gf) and some bivalves (bf). Note also wispy solution seams (ss) associated with organic matter (om), and hardly-distinct mottling in the lower half of the scan due to bioturbation. **(c), (d)** Low-power optical micrographs, both under PPL, illustrating some of the microfossil components of LF6 that include gastropod (gf) and echinoid (ef) fragments, planktonic bivalves (pb), calcispheres (cs), *Lenticulina* spp. (*Le*), *Heterohelix* spp. (*Het*) and *Hedbergella* spp. (*Hed*). **(e), (f)** High-power, backscattered, electron-optical micrographs showing matrix components of LF6, comprising calcite spar and microspar, with coccolith plates (cp), organic matter (woody [wom] and amorphous [aom]), quartz (qz) and pyrite (framboidal [fp] and euhedral [ep]). Note the pervasively sparry-calcite-cemented planktonic forams.

bioclastic grains of this lithofacies are densely packed and stacked, providing evidence of skeletal concentration. Despite being sparry-calcite rich and having the packstone texture, this lithofacies contains considerable amount of organic matter (up to 5.0% TOC, average about 3.6%). Organic matter here is very likely a mixture of both woody and amorphous types (Figure 4.11e and f).

4.5.6.2. Interpretation

The packstone texture and the common occurrence of nonkeeled planktonic foraminifera, disarticulated coccoliths and planktonic bivalves, together with reworked shell fragments and some smaller benthic foraminifera and calcispheres, may indicate that LF6 was deposited in an energetic, open-marine, middle-platform environment, below fair-weather wave base, where wave and/or current energy were sufficient to concentrate skeletal grains but not to remove all carbonate mud (sensu Flügel, 2004). The scoured bottoms of this lithofacies may also suggest sediment reworking by storms (e.g. Brookfield and Brett, 1988). The bioturbation and benthic fauna indicated that stable oxygenated conditions existed at the seafloor.

The considerable amount of organic matter preserved in LF6 might indicate that this lithofacies was deposited when organic-carbon production in the water column was very high, coupled with high input of woody organic matter into the platform, and perhaps higher local rates of sediment accumulation (cf. Hudson and Martill, 1991).

The majority of the pervasive, nonferroan carbonate cement and replacement in this lithofacies might have been precipitated early and in association with the degradation of organic matter (e.g. Machent et al., 2007). The presence of pyrite suggests that part of this early diagenesis involved bacterial sulphate reduction (e.g. Taylor and Macquaker, 2000b).

4.5.7. LF7: Organic-Matter-, Sparry-Calcite-, Coccoliths-, Planktonic-Foraminifera- and Bivalve-Bearing Floatstone

4.5.7.1. Description

LF7 is developed in few horizons in the B2-I subunit, making 0.05- to 0.30-m thick, bivalve floatstones ('shell beds'; Figure 4.12a and b). The calcitic in-place bivalves present in this lithofacies are a combination of thick-shelled oysters and thin-shelled pectens, forming a primary biogenic shell concentration (Figure 4.12a to c). These bivalves are in some places associated with in-place calcareous worm tubes (serpulids; Figure 4.12b and c). Shells are articulated, and the degrees of fragmentation and abrasion are very low. The matrix of these floatstones is composed of coccoliths and planktonic foraminifera (mostly as *Heterohelix* spp., with rare *Hedbergella* spp. and *Whiteinella* spp.), together with nonferroan calcite microspar (average 29.8%) and predominantly amorphous organic matter (up to 7.0% TOC, average 3.6%) [Figure 4.12d to f]. The tests of these planktonic foraminifers are commonly pervasively cemented by nonferroan sparry calcite, but some are infilled with organic matter, pyrite (Figure 4.12e and f) and/or kaolinite. Additionally, some ostracods (including *Cytherella* spp.), planktonic bivalves, and minor detrital quartz (average 5.3%) are present in the background, together with rare clay (average 3.2%), fish debris (average 2.5%), benthic foraminifera, pyrite (average 2.3%) and nonferroan dolomite (average 1.3%) [Figure 4.12d to f].

4.5.7.2. Interpretation

The abundance of articulated, life-positioned bivalves together with common pelagic sediment (including planktonic foraminifers, planktonic bivalves and coccoliths) in this lithofacies indicate deposition in a relatively low-energy, outer-platform environment (Flügel, 2004), well below fair-weather wave base. The presence of these in-place bivalves, together with ostracods and benthic foraminifera, also indicate that oxygenated bottom-water conditions occurred during deposition. The absence of trace fossils in this lithofacies, however, might indicate a comparatively low oxygen concentration (cf. Allison and Brett, 1995).

The high organic-matter content in this lithofacies is probably a result of high primary

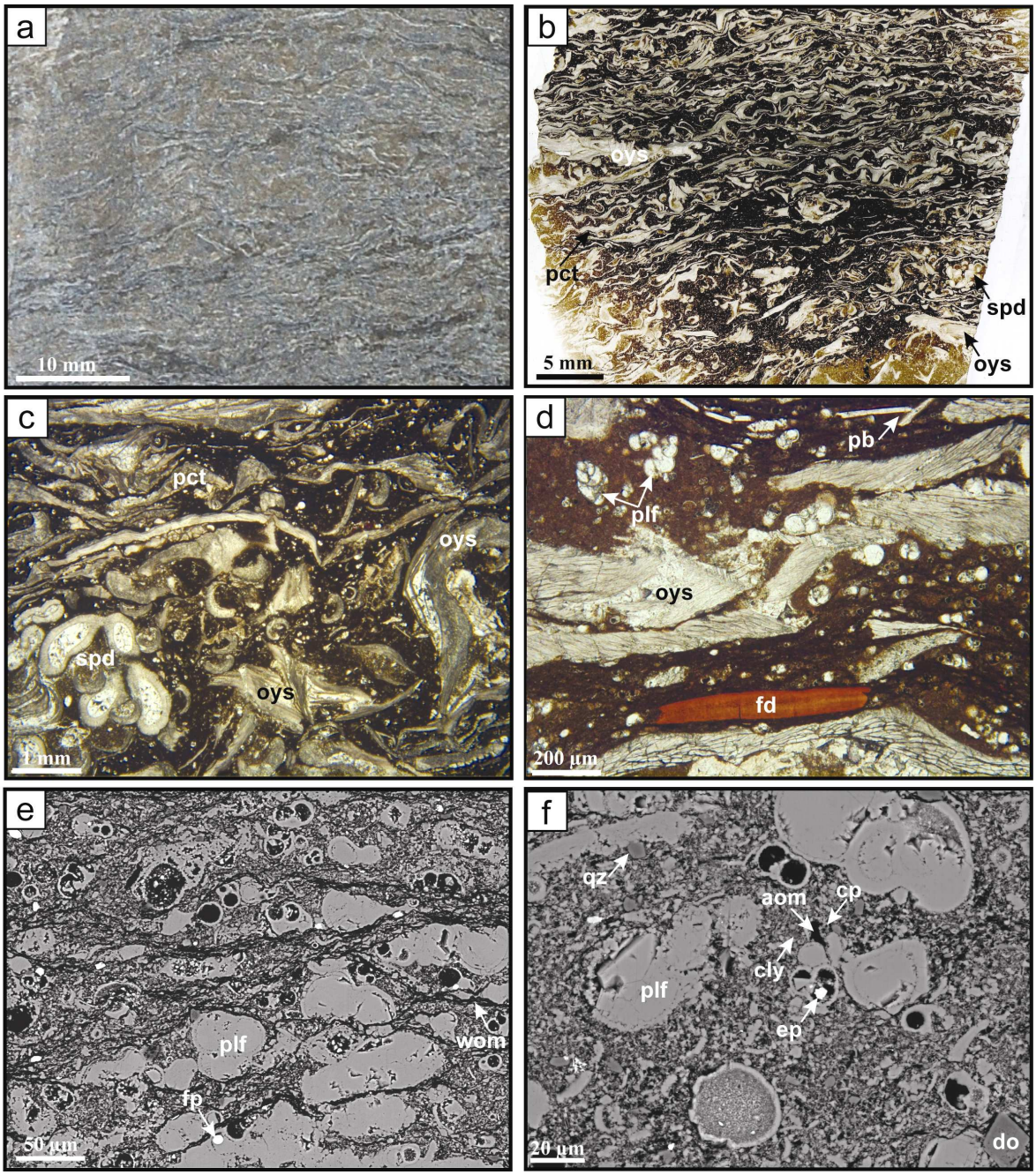

Figure 4.12. (a) Core photograph of LF7 (sample P56; see Figure 4.5 for sample location and other characteristics) illustrating dark-grey, bivalve floatstone ('shell bed'). **(b)** Thin-section scan showing a close-up from (a). Note the primary biogenic shell concentration formed by the in-place growth of oysters (oys) and pectens (pct), as well as serpulids (spd). **(c), (d)** Low-power optical micrographs of the same sample, both under PPL, illustrating the internal microstructures of oysters, pectens and serpulids, and other microfossils present in LF7 including planktonic foraminifers (plf), planktonic bivalves (pb) and fish debris (fd). **(e), (f)** High-power, backscattered, electron-optical micrographs of the same sample illustrating the matrix components of LF7, comprising nonferroan sparry-calcite cement (infilling forams' tests) and nonferroan calcite microspar replacement, together with coccolith plates (cp), organic matter (woody [wom] and amorphous [aom]), quartz (qz), pyrite (framboidal [fp] and euhedral [ep]) and clay (cly). Note also the presence of euhedral dolomite rhombs (do). TOC content of this sample is 2.8%.

organic production at the surface waters, accompanied by episodically-high local rates of sediment accumulation and burial (cf. Hudson and Martill, 1991). Evidence for the latter factor is also provided by the abundant preservation of articulated shells (cf. Brett and Allison, 1998; Lazo et al., 2005).

4.5.8. LF8: Partially-Bioturbated, Organic-Matter-, Sparry-Calcite-, Coccoliths- and Planktonic-Foraminifera-Bearing Mudstone-Wackestone

4.5.8.1. Description

This lithofacies is very important in the Natih-B Member, occurring frequently in the upper units (B2-I and B1), mainly in alternation with LF9 (Figures 4.5 and 4.13). In particular, it accounts for most of the source rock intervals present in the Natih Formation in general and Natih-B Member in particular. Horizons represented by this lithofacies can reach up to 13.7% in TOC (average about 6.1%; 35 samples of LF8 from Natih field), and vary in thickness from 0.015 to 1.650 m (average about 0.175 m).

These horizons are usually grey to very dark-grey in colour, partially bioturbated, and in some places exhibit relict, very thin genetic beds (3 to 30 mm thick), which may have been mistaken for genetic laminae by some geologists (Figure 4.14a and b). The partial bioturbation here is mainly attributed to horizontal and compacted *Planolites* isp. (Figure 4.14a and b), and less commonly to small *Phycosiphon* isp. and *Thalassinoides* isp. In addition, in-place, articulated thick-shelled oysters (including *Exogyra* spp. and *Amphidonte* spp.) and flattened pectens (Figure 4.14a and b) are often well preserved in these horizons, together with some fragmented bivalves and fish debris (Figure 4.14b and c), and few echinoid spines and ostracods (mostly disarticulated). Rare small benthic foraminifera have also been detected in some of these horizons, including the calcareous *Eouvigerina* spp., *Lenticulina* spp. (Figure 4.14c) and *Stilostomella* spp. benthics, and the agglutinated *Marssonella* spp. and *Spiroplectammina* spp. foraminifers.

These mudstone-wackestone horizons are also characterised by the abundant accumulation of calcareous microplankton (planktonic foraminifera) and nanoplankton (coccoliths) that are usually contained in faecal pellets. The planktonic foraminifera here are represented primarily by nonkeeled *Heterohelix* spp. (including *Heterohelix reussi*, *H. moremani* and

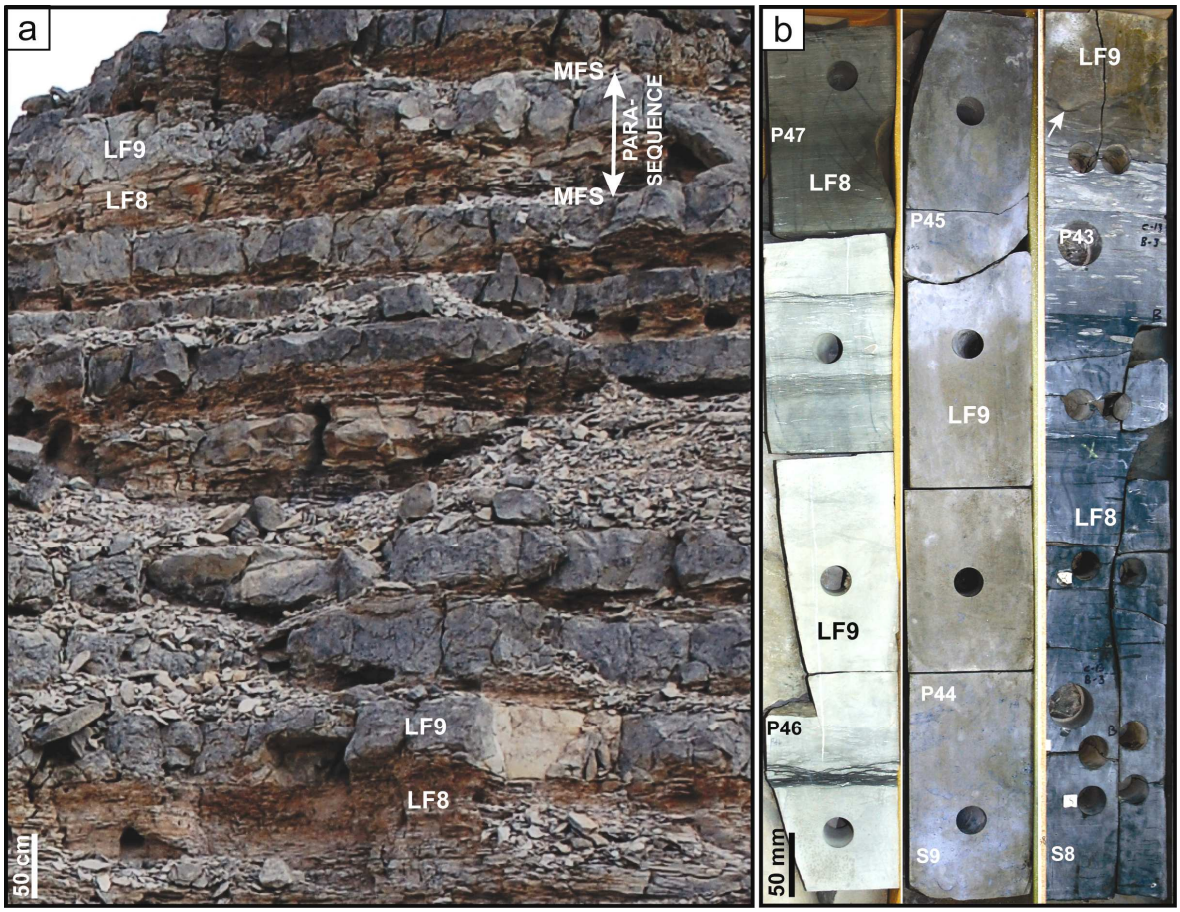

Figure 4.13. (a) Outcrop photograph (Jabal Nahdah) from the middle part of the Natih-B Member (B2-I unit) illustrating the stacking pattern of the intrashelf-basinal lithofacies (LF8: organic-carbon-rich mudstone-wackestone and LF9: sparry-calcite-rich wackestone-packstone) that alternate with one another. Note the relatively soft and fissile nature of LF8 and hard, well-cemented LF9, and the sharp boundaries between them. LF8 and LF9 together stack into shallowing-upward sequences (parasequences) that are capped by marine flooding surfaces (MFS), associated with marine hardgrounds at top of LF9. **(b)** Core photograph (Natih field; see Figure 4.5 for samples depth and other characteristics) from a roughly time-equivalent interval to (a) showing LF8 and LF9 alternating with one another. Note the 50-mm-deep scour feature (arrowed) at the base of LF9. Note also the common bioturbation especially in LF9. See Figure 4.15 for more details on sample P47.

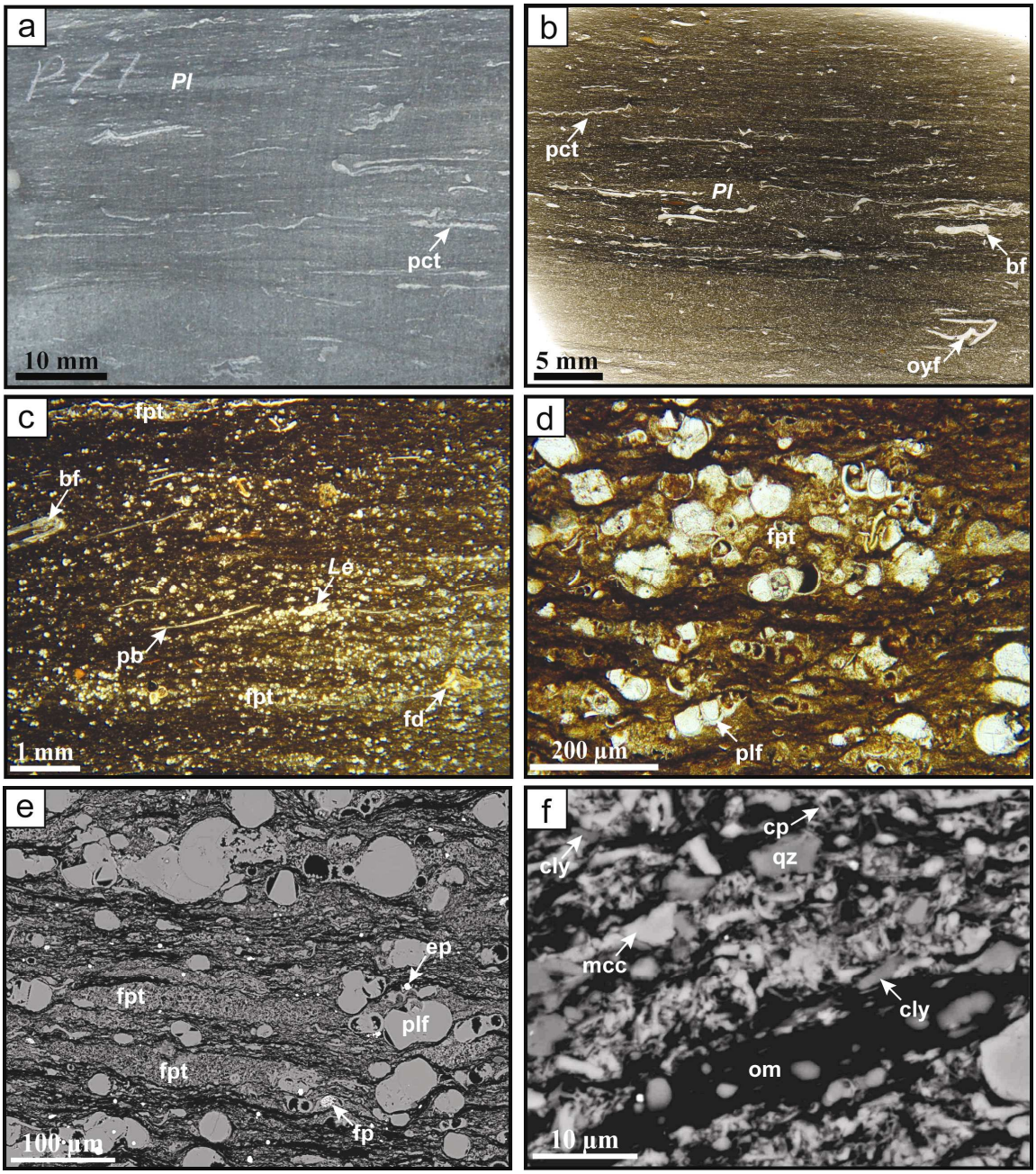

Figure 4.14. (a) Core photograph and **(b)** thin-section scan of LF8 (sample P77; see Figure 4.5 for sample location) illustrating partially-bioturbated, organic-carbon-rich mudstone. Burrowing here is mainly attributed to horizontal, highly-compacted *Planolites* isp. (*Pl*). Note occurrence of in-place pectens (pct) and other fragmented bivalves (bf) and oysters (oyf) present at disrupted and discontinuous bedding surfaces that bound relict thin beds. Note also the irregular and discontinuous laminae of organic matter throughout the sample. **(c), (d)** Low-power optical micrographs, both under PPL, illustrating some of the microfossils present in LF8 that include planktonic bivalves (pb), fish debris (fd), *Lenticulina* sp. (*Le*). Note common occurrence of faecal pellets (fpt) enclosing planktonic foraminifers (plf). **(e), (f)** High-power, backscattered, electron-optical micrographs illustrating the matrix components of LF8, which comprise sparry-calcite-cemented planktonic forams (plf), organic matter (om), disarticulated coccolith plates (cp), microcrystalline calcite ("microspar"; mcc), quartz (qz), clay (cly) and pyrite (framboidal [fp] and euhedral [ep]). Note faecal pellets (fpt) that predominantly enclose coccoliths. TOC content of this sample is 9.9%.

H. pulchra; Figure 4.14d and e) with a few *Hedbergella* spp. (including *H. planispira*) and scarce *Whiteinella* spp. (including *W. baltica*), *Dicarinella* spp., *Guembelitria* spp., *Macroglobigerinelloides* spp. (including *M. bentonensis*) and *Rotalipora* spp. (including *R. appenninica*), in addition to indeterminate, predominantly nonkeeled planktonic foraminifera (disaggregated small and large forms). Disarticulated coccolith plates frequently dominate the rock matrix of these units (Figure 4.14e and f), present in association with some fragments of planktonic foraminifera, microcrystalline calcite ("microspar") replacement, organic matter, together with minor to trace amounts of very fine-grained quartz (average 6.3%), clay (average 4.9%, including kaolinite), dolomite (average 3.4%), pyrite (average 2.9%, both euhedral and framboidal) and phosphatic debris (average 2.9%). Organic matter here is probably a combination of both woody and algal-marine types. Additionally, thin-walled planktonic bivalves are present in this lithofacies (Figure 4.14c) and become frequent in the upper part of Natih-B.

Many of LF8 samples are also characterised by the presence of nonparallel (inclined) lenticular laminae that contain faecal pellets (Figure 4.15). This type of low-angle lamina texture could be mistaken for parallel planar lamination (sensu Macquaker and Bohacs, 2007). Partial bioturbation (*Phycosiphon* isp. and *Planolites* isp.) in these samples disrupted some of these laminae.

The faecal pellets in LF8 are composed of fragmented, nonkeeled planktonic foraminifera (predominantly as *Heterohelix* spp.) and disarticulated coccolith plates (Figure 4.14c to e). These pellets vary in size from 0.1 to 0.5 mm and are commonly flattened by physical compaction parallel/subparallel to bedding. The tests of the planktonic foraminifera are commonly infilled with nonferroan sparry-calcite cement (Figure 4.14e), but organic matter and rare kaolinite, pyrite and/or dolomite can also take part. Few of the planktonic foraminifera have been crushed by compaction.

There is no evidence of stylolites or fracturing in these pelagic, organic-carbon-rich sediments.

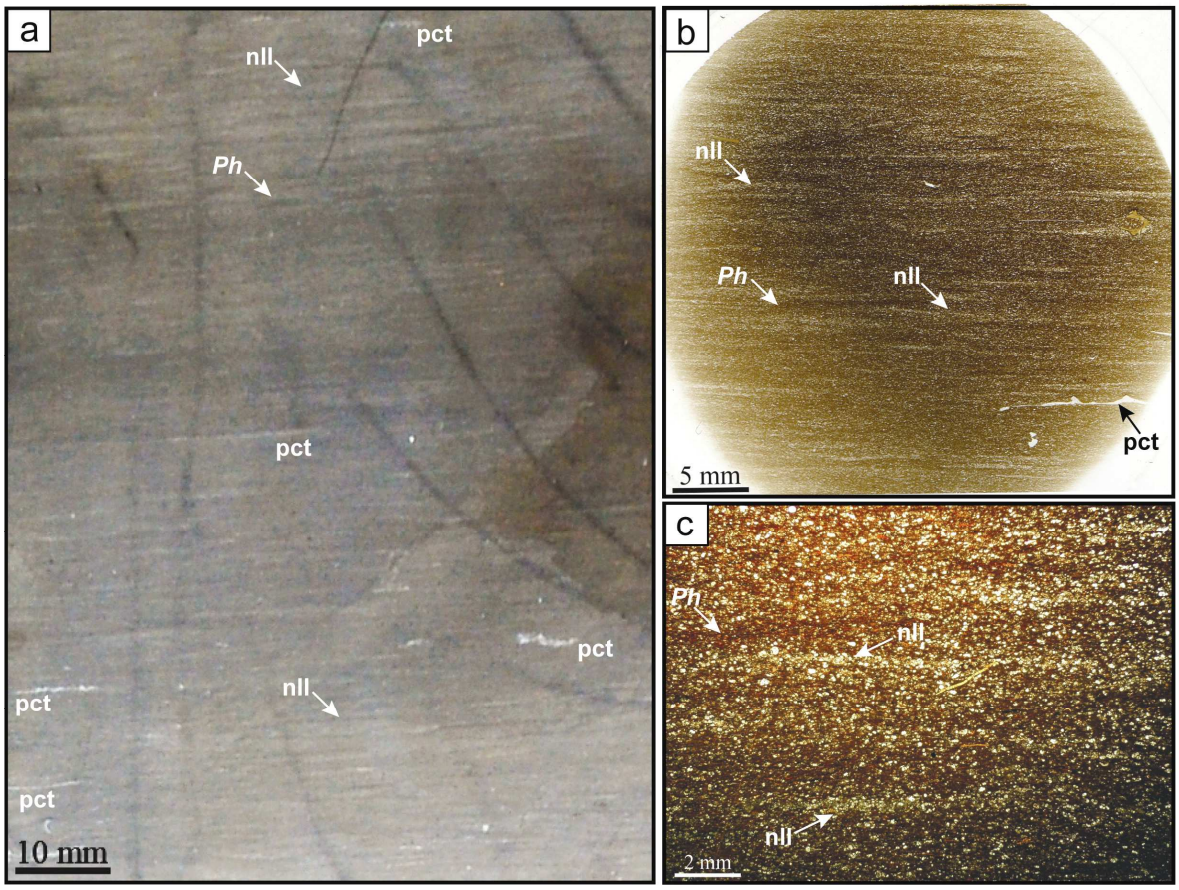

Figure 4.15. (a) Core photograph, **(b)** thin-section scan and **(c)** low-power optical micrograph illustrating characteristic depositional features of LF8 (sample P47; see Figures 4.5 and 4.13b for sample location and other characteristics). Note the nonparallel lenticular lamination (nll) that is partially disrupted by diminutive burrows, mainly attributed here to *Phycosiphon* isp. (*Ph*). These lenticular laminae are composed of faecal pellets, which enclose foraminiferal tests and coccolith plates (Figure 4.14d and e). Note also the remnant thin beds (especially in [a] and [b]) that are bound by laterally-discontinuous bedding surfaces associated with flattened pecten shells. Sample P47 is also characterised by its high TOC content, reaching 11.6%.

4.5.8.2. Interpretation

The increased percentage of planktonic foraminifera in these organic levels of the Natih-B Member indicates an increasing oceanic influence. However, the common occurrence of predominantly nonkeeled planktonic foraminifera (including *Heterohelix* spp. and *Hedbergella* spp.) suggests that the waters were not that ‘deep’ during deposition of LF8 sediments (not deeper than 40 to 60 m). These nonkeeled forms are considered to be shallow-water dwellers, and are the first to colonise new seaways and the last survivors being able to reproduce in shallow waters.

The lack of preserved parallel lamina, presence of bioturbation and occurrence of in-place benthic fauna suggest that, at the time of deposition, the conditions at the sediment/water interface were oxic-dysoxic, rather than persistently anoxic (cf. Hudson and Martill, 1991; Wetzel and Uchmann, 1998; Macquaker et al., 2007). Moreover, the presence of in-place oysters as shell pavements (colonisation surfaces) and moderate bioturbation in many of these horizons suggest that the sediment was firm (rather than "soupy"), and that there were prolonged breaks between sediment supply events (see Kenig et al., 2004; Macquaker et al., 2007). The breaks in sedimentation must have been long enough for some carbonate precipitation to occur (Raiswell et al., 1988) and make the sediment firm, and to allow seafloor colonisation by both the burrowing organisms and oysters.

The lenticular lamina texture and presence of shell fragments in LF8 indicate that relatively more energetic depositional conditions took place, influenced by episodic and advective sedimentation close to storm wave base. The inclined laminae, composed of faecal pellets, are here interpreted as current ripples that were responsible for the lateral transport of the pelagic components (planktonic foraminifers and coccoliths) from the surface waters to the basin centre (sensu Macquaker and Bohacs, 2007). This interpretation is in contrast to traditional assumptions that interpret their deposition as a result of direct settlement from suspension in the water column under persistently low-energy conditions.

The dark colouration of this lithofacies appears to be the dispersed organic matter with clay and pyrite. The carbonate cements infilling the planktonic foraminifera tests in these horizons may be related to very early diagenetic processes, as the tests are uncompacted. The presence of a calcite-pyrite cement assemblage suggests that at least part of this early diagenesis was linked to bacterial decay of organic matter (cf. Irwin, 1980; Taylor and Macquaker, 2000a).

4.5.9. LF9: Extensively-Bioturbated, Shell-fragments, Benthic- and Planktonic-Foraminifera-Bearing, Sparry-Calcite-Rich Wackestone-Packstone

4.5.9.1. Description

LF9 is frequently developed in the upper units of the Natih-B Member. It repeatedly occurs in the B2-I subunit and B1 unit, mostly in alternation with LF8. LF9 is usually light- to dark-grey, well-exposed, laterally-continuous, and very resistant to weathering (Figure 4.13). It is characterised by being strongly calcite cemented and extensively bioturbated. Burrowing in this wackestone-packstone lithofacies is attributed mainly to *Thalassinoides* isp. and rarely to *Planolites* isp. and *Phycosiphon* isp. Both cementation and bioturbation resulted in a mottled and recrystallised appearance of this lithofacies (Figure 4.16a and b).

Horizons consisting of this lithofacies vary in thickness from 0.02 to 1.85 m, but average about 0.21 m. The bases of these horizons are usually sharp and erosive (Figure 4.13), and comprise a mix of disarticulated shells (including bivalves, echinoderms, gastropods and brachiopods). They may exhibit scouring features (Figure 4.13b) and amalgamations of several thin (5 to 50 mm thick), normally-graded, individual beds may occur locally within these horizons.

LF9 is mainly composed of nonferroan calcite spar (average 74.1%), which occurs in the tests of bioclasts as sparry cement as well as in the rock matrix as finely-crystalline (microspar) replacement (Figure 4.16). Reworked, uncompacted shell fragments are common in this lithofacies, mainly of bivalves (including oyster and rudist fragments), together with some ostracods (predominantly disarticulated), gastropods (including both low- and high-spired forms), echinoderms (including echinoid spines and plates) and serpulids (Figure 4.16b to d). Benthic and planktonic foraminifera and coccoliths are also common in this lithofacies, in addition to sparse calcispheres (*Stomiosphaera sphaerica*, *Pithonella ovalis* and *Calcisphaerula innominata*), planktonic bivalves, fine-grained

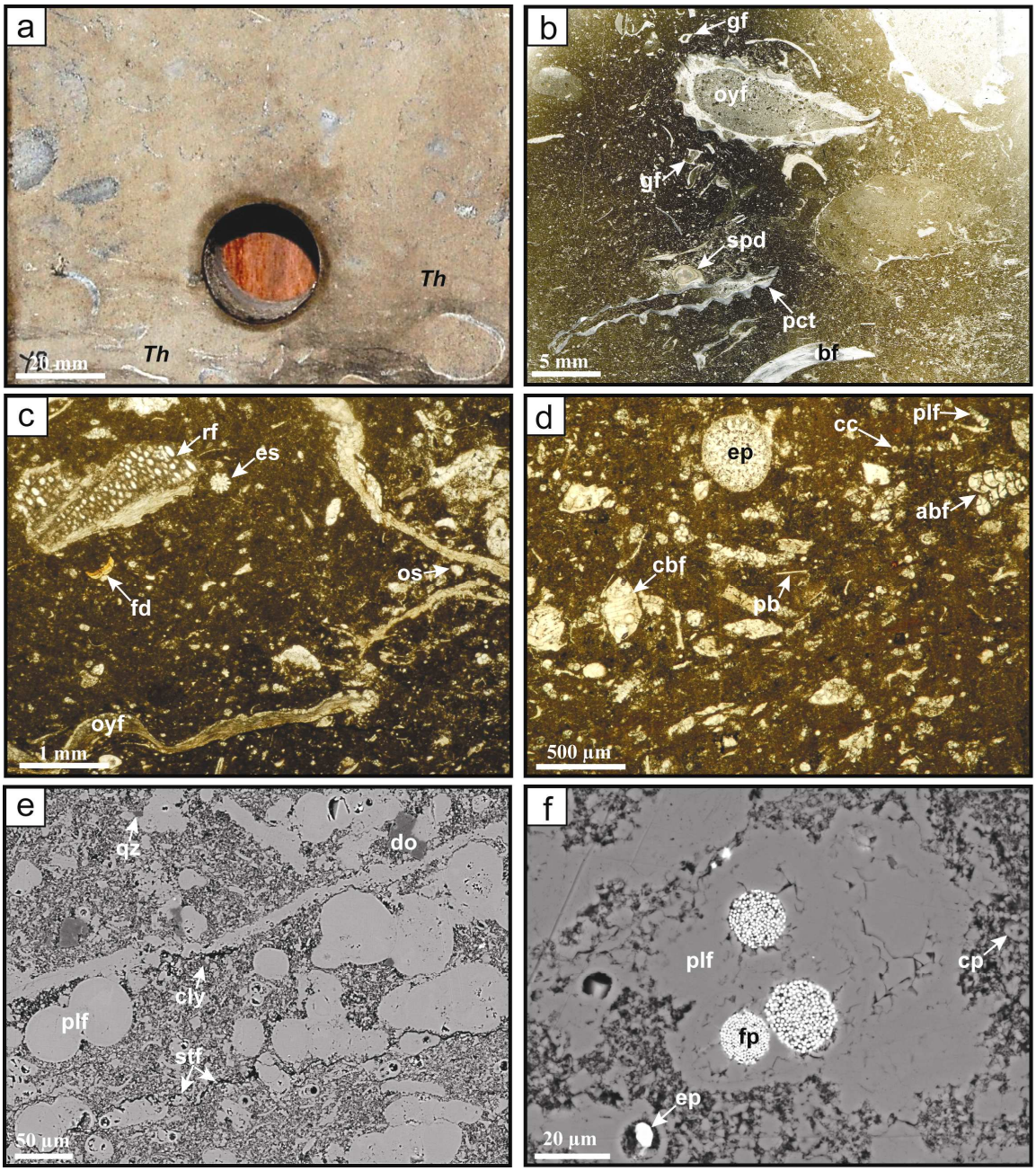

Figure 4.16. (a) Core photograph and **(b)** thin-section scan of LF9 (sample Y8; see Figure 4.5 for sample location) illustrating extensively-bioturbated, shell-fragments-bearing, sparry-calcite-rich wackestone. Bioturbation is mainly attributed to *Thalassinoides* isp. (*Th*). Note abundance and diversity of shell debris of oysters (oyf), pectens (pct), gastropods (gf), serpulids (spd) and indeterminate bivalves (bf). **(c), (d)** Low-power optical micrographs illustrating microfossils present in LF9 that include ostracods (os), fish debris (fd), rudist fragments (rf), echinoid spines (es), echinoid plates (ep), benthic foraminifera (calcareous [cbf] and agglutinated [abf]), planktonic foraminifera (plf), calcispheres (cc) and planktonic bivalves (pb). **(e), (f)** High-power, backscattered, electron-optical micrographs illustrating matrix components of LF9, comprising pervasively sparry-calcite-cemented planktonic forams (plf), disarticulated coccoliths (cp), microcrystalline calcite replacement ("microspar"), quartz (qz), clay (cly) and pyrite (framboidal [fp] and euhedral [ep]). Note the development of stylolite fabrics (stf) along and through planktonic forams, associated with organic matter. Note also how some tests of planktonic forams are being infilled with pyrite.

detrital quartz (average 4.8%), rare pyrite (average 2.1%, euhedral and framboidal), rhombohedral dolomite (average 2.5%), clay (average 2.2%, mostly as kaolinite) and organic matter (average 1.1% TOC), and very rare fish debris (average 0.6%) [Figure 4.16c to d] and wood fragments (average 0.1%).

The benthic foraminifers present in this lithofacies include both calcareous forms (including *Lenticulina* spp., *Trocholina lenticularis, Rotalia cf. skourensis* and *Gavelinella* spp., among other indeterminate calcareous benthics) and agglutinated forms (including *Marssonella* spp., Textularidae, *Marssonella trochus*, *Spiroplectammina* spp. and *Dorothia* spp., along with other indeterminate agglutinated foraminifera). The planktonic foraminifers are mostly represented here by *Heterohelix* spp. (including *H. reussi* and *H. moremani*), *Hedbergella* spp. (including *H. planispira* and *H. delrioensis*) and *Whiteinella* spp., as well as minor *Guembelitria* spp., *Dicarinella* spp., *Macroglobigerinelloides* spp. and *Praeglobotruncana* spp. Some of the planktonic foraminifers in LF9 are concentrated along stylolite fabrics that also in places cut through them (Figure 4.16e).

4.5.9.2. Interpretation

The wackestone-packstone texture, extensive bioturbation, and common occurrence of mixed benthic and planktonic foraminifera and diverse reworked shell fragments, with coccoliths, calcispheres and ostracods, all indicate that LF9 was deposited in a relatively shallow-marine (open outer platform), high-energy, well-oxygenated environment, above storm wave base (e.g. Brett and Allison, 1998; Wetzel and Uchmann, 1998; Hallam et al., 2000). The reworked shell fragments and the erosive bases, coupled with normal grading textures, suggest that sediments of this lithofacies were swept by waning flow currents (likely distal storms) from the surrounding carbonate platform down into the intrashelf basin (cf. Droste, 1990; Hudson and Martill, 1991; Osleger, 1991; Osleger and Read, 1991; Burchette, 1993). In addition, it is likely that the horizons of this lithofacies were formed by the amalgamation and winnowing of individual, thinner storm-generated beds, resulting from the reworking of sediment during major storm events (Banerjee and Kidwell, 1991; Myrow and Southard, 1996; Varban and Plint, 2008). Particular offshore-directed and geostrophic currents produced by storms were probably responsible for erosion, sediment mixing, and both shore-parallel and offshore sediment transport (Aigner, 1982; Burchette and Britton, 1985; Leckie and Krystinik, 1989; Duke, 1990; Duke et al., 1991).

The abundance of early-marine calcite cement and replacement (predating compaction), low preserved organic-matter content, and degree of bioturbation in this wackestone-packstone lithofacies indicate that there was sufficient time for solutes to be diffused to the sites of carbonate precipitation, and for the sediment to be extensively burrowed. Moreover, the abundance of *Thalassinoides* isp. here indicates that between storm events the depositional environment was reasonably quiet, and that overall rates of sediment accumulation were relatively slow.

4.6. Discussion

4.6.1. Overall Depositional Environment

The overall stratigraphy, with the dominance of extensively-bioturbated, algal and benthic-foraminiferal mudstones-wackestones (associated with clays) in the Natih-C and lower Natih-B (B4 and B3 units), extensively-bioturbated bioclastic packstones in middle Natih-B (B2-II) and partially- to extensively-bioturbated pelagic/bioclastic mudstones-wackestones in upper Natih-B Member (B2-I and B1), and the absence of large reefal structures, suggest that overall deposition was initially occurring in shallow-water platform environment that passes gradually into proximal inner- and mid-ramp environments, and further seaward, into distal outer-ramp and intrashelf-basin conditions (see Appendix C and Figure 4.17; Smith et al., 1990; Tucker et al., 1993; van Buchem et al., 2002b; Flügel, 2004; Homewood et al., 2008), with the latter being the most abundant. This, generally, gradually upward-deepening trend represents a progressive transgression, which overall influenced the deposition of the Natih-B Member. The basal Natih-B4 unit (overlying extensively-bioturbated, bored and iron-enriched hardground at top Natih-C) represents the initial stages of this third-order marine transgression (van Buchem et al., 1996). The subsequent units (B3, B2, and B1) represent a generally steadily-rising eustatic sea level, but with several breaks in sedimentation due to high-frequency sea-level fluctuations, associated with the development of several submarine hardgrounds that are linked to breaks in sediment accumulation (Figure 4.13). In addition to these sedimentation breaks, a

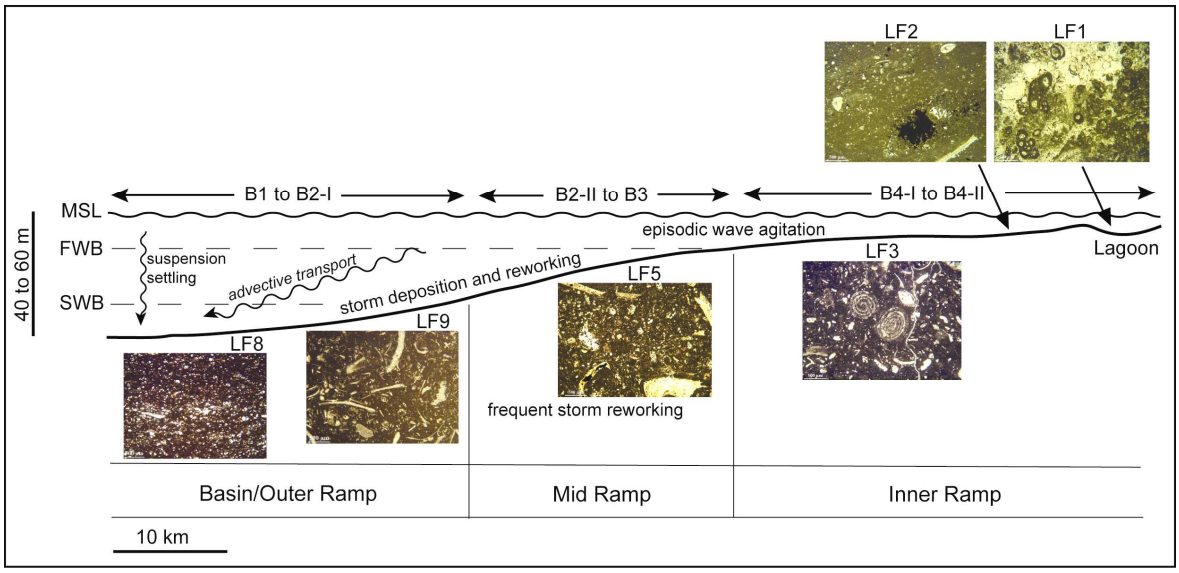

Figure 4.17. Generalised diagram illustrating depositional model of the Natih-B Member, with indication of the likely depositional environments of the main lithofacies present in the succession (sensu Burchette and Wright, 1992). See Figure 4.5 for the vertical distribution of the Natih-B units (B1 to B4) and lithofacies (LF1 to LF9), and the text for their detailed attributes. (MSL = Mean Sea Level; FWB = Fair-weather Wave Base; SWB = Storm Wave Base). Note that palaeopathymetry estimate is based on faunal evidence.

forth-order sequence boundary is placed at the Natih-B3 to B2 transiotion (see Figure 4.3; Grélaud et al., 2006; Homewood et al., 2008).

The faunal and floral content (benthic foraminifera [including miliolids, miliolinid alveolinids, *Nezzazata* spp. and *Dicyclina* spp.], planktonic foraminifera, calcareous algal and shell fragments of bivalves, echinoderms and ostracods) of the B4 (LF1 to LF4) and B3 (LF5) units indicates that they were deposited in an inner-ramp **(<** 35 m deep) environment, which changed into a mid-ramp environment during deposition of the B2-II subunit (LF6, bioturbated skeletal packstones with diverse fossils) [Figure 4.17; Appendix C]. This transgressive event culminated in the development of an outer-ramp and intrashelf-basin (40 to 60 m deep) environments (dominated by nonkeeled planktonic foraminifera, coccoliths and both benthic and planktonic bivalves, together with shallow ramp-derived bioclasts, calcispheres and some fish debris) in which the pelagic-sediment-rich B2-I subunit and B1 unit (LF7 to LF9) were deposited (Figure 4.17; Appendix C). As sea level rose, accommodation increased, which resulted in the dispersion of the mud-dominated carbonate products over wider areas of the basin, resulting in the spatial and temporal distribution of the Natih-B lithofacies.

Specifically, sedimentation in the Natih-B is characterised by the development of stacked

dm- to m-scale shallowing-upward successions (Figure 4.13), where rates of sediment supply were greater than available accommodation. Extensively-bioturbated and pervasively-cemented and microcrystallised submarine hardgrounds are commonly developed at the tops of these thin, upward-shoaling successions (Figure 4.13). Overall, these thin, upward-coarsening cycles are interpreted to be stacked successions of parasequences that are organised into an overall retrogradational trend (sensu Osleger and Read, 1991; Tucker et al., 1993; Bosence and Wilson, 2003; Coe and Church, 2003; Flügel, 2004). Evidence for the latter includes the overall thinning-upaward trend of the alternating LF8 and LF9 horizons (Figure 4.5) and abundance of planktonic bivalves in LF8 towards the top of Natih-B.

4.6.2. Pelagic Sedimentation

The fine-grained carbonates encountered here dominantly comprise detritus composed of coccoliths, planktonic foraminifera and planktonic bivalves, as well as varying proportions of transported shallow-water bioclasts (e.g. bivalve fragments [including rudists], gastropod debris, and echinoid plates and spines), in-place fauna and flora (e.g. bivalves [including oysters and pectens], benthic foraminifera, ostracods and calcispheres), authigenic components, organic matter and detrital siliciclastics. Carbonate mudstones and wackestones that contain assemblages of this sort (i.e. ‘chalks’) are typically interpreted (e.g. Hattin, 1981; Burchette and Britton, 1985; Jenkyns, 1986; Tucker and Wright, 1990; Philip et al., 1995; Flügel, 2004; Homewood et al., 2008) as having been deposited in open-marine environments as pelagic accumulations (e.g. within Upper Cretaceous deposits from North America, Europe and the Middle East). Most sedimentologists assume that such units were deposited as a continuous rain of suspended sediment that settled through the water column under quiescent conditions, in settings where strong bottom currents were largely absent (e.g. Hancock, 1976; Arthur et al., 1984a; Pickering et al., 1986; Caus et al., 1993; Wignall, 1994; Stow et al., 1996; Stow and Tabrez, 1998; Drzewiecki and Simo, 2000; Stow et al., 2001).

While the Natih-B fine-grained carbonates, particularly in the upper part of the succession (units B2 and B1, especially LF9 [Figures 4.13 and 4.16]), have faunal elements that might indicate this depositional style, they are also organised into thin, normally-graded or amalgamated skeletal beds that have erosional and sharp bases and strongly-bioturbated

tops. Such features suggest that deposition occurred from episodic waning flows, which belies their origin as simple suspension-settling sediments deposited as a continuous rain. Instead, these data suggest that deposition may have been episodic, and at least in part driven by erosive events that had the ability to generate some episodic and advective transport of sediment. In this setting, these deposits are likely the products of distal-storm reworking (see Homewood et al., 2008), and are possibly tempestites (sensu Seilacher and Aigner, 1991; Myrow and Southard, 1996). Such an interpretation is supported by the fact that some units (LF8) also contain compacted starved-ripple (lenticular) laminae composed of faecal pellets, inclined at low angles (Figure 4.15).

The internal characteristics of these particular beds (erosional bases, shell concentration and/or amalgamation, overall normally-graded stacking pattern, and current-ripple lamination) suggest that they were likely produced by combined flows, such as either shore-parallel geostrophic currents or wave-enhanced sediment-gravity flows that impinged on the seafloor (e.g. Duke, 1990; Banerjee and Kidwell, 1991; Myrow and Southard, 1996; Molina et al., 1997; Pomar and Tropeano, 2001; Wright et al., 2001; Friedrichs and Wright, 2004; Ichaso and Dalrymple, 2009; Macquaker et al., in press). Such offshore-directed flows are also likely to have been responsible for at least some of the transport of the updip fauna and flora into more downdip settings, which lead to the intermingling of shallow-water biota in the basinal setting (Figure 4.17; e.g. Aigner, 1982; Droste, 1990; Tucker et al., 1993; Pomar and Tropeano, 2001; Flügel, 2004; Pomar et al., 2005; Lasseur et al., 2009).

4.6.2.1 Sediment Reworking, Bioturbation and Dispersion

The abundance of faecal pellets in some units of LF8 (Figures 4.14 and 4.15), composed of phytoplankton detritus (specifically coccolith plates, foraminiferal tests and amorphous organic matter), suggests that, at least occasionally, there was significant primary production in the surface water, and that much of the material in the water column was bundled by filter-feeding organisms (zooplankton) into organominerallic aggregates (sensu Alldredge and Silver, 1988) prior to being delivered to the sediment/water interface. Sediment delivery to the seafloor by this method is commonly much more rapid than by conventional settling of fine-grained sediment and was likely a significant additional

sediment-delivery process, along with the storm-driven advective flows (e.g. Feazel et al., 1985; Pevear and Grabowski, 1985; Schatzinger et al., 1985; Varban and Plint, 2008).

The trace fossils (*Thalassinoides* isp., *Planolites* isp. and *Phycosiphon* isp.) that are recognised throughout the Natih-B succession suggest that the substrate was firm (rather than soupy) and oxygen was available near the sediment/water interface (sensu Bromley, 1975; Kennedy, 1975; Scholle et al., 1983; Ekdale and Bromley, 1984; Schatzinger et al., 1985; Macquaker et al., 2007; Heard et al., 2008), even during the deposition of the most organic-carbon-rich sediments (Al Balushi and Macquaker, in press). The intense burrowing in most of the Natih-B sediments is a result of the large benthic population at the seafloor. Extensive bioturbation and early calcite cementation and microcrystallisation in some horizons (e.g. LF9; Figure 4.16) may imply sharp periodic reduction in sedimentation rates or even nondeposition, which resulted in periodic exposure of the sediment to prolonged burrowing activity and lithification by bottom waters, perhaps connected with an increased current action (Pevear and Grabowski, 1985; Bathurst, 1987; Garrison et al., 1987). Strong bottom-current activity may greatly enhance seafloor lithification by episodically winnowing and sorting the sediment, forming cemented and recrystallised layers (marine hardgrounds) that are irregularly scattered throughout the succession (Figure 4.13; Scholle et al., 1983; Tucker and Wright, 1990; Philip et al., 1995). Part of this cementation and microcrystallisation process was probably associated with the oxidation of the available organic matter (Al Balushi and Macquaker, in press, and references therein). Some hardgrounds in the Natih-B Member can be traced laterally over distances of 100 km between the sections at the Adam Foothills (Immenhauser et al., 2000), reflecting the regionally-consistent and persistent conditions of seafloor cementation and recrystallisation (Kennedy and Garrison, 1975; Tucker and Wright, 1990) and the widespread effect of the fundamental controlling factors, likely high-frequency eustatic sea-level change.

As a result of extensive bioturbation by burrowing organisms and sediment mobilisation by bottom currents, primary sedimentary structures are not commonly preserved in the highly-bioturbated, sparry-calcite-rich intervals of the Natih-B (LF1, LF3, LF5, and LF9). The organic-matter-bearing intervals (e.g. LF8) are, in contrast, partially bioturbated. Most of these organic-matter-bearing intervals were deposited and buried episodically and rapidly and, therefore, less affected by burrowing organisms (Al Balushi and Macquaker, in press,

and references there in). Consequently, these intervals may preserve some relict thin beds or some starved current ripples (Figures 4.14a, b and 4.15a, b). The presence of in-place fauna and burrow fabrics (Figures 4.14a to c and 4.15), nevertheless, suggest that bottom-water anoxia did not exist during the deposition of these organic-carbon-rich units (Schatzinger et al., 1985; Hudson and Martill, 1991; Machhour et al., 1998; Schieber, 2009; Al Balushi and Macquaker, in press).

Combined and geostrophic bottom currents (shore parallel) along and across storm-influenced shelves can rework and resuspend sediment into lags, and may lead to the accumulation of mud in the mid-shelf belt (Scholle et al., 1983; Burchette and Britton, 1985; Pickering et al., 1986; Higgs et al., 1990; Tucker and Wright, 1990; Duke et al., 1991; Varban and Plint, 2008; Plint et al., 2009). It is very likely that the pelleted carbonate muds in the Natih-B was frequently resuspended by storm activity in water depths up to 60 m, and advectively transported both across (sensu Nittrouer and Wright, 1994; Macquaker et al., in press) and obliquely across the shelf (sensu Varban and Plint, 2008; Plint et al., 2009). The onset of deposition by bottom currents in the Natih-B Member is signalled by the development of current-ripple-laminated horizons of LF8 (Figure 4.15), implying that much of the pelagic sediment in these horizons is not simply deposited out of suspension under low-energy conditions (sensu Macquaker and Bohacs, 2007). Current-ripple laminae are suggestive of high-energy turbulent conditions and existence of traction-current activity. However, the absence of buildups in the Natih-B succession may imply deposition in very low-gradient (< 1^{o}) settings, perhaps in homoclinal, ramp-like shelf margin (sensu Ahr, 1973; Read, 1982; Cook et al., 1983; Burchette and Wright, 1992; Stanton and Flügel, 1995; Wright and Burchette, 1996; Pomar, 2001b).

Recent studies have suggested that wave-enhanced sediment-gravity flows may also play a significant role in offshore dispersal of fine-grained sediment in some settings (e.g. Wright et al., 2001; Friedrichs and Wright, 2004; Friedrichs and Scully, 2007; Plint et al., 2009; Macquaker et al., in press). Macquaker et al. (in press) argued that such flows were potential dispersal agents of large volumes of mud rapidly across low-gradient (as low as 0.5m/km) shelves. The distribution of these flows and associated deposits across the shelf is controlled by sediment supply, seabed gradient, and spatial distribution of bottom wave/current energy (Macquaker et al., in press).

Storm-generated waves and currents may deposit tempestites, which may usually show sharp and erosional bases, graded beds, accumulation of reworked shells as basal layers, cross and planar lamination, hummocky cross stratification, and starved ripples (Aigner, 1982; Seilacher and Aigner, 1991; Myrow and Southard, 1996; Molina et al., 1997; Flügel, 2004). However, most of these primary sedimentary structures are rarely preserved in the Natih-B Member due to bioturbation, which in most cases appears to have penetrated deeply into the seafloor and disrupted the sediment for a long period of time after deposition (Bathurst, 1987; Bentley et al., 2006; Lasseur et al., 2009; Macquaker et al., in press). The preservation of some of these structures, however, indicates that sediment delivery was sufficiently rapid, and the recurrence time between delivery events was long enough to ensure that infaunal colonisation was insufficiently pervasive to destroy all the fabrics present (Bentley et al., 2006; Al Balushi and Macquaker, in press; Macquaker et al., in press).

4.6.2.2. Controlling Factors on Sedimentation and Early Diagenesis

The development of the pelagic succession in the upper part of the Natih-B Member, in which organic-matter-bearing horizons (LF8) alternate with sparry-calcite-rich horizons (LF9) [Figure 4.13], is probably in part controlled by changes in sedimentation rate, related to high-frequency variations in eustatic sea level (accommodation), climate, primary production (both organic and inorganic), and bottom currents and circulation patterns (sensu Kennedy and Garrison, 1975; Scholle et al., 1983; Tucker and Wright, 1990; Pomar, 2001a; Flügel, 2004). Changes in sedimentation rate appear to have had strong influence on both organic-matter deposition (LF8) and early carbonate cementation and replacement (LF9) in this succession. In the dynamic and oxic Natih-B intrashelf basin, organic matter in LF8 (average 6.1% TOC) was probably best preserved under higher rates of sediment accumulation at times of relatively high sea-level stands (increased accommodation), associated with increased organic productivity (Arthur et al., 1984b; Hudson and Martill, 1991; Macquaker, 1994; Machhour et al., 1998; Stow et al., 2001; Katz, 2005; Macquaker et al., 2007; Al Balushi and Macquaker, in press). High sedimentation rate may lead to the rapid burial of organic carbon, removing it quickly form the zones of oxic degradation and anaerobic sulphate reduction and ensuring its preservation to form a source rock. On the other hand, reduced sediment accumulation rates at times of relatively low sea-level stands (decreased accommodation), associated with stronger physical (e.g. storms) and biological

(e.g. bioturbation) reworking of the sediment, may enhance carbonate cementation and recrystallisation (and organic-matter oxidation) in LF9, extending the sediment residence time within early-diagenetic zones (Shinn, 1969; Kennedy and Garrison, 1975; Campos and Hallam, 1979; Hattin, 1986; Macquaker, 1994; Taylor et al., 1995; Macquaker et al., 2007; Al Balushi and Macquaker, in press). This means that the pervasively early-cemented and internally-replaced horizons (hardgrounds) at the top of LF9 were produced during times of sediment bypass at the turnarounds from long-term decreasing to increasing accommodation (sensu Macquaker, 1994; Mettraux et al., 1999; Taylor and Macquaker, 2000a). It is also likely that authigenic-carbonate precipitation in these horizons continued through sediment burial as a result of organic-matter oxidation reactions in the overlying organic-carbon-rich mudstones-wackestones (LF8; sensu Taylor et al., 2000).

Changes in accommodation availability also played an important role in the lateral variation of facies across the carbonate ramp (proximal locations) and intrashelf basin (distal locations). In the more proximal locations (inner- and mid-ramp; Jabal Salakh East) there was less accommodation available for sediments to accumulate, which resulted in a slower sedimentation rate that caused the sediments of these setting to be more strongly reworked by storms, extensively bioturbated, and pervasively cemented and replaced early (sensu Macquaker, 1994; Figure 4.18a and b). Organic-carbon-rich units, similar to LF8 in Natih filed (Figure 4.14), were not developed at these locations, as any organic matter being produced was substantially degraded in this relatively shallower, fully oxic environment, where the sediment remained at the sediment/water interface for a prolonged period of time (sensu Taylor et al., 1995). Instead, sparry-calcite-rich units, similar to LF3 and LF5 in Natih field (Figures 4.8 and 4.10), dominated these shallower settings. Moreover, the higher influx of carbonate debris near the basin margin contributed effectively, causing the organic-matter content in these parts of the platform to be autodiluted (van Buchem et al., 2005).

On the other hand, in the more distal locations (outer ramp and intrashelf basin; Jabal Salakh West, Jabal Nahdah, Jabal Qusaybah, and Natih field) and during high relative sea-level stands, there was more accommodation available in the basin to accumulate sediments more rapidly. In these distal locations (especially Natih field), the depositional processes (e.g. high organic productivity, high sedimentation rate, and dysoxic bottom-

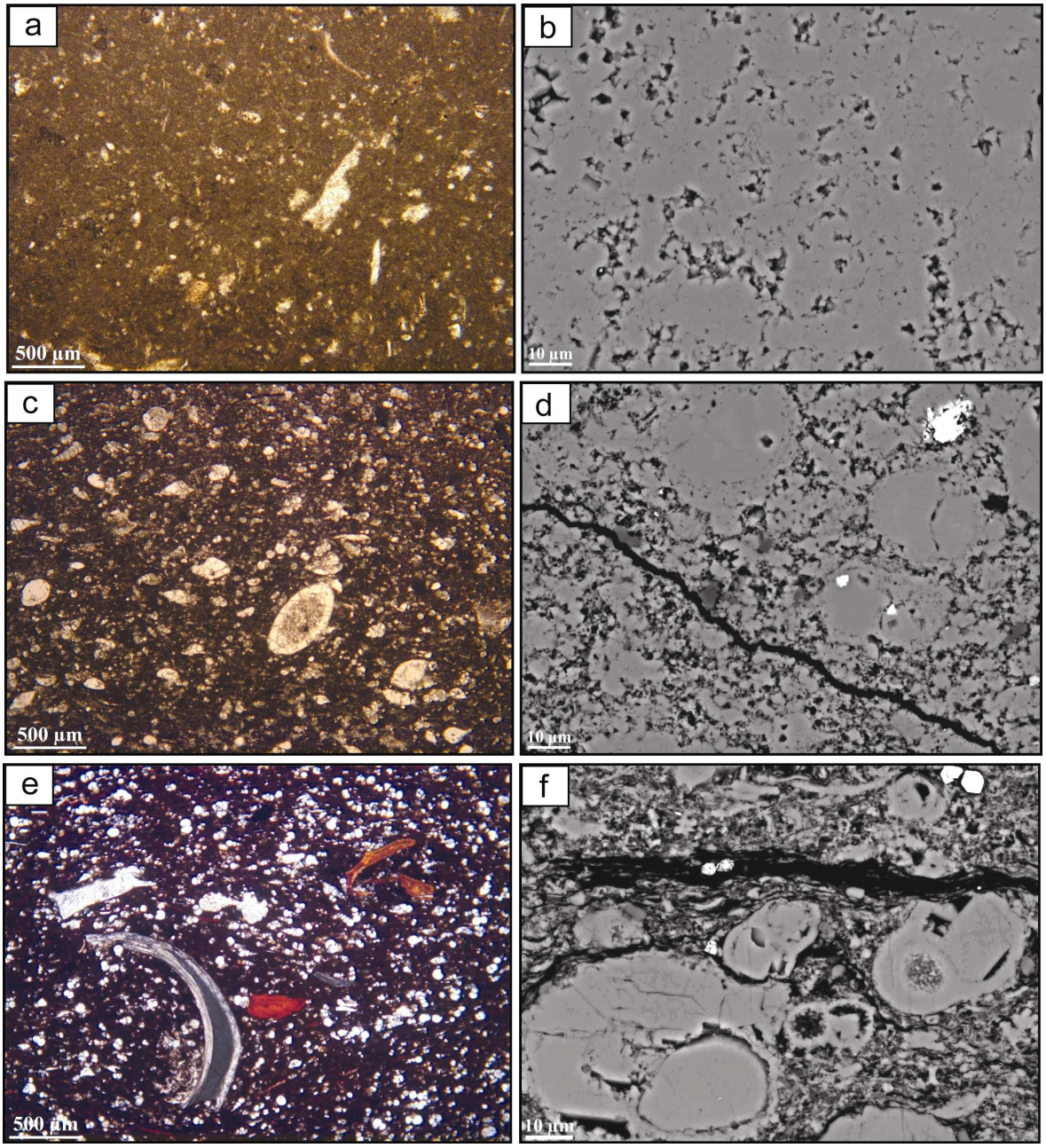

Figure 4.18. Low-power optical and high-power, backscattered, electron-optical photomicrograph pairs illustrating lateral lithofacies variability between proximal location (Jabal Salakh East, photomicrographs **[a]** and **[b]**) and distal locations (Jabal Nahdah, photomicrographs **[c]** and **[d]**; Natih field, photomicrographs **[e]** and **[f]**). Samples were gathered at approximately same timeline in the lower part of the B2-I unit (Figures 4.4 and 4.5). See Figure 4.1 for the lateral spacing between these locations. Note the more extensive sediment reworking and bioturbation, pervasive calcite cementation and recrystallisation, and lack of siliciclastics and organic matter (only 1.0% TOC, sample SE13) in the proximal sample from Jabal Salakh East, in comparison to the distal samples from Jabal Nahdah (2.0% TOC, sample N13) and Natih field (7.1% TOC, sample P34; see Figure 4.5), which are relatively less reworked (biologically and physically) and less pervasively cemented/recrystallised, with better preservation of organic matter and more pelagic and siliciclastic components, especially in the most distal sample from Natih field. See also Appendix B for more information on these samples.

water conditions) are favourable to accumulate pelagic organic-carbon-rich sediments (Figure 4.18c to f). However, during low relative sea-level stands, accommodation was reduced, sedimentation rate was lowered, and the sediment was more strongly winnowed and bioturbated, resulting in the development of hardgrounds (sparry-calcite-rich horizons [LF9; Figures 4.13 and 4.16] and shell pavements [LF7; Figure 4.12]) that indicate breaks in sediment accumulation (depositional hiatuses; sensu Kidwell, 1985; Beckvar and Kidwell, 1988; Röhl and Schmid-Röhl, 2005; Lasseur et al., 2009). It appears that drops in relative sea level (reductions in accommodation) during the deposition of some of the Natih-B intrashelf-basinal sediments (e.g. LF9) were sufficient to periodically expose these sediments to winnowing action by storms and prolong their residence time at the well-oxygenated sediment/water interface, which resulted in their infaunal and epifaunal colonisation, and in the oxidation of any available organic matter (Banerjee and Kidwell, 1991; Taylor et al., 1995; Röhl and Schmid-Röhl, 2005; Macquaker et al., 2007; Al Balushi and Macquaker, in press). These interpretations demonstrate that there is a close correspondence between the incidence of hiatuses in offshore sediments and accommodation availability, as a result of high-frequency sea-level fluctuations (e.g. Scholle et al., 1983; Lasseur et al., 2009).

Fluctuations in relative sea level seem also to have influenced the amount of terrigenous material delivered from the hinterland to the basin across the carbonate ramp (e.g. Shinn, 1969; Kennedy and Garrison, 1975; Scholle et al., 1983; Taylor et al., 1995). Rising sea level shifts the shoreline loci towards the land, such that the supply of siliciclastic detritus retreats away from the basin centre. Under these circumstances carbonate sediments inevitably dominate the centre of the basin (e.g. Pevear and Grabowski, 1985).

It is very likely that the main controlling factors for organic-matter preservation in the Natih-B Member was very high organic production of phytoplankton (planktonic bloom) and rapid sinking and incorporation of organic carbon into the sediments (high sedimentation accumulation rate; see Al Balushi and Macquaker, in press, and references therein). This is suggested by the abundance of faecal pellets in the organic-matter-bearing lithofacies (LF8). Such an increase in organic productivity was probably related to nutrient-loading of the surface waters by outwelling from land, perhaps due to an increase in rainfall (sensu Pevear and Grabowski, 1985). However, it would be expected that such a process would be accompanied by an increased supply of siliciclastics to the basin.

Consequently, a mechanism for trapping sediments at the basin margins (possibly by estuaries or coastal swamps; Leinfelder, 1997) was required. Moreover, the Natih-B intrashelf basin was too shallow and too large for effective upwelling to have occurred in the laterally-extensive Cretaceous carbonate platform (sensu Pevear and Grabowski, 1985; Figure 4.2).

Organic-carbon content in Natih-B (up to 13.7% and average 6.1% TOC, determined from the cored succession from Natih field) varies temporally at the cm to dm scale, as observed from the alternating intrashelf-basinal units of LF8 and LF9 (Figures 4.5 and 4.13b). Spatially, individual organic-carbon-rich horizons can be traced for over 150 km (van Buchem et al., 2002b). Kerogen in these units is immature, with high hydrogen index (HI) values (up to 650) and mainly Type II autochthonous organic matter (van Buchem et al., 2002b, based on samples from Natih filed). It is possible that in other parts of the Fahud and Qarn Alam salt basins, where the Natih-B Member is buried to greater than 1 km, the organic matter is nearing the zone of catagenesis (petroleum formation). The abundance of Type II kerogen suggests that this material is predominantly oil prone (Terken, 1999); that is, it will produce oil rather than gas at these levels of maturation. However, the observation of woody (structured) organic matter in some thin sections from this study (e.g. Figure 4.11e) might suggest the existence of some Type III allochthonous organic matter, which may generate gas (see Ibrahim et al., 2000; Al Balushi and Macquaker, in press). The observation of wood fragments in some thin sections (e.g. Figure 4.10d) provides further evidence for the delivery of woody material into the intrashelf basin.

4.7. Conclusions

High-resolution lithofacies analyses using petrographic, mineralogical and geochemical techniques, in addition to detailed core and field descriptions, have been undertaken on Upper Cretaceous (Natih-B Member), carbonate-dominated successions from North Oman, so that they can be integrated into platform-wide depositional model incorporating an intrashelf basin. In the studied successions, nine lithofacies have been identified based on these analyses. These lithofacies are differentiated from each other based on their sedimentary structures and comparative amounts of autochthonous, allochthonous and authigenic constituents, as well as their depositional textures, with mudstones and

wackestones being the most dominant, together with minor packstones and floatstones. Deposition of these lithofacies occurred in a predominately clastic-starved intrashelf basin (40 to 60 m maximum water depth) and associated outer- and inner-ramp setting where primary production was high and bottom-water conditions varied form oxic to dysoxic. The key factors controlling the development of the nine lithofacies include: sea level, primary production (both organic and inorganic), bottom-water oxygen concentrations, sediment accumulation rates, and early diagenesis. The 50- to 60-m thick Natih-B succession overall deepens upward with the organic-matter-poor (average 0.4% TOC) lagoonal and inner-ramp sediments (B4 and B3 units) developed towards its lower part, in contrast to organic-matter-bearing (up to 13.7% TOC, average 3.7%) outer-ramp and intrashelf-basinal sediments developed towards its middle and upper parts (B2 and B1 units).

Moreover, detailed analyses of sedimentary structures and rock components demonstrate that in these relatively "monotonous", predominantly fine-grained carbonates: a) lithofacies vary greatly at the cm to sub-mm scales; b) some of these sediments display relict, thin (< 5 mm thick) beds; c) many of the organic-matter-bearing sediments are pelleted and display lenticular bedding, suggesting that these sediments were mainly deposited by episodic and advective processes in a relatively energetic environment; d) in some horizons diminutive flattened burrows disrupt depositional laminae, whereas in others extensive bioturbation completely destroys primary structures; e) there were major breaks in sediment accumulation, as indicated by the pervasively-cemented and recrystallised horizons that are present where the stacking patterns change, with the cementation and recrystallisation being promoted, at least in part, by the oxidation of organic matter; f) in addition to this small-scale lithofacies variability, there is a considerable temporal and spatial variability in the Natih-B Member that reflects changes in sediment supply and accommodation availability, as well as local changes in primary production and sedimentation and burial rates that fundamentally controlled organic-matter enrichment in this carbonate-dominated succession.

These high-resolution lithofacies descriptions and interpretations from the Natih-B Member have permitted standard facies analyses to be carried out on predominantly fine-grained carbonates that span an intrashelf basin and surrounding carbonate platform. They illustrate that lithofacies variability exhibited by such carbonate sediments is comparable to

the variability exhibited by siliciclastic mudrocks on continental shelves. This implies that both types (carbonate and siliciclastic) of fine-grained sedimentary rocks can be examined in the same manner, since the main factors influencing their variability are very similar.

Acknowledgements

The authors wish to express gratitude to Petroleum Development Oman (PDO) for the financial and logistic support, and for allowing access to the subsurface core material, seismic data, wireline logs, and reports. We also wish to thank the University of Manchester (School of Earth, Atmospheric and Environmental Sciences) where the polished thin-sections were prepared and petrographic and XRD analyses were performed, and Manchester Metropolitan University (Department of Environmental and Geographical Sciences) where the TOC analyses were performed. Finally, both the Sultanate of Oman Ministry of Oil and Gas (MOG) and PDO are acknowledged for permission to publish this paper.

References

Adams, A.E. and W.S. Mackenzie 1998. A Colour Atlas of Carbonate Sediments and Rocks Under the Microscope. Manson Publishing, 180 p.

Ahr, W.M. 1973. The carbonate ramp: an alternative to the shelf model. Transactions of the Gulf Coast Association of Geological Societies, v. 23, p. 221-225.

Aigner, T. 1982. Calcareous tempestites: storm-dominated stratification in Upper Muschelkalk limestones (Middle Trias, SW Germany). In, G. Einsele and A. Seilacher (Eds.), Cyclic and Event Stratification. Springer-Verlag, p. 180-198.

Aigner, T., M. Doyle, D. Lawrence, M. Epting and A. Van Vliet 1989. Quantitative modeling of carbonate platforms: some examples. In, P.D. Crevello, J.L. Wilson, J.F. Sarg and J.F. Read (Eds.), Controls on Carbonate Platform and Basin Development. SEPM (Society for Sedimentary Geology), Special Publication 44, p. 27-37.

Al-Saad, H. and F.N. Sadooni 2001. A new depositional model and sequence stratigraphic interpretation for the upper Jurassic Arab "D" reservoir in Qatar. Journal of Petroleum Geology, v. 24, no. 3, p. 243-264.

Al Balushi, S.A.K. and J.H.S. Macquaker (in press). Sedimentological evidence for bottom-water oxygenation during deposition of the Natih-B intrashelf-basinal sediments: Upper Cretaceous carbonate source rock, Natih Formation, North Sultanate of Oman. GeoArabia.

Alldredge, A.L. and M.W. Silver 1988. Characteristics, dynamics and significance of marine snow. Progress in Oceanography, v. 20, no. 1, p. 41-82.

Allison, P.A. and C.E. Brett 1995. In situ benthos and paleo-oxygenation in the Middle Cambrian Burgess Shale, British Columbia, Canada. Geology, v. 23, no. 12, p. 1079-1082.

Alsharhan, A.S. 1995. Facies variation, diagenesis, and exploration potential of the Cretaceous rudist-bearing carbonates of the Arabian Gulf. American Association of Petroleum Geologists, v. 79, no. 4, p. 531-550.

Alsharhan, A.S. and A.E.M. Nairn 1988. A review of the Cretaceous formations in the Arabian Peninsula and Gulf: Part II. Mid-Cretaceous (Wasia Group) stratigraphy and palaeogeography. Journal of Petroleum Geology, v. 11, no. 1, p. 89-112.

Alsharhan, A.S. and R.W. Scott 2000. Hydrocarbon potential of Mesozoic carbonate platform-basin systems, U.A.E. In, A.S. Alsharhan and R.W. Scott (Eds.), Middle East Models of Jurassic/Cretaceous Carbonate Systems. SEPM (Society for Sedimentary Geology), Special Publication 69, p. 335-358.

Aqrawi, A.A.M., G.A. Thehni, G.H. Sherwani and B.M.A. Kareem 1998. Mid-Cretaceous rudist-bearing carbonates of the Mishrif Formation: an important reservoir sequence in the Mesopotamian Basin, Iraq. Journal of Petroleum Geology, v. 21, no. 2, p. 57-82.

Arthur, M.A., W.E. Dean and D.A.V. Stow 1984a. The Cenomanian-Turonian oceanic anoxic event II: palaeoceanographic controls on organic-matter production and preservation. In, D.A.V. Stow and D.J.W. Piper (Eds.), Fine-grained Sediments: Deep-Water Processes and Facies. Geological Society, Special Publication 15, p. 527-560.

Arthur, M.A., W.E. Dean and D.A.V. Stow 1984b. Models for the deposition of Mesozoic-Cenozoic fine-grained organic-carbon-rich sediment in the deep sea. Geological Society Special Publications, v. 15, no. 1, p. 527-560.

Azmy, K., D. Lavoie, I. Knight and G. Chi 2008. Dolomitization of the Lower Ordovician Auathuna Formation carbonates, Port au Port Peninsula, western Newfoundland, Canada: implications for a hydrocarbon reservoir. Canadian Journal of Earth Sciences, v. 45, no. 7, p. 795-813.

Baker, P.A. and M. Kastner 1981. Constraints on the formation of sedimentary dolomite. Science, v. 213, no. 4504, p. 214-216.

Banerjee, I. and S.M. Kidwell 1991. Significance of molluscan shell beds in sequence stratigraphy: an example from the Lower Cretaceous Mannville Group of Canada. Sedimentology, v. 38, no. 5, p. 913-934.

Bathurst, R.G.C. 1987. Diagenetically enhanced bedding in argillaceous platform limestones; stratified cementation and selective compaction. Sedimentology, v. 34, no. 5, p. 749-778.

Beckvar, N. and S.M. Kidwell 1988. Hiatal shell concentrations, sequence analysis, and sea-level history of a Pleistocene coastal alluvial fan, Punta Chueca, Sonora. Lethaia, v. 21, no. 3, p. 257-270.

Bentley, S.J., A. Sheremet and J.M. Jaeger 2006. Event sedimentation, bioturbation, and preserved sedimentary fabric: field and model comparisons in three contrasting marine settings. Continental Shelf Research, v. 26, no. 17-18, p. 2108-2124.

Berner, R.A. 1978. Sulfate reduction and the rate of deposition of marine sediments. Earth and Planetary Science Letters, v. 37, no. 3, p. 492-498.

Berner, R.A. 1981. A new geochemical classification of sedimentary environments. Journal of Sedimentary Research v. 51, no. 2, p. 359-365.

Bosence, D.W.J. and R.C.L. Wilson 2003. Sequence stratigraphy of carbonate depositional systems. In, A.L. Coe (Ed.), The Sedimentary Record of Sea-Level Change. Cambridge University Press, p. 234-256.

Brett, C.E. and P.A. Allison 1998. Palaeontological approaches to the environmental interpretation of marine mudrocks. In, J. Schieber, W. Zimmerle and P. Sethi (Eds.), Shales and Mudstones I: Basin Studies, Sedimentology, and Palaeontology. E. Schweizerbart'sche Verlagsbuchhandlung, p. 384.

Bromley, R.G. 1975. Trace fossils at omission surfaces. In, R.W. Frey (Ed.), The Study of Trace Fossils. Springer-Verlag, p. 399-428.

Brookfield, M.E. and C.E. Brett 1988. Paleoenvironments of the mid-Ordovician (Upper Caradocian) Trenton limestones of southern Ontario, Canada: storm sedimentation on a shoal-basin shelf model. Sedimentary Geology, v. 57, no. 1-2, p. 75-105.

Burchette, T.P. 1993. Mishrif Formation (Cenomanian–Turonian), southern Arabian Gulf: carbonate platform growth along a cratonic basin margin. In, J.A.T. Simo, R.W. Scott and J.P. Masse (Eds.), Cretaceous Carbonate Platforms. American Association of Petroleum Geologists, Memoir 56, p. 185-200.

Burchette, T.P. and S.R. Britton 1985. Carbonate facies analysis in the exploration for hydrocarbons: a case study from the Cretaceous of the Middle East. In, P.J. Brenchley and B.P.J. Williams (Eds.), Sedimentology: Recent Developments and Applied Aspects. Geological Society, Special Publication 18, p. 311-338.

Burchette, T.P. and V.P. Wright 1992. Carbonate ramp depositional systems. Sedimentary Geology, v. 79, no. 1-4, p. 3-57.

Campbell, C.V. 1967. Lamina, laminaset, bed and bedset. Sedimentology, v. 8, no. 1, p. 7-26.

Campos, H.S. and A. Hallam 1979. Diagenesis of English Lower Jurassic limestones as inferred from oxygen and carbon isotope analysis. Earth and Planetary Science Letters, v. 45, no. 1, p. 23-31.

Caus, E., A. Gómez-Garrido, A. Simó and K. Soriano 1993. Cenomanian-Turonian platform to basin integrated stratigraphy in the South Pyrenees (Spain). Cretaceous Research, v. 14, no. 4-5, p. 531-551.

Coe, A.L. and K.D. Church 2003. Sequence stratigraphy and sea-level change. In, A.L. Coe (Ed.), The Sedimentary Record of Sea-Level Change. Cambridge University Press, p. 57-98.

Compton, J.S. 1988. Sediment composition and precipitation of dolomite and pyrite in the Neogene Monterey and Sisquoc formations, Santa Maria Basin Area, California. In, V. Shukla and P.A. Baker (Eds.), Sedimentology and Geochemistry of Dolostones. SEPM (Society for Sedimentary Geology), Special Publication 43, p. 53-64.

Connally, T.C. and R.W. Scott 1985. Carbonate sediment-fill of an oceanic shelf, Lower Cretaceous, Arabian Peninsula. In, P.D. Crevello and P.M. Harris (Eds.), Deep-Water Carbonate: Buildups, Turbidites, Debris Flows and Chalks - A Core Workshop. SEPM (Society for Sedimentary Geology), Core Workshop 6, p. 266-302.

Cook, H.E., A.C. Hine and H.T. Mullins 1983. Platform Margin and Deep Water Carbonates. SEPM (Society for Sedimentary Geology), Short Course 12, 563 p.

Dickson, J.A.D. 1965. A Modified staining technique for carbonates in thin section. Nature, v. 205, no. 4971, p. 587.

Droste, H. 1990. Depositional cycles and source rock development in an epeiric intraplatform basin: the Hanifa Formation of the Arabian Peninsula. Sedimentary Geology, v. 69, p. 281-296.

Droste, H. 2003. Intra-platform basins in the Cretaceous carbonate platform of Oman (abstract). AAPG International Conference, Barcelona, Spain. American Association of Petroleum Geologists.

Droste, H. and M. Van Steenwinkel 2004. Stratal geometries and patterns of platform carbonates: the Cretaceous of Oman. In, G. Eberli, J.L. Massaferro and J.F.R. Sarg (Eds.), Seismic Imaging of Carbonate Reservoirs and Systems. American Association of Petroleum Geologists, Memoir 81, p. 185-206.

Drzewiecki, P.A. and J.A. Simo 2000. Tectonic, eustatic and environmental controls on mid-Cretaceous carbonate platform deposition, south-central Pyrenees, Spain. Sedimentology, v. 47, no. 3, p. 471-495.

Duke, W.L. 1990. Geostrophic circulation or shallow-marine turbidity currents? The dilemma of paleoflow patterns in storm-influenced prograding shoreline systems. Journal of Sedimentary Research, v. 60, no. 6, p. 870-883.

Duke, W.L., R.W.C. Arnott and R.J. Cheel 1991. Shelf sandstones and hummocky cross-stratification: new insights on a stormy debate. Geology, v. 19, no. 6, p. 625-628.

Dunham, J.B. and E.R. Olson 1980. Shallow subsurface dolomitization of subtidally deposited carbonate sediments in the Hanson Creek Formation (Ordovician-Silurian) of Central Nevada. In, D.H. Zenger, J.B. Dunham and R.L. Ethington (Eds.), Concepts and Models of Dolomitization. SEPM (Society for Sedimentary Geology), Special Publication 28, p. 139-161.

Dunham, R.J. 1962. Classification of carbonate rocks according to depositional texture. In, W.E. Ham (Ed.), Classification of carbonate rocks, A symposium. American Association of Petroleum Geologists, Memoir 1, p. 108-171.

Ekdale, A.A. and R.G. Bromley 1984. Cretaceous chalk ichnofacies in Northern Europe. Geobios, v. 17, no. SUPPL. 1, p. 201-204.

Ekdale, A.A. and R.G. Bromley 1991. Analysis of composite ichnofabrics; an example in Uppermost Cretaceous chalk of Denmark. Palaios, v. 6, no. 3, p. 232-249.

Embry, A.F. and J.E. Klovan 1971. A late Devonian reef tract on northeastern Banks Island Nordwest Territories. Bulletin of Canadian Petroleum Geology, v. 19, p. 730-781.

Feazel, C.T., J. Keany and R.M. Peterson 1985. Cretaceous and Tertiary chalk of the Ekofisk field area, central North Sea. Carbonate Petroleum Reservoirs, p. 495-507.

Flügel, E. 2004. Microfacies of Carbonate Rocks: Analysis, Interpretation and Application. Springer, 976 p.

Friedman, G.M. 1964. Early diagenesis and lithification in carbonate sediments. Journal of Sedimentary Research, v. 34, no. 4, p. 777-813.

Friedrichs, C.T. and M.E. Scully 2007. Modeling deposition by wave-supported gravity flows on the Po River prodelta: from seasonal floods to prograding clinoforms. Continental Shelf Research, v. 27, no. 3-4, p. 322-337.

Friedrichs, C.T. and L.D. Wright 2004. Gravity-driven sediment transport on the continental shelf: implications for equilibrium profiles near river mouths. Coastal Engineering, v. 51, no. 8-9, p. 795-811.

Garrison, R.E., W.J. Kennedy and T.J. Palmer 1987. Early lithification and hardgrounds in upper Albian and Cenomanian calcarenites, southwest England. Cretaceous Research, v. 8, no. 2, p. 103-140.

Gingras, K.M., S.G. Pemberton, K. Muelenbachs and H. Machel 2004. Conceptual models for burrow-related, selective dolomitization with textural and isotopic evidence from the Tyndall Stone, Canada. Geobiology, v. 2, no. 1, p. 21-30.

Glennie, K.W. 2000. Cretaceous tectonic evolution of Arabia's eastern plate margin: a tale of two oceans. In, A.S. Alsharhan and R.W. Scott (Eds.), Middle East Models of Jurassic/Cretaceous Carbonate Systems. SEPM (Society for Sedimentary Geology), Special Publication 69, p. 9-20.

Gradstein, F.M., J.G. Ogg and A.G. Smith 2004. A Geologic Time Scale 2004. Cambridge University Press, 589 p.

Grantham, P.J., G.W.M. Lijmbach, J. Posthuma, M.W. Hughes Clarke and R.J. Willink 1987. Origin of crude oils in Oman. Journal of Petroleum Geology, v. 11, no. 1, p. 61-80.

Gregg, J.M. and D.F. Sibley 1984. Epigenetic dolomitization and the origin of xenotopic dolomite texture. Journal of Sedimentary Petrology, v. 54, no. 3, p. 908-931.

Grélaud, C., P. Razin, P.W. Homewood and A.M. Schwab 2006. Development of incisions on a periodically emergent carbonate platform (Natih Formation, Late Cretaceous, Oman). Journal of Sedimentary Research, v. 76, no. 4, p. 647-669.

Grotzinger, J.P. 1989. Facies and evolution of Precambrian carbonate depositional systems: emergence of the modern platform archetype In, P.D. Crevello, J.L. Wilson, J.F. Sarg and J.F. Read (Eds.), Controls on Carbonate Platform and Basin Development. SEPM (Society for Sedimentary Geology), Special Publication 44, p. 79-106.

Grover, G. 1993. Intrashelf basins: a geologic model for source-bed and reservoir facies deposition within carbonate shelves (abstract), AAPG International Conference. The Hague, Netherlands, American Association of Petroleum Geologists Bulletin, v. 77, p. 1629.

Hallam, A., P.B. Wignall, J. Yin and J.B. Riding 2000. An investigation into possible facies changes across the Triassic-Jurassic boundary in southern Tibet. Sedimentary Geology, v. 137, no. 3-4, p. 101-106.

Hancock, J.M. 1976. The petrology of the chalk, v. 86, p. 499-535.

Harris, P.M. and S.H. Frost 1984. Middle Cretaceous carbonate reservoirs, Fahud field and northwestern Oman. American Association of Petroleum Geologists Bulletin, v. 68, no. 5, p. 649-658.

Hattin, D.E. 1981. Petrology of Smoky Hill Member, Niobrara Chalk (Upper Cretaceous) in type area, Western Kansas. American Association of Petroleum Geologists Bulletin, v. 65, no. 12, p. 831-849.

Hattin, D.E. 1986. Carbonate substrates of the Late Cretaceous Sea, central Great Plains and southern Rocky Mountains. Palaios, v. 1, no. 4, p. 347-367.

Heard, T.G., K.T. Pickering and S.A. Robinson 2008. Milankovitch forcing of bioturbation intensity in deep-marine thin-bedded siliciclastic turbidites. Earth and Planetary Science Letters, v. 272, no. 1-2, p. 130-138.

Higgs, R., B.S. Hart, R.M. Vantfoort, A.G. Plint, D.A. Leckie and L.F. Krystinik 1990. Is there evidence for geostrophic currents preserved in the sedimentary record of inner to middle shelf deposits? Discussion and reply. Journal of Sedimentary Research, v. 60, no. 4, p. 630-637.

Holail, H., K.C. Lohmann and I. Sanderson 1988. Dolomitization and dedolomitization of Upper Cretaceous carbonates: Bahariya Oasis, Egypt. In, V. Shukla and P.A. Baker (Eds.), Sedimentology and Geochemistry of Dolostones SEPM (Society for Sedimentary Geology), Special Publication 43, p. 191-207.

Homewood, P., P. Razin, C. Grélaud, H. Droste, V. Vahrenkamp, M. Mettraux and J. Mattner 2008. Outcrop sedimentology of the Natih Formation, northern Oman: a field guide to selected outcrops in the Adam Foothills and Al Jabal Al Akhdar areas. GeoArabia, v. 13, no. 3, p. 39-120.

Hudson, J.D. and D.M. Martill 1991. The Lower Oxford Clay: production and preservation of organic matter in the Callovian (Jurassic) of central England. In, R.V. Tyson and T.H.

Pearson (Eds.), Modern and Ancient Continental Shelf Anoxia. Geological Society, Special Publication 58, p. 363-379.

Hughes Clarke, M.W. 1988. Stratigraphy and rock units nomenclature in the oil-producing area of interior Oman. Journal of Petroleum Geology, v. 11, no. 1, p. 5-60.

Hunt, D., T. Allsop and R.E. Swarbrick 1996. Compaction as a primary control on the architecture and development of depositional sequences: conceptual framework, applications and implications. In, J.A. Howell and J.F. Aitken (Eds.), High Resolution Sequence Stratigraphy: Innovations and Applications. Geological Society, Special Publication 104, p. 321-345.

Ibrahim, M.I.A., H.H.A. Al-Hitmi and S.E. Kholeif 2000. Albian-Cenomanian Palynology, Paleoecology and Organic Thermal Maturity of Well DK-B in the Dukhan Oil Field of Western Qatar. GeoArabia, v. 5, no. 4, p. 483-508.

Ichaso, A.A. and R.W. Dalrymple 2009. Tide- and wave-generated fluid mud deposits in the Tilje Formation (Jurassic), offshore Norway. Geology, v. 37, no. 6, p. 539-542.

Immenhauser, A., A. Creusen, M. Esteban and H.B. Vonhof 2000. Recognition and interpretation of polygenic discontinuity surfaces in the Middle Cretaceous Shu'aiba, Nahr Umr, and Natih formations of northern Oman. GeoArabia, v. 5, no. 2, p. 299-322.

Immenhauser, A., W. Schlager, S.J. Burns, R.W. Scott, T. Geel, J. Lehmann, S. Van Der Gaast and L.A. Bolder-Schrijver 1999. Late Aptian to late Albian sea-level fluctuations constrained by geochemical and biological evidence (Nahr Umr Formation, Oman). Journal of Sedimentary Research, v. 69, no. 2, p. 434-446.

Irwin, H. 1980. Early diagenetic carbonate precipitation and pore-fluid migration in the Kimmeridge Clay of Dorset, England. Sedimentology, v. 27, no. 5, p. 577-591.

Jenkyns, H.C. 1986. Pelagic environments. In, H.G. Reading (Ed.), Sedimentary Environments and Facies. Blackwell Scientific Publications, p. 343-397.

Kastner, M. 1984. Sedimentology: control of dolomite formation. Nature, v. 311, no. 5985, p. 410-411.

Katz, B.J. 2005. Controlling factors on source rock development - a review of productivity, preservation, and sedimentation rate. In, N.B. Harris (Ed.), The Deposition of Organic-Carbon-Rich Sediments: Models, Mechanisms, and Consequences. SEPM (Society for Sedimentary Geology), Special Publication 82, p. 7-16.

Kenig, F., J.D. Hudson, J.S.S. Damste and B.N. Popp 2004. Intermittent euxinia: reconciliation of a Jurassic black shale with its biofacies. Geology, v. 32, no. 5, p. 421-424.

Kennedy, M.J. and R.E. Garrison 1975. Morphology and genesis of nodular chalks and hardgrounds in the Upper Cretaceous of southern England. Sedimentology, v. 22, no. 3, p. 311-386.

Kennedy, W.J. 1975. Trace Fossils in Carbonate Rocks. In, R.W. Frey (Ed.), The Study of Trace Fossils. Springer-Verlag, p. 377-398.

Kidwell, S.M. 1985. Palaeobiological and sedimentological implications of fossil concentrations. Nature, v. 318, no. 6045, p. 457-460.

Kirmaci, M.Z. 2008. Dolomitization of the late Cretaceous-Paleocene platform carbonates, Gölköy (Ordu), eastern Pontides, NE Turkey. Sedimentary Geology, v. 203, no. 3-4, p. 289-306.

Lasseur, E., F. Guillocheau, C. Robin, F. Hanot, D. Vaslet, R. Coueffe and D. Neraudeau 2009. A relative water-depth model for the Normandy Chalk (Cenomanian-Middle Coniacian, Paris Basin, France) based on facies patterns of metre-scale cycles. Sedimentary Geology, v. 213, no. 1-2, p. 1-26.

Lazo, D.G., M. Cichowolski, D.L. Rodriguez and M.B. Aguirre-Urreta 2005. Lithofacies, palaeoecology and palaeoenvironments of the Agrio Formation, Lower Cretaceous of the Neuquen Basin, Argentina. Geological Society Special Publications, v. 252, no. 1, p. 295-315.

Leckie, D.A. and L.F. Krystinik 1989. Is there evidence for geostrophic currents preserved in the sedimentary record of inner- to middle-shelf deposits? Journal of Sedimentary Research, v. 59, no. 5, p. 862-870.

Lee, Y.I. and G.M. Friedman 1987. Deep-burial dolomitization in the Ordovician Ellenburger Group carbonates, West Texas and southeastern New Mexico. Journal of Sedimentary Research, v. 57, no. 3, p. 544-557.

Leinfelder, R. 1997. Coral reefs and carbonate platforms within a siliciclastic setting: general aspects and examples from the late Jurassic of Portugal. In, H.A. Lessios and I.G. Macintyre (Eds.), Proceedings of the 8th International Coral Reef Symposium. Smithsonian Tropical Research Institute, Panama, v. 2, p. 1737-1742.

Machent, P.G., K.G. Taylor, J.H.S. Macquaker and J.D. Marshall 2007. Patterns of early post-depositional and burial cementation in distal shallow-marine sandstones: Upper Cretaceous Kenilworth Member, Book Cliffs, Utah, USA. Sedimentary Geology, v. 198, no. 1-2, p. 125-145.

Machhour, L., J.P. Masse, J.L. Oudin, B. Lambert and P. Lapointe 1998. Petroleum potential of dysaerobic carbonate source rocks in an intra-shelf basin: the Lower Cretaceous of Provence, France. Petroleum Geoscience, v. 4, no. 2, p. 139-146.

Macquaker, J.H.S. 1994. A lithofacies study of the Peterborough Member, Oxford Clay Formation (Jurassic), UK: an example of sediment bypass in a mudstone succession. Journal of the Geological Society, v. 151, no. 1, p. 161-172.

Macquaker, J.H.S. and A.E. Adams 2003. Maximizing information from fine-grained sedimentary rocks: an inclusive nomenclature for mudstones. Journal of Sedimentary Research, v. 73, no. 5, p. 735-744.

Macquaker, J.H.S., S.J. Bentley and K.M. Bohacs (in press). Wave-enhanced sediment-gravity flows and mud dispersal across continental shelves: reappraising sediment transport processes operating in ancient mud-dominated successions. Geology.

Macquaker, J.H.S. and K.M. Bohacs 2007. On the accumulation of mud. Science, v. 318, no. 5857, p. 1734-1735.

Macquaker, J.H.S., R.L. Gawthorpe, K.G. Taylor and M.J. Oates 1998. Heterogeneity, stacking patterns and sequence stratigraphic interpretation in distal mudstone successions: examples from the Kimmeridge Clay Formation, U.K. In, J. Schieber, W. Zimmerle and P. Sethi (Eds.), Shales and Mudstones, Volume I: Basin Studies, Sedimentology, and Palaeontology. E. Schweizerbart'sche Verlagsbuchhandlung, p. 163-186.

Macquaker, J.H.S. and C.R. Jones 2002. A sequence-stratigraphic study of mudstone heterogeneity: a combined petrographic/wireline log investigation of Upper Jurassic mudstones from the North Sea (U.K.). In, M. Lovell and N. Parkinson (Eds.), Geological Applications of Well Logs. American Association of Petroleum Association, Methods in Exploration 13, p. 123-141.

Macquaker, J.H.S., K.G. Taylor and R.L. Gawthorpe 2007. High-resolution facies analyses of mudstones: implications for palaeoenvironmental and sequence-stratigraphic interpretations of offshore ancient mud-dominated successions. Journal of Sedimentary Research, v. 77, no. 3-4, p. 324-339.

Markello, J.R. and J.F. Read 1982. Upper Cambrian intrashelf basin, Nolichucky Formation, southwest Virginia Appalachians. American Association of Petroleum Geologists Bulletin, v. 66, no. 7, p. 860-878.

Mazzullo, S.J. 2000. Organogenic dolomitization in peritidal to deep-sea sediments. Journal of Sedimentary Research, v. 70, no. 1, p. 10-23.

Mazzullo, S.J. 2006. Late Pliocene to Holocene platform evolution in northern Belize, and comparison with coeval deposits in southern Belize and the Bahamas. Sedimentology, v. 53, no. 5, p. 1015-1047.

Mazzullo, S.J., W.D. Bischoff and C.S. Teal 1995. Holocene shallow-subtidal dolomitization by near-normal seawater, northern Belize. Geology, v. 23, no. 4, p. 341-344.

Mettraux, M., P. Homewood, A.M. Schwab and F. Guillocheau 1999. Sedimentology and accommodation cycles of Paris Basin Campanian Chalk: the key to high-resolution stratigraphy and seismic signature. In, P.M. Harris, A.H. Saller and J.A. Simo (Eds.), Advances in Carbonate Sequence Stratigraphy: Application to Reservoirs, Outcrops and Models. SEPM (Society for Sedimentary Geology), Special Publication 63, p. 317-334.

Molina, J.M., P.A. Ruiz-Ortiz and J.A. Vera 1997. Calcareous tempestites in pelagic facies (Jurassic, Betic Cordilleras, Southern Spain). Sedimentary Geology, v. 109, no. 1, p. 95-109.

Murris, R.J. 1980. Middle East: stratigraphic evolution and oil habitat. American Association of Petroleum Geologists Bulletin, v. 64, no. 5, p. 597-618.

Myrow, P.M. and J.B. Southard 1996. Tempestite deposition. Journal of Sedimentary Research, v. 66, no. 5, p. 875-887.

Nittrouer, C.A. and L.D. Wright 1994. Transport of particles across continental shelves. Reviews of Geophysics, v. 32, no. 1, p. 85-113.

Osleger, D. 1991. Subtidal carbonate cycles: implications for allocyclic vs. autocyclic controls. Geology, v. 19, no. 9, p. 917-920.

Osleger, D. and J.F. Read 1991. Relation of eustasy to stacking patterns of metre-scale carbonate cycles, late Cambrian, USA. Journal of Sedimentary Research, v. 61, no. 7, p. 1225-1252.

Pevear, D.R. and G.J. Grabowski 1985. Geology and geochemistry of the Toolebuc Formation, an organic-rich chalk from the Lower Cretaceous of Queensland, Australia. In, P.D. Crevello and P.M. Harris (Eds.), Deep-Water Carbonates: Buildups, Turbidites, Debris Flows and Chalks - A Core Workshop. SEPM (Society for Sedimentary Geology), Core Workshop 6, p. 303-341.

Philip, J., J. Borgomano and S. Al-Maskiry 1995. Cenomanian-Early Turonian carbonate platform of northern Oman: stratigraphy and palaeoenvironments. Palaeogeography, Palaeoclimatology, Palaeoecology, v. 119, p. 77-92.

Pickering, K., D. Stow, M. Watson and R. Hiscott 1986. Deep-water facies, processes and models: a review and classification scheme for modern and ancient sediments. Earth Science Reviews, v. 23, no. 2, p. 75-174.

Plint, A.G., A. Tyagi, M.J. Hay, B.L. Varban, H. Zhang and X. Roca 2009. Clinoforms, Paleobathymetry, and Mud Dispersal Across the Western Canada Cretaceous Foreland Basin: evidence from the Cenomanian Dunvegan Formation and Contiguous Strata. Journal of Sedimentary Research, v. 79, no. 3, p. 144-161.

Pomar, L. 2001a. Ecological control of sedimentary accommodation: evolution from a carbonate ramp to rimmed shelf, Upper Miocene, Balearic Islands. Palaeogeography, Palaeoclimatology, Palaeoecology, v. 175, no. 1-4, p. 249-272.

Pomar, L. 2001b. Types of carbonate platforms: a genetic approach. Basin Research, v. 13, no. 3, p. 313-334.

Pomar, L., E. Gili, A. Obrador and W.C. Ward 2005. Facies architecture and high-resolution sequence stratigraphy of an Upper Cretaceous platform margin succession, southern central Pyrenees, Spain. Sedimentary Geology, v. 175, no. 1-4 SPEC. ISS., p. 339-365.

Pomar, L. and M. Tropeano 2001. The Calcarenite di Gravina formation in Matera (Southern Italy): new insights for coarse-grained, large-scale, cross-bedded bodies encased in offshore deposits. American Association of Petroleum Geologists Bulletin, v. 85, no. 4, p. 661-689.

Purdy, E.G., E. Gischler and A.J. Lomando 2003. The Belize margin revisited. 2. Origin of Holocene antecedent topography. International Journal of Earth Sciences, v. 92, no. 4, p. 552-572.

Purser, B.H., M.E. Tucker and D.H. Zenger 1994. Problems, progress and future research concerning dolomites and dolomitization. In, B.H. Purser, M.E. Tucker and D.H. Zenger

(Eds.), Dolomites: A Volume in Honour of Dolomieu. International Association of Sedimentologists, Special Publication 21, p. 3-20.

Raiswell, R., F. Buckley, R.A. Berner and T.F. Anderson 1988. Degree of pyritization of iron as a paleoenvironmental indicator of bottom-water oxygenation. Journal of Sedimentary Research, v. 58, no. 5, p. 812-819.

Rameil, N. 2008. Early diagenetic dolomitization and dedolomitization of Late Jurassic and earliest Cretaceous platform carbonates: a case study from the Jura Mountains (NW Switzerland, E France). Sedimentary Geology, v. 212, no. 1-4, p. 70-85.

Read, J.F. 1982. Carbonate platforms of passive (extensional) continental margins: types, characteristics and evolution. Tectonophysics, v. 81, no. 3-4, p. 195-212.

Read, J.F. 1985. Carbonate platform facies models. American Association of Petroleum Geologists Bulletin, v. 69, no. 1, p. 1-21.

Reid, R.P. and I.G. Macintyre 1998. Carbonate recrystallization in shallow marine environments: a widespread diagenetic process forming micritized grains. Journal of Sedimentary Research, v. 68, no. 5, p. 928-946.

Reid, R.P., I.G. Macintyre and N.P. James 1990. Internal precipitation of microcrystalline carbonate: a fundamental problem for sedimentologists. Sedimentary Geology, v. 68, no. 3, p. 163-170.

Robertson, A.H.F. 1998. Lithofacies evidence for the Cretaceous-Paleogene sedimentary history of Eratosthenes Seamount, eastern Mediterranean, in its regional tectonic context Sites 966 and 967. Proceedings of the Ocean Drilling Program: Scientific Results, v. 160, p. 403-418.

Röhl, H.-J. and A. Schmid-Röhl 2005. Lower Toarcian (Upper Liassic) black shales of the Central European Epicontinental Basin: a sequence stratigraphic case study from SW German Posidonia Shale. In, N.B. Harris (Ed.), The Deposition of Organic-Carbon-Rich Sediments: Models, Mechanisms, and Consequences. SEPM (Society for Sedimentary Geology), Special Publication 82, p. 165-189.

Sadooni, F.N. and A.S. Alsharhan 2004. Stratigraphy, lithofacies distribution, and petroleum potential of the Triassic strata of the northern Arabian plate. American Association of Petroleum Geologists Bulletin, v. 88, no. 4, p. 515-538.

Saller, A.H. 1996. Differential compaction and basinward tilting of the prograding capitan reef complex, Permian, west Texas and southeast New Mexico, USA. Sedimentary Geology, v. 101, no. 1-2, p. 21-30.

Scasso, R.A., M.S. Alonso, S. Lanes, H.J. Villar and G. Laffitte 2005. Geochemistry and petrology of a Middle Tithonian limestone-marl rhythmite in the Neuquen Basin, Argentina: depositional and burial history. Geological Society Special Publications, v. 252, no. 1, p. 207-229.

Schatzinger, R.A., C.T. Feazel and W.E. Henry 1985. Evidence of resedimentation in chalk from the Central Graben, North Sea. Deep-water carbonates. Core workshop, New Orleans, 1985, p. 342-385.

Schieber, J. 1999. Distribution and deposition of mudstone facies in the Upper Devonian Sonyea Group of New York. Journal of Sedimentary Research, v. 69, no. 4, p. 909-925.

Schieber, J. 2003. Simple gifts and buried treasures – implications of finding bioturbation and erosion surfaces in black shales. The Sedimentary Record, v. 1, no. 2, p. 4-8.

Schieber, J. 2009. Discovery of agglutinated benthic foraminifera in Devonian black shales and their relevance for the redox state of ancient seas. Palaeogeography, Palaeoclimatology, Palaeoecology, v. 271, no. 3-4, p. 292-300.

Scholle, P.A., M.A. Arthur and A.A. Ekdale 1983. Pelagic Environment. In, P.A. Scholle, D.G. Bebout and C.H. Moore (Eds.), Carbonate Depositional Environments. American Association of Petroleum Geologists, Memoir 33, p. 619-691.

Scott, R.W. 1990. Chronostratigraphy of Cretaceous carbonate shelf, southeastern Arabia. In, A.H.F. Robertson, M.P. Searle and A.C. Ries (Eds.), The Geology and Tectonics of the Oman Region. Geological Society, Special Publication 49, p. 89-108.

Seilacher, A. and T. Aigner 1991. Storm deposition at the bed, facies, and basin scale: the geologic perspective. In, G. Einsele, A. Ricken and A. Seilacher (Eds.), Cycles and Events in Stratigraphy. Springer-Verlag, p. 249-267.

Sharief, F.A., K. Magara and H.M. Abdulla 1989. Depositional system and reservoir potential of the Middle Cretaceous Wasia Formation in central-eastern Arabia. Marine and Petroleum Geology, v. 6, no. 4, p. 303-315.

Sharland, P.R., R. Archer, D.M. Casey, R.B. Davies, S.H. Hall, A.P. Heward, A.D. Horbury and M.D. Simmons 2001. Arabian Plate Sequence Stratigraphy. GeoArabia, Special Publication 2, 371 p.

Shinn, E.A. 1969. Submarine lithification of Holocene carbonate sediments in the Persian Gulf. Sedimentology, v. 12, no. 1-2, p. 109-144.

Sibley, D.F. and J.M. Gregg 1987. Classification of dolomite rock textures. Journal of Sedimentary Petrology, v. 57, no. 6, p. 967-975.

Smith, A.B., M.D. Simmons and A. Racey 1990. Cenomanian echinoids, larger foraminifera and calcareous algae from the Natih Formation, central Oman Mountains. Cretaceous Research, v. 11, no. 1, p. 29-69.

Stanton, R.J. and E. Flügel 1995. An accretionary distally steepened ramp at an intrashelf basin margin: an alternative explanation for the Upper Triassic Steinplatte "reef" (Northern Calcareous Alps, Austria). Sedimentary Geology, v. 95, no. 3-4, p. 269-286.

Stow, D.A.V., A.Y. Huc and P. Bertrand 2001. Depositional processes of black shales in deep water. Marine and Petroleum Geology, v. 18, no. 4, p. 491-498.

Stow, D.A.V., H.G. Reading and J.D. Collins 1996. Deep seas. In, H.G. Reading (Ed.), Sedimentary Environments: Processes, Facies and Stratigraphy. Blackwell Science, p. 395-453.

Stow, D.A.V. and A.R. Tabrez 1998. Hemipelagites: processes, facies and model. In, M.S. Stoker, D. Evans and A. Cramp (Eds.), Geological Processes on Continental Margins: Sedimentation, Mass-Wasting and Stability. Geological Society, Special Publication 129, p. 317-337.

Swart, P.K., D.L. Cantrell, H. Westphal, C.R. Handford and C.G. Kendall 2005. Origin of dolomite in the Arab-D reservoir from the Ghawar field, Saudi Arabia: evidence from petrographic and geochemical constraints. Journal of Sedimentary Research, v. 75, no. 3, p. 476-491.

Taghavi, A.A., A. Mørk and E. Kazemzadeh 2007. Flow unit classification for geological modelling of a heterogeneous carbonate reservoir: Cretaceous Sarvak Formation, Dehluran field, SW Iran. Journal of Petroleum Geology, v. 30, no. 2, p. 129-146.

Taylor, K.G., R.L. Gawthorpe, C.D. Curtis, J.D. Marshall and D.N. Awwiller 2000. Carbonate cementation in a sequence-stratigraphic framework: Upper Cretaceous sandstones, Book Cliffs, Utah-Colorado. Journal of Sedimentary Research, v. 70, no. 2, p. 360-372.

Taylor, K.G., R.L. Gawthorpe and J.C. Van Wagoner 1995. Stratigraphic control on laterally persistent cementation, Book Cliffs, Utah. Journal of the Geological Society, v. 152, no. 2, p. 225-228.

Taylor, K.G. and J.H.S. Macquaker 2000a. Early diagenetic pyrite morphology in a mudstone-dominated succession: the Lower Jurassic Cleveland Ironstone Formation, eastern England. Sedimentary Geology, v. 131, no. 1-2, p. 77-86.

Taylor, K.G. and J.H.S. Macquaker 2000b. Spatial and temporal distribution of authigenic minerals in continental shelf sediments: implications for sequence stratigraphic analysis. In, C.R. Glen, L. Prévôt-Lucas and J. Lucas (Eds.), Marine Authigenesis: From Global to Microbial. SEPM (Society for Sedimentary Geology), Special Publication 66, p. 309-323.

Taylor, T.R. and D.F. Sibley 1986. Petrographic and geochemical characteristics of dolomite types and the origin of ferroan dolomite in the Trenton Formation, Ordovician, Michigan Basin, USA. Sedimentology, v. 33, no. 1, p. 61-86.

Teal, C.S., S.J. Mazzullo and W.D. Bischoff 2000. Dolomitization of Holocene shallow-marine deposits mediated by sulfate reduction and methanogenesis in normal-salinity seawater, northern Belize. Journal of Sedimentary Research, v. 70, no. 3, p. 649-663.

Terken, J.M.J. 1999. The Natih petroleum system of north Oman. GeoArabia, v. 4, no. 2, p. 157-180.

Tucker, M.E., F. Calvet and D. Hunt 1993. Sequence stratigraphy of carbonate ramps: systems tracts, models and application to the Muschelkalk carbonate platforms of eastern Spain. Sequence stratigraphy and facies associations, p. 397-415.

Tucker, M.E. and V.P. Wright 1990. Carbonate Sedimentology. Blackwell Science, 482 p.

van Buchem, F.S.P., A.Y. Huc, B. Pradier and M. Stefani 2005. Stratigraphic patterns in carbonate source-rock distribution: second-order to fourth-order control and sediment flux. In, N.B. Harris (Ed.), The Deposition of Organic-Carbon-Rich Sediments: Models,

Mechanisms, and Consequences. SEPM (Society for Sedimentary Geology), Special Publication 82, p. 191-223.

van Buchem, F.S.P., B. Pittet, H. Hillgärtner, J. Grötsch, A.I. Al Mansouri, I.M. Billing, H.H.J. Droste, W.H. Oterdoom and M. van Steenwinkel 2002a. High-resolution sequence stratigraphic architecture of Barremian/Aptian carbonate systems in northern Oman and the United Arab Emirates (Kharaib and Shu'aiba formations). GeoArabia, v. 7, no. 3, p. 461-500.

van Buchem, F.S.P., P. Razin, P.W. Homewood, W.H. Oterdoom and J. Philip 2002b. Stratigraphic organization of carbonate ramps and organic-rich intrashelf basins: Natih Formation (middle Cretaceous) of northern Oman. American Association of Petroleum Geologists Bulletin, v. 86, no. 1, p. 21-53.

van Buchem, F.S.P., P. Razin, P.W. Homewood, J.M. Philip, G.P. Eberli, J.P. Platel, J. Roger, R. Eschard, G.M.J. Desaubliaux, T. Boisseau, J.P. Leduc, R. Labourdette and S. Cantaloube 1996. High-resolution sequence stratigraphy of the Natih Formation (Cenomanian/Turonian) in northern Oman: distribution of source rocks and reservoir facies. GeoArabia, v. 1, no. 1, p. 65-91.

Van Lith, Y., R. Warthmann, C. Vasconcelos and J.A. McKenzie 2003. Microbial fossilization in carbonate sediments: a result of the bacterial surface involvement in dolomite precipitation. Sedimentology, v. 50, no. 2, p. 237-245.

Varban, B.L. and A.G. Plint 2008. Palaeoenvironments, palaeogeography, and physiography of a large, shallow, muddy ramp: Late Cenomanian-Turonian Kaskapau Formation, western Canada foreland basin. Sedimentology, v. 55, no. 1, p. 201-233.

Ward, R.F., C.G.S.C. Kendall and P.M. Harris 1986. Upper Permian (Guadalupian) Facies and their Association with Hydrocarbons - Permian Basin, West Texas and New Mexico. American Association of Petroleum Geologists Bulletin, v. 70, no. 3, p. 239-262.

Warren, J. 2000. Dolomite: occurrence, evolution and economically important associations. Earth Science Reviews, v. 52, no. 1-3, p. 1-81.

Wetzel, A. and A. Uchmann 1998. Biogenic sedimentary structures in mudstones - an overview. In, J. Schieber, W. Zimmerle and P. Sethi (Eds.), Shales and Mudstones, Volume I: Basin Studies, Sedimentology, and Palaeontology. E. Schweizerbart'sche Verlagsbuchhandlung, p. 351-369.

Whitaker, F.F. and P.L. Smart 2007. Geochemistry of meteoric diagenesis in carbonate islands of the northern Bahamas: 1. evidence from field studies. Hydrological Processes, v. 21, no. 7, p. 949-966.

Wiggins, W.D. and P.M. Harris 1985. Burial diagenetic sequence in deep-water allochthonous dolomites Permian Bone Spring Formation, southeast New Mexico. In, P.D. Crevello and P.M. Harris (Eds.), Deep-Water Carbonate: Buildups, Turbidites, Debris Flows and Chalks - A Core Workshop. SEPM (Society for Sedimentary Geology), Core Workshop 6, p. 140-173.

Wignall, P.B. 1994. Black shales - Oxford Monographs Geol. Geophys., 30, 127 pp., Oxford (Oxford Univ. Press).

Wright, L.D., C.T. Friedrichs, S.C. Kim and M.E. Scully 2001. Effects of ambient currents and waves on gravity-driven sediment transport on continental shelves. Marine Geology, v. 175, no. 1-4, p. 25-45.

Wright, V.P. and T.P. Burchette 1996. Shallow-water carbonate environments. In, H.G. Reading (Ed.), Sedimentary Environments: Processes, Facies and Stratigraphy. Blackwell Science, p. 325-394.

Yoo, C.M., J.M. Gregg and K.L. Shelton 2000. Dolomitization and dolomite neomorphism: Trenton and Black River Limestones (Middle Ordovician) Northern Indiana, U.S.A. Journal of Sedimentary Research, v. 70, no. 1, p. 265-274.

Chapter 5

Influence of early oxic diagenesis on source potential and lithofacies cyclicity: new insight from the intrashelf-basinal carbonates of the Natih-B Member (Upper Cretaceous Natih Formation, North Oman)

Said A.K. Al Balushi, Joe H.S. Macquaker, and Cathy Hollis

5.1. Abstract

The key processes that control organic-carbon enrichment in ancient intrashelf basins, preserved in carbonate dominated successions are complicated. These data suggest that the observed diagenetic variability is primarily controlled by changes in primary production, sedimentation rate, accommodation availability, bottom-current activity, and microbial processes. All these are related to relative sea-level fluctuations. Although some of the processes are relatively well understood, the varying role of microbial metabolism as a control on early diagenesis has been underestimated. Investigation of core and outcrop samples of the Cenomanian Natih-B Member (North Oman) indicates that this succession experienced differential diagenetic alterations immediately post-deposition, at the sediment/water interface or under a few centimetres of sediment. Transmitted light, cathodoluminescence, and backscattered scanning-electron microscopy, as well as stable-isotopic ($\delta^{13}C$ and $\delta^{18}O$), X-ray diffraction and total organic-carbon (TOC) analyses have been employed to delineate the major controls on the cyclic pattern of early diagenesis and hydrocarbon source potential.

The Natih-B Member is composed of pelagic sediments that exhibit a manifest, high-frequency cyclicity marked by decimetre-thick lithofacies alternations, mainly between: Lithofacies A) compacted, partially-bioturbated, skeletal, organic-carbon-rich mudstone-wackestone, and Lithofacies B) uncompacted, extensively-bioturbated, skeletal, sparry-calcite-rich wackestone-packstone. Studies indicate that sediments were locally reworked

by bottom currents and storms, although bioturbation and cementation at the seafloor obliterated most of the depositional structures, especially in Lithofacies B. The individual units are variously composed of authigenic and biogenic calcite (58.1 to 97.6%, average 78.5%) and organic matter (0.3 to 13.7% TOC, average 3.6%), together with minor detrital quartz and clay, replacive and pore-filling pyrite and dolomite, and phosphate (fish debris). Lithofacies A contains relatively more organic matter, clay, pyrite, and dolomite than Lithofacies B, and constitutes an excellent source for hydrocarbons. Diagenetic textures of Lithofacies A are dominated by compactional deformation of burrow fabrics, faecal pellets and solution seams, in addition to zoned to bright-luminescent, nonferroan sparry- and isopachous-calcite cement in and around uncompacted foraminiferal tests, in an uncemented matrix. In contrast, Lithofacies B does not show any signs of compaction other than microstylolites, and it is dominated by zoned to dull-luminescent, nonferroan, microcrystalline calcite ("microspar") replacement, in addition to pore-filling, predominantly dull-luminescent, nonferroan sparry-calcite cement. Moreover, Lithofacies B shows evidence of isopachous- and meniscus-style cementation, together with geopetal structures and mictritic peloids. Stable-isotopic compositions of both lithofacies were determined from whole-rock samples ($\delta^{13}C$ = −0.9 to +0.9‰, average +0.3‰; $\delta^{18}O$ = −5.6 to −3.7‰, average −4.8‰) and sparry-calcite (both cement and matrix) subsamples ($\delta^{13}C$ = −0.6 to +1.2‰, average +0.6‰; $\delta^{18}O$ = −5.7 to −3.7‰, average −4.3‰); all results being relative to VPDB (Vienna Pee Dee Belemnite).

These petrographic and isotopic characteristics suggest that the Natih-B abundant calcite cements and replacements were precipitated early, prior to compaction, mainly from 'normal' (open, oxic) seawater at slightly elevated depositional temperatures. Some of the slightly negative $\delta^{13}C$ values, however, may argue for an isotopically-light carbon addition, probably derived from organic-matter oxidation by molecular-oxygen respiration, to the 'normal-marine' porewater during syndepositional cementation and microcrystallisation. Based on evidence of extensive seafloor bioturbation and cementation, and their position within the depositional succession, the tops of Lithofacies B are interpreted as hard-/firmgrounds (discontinuity surfaces) that cap shallowing-upward, fifth-order cycles, formed as a function of sediment starvation and increased bottom-current activity during relative sea-level falls. In contrast, Lithofacies A is believed to reflect high organic production coupled with high sedimentation rate and rapid burial, which limited total infaunal colonisation and extensive calcite precipitation, and preserved organic matter

together with some escape burrows and in-place fauna, suggesting episodic sediment influx when more accommodation was available and seafloor diagenesis was minimised during relative sea-level rises. The relatively higher amounts of pyrite and dolomite in Lithofacies A might indicate organic-matter degradation by bacterial sulphate reduction in anoxic sediment during shallow burial.

These are the first reported examples of early normal-marine carbonate precipitation and oxic-respiration processes affecting the Natih-B sediments, which also provide new insight into the overall depositional and diagenetic history of this source-rock-bearing succession that has often been assumed to be dominated by "anoxic" processes.

5.2. Introduction

Fewer diagenetic studies have been conducted on ancient, basinal, fine-grained carbonates (mudstones and wackestones) compared to the equivalent coarser-grained platform carbonates (e.g. grainstones) (e.g. Schneidermann and Harris, 1985; Moore, 1989; Tucker and Wright, 1990; Alsharhan and Scott, 2000; Scholle and Ulmer-Scholle, 2003; Flügel, 2004). This is probably due to the apparently homogenous appearance of most fine-grained sedimentary rocks in core and outcrop, the fact that determining the origin of the individual components is difficult to distinguish using core-/outcrop-based analytical methods, and their apparent insignificance as conventional hydrocarbon reservoirs (Heydari and Wade, 2002). However, recent high-resolution characterisation utilising optical and backscattered electron-optical methods, in addition to mineralogical and geochemical techniques, demonstrate that fine-grained carbonates display significant depositional and diagenetic variability at the centimetre to millimetre scales, and that careful analyses using these techniques allows the origin of the individual components to be determined (Heydari and Wade, 2002; Macquaker and Adams, 2003; Mallon and Swarbrick, 2008; Al Balushi et al., in review). Moreover, organic-carbon-rich carbonate mudstones can be excellent petroleum source rocks in carbonate-dominated hydrocarbon systems (e.g. Sassen et al., 1987; Summerhayes, 1987; Droste, 1990; Klemme and Ulmishek, 1991; Machhour et al., 1998; Demirel and Guneri, 2000; Katz et al., 2000; Doyle et al., 2005; van Buchem et al., 2005; Al Balushi and Macquaker, in press) and, therefore, warrant further investigation.

High-resolution sedimentological and stratigraphic studies of carbonate source rocks have improved our understanding of the key factors controlling their deposition and distribution (e.g. Bohacs, 1998; Bombardiere and Gorin, 2000; Heydari and Wade, 2002; van Buchem et al., 2005; Al Balushi and Macquaker, in press). In spite of recent advances in sedimentary petrology and geochemistry, however, the control on the specific genesis of primary and diagenetic textures of these rocks remains debatable (Munnecke et al., 1997; Heydari and Wade, 2002). For instance, early diagenesis in fine-grained organic-carbon-rich successions is commonly interpreted to be dominated by anoxic processes, with the diagenetic reactions taking place in a closed (or partly-closed) system that is dominated by carbonate precipitation/dissolution reactions, in porewaters that are significantly evolved from marine porewater by contributions due to organic-matter decay (e.g. Hudson, 1977; Brand and Veizer, 1981; Baker et al., 1982; Pingitore, 1982; Czerniakowski et al., 1984; Ricken, 1986; Sansone et al., 1990). In contrast to this, some researchers (e.g. Bathurst, 1979; Patterson and Walter, 1994; Booler and Tucker, 2002; Caron et al., 2005; Raven and Dickson, 2007) have also argued that diagenesis in fine-grained carbonates usually occurs in an open system as a result of precipitation associated with large volumes of migrating, marine-derived water flushing through the pores, especially in the presence of active circulation and bioturbation that also allow constant solutes exchange in the system (see also Hendry, 1993; Hendry and Kalin, 1997). This debate centres on the fact that the degree to which the porewaters are open or closed in these systems is commonly not known. Detailed petrographic, mineralogical, and geochemical investigations of the Upper Cretaceous Natih-B Member (North Oman; Figure 5.1) intrashelf-basinal source lithofacies may help in resolving some uncertainity in this debate.

The effect of carbonate diagenesis within epeiric intrashelf basins was extensive and may had a significant effect on the macroscopic, microscopic and petrophysical characteristics of sedimentary successions (e.g. Machent et al., 2007; Beltran et al., 2009). Intrashelf-basinal, fine-grained carbonates may become replaced and cemented during early diagenesis, prior to significant compaction. The most evident form of this early diagenesis is the development of uncompacted, sparry-calcite-rich units that alternate with compacted organic-carbon-rich units (e.g. Molenaar and Zijlstra, 1997; Westphal and Munnecke, 1997; Westphal et al., 2004; Al Balushi and Macquaker, in press). In these settings, it is commonly postulated that early carbonate precipitation is mainly driven by dissolution

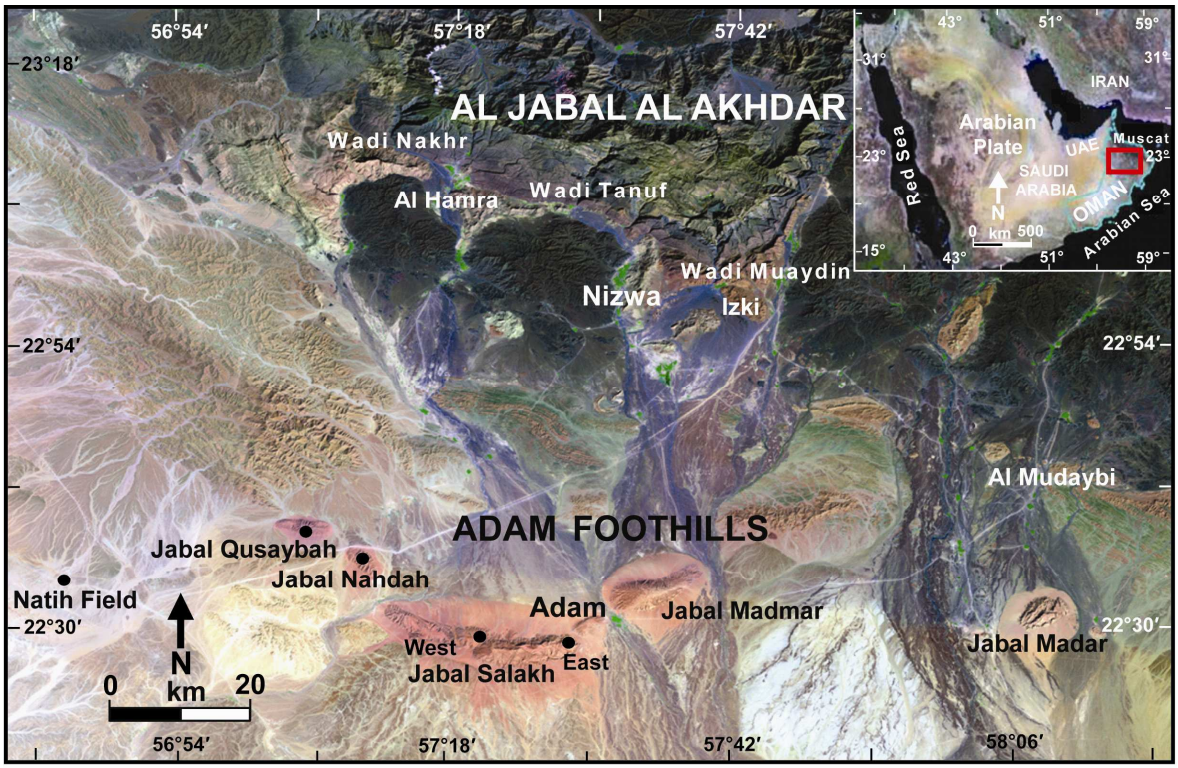

Figure 5.1. Satellite images (source: Petroleum Development Oman [PDO]) illustrating the area of study in North Oman, mainly Adam Foothills exposures (Jabal Salakh East, Jabal Salakh West, Jabal Nahdah and Jabal Qusaybah) and a well from Natih field. Note that in this transect, the well from Natih field is the most distal (i.e. centre of the Natih-B intrashelf basin) and the section from Jabal Salakh East is the most proximal (i.e. margin of the Natih-B intrashelf basin).

and diffusion in response to disturbances of redox profiles through bioturbation of erosional/depositional events (sensu Molenaar and Zijlstra, 1997). This preferential early diagenesis of basinal carbonates has been interpreted to be dependant upon changes in several key factors, including primary lithofacies, mineralogy, sedimentation rate, climate, and seafloor currents and circulation patterns (Tucker and Wright, 1990; Moss and Tucker, 1995).

Cyclic or rhythmic successions with repeated lithofacies motifs of different ages and depositional settings are frequent worldwide (e.g. Weedon, 1986; Droste, 1990; Macquaker and Taylor, 1996; Macquaker et al., 1998; Scasso et al., 2005; van Buchem et al., 2005; Varban and Plint, 2008). In particular, Upper Cretaceous pelagic sequences with carbonate-rich/organic-rich alternation have been the focus of substantial research for many years (e.g. Scholle and Arthur, 1980; Arthur et al., 1984; Hallam, 1987; Ditchfield and Marshall, 1989; Burchette, 1993; Savrda and Bottjer, 1994; Ricken, 1996; Schröder-

Adams et al., 1996; Kuhnt et al., 1997; Scholle et al., 1998; van Buchem et al., 2002; Damholt and Surlyk, 2004; Westphal et al., 2004; Al Balushi and Macquaker, in press). These alternating lithofacies record cyclic changes in the amounts of calcium carbonate and organic carbon, as well as the intensity of bioturbation (Weedon, 1986).

The sole cause of this cyclicity, specifically if it is driven by environmental change or diagenetic alteration, has been the subject of a long-standing debate (see e.g. Hallam, 1986; Weedon, 1986; Savrda and Bottjer, 1994; Böhm et al., 2003; Biernacka et al., 2005; Reuning et al., 2006; Bádenas et al., 2009). Although pelagic carbonate cyclicity in some sequences is primarily a function of primary depositional processes, as revealed by differences in texture, mineralogical composition, fossil type and content, and amount of organic matter (e.g. Fischer et al., 1985; Weedon and Jenkyns, 1999; Fiet and Gorin, 2000; Pittet and Mattioli, 2002; Niebuhr, 2005; Tucker et al., 2009), most rhythmites undoubtedly have, to varying degrees, been diagenetically modified (e.g. Hallam, 1986; Ricken, 1986; Bathurst, 1987; Frank et al., 1999; Westphal et al., 2000; Westphal et al., 2004; Westphal et al., 2008). This is demonstrated by differences in the extent of bioturbation, volume of carbonate cementation/replacement, extent of compaction, and thier isotopic signature.

Recent work by Al Balushi and Macquaker (in press) and Al Balushi et al. (in review) demonstrates that the decimetre- to metre-scale cyclicity (couplets composing both alternating organic-carbon-rich/sparry-calcite-rich lithofacies) in the Cenomanian-aged Natih-B Member intrashelf basin reflects the detailed interplay of several depositional and diagenetic factors, including subtle changes in: a) primary organic and inorganic production, b) porewater oxygen concentration, c) clastic input, d) intensity of bottom-water currents, e) rate of sediment accumulation and burial, f) early (syndepositional) carbonate precipitation, and g) late (burial) compaction. All of these factors, with the exception of the latter (g), appear to be more or less related to high-frequency eustatic sea-level fluctuations and accommodation availability. Van Buchem et al. (2005) estimated the duration of each cycle (couplet) to be in the order of 10,000 to 15,000 years, which indicates a ffith-order cycle range.

In the light of these overarching controls, this paper aims to extend the work of Al Balushi and Macquaker (in press) and Al Balushi et al. (in review), which investigated the

sedimentological and stratigraphical aspects of the Natih-B Member, and discussed the depositional controls on its lithofacies variability and organic-matter enrichment. In particular, it aims to illustrate the relative importance of differential early diagenesis in enhancing lithofacies cyclicity and its influence on organic-matter degradation within a carbonate-dominated, source-rock-bearing succession, as well as investigating the processes that fundamentally controlled early carbonate precipitation in these units. To meet these aims, detailed description of the nature and style of the early-diagenetic features of the two main alternating units (carbonate-rich and organic-rich lithofacies) in the Natih-B Member have been generated.

The interpretations presented in this paper are based upon a comprehensive sedimentological and diagenetic characterisation of the Natih-B Member in the Adam Foothills, where it is best exposed, and from the continuous core within a well in the nearby Natih field (Figure 5.1). The samples were then analysed using optical, cathodoluminescence, backscattered electron-optical, mineralogical (X-ray diffraction [XRD], and geochemical (TOC and stable isotopes) techniques, in order to obtain detailed textural, mineralogical and isotopic data of the carbonate cements/replacements present. On the basis of this investigation, an improved understanding of the processes that resulted in the alternating spar-rich, TOC-depleted carbonates/spar-depleted, carbonaceous mudstones is presented.

5.3. Geological and Stratigraphic Setting of the Natih-B Member

The carbonate-dominated, middle-late Cenomanian sediments of the Natih-B Member were deposited in an intrashelf (intraplatform) basin during a worldwide marine transgression, surrounded by a carbonate-ramp system (Figure 5.2; van Buchem et al., 2002; van Buchem et al., 2005; Al Balushi et al., in review). The Natih-B Member forms part of the late Albian-early Turonian Natih Formation (upper unit of the Wasia Group; Figure 5.2), which is well known in the subsurface of interior Oman and in the excellent outcrops of the Oman Mountains (southern flank of Al Jebel Al Akhdar) and the Adam Foothills in North Oman (e.g. Homewood et al., 2008; Figure 5.1).

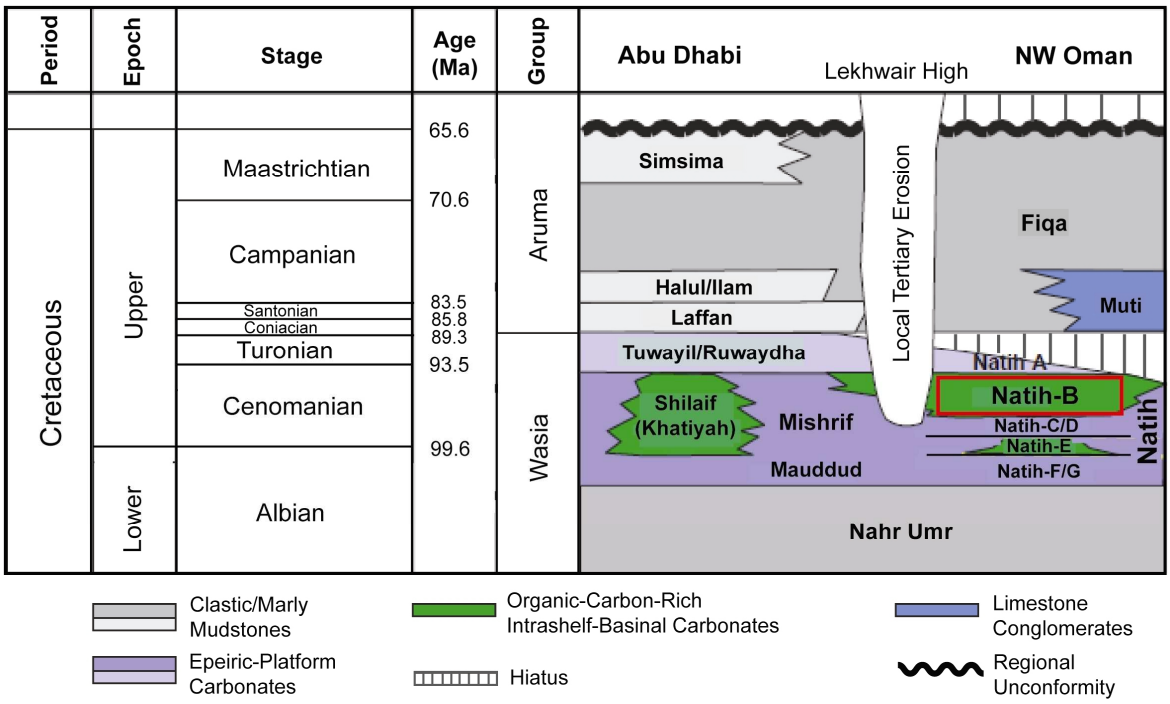

Figure 5.2. Upper Cretaceous stratigraphic columns of Oman and UAE, illustrating the regional lithostratigraphic and chronostratigraphic framework of the Wasia and Aruma groups (modified from van Buchem et al., 2002; original source: Burchette, 1993). Note the temporal and spatial distribution of the Natih-B Member – focus of this study – that is one of seven lithostratigraphic units (members Natih-G to A) within the Natih Formation. Stage subdivisions for the Wasia Group are based on ammonites (see van Buchem et al., 2005), and absolute ages are after Gradstein et al. (2004).

During the time from late Albian to early Turonian, a major phase of carbonate-platform growth took place in Oman, recording the deposition of the Natih Formation shallow-water carbonates over siliciclastic-dominated deposits of the Nahr Umr Formation (e.g. van Buchem et al., 2002; Figure 5.2). Seven lithostratigraphic units have been identified in the Natih Formation (members Natih-G to Natih-A upward; Figure 5.2; e.g. Harris and Frost, 1984; Hughes Clarke, 1988), with characteristic wireline-log responses. The Natih Formation has also been interpreted in terms of a high-resolution sequence-stratigraphic model, where three third-order and fourteen fourth-order depositional sequences have been identified (see Grélaud et al., 2006) based on the outcrop successions in North Oman (cf. Philip et al., 1995; van Buchem et al., 1996; van Buchem et al., 2002). Uplift and erosion in the Turonian terminated sedimentation on the Natih carbonate platform, which was eventually buried beneath an influx of fine-grained terrigenous sediments of the Fiqa Formation (Aruma Group) from the Arabian craton in the Santonian (e.g. Robertson, 1987; Droste and Van Steenwinkel, 2004; Figure 5.2).

Intrashelf-basins developed at two key periods in the late Albian-early Cenomanian and middle-late Cenomanian, in lower Natih-E and upper Natih-B (Figure 5.2; e.g. van Buchem et al., 1996), during high relative sea level, in areas with minor topographic depressions and relatively low rates of carbonate-platform growth, which enhanced the accommodation availability (van Buchem et al., 2002; Droste and Van Steenwinkel, 2004). This study is focused on the Natih-B Member (Figure 5.2), which is around 55 m thick and includes abundant organic-carbon-rich sediments, reaching up to 13.7% TOC (average 5.4%). The Natih-B intrashelf-basinal sediments probably sourced hydrocarbons to the adjacent (intraformational) shoal deposits updip (Grantham et al., 1987; Terken, 1999; Homewood et al., 2008). These subsurface source rocks are characterised by high hydrogen index (400 to 650) and dominated by Type-II kerogen composition (van Buchem et al., 2005) that indicate the predominance of amorphous organic matter, together with some woody material (see Al Balushi and Macquaker, in press; Al Balushi et al., in review). Examples of time-equivalent intrashelf-basinal carbonates to those of the Natih-B Member in the Gulf region include the upper Shilaif/Khatiah Formation of UAE (Figure 5.2), Rumaila Formation of eastern Saudi Arabia, Kuwait and southern Iraq, and upper Sarvak Formation of southwestern Iran (Alsharhan and Nairn, 1988; Burchette, 1993; Aqrawi et al., 1998; van Buchem et al., 2002; Taghavi et al., 2007).

The Natih-B Member is subdivided in the subsurface into four main lithostratigraphic units (B4 to B1, bottom to top), based on gamma-ray readings from wells located in more distal locations of the Natih-B intrashelf basin. Similar pattern of subdivision is followed in the studied cores and exposures, but with the further subdivision of the B4 unit into B4-II and B4-I subunits, and B2 unit into B2-II and B2-I subunits, based on detailed lithological characteristics (see Al Balushi et al., in review; Figures 5.3 and 5.4).

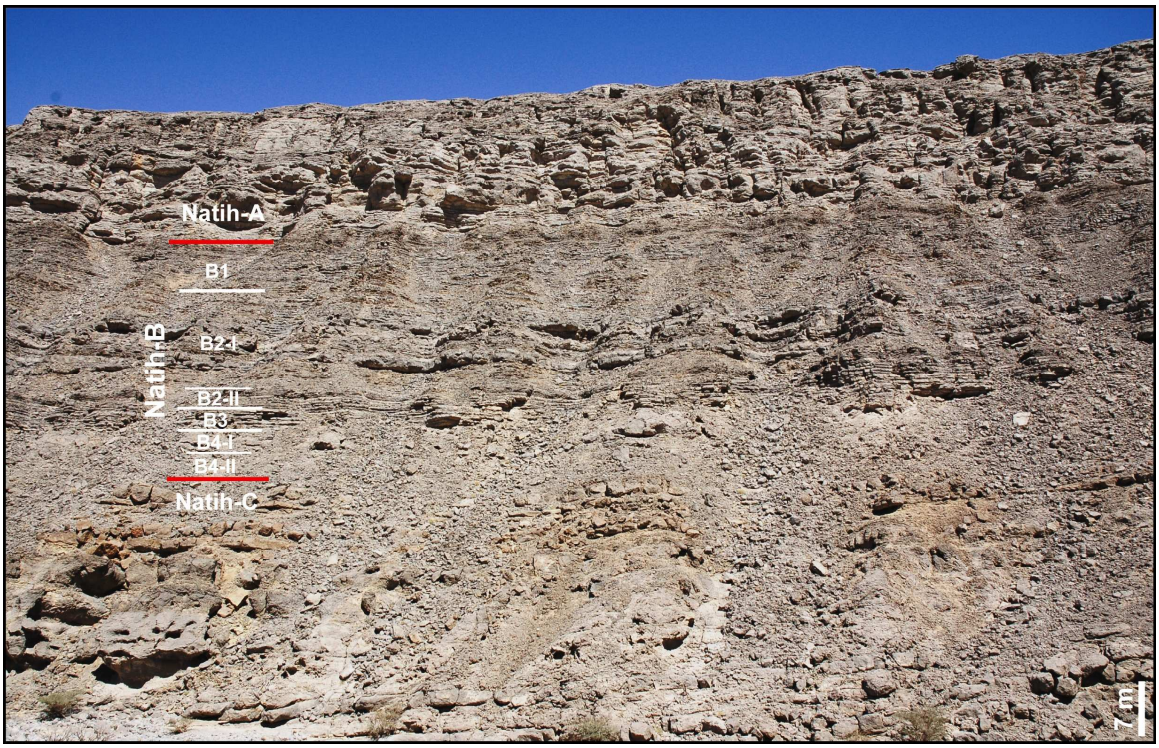

Figure 5.3. Looking NNW; outcrop section in Jabal Salakh West (see Figure 5.1 for location) showing upper members of the Natih Formation (Natih-C to Natih-A), with subdivision of the Natih-B succession. The Natih-B Member overlies brownish, iron-enriched, strongly-bioturbated, bored hardground (top Natih-C), and is overlain by whitish, well-bedded unit of Natih-A with an eroded top.

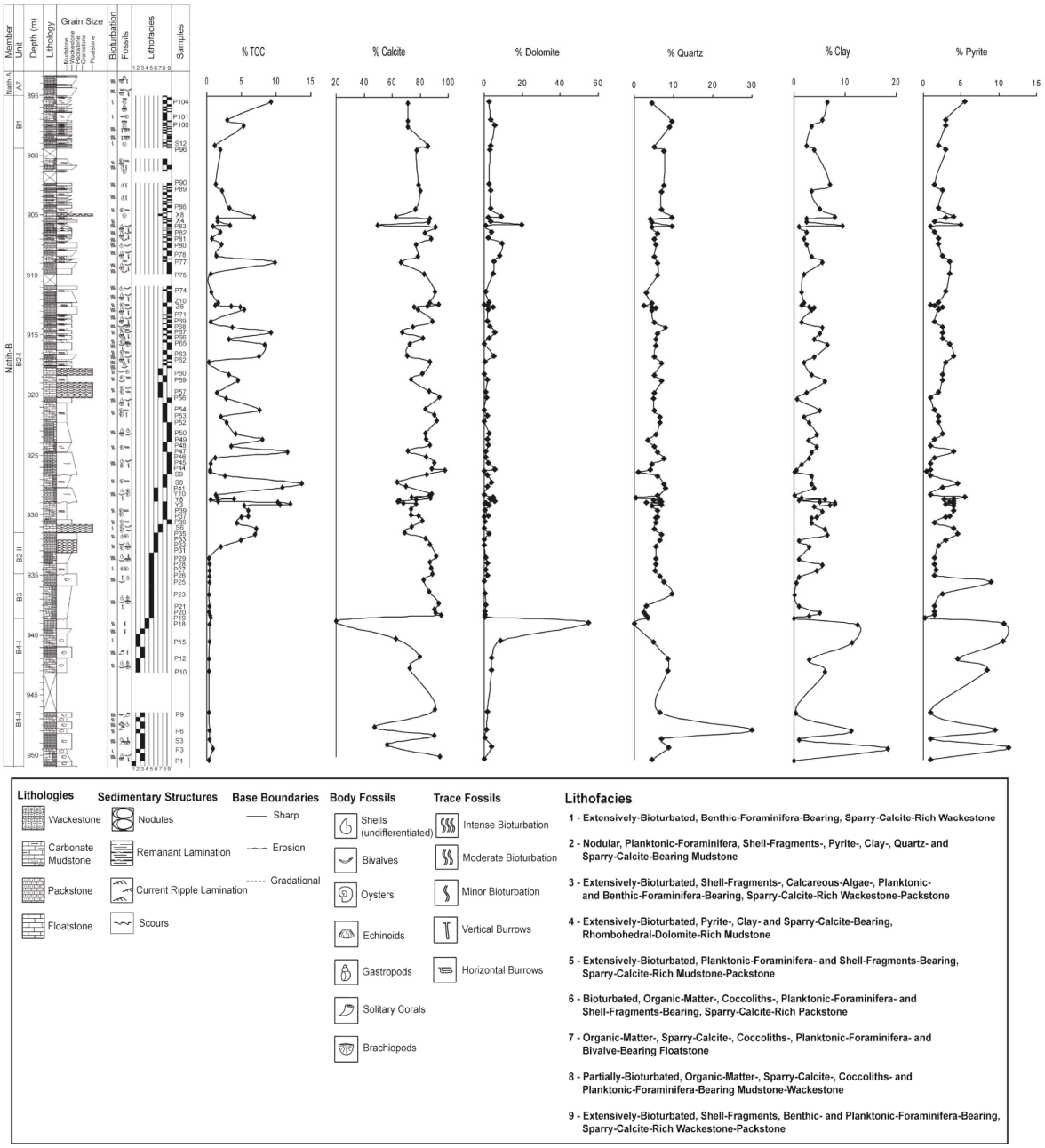

Figure 5.4. Graphic log of the Natih-B Member based on core from a well in Natih field (see Figure 5.1 for location) illustrating the internal lithostratigraphy and temporal lithofacies variability (Lithofacies 1 to 9; see also Al Balushi et al., in review), with indication of sample locations and their TOC and mineralogical percentages (see also Appendices B and C). Mineralogical contents were estimated from combined XRD and petrographic analyses. Note the fluctuating trend of these percentages, especially with TOC in units B2 and B1, reflecting rhythmic bedding, predominantly between Lithofacies 8 and 9, which are referred to in this study as Lithofacies A and Lithofacies B, respectively. The depth referred to here is driller's depth.

5.4. Methods

5.4.1. Outcrop- and Core-based Analyses

This study is based on macroscopic observations at the exposures and core shed, and on data from microscopic, mineralogical, and geochemical investigations at the laboratory. Four outcrop Natih-B sections in the Adam Foothills (Jabal Salakh East, Jabal Salakh West, Jabal Nahdah, and Jabal Qusaybah) and a subsurface core section in the nearby Natih field, North Oman (Figure 5.1) were studied. High-resolution sedimentary logs were measured (see Appendix A), and samples were collected along a 100-km-long transect from the five locations across the Natih-B intrashelf basin. Overall, the logs from these locations enabled the recognition of recurring lithofacies and associated carbonate-cemented horizons, identification of shell concentrations and key surfaces separating the various lithofacies or groups of lithofacies, and determination of sequence architecture and stacking patterns (e.g. Figure 5.4). Identification of the cemented (and replaced) horizons was achievable from the studied sections due to their characteristic whitish and light-grey colour in the core and strong resistance to weathering in the field. Specific horizons were traced to determine lateral continuity and overall lithofacies variability.

The focus of this paper is primarily placed on the textural observations and geochemical investigations of early-lithified features and marine cementation and replacement of calcite. Over 300 fresh, least-weathered samples of spar-rich and organic-rich carbonates were hand collected from the five-studied sections. In preparation for detailed petrographic analyses, 286 polished thin sections (≤ 30 µm thick) were made. Prior to thin-section preparation, sliced and slabbed specimens were studied, and macro-sedimentary features were recorded. Compositional and diagenetic characteristics of the lithified layers and their encasing lithologies are based on combined optical and electron-optical petrography of thin sections.

5.4.2. Petrographic Analyses

Thirty four selected thin sections were half stained using a combined Alizarin Red S and potassium ferricyanide solution to differentiate dolomite from calcium carbonate, and also

to determine whether their cements/replacements are ferroan or nonferroan (see Dickson, 1965; Adams and Mackenzie, 1998). All the 286 prepared thin sections were scanned utilising a flatbed scanner (Epson Perfection 3170 Photo) to generate high-quality digital images of whole thin sections and record textural details at low resolution (10^{-2} to 10^{-3} m scale). The thin sections were then examined optically at low to medium resolution under transmitted light (TL), both plane-polarised light (PPL) and cross-polarised light (XPL), using a petrographic microscope (Nikon Optiphot2-Pol). The microscope was attached to a digital camera (Jenoptik Jena D-07739), and a set of photomicrographs were captured from 142 selected thin sections. This standard petrographic investigation helped to obtain lithological, textural, compositional, and diagenetic information at 10^{-3} to 10^{-4} m scales.

For the discrimination of the different carbonate-cement fabrics, generations and zonations, 68 polished thin sections were investigated by cold-cathode cathodoluminescence (CL). A CITL Cathodoluminescence Unit (Model CCL 8200 mk3) was employed together with an Olympus BH-2 petrographic microscope. Operating conditions for the CL Unit were maintained at approximately 20.0 kV cathode voltage, 300.0 μA electron-beam current, and 0.2 torr vacuum. Photomicrographs (under both PPL and CL) from each thin section were obtained using a digital camera (Jenoptik Jena D-07739).

After initial optical investigations (TL and CL microscopy), 133 thin sections were chosen for detailed electron-optical analyses to examine the textures and constituents at even higher resolution (10^{-4} to 10^{-5} m scale). A JEOL 6400 scanning electron microscope (SEM) equipped with a solid-state, Link Systems 4-Quadrant, backscattered electron (BSE) detector was used to analyse the carbon-coated thin sections. The SEM was operated at 20 kV, 2 nA and 15-mm working distance, and BSE photomicrographs were recorded from each thin section using a Semafore digital framestore. Minerals were identified utilising a semiquantitative, energy-dispersive, X-ray microanalysis system that determined the major elemental compositions (including Ca, Si, Al, Fe, S, Mg, P, and K) of individual grains and cements/replacements within the samples. The BSE microscopy was a crucial element of this study and was used to characterise and geochemically quantify the diagenetic phases of carbonates and other minerals.

5.4.3. Mineralogical and Geochemical Analyses

The main mineral phases in the different Natih-B lithofacies were determined by XRD on 91 bulk samples. A Philips PW1730 X-ray diffractometer (Cu Kα radiation) was employed, utilising a tube voltage of 40 kV and a tube current of 20 mA, with a step size of 0.01º and time constant of 2.00 s. During each XRD analysis, a thin smear was prepared by mixing approximately 0.5 g of the powdered sample with a few drops of amyl acetate and then left to dry on a small glass slide, which is then inserted in the diffractometer. Semiquantitative estimations of bulk-mineralogy fractions were carried out using peak area measurements (sensu Schultz, 1964).

TOC contents were measured by combustion under oxygen flow, utilising an induction furnace on a LECO carbon and nitrogen analyser (TruSpec CN) at the Department of Environmental and Geographical Sciences, Manchester Metropolitan University (UK). The TOC measurements were conducted after treating the powdered bulk samples with hydrochloric acid (1 M HCl) to remove carbonate carbon. Total carbon (TC) of each untreated sample had been previously determined using the same furnace. The difference between the TC and TOC values yielded the total carbonate carbon (TCC) content. Sample reproducibility is estimated at about 0.1% for all values.

In addition to whole-rock TOC and XRD data, component abundances in each sample were quantified by visual estimation from the optical and electron-optical photomicrographs, and with reference to standard comparison charts (see Flügel, 2004). Some of these data are reported in Figure 5.4 (see also Appendices B and C).

Carbon and oxygen stable-isotope analyses were performed on 25 powdered bulk samples and carefully-selected subsamples from both intrashelf-basinal, alternating organic-carbon-rich and sparry-calcite-rich intervals (see Table 5.1 and Figure 5.5), in order to unravel the diagenetic history of these carbonates, which comprise mixtures of authigenic and biogenic materials. The subsamples were extracted with a steel needle from the same cut rock faces from which the thin sections were prepared, so isotope subsamples can be directly related to the microscopically-identified calcite fractions – whether diagenetic or original. The separate subsamples were taken from unaltered oyster and pecten shells (5 subsamples), sparry-calcite-cemented shell fragments (4 subsamples), sparry-calcite-cemented

Table 5.1. Mineralogical and isotopic compositions of selected Lithofacies A and Lithofacies B samples (Natih field; see Figure 5.4 and Appendix B). Abbreviations: dd = driller's depth; Cal = calcite; Dol = dolomite; Qua = quartz; Pyr = pyrite; Cla = clay; WR = whole-rock sample; M = matrix subsample; CS = calcite-cemented shell subsample; US = unaltered shell subsample; CF = calcite-cemented fracture subsample.

General Sample Data				Whole-Rock Semiquantitative Mineralogical Data (%)							$\delta^{13}C$ (‰ VPDB)					$\delta^{18}O$ (‰ VPDB)				
Name	Unit	Lithofacies	Depth (m dd)	TOC	Cal (Total)	Cal (Cement)	Dol	Qua	Pyr	Cla	WR	M	CS	US	CF	WR	M	CS	US	CF
P96	B1	A	898.50	2.0	77.5	62.5	3.0	7.5	3.0	4.0	0.9	0.8	-0.1	1.0		-5.2	-4.3	-3.8	-4.2	
X4	B2-I	B	904.60	1.5	86.0	36.0	3.5	4.5	1.5	2.5	0.6	0.7		1.7	1.3	-5.3	-4.3		-4.1	-9.3
P67	B2-I	A	914.00	9.3	67.2	18.2	5.5	6.0	2.5	5.0	0.5	0.4		1.1		-5.6	-5.7		-4.3	
P56	B2-I	A	919.50	2.8	93.6	24.1	1.1	4.8	0.9	0.6	0.2		1.2	0.8		-4.9		-4.0	-4.3	
P44	B2-I	B	925.50	0.5	88.3	80.3	5.5	4.0	1.0	0.5	-0.9	-0.6				-3.7	-3.9			
S9	B2-I	B	925.65	0.5	97.7	89.0	0.1	1.0	0.4	0.1	-0.7	-0.2	1.0			-3.8	-4.0	-3.7		
Y8	B2-I	B	927.90	1.5	86.4	65.4	4.5	0.5	5.5	1.5	0.8	0.5		1.2		-5.1	-5.3		-4.7	
P31	B2-II	A	932.00	2.0	87.1	63.2	0.0	5.5	2.0	3.0	0.6	0.7	1.2			-4.7	-4.6	-5.1		

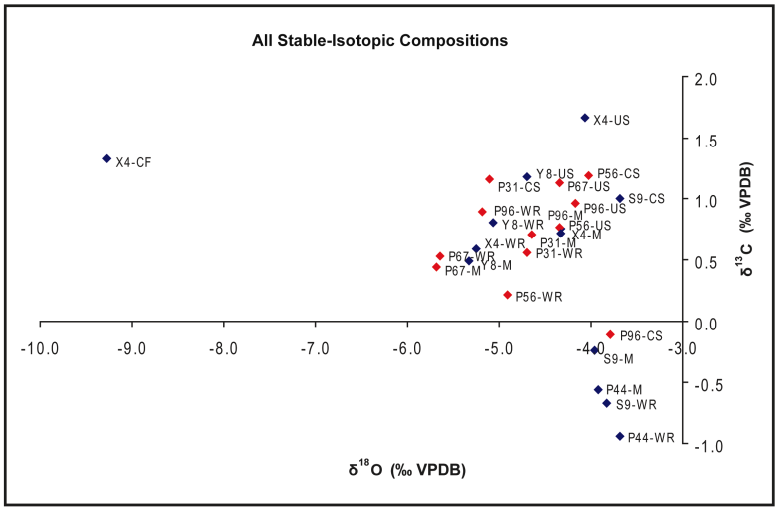

Figure 5.5. Cross-plot showing all the carbon and oxygen stable-isotopic compositions from Table 5.1. The red dots refer to Lithofacies A and the blue dots refer to Lithofacies B (see Table 5.1 above for abbreviations). The average stable-isotopic composition of all analysed samples and subsamples of both lithofacies is +0.6‰ VPDB $\delta^{13}C$ and −4.7‰ VPDB $\delta^{18}O$. The average for Lithofacies A is +0.7‰ VPDB $\delta^{13}C$ and −4.7‰ VPDB $\delta^{18}O$; and for Lithofacies B is +0.5‰ VPDB $\delta^{13}C$ and −4.8‰ VPDB $\delta^{18}O$.

microfracture (1 subsample) and sparry-calcite-dominated, fine-grained matrix (7 subsamples), in addition to 8 homogenised bulk samples (4 from each lithofacies) [see Table 5.1 and Figure 5.5]. Isotopic analyses of calcite were conducted after detailed petrographic study (thin-section staining, TL, CL, and BSE microscopy) and XRD and TOC analyses. Dolomitised samples were not collected for stable-isotope analyses because they are rare in the Natih-B intrashelf-basinal sediments; and it is very difficult to separate dolomite from calcite and other components due to their very fine-grain size.

Before performing the stable-isotopic analyses, all the powdered samples were treated by overnight combustion in an oxygen atmosphere at a pressure of 0.2 mbar in order to remove any organic matter. CO_2 gases were generated by reacting around 3.0 mg of

powdered sample with about 2.0 mL of anhydrous 100% orthophosphoric acid (H_3PO_4) in an online-automated preparation system at 25°C (sensu McCrea, 1950). The evolved CO_2 gases were collected cryogenically (−200°C) at regular intervals and analysed for calcite on an automated VG SIRA-12, gas-sourced mass spectrometer in the University of Liverpool Stable Isotope laboratory (UK) where $^{13}C/^{12}C$ and $^{18}O/^{16}O$ ratios were measured. Isotopic ratios were corrected by standard procedures (sensu Craig, 1957). All results are presented in conventional delta (δ) notation as parts per mil (‰) deviation from the Vienna Pee Dee Belemnite (VPDB) international standard (Coplen, 1994). The analytical precision is better than 0.1‰ for both $\delta^{13}C$ and $\delta^{18}O$ values.

5.5. Background to all Lithofacies in the Natih-B Member and their Depositional Environments

5.5.1. General Characteristics

The majority of the carbonate sediments encountered in the Natih-B Member have mudstone through to packstone textures, together with some floatstones ('shell beds'). Mudstones and wackestones, however, are the most abundant (Figure 5.4). High-resolution lithofacies analyses using petrographic, mineralogical and geochemical techniques, in addition to core and field descriptions, have enabled the identification of nine lithofacies in this succession (Figure 5.4; Lithofacies 1 to Lithofacies 9; see Al Balushi et al., in review for more detailed descriptions). These lithofacies are differentiated from one another on the basis of their sedimentary structures and relative proportions of biogenic, detrital and authigenic components, as well as their depositional textures. In these lithofacies, the calcite content varies from 19.7 to 97.6% (average 78.3%), quartz content from 0.0 to 29.9% (average 5.9%), clay content from 0.0 to 18.4% (average 3.9%), TOC content from 0.3 to 13.7% (average 3.3%), with dolomite, pyrite and phosphate (fish debris) each varying from 0.0 to 55.5% (average 3.2%), 0.2 to 11.3% (average 3.0%) and 0.0 to 5.0% (average 1.6%), respectively (see Figure 5.4).

The common occurrence of mixed skeletal debris and presence of scoured surfaces and lenticular laminae suggest that the Natih-B sediments were locally reworked by storms and bottom currents (Al Balushi and Macquaker, in press; Al Balushi et al., in review).

Bioturbation and carbonate replacement and cementation, however, obliterated most of the depositional structures in these sediments, especially in the sparry-calcite-rich units (e.g. Lithofacies 9; Al Balushi et al., in review). The organic-carbon-rich units (e.g. Lithofacies 8), following compaction, developed thin depositional beds (thin partings) that could be mistakenly identified as depositional laminae. Moreover, these units contain evidence of in-place fauna, including thick-shelled oysters, flattened pectens and benthic foraminifera (Al Balushi and Macquaker, in press).

5.5.2. Depositional Environments

The overall Natih-B Member depositional environment represents a transition from a proximal lagoon and inner-ramp setting to a distal outer-ramp and intrashelf-basin environment where primary production was high and bottom-water conditions varied form oxic to dysoxic (Al Balushi and Macquaker, in press; Al Balushi et al., in review). The presence of benthic foraminifera (including miliolids, miliolinid alveolinids, *Nezzazata* spp. and *Dicyclina* spp.), planktonic foraminifera, calcareous algae and shells (including bivalves, echinoderms and ostracods) in the B4 unit (Lithofacies 1 to 4; Figure 5.4) and B3 unit (Lithofacies 5; Figure 5.4) suggests that these units were deposited in an inner-ramp (< 35 m deep) environment. Subsequently, the inner-ramp environment changed into a mid-ramp environment during deposition of the B2-II subunit (Lithofacies 6, bioturbated skeletal packstones with diverse fauna and flora; Figure 5.4). This transgressive event recorded the development of an outer-ramp and intrashelf-basin (40 to 60 m maximum water depth) environment, with sedimentation dominated by the accumulation of benthic and planktonic foraminifera, coccoliths, and both benthic and planktonic bivalves, together with shallow-platform-derived skeletal debris, calcispheres and some fish debris. It was in this environment that the pelagic-sediment-rich B2-I subunit and B1 unit (Lithofacies 7 to 9; Figure 5.4) were deposited (Al Balushi et al., in review).

This study is focused on the upper half of the Natih-B Member (B2 and B1 units; Figures 5.3 and 5.4) where the pelagic, intrashelf-basinal deposits occur. Specifically, this contribution will concentrate on the alternating organic-carbon-rich (Lithofacies 8)/sparry-calcite-rich (Lithofacies 9) deposits (see Figures 5.4 and 5.6). In this paper we refer to Lithofacies 8 as Lithofacies A and Lithofacies 9 as Lithofacies B, in order to avoid confusion with our previous work on the Natih-B Member (Al Balushi and Macquaker, in

press; Al Balushi et al., in review). Lithofacies A is here described as compacted, partially-bioturbated, skeletal, organic-carbon-rich mudstone-wackestone, and Lithofacies B as uncompacted, extensively-bioturbated, skeletal, sparry-calcite-rich wackestone-packstone. In this paper, these lithofacies are described and interpreted in terms of both their depositional features and their diagenetic overprints (including bioturbation, cementation, recrystallisation, and compaction).

5.6. Detailed Characteristics of Lithofacies A

5.6.1. Description

Lithofacies A represents the bulk of the source-rock intervals in the Natih-B Member. It is characterised by high organic-matter contents that reach up to 13.7% in TOC (average about 6.1%, based on 35 samples form a well in the Natih field; Figure 5.4). Horizons represented by this lithofacies vary in thickness from 0.015 to 1.650 m (average about 0.175 m; Figure 5.6). Typically, Lithofacies A is fine-grained, with mudstone to wackestone textures, compacted, and appears grey to very dark grey, or even black, on fresh surfaces (Figure 5.6). In the field, the units exhibit a well-defined fissility (Figures 5.6b and 5.7a) with some in-place, thick-shelled oysters being well preserved along many thin partings (Figure 5.7a).

Lithofacies A is partially bioturbated (Figure 5.6a), displaying textures of compressed *Planolites* isp. and *Phycosiphon* isp. (Figures 5.6a and 5.7b to f), with rare *Thalassinoides* isp. In addition, in-place flattened pectens are commonly well preserved (Figure 5.7f), together with some other undifferentiated bivalve fragments and fish debris, and a few echinoid spines and ostracods (mostly disarticulated). Rare small, calcareous, benthic foraminifera have also been detected in these units. The partial bioturbation of the sediment disrupted most of the primary sedimentary structures in the rock, and left only some remnant thin bedding planes (spaced from 3 to 30 mm apart; Figures 5.6a and 5.7e, f) and mostly bounded by either flattened bivalve shells (e.g. pectens; Figure 5.7f) or concentrations of planktonic foraminifera (Figure 5.7e).

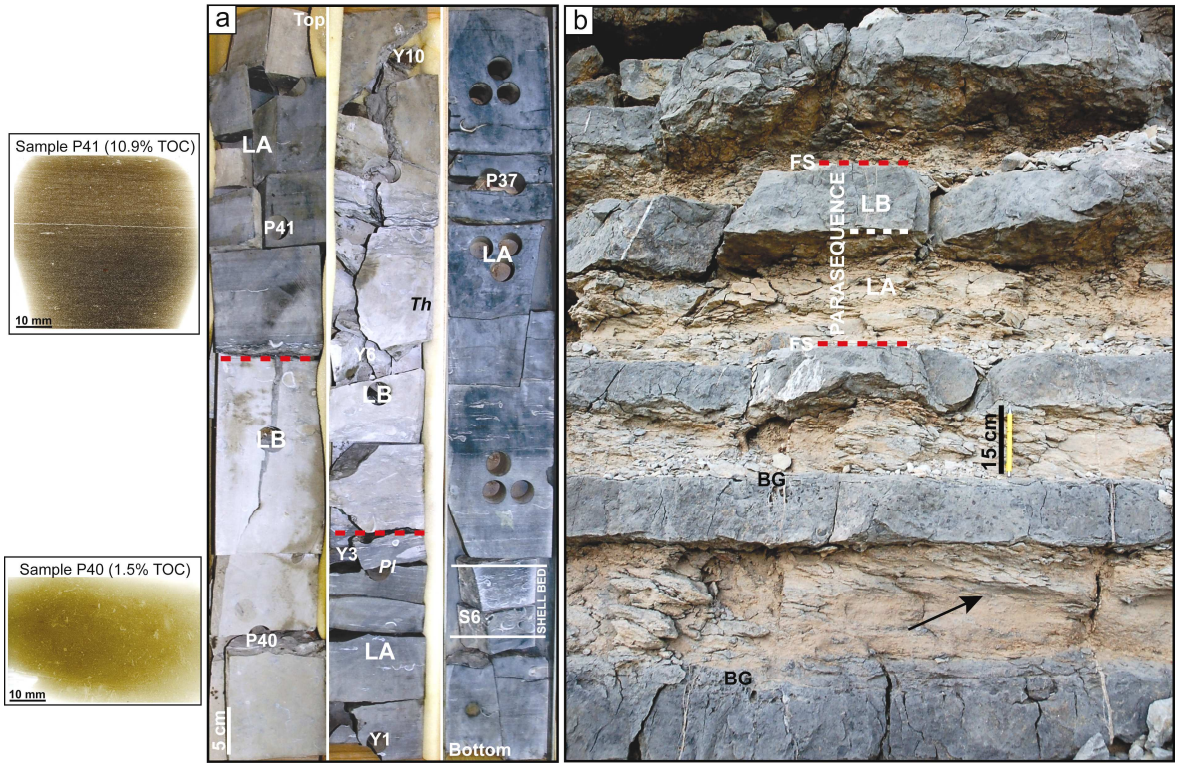

Figure 5.6. (a) Core photograph (Natih field, lower Natih-B2-I; see Figure 5.4 for samples depth and other characteristics) and **(b)** outcrop photograph (Jabal Salakh West, upper Natih-B1), both illustrating macroscopic characteristics of the intrashelf-basinal, alternating units: Lithofacies A (LA; compacted, partially-bioturbated, skeletal, organic-carbon-rich mudstone-wackestone) and Lithofacies B (LB; uncompacted, extensively-bioturbated, skeletal, sparry-calcite-rich wackestone-packstone). Note in (a) the uncompacted bioclasts and trace fossils (predominantly *Thalassinoides* isp. [*Th*]) in lithofacies B, and relatively compacted bivalves and compressed burrows (predominantly *Planolites* isp. [*Pl*] in lithofacies A, with relict, thin (cm-thick), depositional beds. Together, these lithofacies form dm- to m-thick shallowing-upward parasequences, capped by marine flooding surfaces (FS) associated with marine hard-/firmgrounds (discontinuities). Note, in photograph b, some boring (BG) features at the top of Lithofacies B. At the exposure, as in (b), Lithofacies A appears fissile and strongly weathered in comparison to Lithofacies B, which looks hard, well-cemented, and more resistant to weathering. Note also the inclined, nonparallel, lenticular lamination in Lithofacies A, arrowed in (b), enhanced by compaction and weathering.

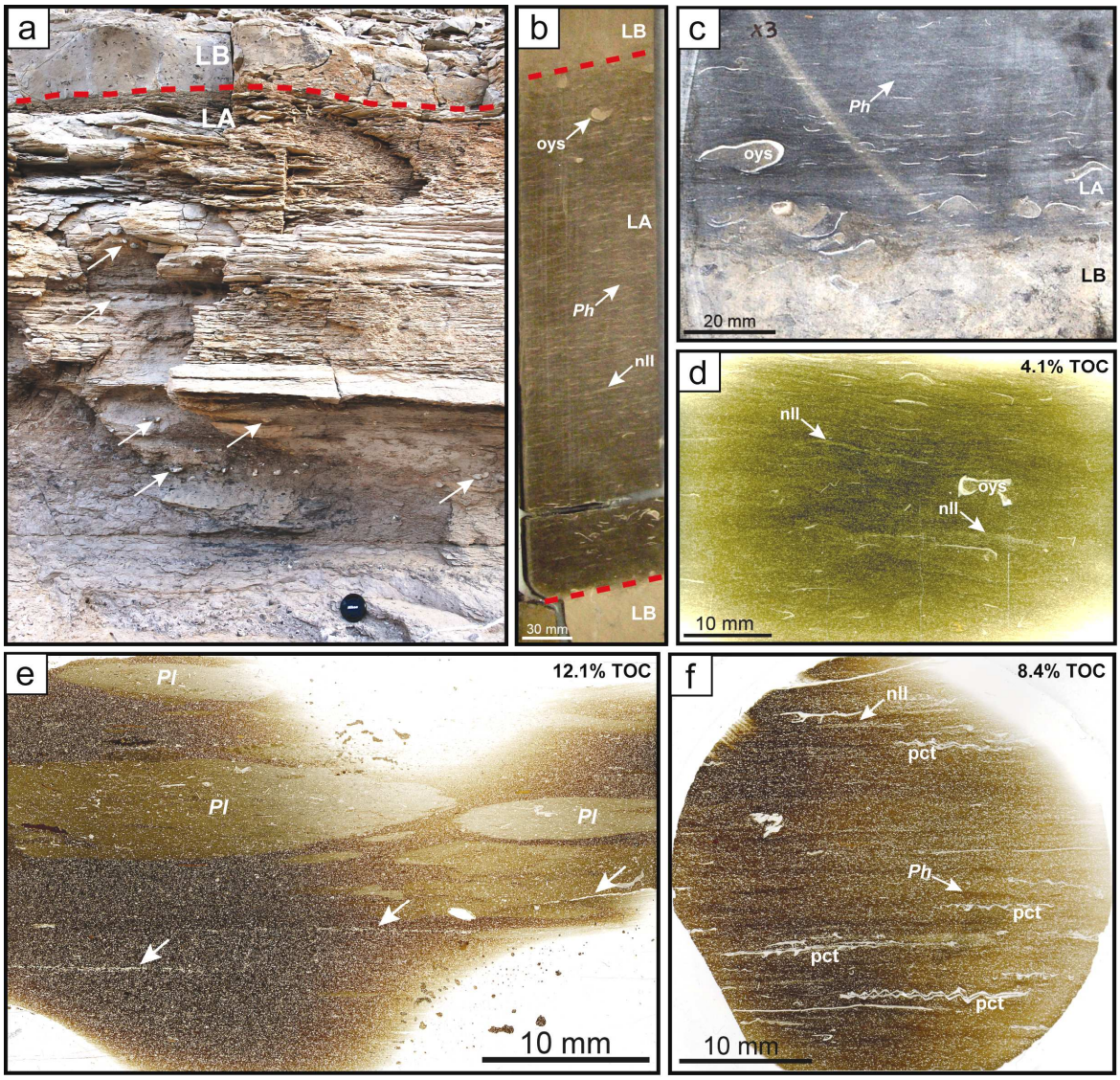

Figure 5.7. Outcrop and core photographs and thin-section scans illustrating characteristic macroscopic features of Lithofacies A (LA). **(a)** Outcrop photograph (Jabal Salakh West, upper Natih-B2) showing well-developed fissility in Lithofacies A, with well-preserved, in-place oysters (arrowed) present along many thin partings. Note the oyster-colonised surface at the bottom of the photograph and the black fresh (least weathered) colour of this organic-carbon-rich lithofacies. Note also the sharp boundary between Lithofacies A and Lithofacies B (LB). Lens cap 5 cm across. **(b)** Core photograph (Fahud field, core depth interval: 584.30 to 583.62 m driller's depth) illustrating evidence of nonparallel, lenticular lamination (nll), partial bioturbation attributed here to *Phycosiphon* isp. (*Ph*), in-place oysters (oys) and reworked shell fragments in Lithofacies A. **(c)** Core photograph (sample X3; see Figure 5.4 for sample depth and other characteristics) illustrating similar features as in (b). **(d)** Thin-section scan showing detail of (d). **(e)** Thin-section scan (sample Y3; Figure 5.4) showing compressed *Planolites* isp. (*Pl*) and relict thin beds capped by discontinuous bands (arrowed) of concentrated planktonic foraminifera. **(f)** Thin-section scan (sample P65; Figure 5.4) illustrating similar features as in (b), (c) and (d), as well as the presence of flattened pectens (pct) at bedding planes of relict, thin, depositional beds.

Lithofacies A is also characterised by the development of lenticular (inclined) laminae (Figures 5.6 and 5.7) that are often disrupted by a burrowing infauna. These nonparallel laminae usually contain compacted faecal pellets, which enclose fragmented planktonic foraminifera, disarticulated coccoliths, and organic matter (Figure 5.8).

The matrix of this lithofacies is dominated by coccoliths and nonkeeled planktonic foraminifera, together with organic matter (predominantly amorphous; 2.0 to 13.7% TOC, average 6.1%, based on subsurface samples), planktonic bivalves and rare zoned to dull-luminescent, nonferroan microcrystalline calcite ("microspar") [Figure 5.8]. Minor detrital quartz (Figure 5.8f; average 6.3%), clay (average 4.9%, including kaolinite [Figure 5.8d and e]) and dolomite (average 3.4%) are present in the rock matrix, together with rare pyrite (average 2.9%, both framboidal and euhedral; Figure 5.8e and f). The dolomite predominantly occurs as replacive, nonferroan, euhedral (planar-e type) rhombs up to 100 µm across (Figure 5.8e and f), sparsely scattered throughout Lithofacies A. The dolomite rhombs are also present within and along pressure-solution seams (Figure 5.8f), and in places crosscut by them. Pressure-solution seams also frequently cut through uncompacted, sparry-calcite-cemented tests of planktonic foraminifers (Figure 5.8e and f). They are commonly associated with concentrations of organic matter and clay, and exhibit discrete, wispy ('horsetail) textures (Figure 5.8e and f).

The majority of the tests of the planktonic foraminifera are uncompacted, and their shelter porosity is commonly filled with zoned and bright-luminescent, nonferroan sparry calcite (Figure 5.8). This shelter porosity is rarely filled/co-filled with zoned, nonferroan sparry dolomite, pyrite (both framboidal and euhedral), and/or kaolinite (predominantly as curved booklets) that in places is engulfed by growth of calcite crystals (Figure 5.8e). Moreover, isopachous crusts of fibrous to bladed, nonferroan, high-Mg calcite cements are commonly well developed around the outer tests of the planktonic foraminifera (Figure 5.8c to e). Where foraminiferal tests are partly cemented, they have been crushed by compaction (Figure 5.8c). The sediment surrounding foraminiferal tests is also strongly compacted (Figure 5.8c to f). In addition to the calcite cement in the foraminiferal tests, the shelter porosity of the oysters is commonly infilled with nonferroan sparry-calcite cement (Figure 5.8a and b).

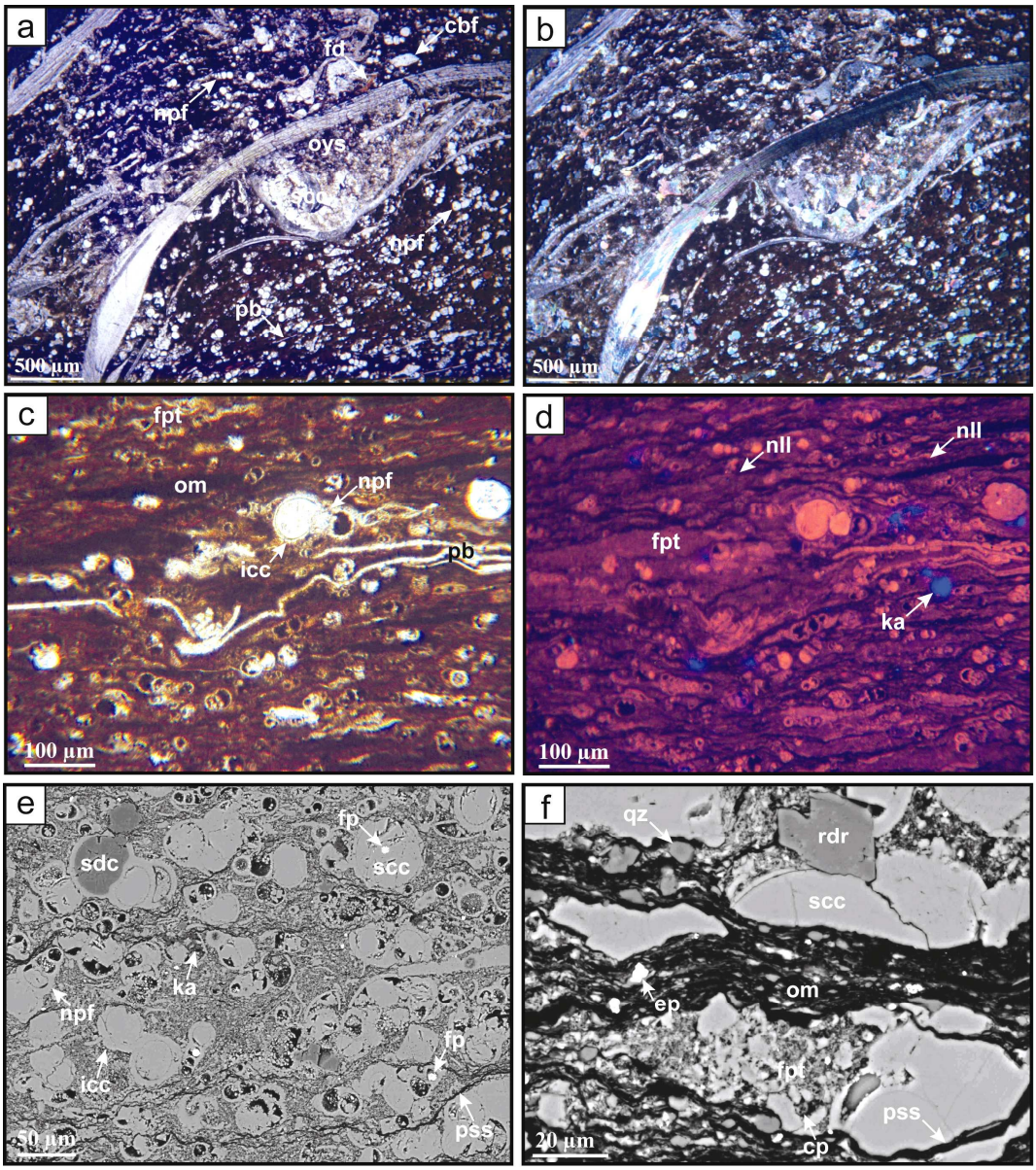

Figure 5.8. Thin-section micrographs illustrating microscopic features of Lithofacies A. **(a, b)** Under PPL and XPL respectively (sample P33; Figure 5.4). Note abundance of uncompacted, sparry-calcite-cemented, nonkeeled planktonic foraminifera (npf) and organic-matter-rich matrix, together with oysters (oys), planktonic bivalves (pb), fish debris (fd) and calcareous benthic foraminifera (cbf). Note also the nonferroan sparry-calcite cement (scc) in the shelter porosity of oyster. **(c, d)** Under PPL and CL respectively (sample S8; Figure 5.4). Note abundance of compacted faecal pellets (fpt) containing organic matter (OM) and other aggregates, resulting in nonparallel, lenticular lamination (nll), and sparry-calcite-cemented (zoned, nonferroan) and porous planktonic forams. Note also the isopachous calcite cement (icc) around a foram's test in the middle of the micrograph. The blue material in (d) is most likely kaolinite (ka). **(e, f)** Backscattered electron micrographs (samples X8 and P39 respectively; Figure 5.4). Note abundance of nonferroan sparry-calcite cement in the forams' tests, occasionally in association with framboidal pyrite (fp), sparry dolomite cement (sdc) or kaolinite (ka). Note also in (e) the development of isopachous calcite cements around most of forams' tests. Finally, note in both micrographs the rhombohedral dolomite replacements (rdr) and pressure-solution seams (pss); as well as organic matter (om), quartz (qz), euhedral pyrite (ep), and a faecal pellet enclosing forams, coccolith plates (cp), and microcrystalline calcite ("microspar").

Four samples were chosen for the determination of stable-isotopic compositions of calcite in Lithofacies A (see Table 5.1 and Figure 5.5). The whole-rock samples gave $\delta^{13}C$ values of +0.6, +0.2, +0.5 and +0.9‰ (average +0.6‰ VPDB), and respectively $\delta^{18}O$ values of −4.7, −4.9, −5.6 and −5.2‰ (average −5.1‰ VPDB). Three matrix subsamples gave values close to the values of their whole-rock samples; $\delta^{13}C$ of +0.7, +0.4 and +0.8‰ (average +0.6‰ VPDB), and $\delta^{18}O$ of −4.6‰, −5.7‰ and −4.3‰ (average −4.9‰ VPDB). Additionally, three subsamples from diagenetically-unaltered (original) parts of bivalve shells (oysters and pectens) gave $\delta^{13}C$ values of +0.8, +1.1 and +1.0 (average +1.0‰ VPDB), and respectively $\delta^{18}O$ values of −4.3, −4.3 and −4.2‰ (average −4.3‰ VPDB). Finally, three subsamples from sparry-calcite-cemented gastropods and oysters gave $\delta^{13}C$ values of +1.2, +1.2 and −0.1‰ (average +0.8‰ VPDB), and respectively $\delta^{18}O$ values of −5.1, −4.0, and −3.8‰ (average −4.3‰ VPDB). Overall, the average stable-isotopic composition of all analysed samples and subsamples of Lithofacies A is +0.7‰ VPDB for $\delta^{13}C$ and −4.7‰ VPDB for $\delta^{18}O$.

5.6.2. Interpretation

The mudstone-wackestone texture of Lithofacies A with abundant planktonic foraminifera and coccoliths suggest that these organic-carbon-rich units were deposited in an open-marine, basinal environment (e.g. Markello and Read, 1982; Burchette and Britton, 1985; Droste, 1990; Philip et al., 1995; van Buchem et al., 1996; Kuhnt et al., 1997; Al Balushi et al., in review). The occurrence of in-place benthic fauna (including oysters, pectens and some small benthic foraminifera) together with some burrows, and the fact that the planktonic foraminifers are predominantly nonkeeled (Figures 5.7 and 5.8), indicate that the depositional intrashelf basin was relatively shallow (probably in the order of 40 to 60 m) and predominantly oxic (Hudson and Martill, 1991; Machhour et al., 1998; Schieber, 2003; Marynowski et al., 2007; Schieber, 2009; Al Balushi and Macquaker, in press; Al Balushi et al., in review).

The preservation of relict thin beds, organo-mineralic aggregates, lenticular lamination and partial bioturbation in many of these sediments (Figures 5.7 and 5.8) suggest that Lithofacies A, instead of being deposited predominantly from suspension settling under quiet, anoxic conditions, was probably emplaced, at least in parts, by episodic and advective processes in a relatively dynamic, oxic-dysoxic environment, close to storm

wave base (Schieber, 1994; Macquaker and Bohacs, 2007; Schieber et al., 2007; Schieber and Southard, 2009; Macquaker et al., in press; Al Balushi et al., in review). This depositional setting was very likely associated with energetic bottom currents, which were able to episodically and advectively rework and agitate fine-grained sediments from the substrate before they were accumulated at the sediment/water interface, where they were subsequently burrowed by diminutive infauna (sensu Reid et al., 1990). These sediments, as a result of compaction, developed thin partings (sensu Campbell, 1967; Bathurst, 1987) that gave them a strongly-fissile appearance (especially at the exposure, enhanced by weathering; Figure 5.7a). This well-developed fissility is commonly misinterpreted as depositional parallel laminae (sensu Campbell, 1967).

The dark colouration of Lithofacies A is a result of the dispersed organic matter, together with clay and pyrite. The high organic-matter content (up to 13.7% TOC) in this lithofacies is interpreted to be mainly a result of high primary organic-carbon production in the water column, coupled with episodically-high local rates of sediment accumulation and burial (Hudson and Martill, 1991; Arthur and Sageman, 1994; Canfield, 1994; Hochuli et al., 1999; Katz, 2005; Macquaker et al., 2007; Al Balushi and Macquaker, in press). Evidence for the latter factor is also provided by the abundant preservation of articulated shells, as well as the presence of some relict thin beds and lenticular laminae (Brett and Allison, 1998; Lazo et al., 2005; Machent et al., 2007; Al Balushi et al., in review; Figure 5.7).

The nonferroan calcite cements infilling the shelter porosity of planktonic foraminiferal tests, as well as the oysters, in this lithofacies (Figure 5.8) may be related to very early diagenetic processes, as these tests appear uncompacted (e.g. Bathurst, 1974; Macquaker et al., 2007). Based on the interpretation that this lithofacies was deposited in a relatively shallow, oxic-dysoxic intrashelf-basinal environment with evidence of physical and biological sediment reworking, isopachous high-Mg calcite cementation around the foraminifers' tests (Figures 5.7 and 5.8), and the stable-isotopic compositions of the various calcite components (Table 5.1 and Figure 5.5), it is very likely that the majority of the calcite cement in Lithofacies A was derived from normal-marine, oxic porewaters (e.g. Hudson, 1977; Dickson and Coleman, 1980; Dickson, 1985; Curtis and Coleman, 1986; Muchez et al., 1991; Frank and Lohmann, 1996; Adams and Mackenzie, 1998; Nelson and James, 2000; Scholle and Ulmer-Scholle, 2003; Allison et al., 2008). The slightly negative $\delta^{18}O$ values might suggest that the depositional temperature was relatively high, which was

likely during the Cenomanian time (cf. de Boer, 1982). An estimate of seawater palaeotemperature from $\delta^{18}O$ compositions of unaltered bivalves has been calculated for the Natih-B Member (see Section 5.8).

Despite the overriding marine signature recorded isotopically, zoned and bright-luminescent, nonferroan, pore-filling sparry calcite, and both replacive and pore-filling, nonferroan, finely-crystalline, rhombohedral dolomite (cross-cut by solution seams), as well as the presence of framboidal pyrite (Figure 5.8e and f), are all suggestive of early diagenetic processes taking place in suboxic conditions during organic-matter decay (i.e. "organogenesis"; e.g. Irwin, 1980; Compton, 1988; Holail et al., 1988; Ader and Javoy, 1998; Mazzullo, 2000; Taylor and Macquaker, 2000a; Machent et al., 2007; Dickson et al., 2008; Rachidi et al., 2009). Specifically, it is likely that bacterial sulphate reduction occurring within anoxic sediment (< 20 cm below the sediment/water interface) was contributing in the oxidation of organic matter, producing hydrogen sulphide (e.g. Berner, 1978; Canfield, 1989, 1994; Taylor and Macquaker, 2000b), and liberating bicarbonate into the porewaters. The zonation of the calcite and dolomite cements and replacements revealed by CL (Figure 5.8d) implies that the chemistry of the diagenetic porefluids varied during carbonate precipitation (e.g. Azmy et al., 2008). The requisite Mg^{2+} and Ca^{2+} ions for dolomitisation were probably provided by early diffusion from overlying seawater, with CO_3^{2-} ions (plus additional Ca^{2+} ions) being supplied mainly by both organic-matter degradation and precursor carbonates dissolution (Baker and Burns, 1985; Compton and Siever, 1986; Compton, 1988; Mazzullo, 2000; Swart et al., 2005). It is noteworthy that the isotopic data for Lithofacies A does not provide evidence for organogenesis through depleted $\delta^{13}C$ values. This could reflect either the limitations of the sampling, or buffering of low isotopic $\delta^{13}C$ values by seawater.

The kaolinite cement that co-fills the tests of the planktonic foraminifers (Figure 5.8e) is interpreted here to have precipitated during late diagenesis in either normal-marine or modified-marine porewaters (sensu Maliva et al., 1999). The association of kaolinite cement with organic matter in Lithofacies A might suggest that late-diagenetic organic complexing of aluminium was responsible for kaolinite cementation (cf. Maliva et al., 1999) in these organic-carbon-rich carbonate mudstones-wackestones. This was probably a result of bacterial or thermal decarboxylation of organic compounds, which perhaps

released organo-aluminium complexes responsible for the precipitation of kaolinite cement (Maliva et al., 1999).

The development of compacted sediment around the foraminiferal tests as well as the compressed horizontal burrows and faecal pellets, and the occurrence of pressure-solution seams (Figures 5.7 and 5.8) indicate that both physical and chemical compaction processes dominated the late diagenetic history of this lithofacies (sensu Shinn and Robbin, 1983). Pressure solution in these organic-rich mudstones caused the sediment to develop fissility (Figure 5.7a; cf. Bathurst, 1987). There is no petrographic or isotopic evidence from these units to suggest a late burial recrystallisation.

5.7. Detailed Characteristics of Lithofacies B

5.7.1. Description

Lithofacies B comprises uncompacted, extensively bioturbated, and pervasively calcite-cemented and replaced skeletal wackestone-packstone, with a relatively low concentration of organic matter (0.5 to 1.6% TOC, average 1.1%; see Figures 5.4, 5.6 and 5.9). It is well exposed, laterally-continuous, and very resistant to weathering (Figure 5.6b). It varies in colour from whitish and very light grey to dark grey (Figures 5.6a and 5.9a, c, d). Horizons formed by this lithofacies vary in thickness from 0.02 to 1.85 m (average about 0.21 m; Figure 5.6). These horizons commonly exhibit sharp and erosive bases (including cm-scale scour-lag features; Figure 5.9e), frequently associated with concentrations of reworked shell fragments of bivalves, gastropods, echinoderms and brachiopods. Amalgamation of thin (5 to 50 mm thick), normally-graded depositional beds may be observed within some of these horizons (Figure 5.9f). Moreover, Lithofacies B shows evidence of macroscopic geopetal structures (Figure 5.9a).

Overall, extensive bioturbation and carbonate precipitation in these horizons have destroyed most of the primary sedimentary structures, causing these units to exhibit a mottled appearance (Figures 5.6 and 5.9). Burrowing here is predominantly attributed to open (unlined) *Thalassinoides* isp. (Figure 5.6a and 5.9a to d), and rarely to *Planolites* isp. and *Phycosiphon* isp. Both bioturbation and carbonate precipitation become increasingly

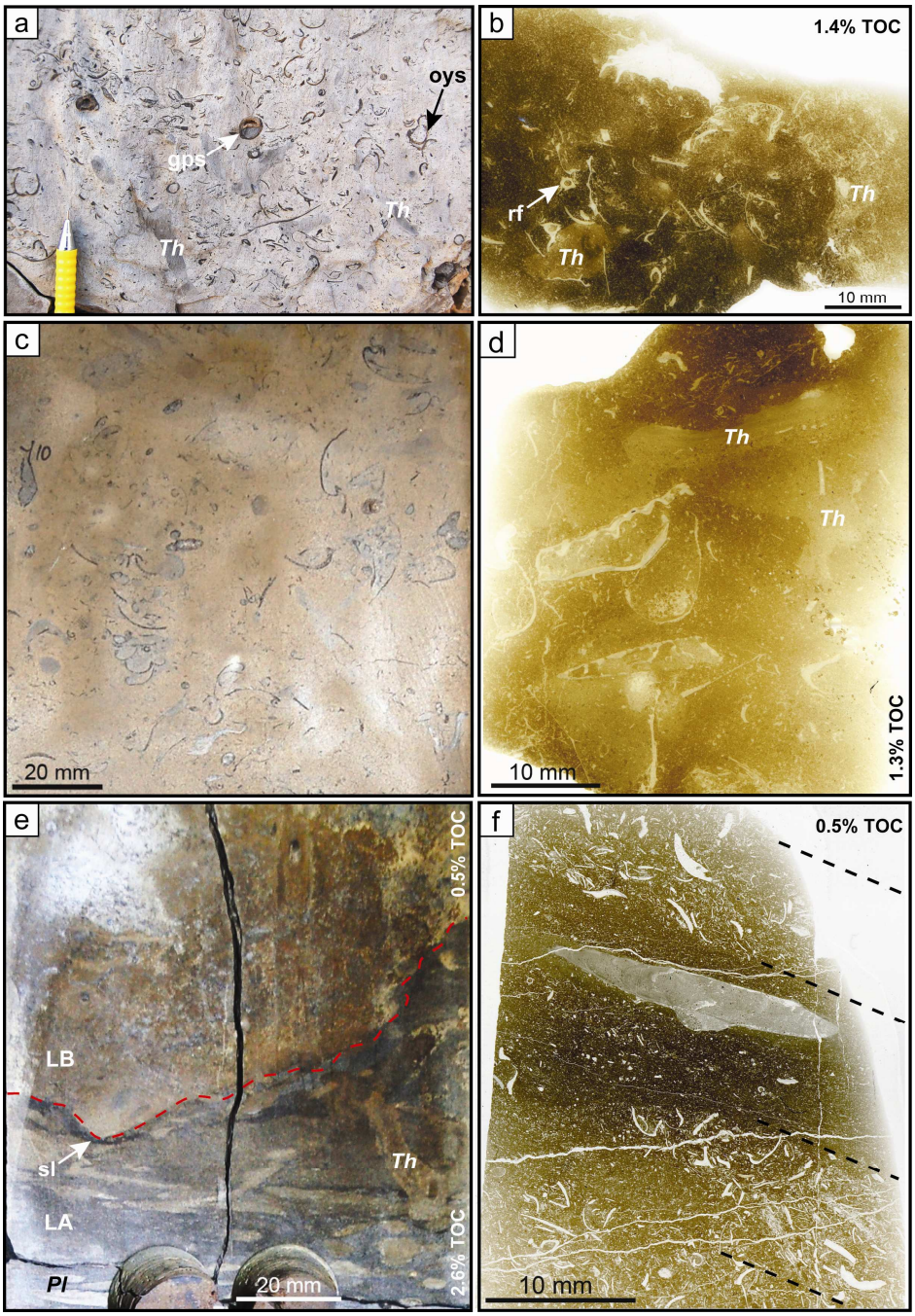

Figure 5.9. Hand-specimen photograph and thin-section scan pairs illustrating characteristic macroscopic features of Lithofacies B. **(a, b)** Outcrop photograph and thin-section scan, respectively, of sample Q52 (Jabal Qusaybah) showing evidence of extensive bioturbation (*Thalassinoides* isp. [*Th*]) and skeletal debris (including oyster [oys] and rudist [rf] fragments) concentration. Note geopetal structure (gps) in (a) within a gastropod fragment. **(c, d)** Core photograph and thin-section scan, respectively, of sample Y10 (Figures 5.4 and 5.6a) illustrating similar features as in (a, b), but note the strongly mottled, uncompacted appearance as a result of extensive bioturbation and early cementation. **(e, f)** Core photograph and thin-section scan, respectively, of sample S9 (Figure 5.4). Note in (e) erosive boundary between Lithofacies A (LA) and Lithofacies B (LB) associated with a scour-lag (sl), and progressive increase of bioturbation intensity in LA with *Planolites* isp. (*Pl*) near the bottom and *Thalassinoides* isp. (*Th*) near the top. Note in (f) amalgamation of thin, normally-graded depositional beds with concentration of skeletal debris.

more intense towards the unit tops, in places associated with boring features (Figure 5.6b).

Lithofacies B is largely composed of nonferroan sparry calcite (average 74.1%), which occupies the pore-spaces of uncompacted skeletal material and some of the intergranular porosity as predominantly zoned to dull-luminescent, meniscus-style cement, as well as the matrix of the rock as zoned and dull-luminescent, finely-crystalline spar ("microspar") [Figure 5.10]. In addition, isopachous crusts of fibrous to bladed, nonferroan, high-Mg calcite cements are usually well developed around the tests of the planktonic foraminifera and some other bioclasts (Figure 5.10a, b, e, and f). Reworked shell fragments of bivalves (including oysters and rudists; Figure 5.9a and b), ostracods, gastropods, echinoderms and serpulids are common in this lithofacies, together with benthic (both calcareous and agglutinated) and nonkeeled planktonic foraminifera, calcispheres, peloids and coccoliths (Figure 5.10). Many of the skeletal allochems are densely packed and stacked, providing evidence of skeletal concentration (Figure 5.9a and f). Other minor components include fine-grained detrital quartz (average 4.8%), nonferroan dolomite (average 2.5%, mostly as scattered rhombs), detrital clay (average 2.2%, mostly as kaolinite), pyrite (average 2.1%, both euhedral and framboidal), organic matter (average 1.3%, both amorphous and woody), fish debris (average 0.6%), and wood fragments (average 0.1%).

There is no evidence of mechanical compaction in Lithofacies B. However, a few discrete, low-amplitude microstylolites, associated with organic matter, are present dissecting both matrix and pore-filling cements. Lithofacies B is also dissected by nonferroan, bright-luminescent, sparry-calcite-cemented fractures (Figure 5.10c and d).

Four samples were selected for the determination of stable-isotopic compositions of calcite (both biogenic and authigenic, as well as mixtures of both) in Lithofacies B (see Table 5.1 and Figure 5.5). The whole-rock samples gave $\delta^{13}C$ values of +0.8, −0.7, −0.9 and +0.6‰ (average −0.1‰ VPDB), and respectively $\delta^{18}O$ values of −5.1, −3.8, −3.7 and −5.3‰ (average −4.5‰ VPDB). The matrix subsamples (dominated by microcrystalline calcite ["microspar"]) gave values close to the values of their whole-rock samples; $\delta^{13}C$ of +0.5, −0.2, −0.6 and +0.7‰ (average +0.1‰ VPDB), and $\delta^{18}O$ of −4.6, −5.7 and −4.3‰ (average −4.4‰ VPDB). In addition, two subsamples from diagenetically-unaltered (original) parts of shell fragments gave $\delta^{13}C$ values of +1.2 and +1.7‰ VPDB, and

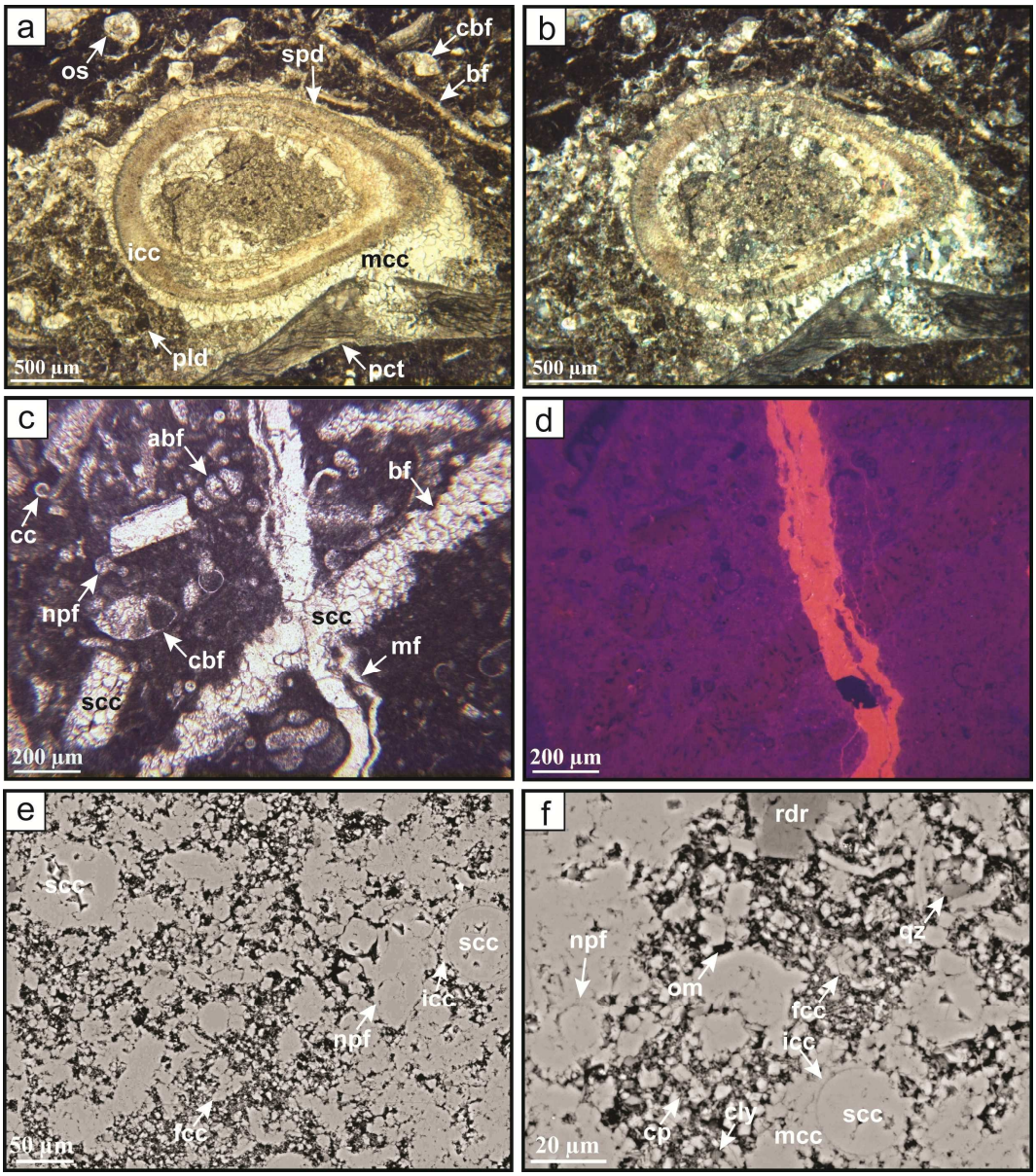

Figure 5.10. Thin-section micrographs illustrating microscopic features of Lithofacies B. **(a, b)** Under PPL and XPL respectively (sample Y8; Figure 5.4) showing uncompacted, sparry-calcite-cemented (nonferroan) bioclasts, including serpulids (spd), ostracods (os), calcareous benthic foraminifera (cbf) and bivalve fragments (bf), together with micritic peloids (pld) and less-altered pectens (pct). Note also the nonferroan, isopachous calcite cement (icc) around the serpulid and nonferroan meniscus-style calcite cement (mcc) between the serpulid and pecten. **(c, d)** Under PPL and CL, respectively (sample S9; Figure 5.4) showing a mixture of predominantly sparry-calcite-cemented (scc; nonferroan, zoned to dull-luminescent) bioclasts, including bivalve fragments (bf), agglutinated benthic foraminifera (abf), calcareous benthic foraminifera (cbf), nonkeeled planktonic foraminifera (npf) and calcispheres (cc). Note also the sparry-calcite-cemented (nonferroan, bright-luminescent) microfracture (mf). **(e, f)** Backscattered electron micrographs (sample P90; Figure 5.4) illustrating the matrix composition, which is dominated by nonferroan, finely-crystalline calcite (fcc) ["microspar"]. Note the pervasively sparry-calcite-cemented (scc; nonferroan) tests of nonkeeled planktonic forams (npf) and development of nonferroan, isopachous calcite cement (icc) around them. Note also the scarce organic matter (om), rhombohedral dolomite replacement (rdr), quartz (qz), coccolith plates (cp), and clay.

respectively $\delta^{18}O$ values of −4.7 and −4.1‰ VPDB. Finally, a subsample from a sparry-calcite-cemented shell fragment and another from a sparry-calcite-cemented microfracture gave, respectively, $\delta^{13}C$ values of +1.0 and +1.3‰ VDPB, and $\delta^{18}O$ values of −3.7 and −9.3‰ VPDB. Overall, the average stable-isotopic composition of all analysed samples and subsamples of Lithofacies B is +0.5‰ VPDB for $\delta^{13}C$ and −4.8‰ VPDB for $\delta^{18}O$.

5.7.2. Interpretation

The extensively-bioturbated wackestone-packstone texture of Lithofacies B and the common occurrence of mixed benthic and nonkeeled planktonic foraminifera, together with a diverse assemblage of reworked skeletal debris, disarticulated coccoliths and calcispheres, and the presence of scoured surfaces (Figures 5.9 and 5.10) suggest that these sediments were deposited in an outer-ramp setting, in relatively shallower-water, better-oxygenated, higher-energy conditions, in comparison with Lithofacies A, above storm wave base (e.g. Brett and Allison, 1998; Wetzel and Uchmann, 1998; Hallam et al., 2000; Flügel, 2004; Al Balushi and Macquaker, in press; Al Balushi et al., in review). The frequent occurrence of mixtures of winnowed shell fragments and the presence of erosive bases in this lithofacies, associated with normally-graded, amalgamated, thin beds and bioturbated tops may imply that these units are distal tempestites (Figure 5.9; e.g. Aigner, 1982; Myrow and Southard, 1996; Meng et al., 1997; Molina et al., 1997; Savrda and Nanson, 2003). It is very likely that the majority of sediment components in Lithofacies B were derived from the surrounding carbonate platform, swept into the intrashelf basin by waning flow currents during major storm events (Brookfield and Brett, 1988; Droste, 1990; Hudson and Martill, 1991; Osleger, 1991; Osleger and Read, 1991; Burchette, 1993; Myrow and Southard, 1996; Varban and Plint, 2008; Al Balushi and Macquaker, in press).

The intense burrowing (predominantly attributed to open *Thalassinoides* isp.; Figure 5.9a to d) indicates that stable and well-oxygenated substrate conditions occurred during deposition of Lithofacies B (e.g. Fisher and Hudson, 1987; Ekdale and Bromley, 1991; Philip et al., 1995; Savrda et al., 2001; Damholt and Surlyk, 2004). Moreover, the three-dimensional preservation of trace fossils and bioclasts, and the formation of geopetal structures, micritic peloids and meniscus textures (Figures 5.9 and 5.10) suggest that most of the calcite precipitation process (both in the matrix and bioclast tests) occurred early, prior to significant compaction and burial, at or near the sediment/water interface (e.g.

Berner, 1981; Ricken and Hemleben, 1982; Reid et al., 1990; Tucker and Wright, 1990; Westphal and Munnecke, 1997; Reid and Macintyre, 1998; Hall et al., 2004; Westphal, 2006; Breesch et al., 2007; Macquaker et al., 2007; Collin et al., 2009). Additionally, both extensive bioturbation and the pervasive carbonate cementation and replacement, especially at unit tops, imply prolonged breaks in sediment accumulation (e.g. Ruffell and Watch, 1998; Gruszczynski et al., 2008). Therefore, the tops of these units, which cap shallowing-upward parasequences (Figure 5.6; see also Al Balushi and Macquaker, in press; Al Balushi et al., in review), may be interpreted as marine hard-/firmgrounds (discontinuity surfaces; e.g. Philip et al., 1995; van Buchem et al., 1996; Ruffell and Watch, 1998; van Buchem et al., 2002; Carmona et al., 2007) that were developed when facies stacking-pattern changes (see discussion in Al Balushi and Macquaker, in press). This development was probably a function of sediment starvation at the seafloor (Savrda et al., 2001) and increased bottom-current activity during relative sea-level fall and associated decrease in accommodation such that sediment supply to the basin was reduced (Ruffell and Watch, 1998; Gruszczynski et al., 2008).

The stable-isotopic compositions of the various calcite components (including replacements and cements, except those from the microfracture; see Table 5.1 and Figure 5.5) of this lithofacies ($\delta^{13}C$ = −0.9 to +1.7‰ [average +0.5‰ VPDB]; $\delta^{18}O$ = −5.7 to −3.7‰ [average −4.8‰ VPDB]), together with evidence of strong sediment reworking by storms and burrowing organisms, and precipitation of isopachous cements (Figures 5.9 and 5.10), suggest that the majority of the nonferroan calcite (both replacive and pore-filling) in Lithofacies B was probably derived from normal-marine, fully-oxic porewaters (e.g. Hudson, 1977; Dickson and Coleman, 1980; Marshall and Ashton, 1980; Dickson, 1985; Curtis and Coleman, 1986; Ditchfield and Marshall, 1989; Muchez et al., 1991; Frank and Lohmann, 1996; Adams and Mackenzie, 1998; Scholle and Ulmer-Scholle, 2003; Flügel, 2004; Preto et al., 2009). The $\delta^{18}O$ values in this lithofacies are very similar to those of Lithofacies A (see Table 5.1 and Figure 5.5), meaning that similar elevated seawater temperature occurred during syndepositional calcite precipitation of Lithofacies B (see Section 5.8). The more negative $\delta^{18}O$ value (−9.2‰ VPDB) from the bright-luminescent, calcite-cemented fracture, however, suggests even higher temperature of precipitation, still more consistent with burial cementation. No evidence has been found to link the negative $\delta^{18}O$ values to meteoric diagenesis (e.g. subaerial exposure) or late-burial recrystallisation (e.g. blocky calcite cement).

The whole-rock and matrix samples of Lithofacies B are slightly more depleted in $\delta^{13}C$, compared to those of Lithofacies A (see Table 5.1 and Figure 5.5). This might suggest that there was a relatively higher input of depleted carbon to the system when Lithofacies B was being lithified early. It is very likely that this isotopically-light carbon was mainly produced by oxic respiration of organic-matter at the sediment/water interface (e.g. Froelich et al., 1979; Berner, 1984; Canfield, 1989; Hendry, 1993; Reid and Macintyre, 1998; Machent et al., 2007). This argument is also supported by the fact that Lithofacies B contains less organic carbon than Lithofacies A, and by the interpretation that it was deposited very slowly, prolonging the residence time of residual organic matter at the oxic zone and allowing it to be more substantially oxidised. The relatively smaller amounts of both pyrite and dolomite, and the predominantly dull-luminescent nature of sparry calcite in this lithofacies might indicate that bacterial sulphate reduction played a less significant role in the early organogenesis of these units. The slightly varying levels of CL of the various cements and replacements in this lithofacies (Figure 5.10d) suggest that the porewaters chemistry was fluctuating slightly during carbonate precipitation (e.g. Azmy et al., 2008).

5.8. Discussion and Conclusion

Detailed petrographic, mineralogical, and geochemical analyses of alternating organic-carbon-rich/sparry-calcite-rich fine-grained carbonates from the Upper Cretaceous Natih-B Member demonstrate that the manifest, high-frequency cyclicity expressed by these intrashelf-basinal lithofacies was to some extent influenced by diagenesis. The organic-carbon-rich units are strongly compacted and display well-developed fissility, with insignificant carbonate precipitation in the matrix but with pervasive sparry and isopachous calcite cementation in the uncompacted tests of planktonic foraminifers. In contrast, the sparry-calcite-rich units are uncompacted and with abundant sparry-calcite cements and replacements in the bioclasts tests and matrix, in addition to meniscus-style cements, micritic peloids and geopetal structures (see Ricken and Hemleben, 1982; Westphal and Munnecke, 1997; Westphal, 2006).

Although these alternating units vary in the degree of compaction, the majority of the sparry calcite in both lithofacies, however, was precipitated early, prior to compaction and

significant burial. The stable-isotopic results suggest that these early cements and replacements were mainly derived from normal-marine, oxic porewaters, with little contribution of isotopically-light carbon from early organogenesis (cf. Raven and Dickson, 2007). The relatively higher amounts of framboidal pyrite, rhombohedral dolomite and authigenic kaolinite, in the partially-bioturbated, skeletal, organic-carbon-rich units might indicate that the very small amount of isotopically-light carbon in this lithofacies was produced by organic-matter decay as a result of bacterial sulphate reduction. In contrast, the relatively smaller amounts of framboidal pyrite and rhombohedral dolomite, and the lack of authigenic kaolinite, in the extensively-bioturbated, skeletal, sparry-calcite-rich intervals might suggest that the slightly depleted $\delta^{13}C$ in this lithofacies was a result of organic-matter degradation by molecular-oxygen respiration at or near the sediment/water interface.

The seawater palaeotemperature during deposition of the Natih-B sediments can be estimated from the $\delta^{18}O$ composition of diagenetically-unaltered bivalve calcite (texturally-pristine oysters and pectens, nonluminescent under CL), as most marine molluscs (including bivalves) are known to secrete their shells in oxygen-isotopic equilibrium with the surrounding seawater (e.g. Brigaud et al., 2008, and references therein). There is no evidence to suggest that the low $\delta^{18}O$ values of the Natih-B unaltered shells (Table 5.1; average −4.3‰ VPDB) reflect freshwater input and/or reduced seawater salinity. In calculating the palaeotemperature of calcite, the equation of Epstein et al. (1953) and Craig and Gordon (1965), as modified by Anderson and Arthur (1983), has been used because it was primarily based on molluscan-calcite isotope data:

$$T = 16.00 - 4.14\,(\delta^{18}O_{calcite} - \delta^{18}O_{seawater}) + 0.13\,(\delta^{18}O_{calcite} - \delta^{18}O_{seawater})^2$$

In this equation, T is the temperature in degrees Celsius (ºC), $\delta^{18}O_{calcite}$ equals the oxygen isotope composition of calcite with respect to the VPDB international standard, and $\delta^{18}O_{seawater}$ equates to the oxygen isotope ratio of seawater relative to the (Vienna Standard Mean Ocean Water) VSMOW standard. This palaeotemperature calculation involves an assumption for the oxygen isotope composition of Cretaceous seawater. A $\delta^{18}O_{seawater}$ value of −1.0‰ VSMOW is generally assumed for an “ice-free” time period (Shackleton and Kennett, 1975), which has often been suggested for the Upper Cretaceous due to the nonexistence of glacial deposits (e.g. Steuber et al., 2005, and references therein). Based

on this assumption and an average $\delta^{18}O_{calcite}$ value of −4.3‰ VPDB from unaltered shells (see Table 5.1), the mean seawater palaeotemperature for the Natih-B is worked out to be 31.4ºC, varying from 30.1ºC (for $\delta^{18}O_{calcite}$ = −4.1‰ VPDB) to 33.1ºC (for $\delta^{18}O_{calcite}$ = −4.7‰ VPDB).

The results of our study show the complex interplay of the different factors that controlled diagenetic variability and organic-matter preservation in predominantly fine-grained intrashelf-basinal carbonates. The main factors that controlled these changes are predominantly related to high-frequency (fifth-order scale) eustatic sea-level fluctuations and associated accommodation availability. These include changes in primary production, local rates of sediments accumulation, bottom-current activity, and early diagenesis. The organic-carbon-rich units reflect the processes of high primary organic production, episodic, and rapid sedimentation and burial during relative sea-level rise and increase of accommodation, which resulted in the better preservation of organic matter by removing it quickly from the zone of substantial oxic respiration. On the other hand, the sparry-calcite-rich units represent relatively higher primary inorganic production, increased bottom-current activity, slow sedimentation and burial during relative sea-level fall and decrease of accommodation, which resulted in the development of early-cemented and replaced hard-/firmgrounds, and in the substantial autodilution and mineralisation of organic matter in the oxic zone.

In conclusion, the abundance of normal-marine-derived calcite precipitates and evidence of sediment reworking by both bottom currents and burrowing organisms throughout the Natih-B Member illustrate the significant role that early oxic processes played in controlling lithofacies variability in this source-rock-bearing succession, which is often misinterpreted to be predominantly controlled by changes in bottom-water anoxia (e.g. Murris, 1980; Scott, 1990; Philip et al., 1995; Droste and Van Steenwinkel, 2004; Homewood et al., 2008).

Acknowledgements

The authors wish to convey special appreciation to Petroleum Development Oman (PDO) for providing financial support and for allowing access to the subsurface core material, seismic data, wireline logs, and internal technical reports. We also would like to extend thanks to the University of Manchester, where the polished thin-sections were prepared (by Harry Williams and Stephen Stockley) and the petrographic and XRD analyses were performed (with an initial aid from Steve Caldwell, David Plant, and John Waters). The University of Liverpool is greatly acknowledged, where the stable-isotopic analyses were run (under the guidance of Jim Marshall and assistance of James Ball). Finally, we are very grateful to the Manchester Metropolitan University where the TOC analyses were performed (under the guidance of Kevin Taylor and assistance of David McKendry).

References

Adams, A.E. and W.S. Mackenzie 1998. A Colour Atlas of Carbonate Sediments and Rocks Under the Microscope. Manson Publishing, 180 p.

Ader, M. and M. Javoy 1998. Early diagenesis in a sulphate-reducing environment: an isotopic study in the Lower Jurassic of the Paris Basin. Diagenese precoce en milieu sulfure reducteur: Une etude isotopique dans le Jurassique basal du Bassin parisien, v. 327, no. 12, p. 803-809.

Aigner, T. 1982. Calcareous tempestites: storm-dominated stratification in Upper Muschelkalk limestones (Middle Trias, SW Germany). In, G. Einsele and A. Seilacher (Eds.), Cyclic and Event Stratification. Springer-Verlag, p. 180-198.

Al Balushi, S.A.K. and J.H.S. Macquaker (in press). Sedimentological evidence for bottom-water oxygenation during deposition of the Natih-B intrashelf-basinal sediments: Upper Cretaceous carbonate source rock, Natih Formation, North Sultanate of Oman. GeoArabia.

Al Balushi, S.A.K., J.H.S. Macquaker and C. Hollis (in review). High-resolution lithofacies analyses of predominantly fine-grained carbonates in and around an intrashelf basin: an example from the Upper Cretaceous Natih-B Member of North Oman.

Allison, P.A., S.P. Hesselbo and C.E. Brett 2008. Methane seeps on an Early Jurassic dysoxic seafloor. Palaeogeography, Palaeoclimatology, Palaeoecology, v. 270, no. 3-4, p. 230-238.

Alsharhan, A.S. and A.E.M. Nairn 1988. A review of the Cretaceous formations in the Arabian Peninsula and Gulf: Part II. Mid-Cretaceous (Wasia Group) stratigraphy and palaeogeography. Journal of Petroleum Geology, v. 11, no. 1, p. 89-112.

Alsharhan, A.S. and R.W. Scott (Eds.) 2000. Middle East Models of Jurassic/Cretaceous Carbonate Systems. SEPM (Society for Sedimentary Geology), Special Publication 69, 364 p.

Anderson, T.F. and M.A. Arthur 1983. Stable isotopes of oxygen and carbon and their application to sedimentologic and palaeoenvironmental problems. SEPM (Society for Sedimentary Geology), Short Course 10, 151 p.

Aqrawi, A.A.M., G.A. Thehni, G.H. Sherwani and B.M.A. Kareem 1998. Mid-Cretaceous rudist-bearing carbonates of the Mishrif Formation: an important reservoir sequence in the Mesopotamian Basin, Iraq. Journal of Petroleum Geology, v. 21, no. 2, p. 57-82.

Arthur, M.A., W.E. Dean and D.A.V. Stow 1984. Models for the deposition of Mesozoic-Cenozoic fine-grained organic-carbon-rich sediment in the deep sea. Geological Society Special Publications, v. 15, no. 1, p. 527-560.

Arthur, M.A. and B.B. Sageman 1994. Marine black shales: depositional mechanisms and environments of ancient deposits. Annual Review of Earth and Planatary Sciences, v. 22, p. 499-551.

Azmy, K., D. Lavoie, I. Knight and G. Chi 2008. Dolomitization of the Lower Ordovician Auathuna Formation carbonates, Port au Port Peninsula, western Newfoundland, Canada: implications for a hydrocarbon reservoir. Canadian Journal of Earth Sciences, v. 45, no. 7, p. 795-813.

Bádenas, B., M. Aurell, J.C. García-Ramos, B. González and L. Piñuela 2009. Sedimentary vs. diagenetic control on rhythmic calcareous successions (Pliensbachian of Asturias, Spain). Terra Nova, v. 21, no. 3, p. 162-170.

Baker, P.A. and S.J. Burns 1985. Occurrence and formation of dolomite in organic-rich continental margin sediments. American Association of Petroleum Geologists Bulletin, v. 69, no. 11, p. 1917-1930.

Baker, P.A., J.M. Gieskes and H. Elderfield 1982. Diagenesis of carbonates in deep-sea sediments - evidence from Sr/Ca ratios and interstitial dissolved Sr^{2+} data. Journal of Sedimentary Research, v. 52, no. 1, p. 71-82.

Bathurst, R.G.C. 1974. Marine Diagenesis of Shallow Water Calcium Carbonate Sediments. Annual Review of Earth and Planetary Sciences, v. 2, no. 1, p. 257-274.

Bathurst, R.G.C. 1979. Diagenesis in carbonate sediments: a review. Geologische Rundschau, v. 68, no. 3, p. 848-855.

Bathurst, R.G.C. 1987. Diagenetically enhanced bedding in argillaceous platform limestones; stratified cementation and selective compaction. Sedimentology, v. 34, no. 5, p. 749-778.

Beltran, C., M. de Rafelis, A. Person, F. Stalport and M. Renard 2009. Multiproxy approach for determination of nature and origin of carbonate micro-particles so-called "micarb" in pelagic. Sedimentary Geology, v. 213, no. 1, p. 64-76.

Berner, R.A. 1978. Sulfate reduction and the rate of deposition of marine sediments. Earth and Planetary Science Letters, v. 37, no. 3, p. 492-498.

Berner, R.A. 1981. A new geochemical classification of sedimentary environments. Journal of Sedimentary Research v. 51, no. 2, p. 359-365.

Berner, R.A. 1984. Sedimentary pyrite formation: an update. Geochimica et Cosmochimica Acta, v. 48, no. 4, p. 605-615.

Biernacka, J., K. Borysiuk and P. Raczyński 2005. Zechstein (Ca1) limestone-marl alternations from the North-Sudetic Basin, Poland: depositional or diagenetic rhythms? Geological Quarterly, v. 49, no. 1, p. 1-14.

Bohacs, K.M. 1998. Contrasting expressions of depositional sequences in mudrocks from marine to non marine environments. In, J. Schieber, W. Zimmerle and P. Sethi (Eds.), Shales and Mudstones, Volume I: Basin Studies, Sedimentology, and Palaeontology. E. Schweizerbart'sche Verlagsbuchhandlung, p. 33-78.

Böhm, F., H. Westphal and S. Bornholdt 2003. Required but disguised: environmental signals in limestone-marl alternations. Palaeogeography, Palaeoclimatology, Palaeoecology, v. 189, no. 3-4, p. 161-178.

Bombardiere, L. and G.E. Gorin 2000. Stratigraphical and lateral distribution of sedimentary organic matter in Upper Jurassic carbonates of SE France. Sedimentary Geology, v. 132, no. 3-4, p. 177-203.

Booler, J. and M.E. Tucker 2002. Distribution and geometry of facies and early diagenesis: the key to accommodation space variation and sequence stratigraphy: Upper Cretaceous Congost Carbonate platform, Spanish Pyrenees. Sedimentary Geology, v. 146, no. 3-4, p. 225-247.

Brand, U. and J. Veizer 1981. Chemical diagenesis of a multicomponent carbonate system; 2, Stable isotopes. Journal of Sedimentary Research, v. 51, no. 3, p. 987-997.

Breesch, L., R. Swennen, B. Dewever and A. Mezini 2007. Deposition and diagenesis of carbonate conglomerates in the Kremenara anticline, Albania: a paragenetic time marker in the Albanian foreland fold-and-thrust belt. Sedimentology, v. 54, no. 3, p. 483-496.

Brett, C.E. and P.A. Allison 1998. Palaeontological approaches to the environmental interpretation of marine mudrocks. In, J. Schieber, W. Zimmerle and P. Sethi (Eds.), Shales and Mudstones I: Basin Studies, Sedimentology, and Palaeontology. E. Schweizerbart'sche Verlagsbuchhandlung, p. 384.

Brigaud, B., E. Pucéat, P. Pellenard, B. Vincent and M.M. Joachimski 2008. Climatic fluctuations and seasonality during the Late Jurassic (Oxfordian-Early Kimmeridgian) inferred from $\delta^{18}O$ of Paris Basin oyster shells. Earth and Planetary Science Letters, v. 273, no. 1-2, p. 58-67.

Brookfield, M.E. and C.E. Brett 1988. Paleoenvironments of the mid-Ordovician (Upper Caradocian) Trenton limestones of southern Ontario, Canada: storm sedimentation on a shoal-basin shelf model. Sedimentary Geology, v. 57, no. 1-2, p. 75-105.

Burchette, T.P. 1993. Mishrif Formation (Cenomanian–Turonian), southern Arabian Gulf: carbonate platform growth along a cratonic basin margin. In, J.A.T. Simo, R.W. Scott and J.P. Masse (Eds.), Cretaceous Carbonate Platforms. American Association of Petroleum Geologists, Memoir 56, p. 185-200.

Burchette, T.P. and S.R. Britton 1985. Carbonate facies analysis in the exploration for hydrocarbons: a case study from the Cretaceous of the Middle East. In, P.J. Brenchley and B.P.J. Williams (Eds.), Sedimentology: Recent Developments and Applied Aspects. Geological Society, Special Publication 18, p. 311-338.

Campbell, C.V. 1967. Lamina, laminaset, bed and bedset. Sedimentology, v. 8, no. 1, p. 7-26.

Canfield, D.E. 1989. Sulfate reduction and oxic respiration in marine sediments: implications for organic carbon preservation in euxinic environments. Deep Sea Research Part A, Oceanographic Research Papers, v. 36, no. 1, p. 121-138.

Canfield, D.E. 1994. Factors influencing organic-carbon preservation in marine sediments. Chemical Geology, v. 114, no. 3-4, p. 315-329.

Carmona, N.B., M.G. MÃ¡ngano, L.A. Buatois and J.J. Ponce 2007. Bivalve trace fossils in an early Miocene discontinuity surface in Patagonia, Argentina: burrowing behavior and implications for ichnotaxonomy at the firmground-hardground divide. Palaeogeography, Palaeoclimatology, Palaeoecology, v. 255, no. 3-4, p. 329-341.

Caron, V., C.S. Nelson and P.J.J. Kamp 2005. Sequence stratigraphic context of syndepositional diagenesis in cool-water shelf carbonates: Pliocene limestones, New Zealand. Journal of Sedimentary Research, v. 75, no. 2, p. 231-250.

Collin, P.Y., S. Kershaw, S. Crasquin-Soleau and Q. Feng 2009. Facies changes and diagenetic processes across the Permian-Triassic boundary event horizon, Great Bank of Guizhou, South China: a controversy of erosion and dissolution. Sedimentology, v. 56, no. 3, p. 677-693.

Compton, J.S. 1988. Sediment composition and precipitation of dolomite and pyrite in the Neogene Monterey and Sisquoc formations, Santa Maria Basin Area, California. In, V. Shukla and P.A. Baker (Eds.), Sedimentology and Geochemistry of Dolostones. SEPM (Society for Sedimentary Geology), Special Publication 43, p. 53-64.

Compton, J.S. and R. Siever 1986. Diffusion and mass balance of Mg during early dolomite formation, Monterey Formation. Geochimica et Cosmochimica Acta, v. 50, no. 1, p. 125-135.

Coplen, T.B. 1994. Reporting of stable hydrogen, carbon and oxygen isotope abundances. Pure and Applied Chemistry, v. 66, no. 2, p. 273-276.

Craig, H. 1957. Isotopic standards for carbon and oxygen and correction factors for mass-spectrometric analysis of carbon dioxide. Geochimica et Cosmochimica Acta, v. 12, no. 1-2, p. 133-149.

Craig, H. and L.I. Gordon 1965. Deuterium and oxygen-18 variations in the ocean and the marine atmosphere. Proceedings of a Conference on Stable Isotopes in Oceanographic Studies and Paleotemperatures, Spoleto, Italy, p. 9–130.

Curtis, C.D. and M.L. Coleman 1986. Controls on the precipitation of early diagenetic calcite, dolomite and siderite concretions in complex depositional sequences. In, D.L. Gautier (Ed.), Roles of Organic Matter in Sediment Diagenesis. SEPM (Society for Sedimentary Geology), Special Publication 38, p. 23-33.

Czerniakowski, L.A., K.C. Lohmann and J.L. Wilson 1984. Closed-system marine-burial diagenesis: isotopic data from the Austin Chalk and its components. Sedimentology, v. 31, no. 6, p. 863-877.

Damholt, T. and F. Surlyk 2004. Laminated-bioturbated cycles in Maastrichtian chalk of the North Sea: oxygenation fluctuations within the Milankovitch frequency band. Sedimentology, v. 51, no. 6, p. 1323-1342.

de Boer, P.L. 1982. Some remarks about the stable isotope composition of cyclic pelagic sediments from the Cretaceous in the Apennines (Italy). In, S.O. Schlanger and M.B. Cita (Eds.), Nature and Origin of Cretaceous Carbon-Rich Facies, p. 129-143.

Demirel, I.H. and S. Guneri 2000. Cretaceous carbonates in the Adiyaman region, SE Turkey: an assessment of burial history and source-rock potential. Journal of Petroleum Geology, v. 23, no. 1, p. 91-106.

Dickson, J.A.D. 1965. A Modified staining technique for carbonates in thin section. Nature, v. 205, no. 4971, p. 587.

Dickson, J.A.D. 1985. Diagenesis of shallow-marine carbonates. Geological Society Special Publications, v. 18, no. 1, p. 173-188.

Dickson, J.A.D. and M.L. Coleman 1980. Changes in carbon and oxygen isotope composition during limestone diagenesis. Sedimentology, v. 27, no. 1, p. 107-118.

Dickson, J.A.D., R.A. Wood, H. Bu Al Rougha and H. Shebl 2008. Sulphate reduction associated with hardgrounds: lithification afterburn! Sedimentary Geology, v. 205, no. 1-2, p. 34-39.

Ditchfield, P. and J.D. Marshall 1989. Isotopic variation in rhythmically bedded chalks: paleotemperature variation in the Upper Cretaceous. Geology, v. 17, no. 9, p. 842-845.

Doyle, P., D.G. Poire, L.A. Spalletti, D. Pirrie, P. Brenchley and S.D. Matheos 2005. Relative oxygenation of the Tithonian-Valanginian Vaca Muerta-Chachao formations of the Mendoza Shelf, Neuquen Basin, Argentina. Geological Society Special Publications, v. 252, no. 1, p. 185-206.

Droste, H. 1990. Depositional cycles and source rock development in an epeiric intraplatform basin: the Hanifa Formation of the Arabian Peninsula. Sedimentary Geology, v. 69, p. 281-296.

Droste, H. and M. Van Steenwinkel 2004. Stratal geometries and patterns of platform carbonates: the Cretaceous of Oman. In, G. Eberli, J.L. Massaferro and J.F.R. Sarg (Eds.),

Seismic Imaging of Carbonate Reservoirs and Systems. American Association of Petroleum Geologists, Memoir 81, p. 185-206.

Ekdale, A.A. and R.G. Bromley 1991. Analysis of composite ichnofabrics; an example in Uppermost Cretaceous chalk of Denmark. Palaios, v. 6, no. 3, p. 232-249.

Epstein, S., R. Buchsbaum, H.A. Lowenstam and H.C. Urey 1953. Revised carbonate–water isotopic temperature scale. Bulletin of the Geological Society of America, v. 64, p. 1315–1325.

Fiet, N. and G. Gorin 2000. Lithological expression of Milankovitch cyclicity in carbonate-dominated, pelagic, Barremian deposits in central Italy. Cretaceous Research, v. 21, no. 4, p. 457-467.

Fischer, A.G., T. Herbert and I.P. Silva 1985. Carbonate bedding cycles in Cretaceous pelagic and hemipelagic sequences. Fine-grained deposits and biofacies of the Cretaceous Western Interior Seaway. Field trip, Golden, CO, 1985, p. 1-10.

Fisher, I.S. and J.D. Hudson 1987. Pyrite formation in Jurassic shales of contrasting biofacies. In, A.J. Fleet and J. Brooks (Eds.), Marine Petroleum Source Rocks. Geological Society, Special Publication 26, p. 69-78.

Flügel, E. 2004. Microfacies of Carbonate Rocks: Analysis, Interpretation and Application. Springer, 976 p.

Frank, T.D., M.A. Arthur and W.E. Dean 1999. Diagenesis of lower Cretaceous pelagic carbonates, North Atlantic: paleoceanographic signals obscured. Journal of Foraminiferal Research, v. 29, no. 4, p. 340-351.

Frank, T.D. and K.C. Lohmann 1996. Diagenesis of fibrous magnesian calcite marine cement: implications for the interpretation of $\delta^{18}O$ and $\delta^{13}C$ values of ancient equivalents. Geochimica et Cosmochimica Acta, v. 60, no. 13, p. 2427-2436.

Froelich, P.N., G.P. Klinkhammer, M.L. Bender, N.A. Luedtke, G.R. Heath, D. Cullen, P. Dauphin, D. Hammond, B. Hartman and V. Maynard 1979. Early oxidation of organic matter in pelagic sediments of the eastern equatorial Atlantic: suboxic diagenesis. Geochimica et Cosmochimica Acta, v. 43, no. 7, p. 1075-1090.

Gradstein, F.M., J.G. Ogg and A.G. Smith 2004. A Geologic Time Scale 2004. Cambridge University Press, 589 p.

Grantham, P.J., G.W.M. Lijmbach, J. Posthuma, M.W. Hughes Clarke and R.J. Willink 1987. Origin of crude oils in Oman. Journal of Petroleum Geology, v. 11, no. 1, p. 61-80.

Grélaud, C., P. Razin, P.W. Homewood and A.M. Schwab 2006. Development of incisions on a periodically emergent carbonate platform (Natih Formation, Late Cretaceous, Oman). Journal of Sedimentary Research, v. 76, no. 4, p. 647-669.

Gruszczynski, M., J.D. Marshall, R. Goldring, M.L. Coleman, K. Malkowski, E. Gazdzicka, J. Semil and P. Gatt 2008. Hiatal surfaces from the Miocene Globigerina Limestone Formation of Malta: biostratigraphy, sedimentology, trace fossils and early

diagenesis. Palaeogeography, Palaeoclimatology, Palaeoecology, v. 270, no. 3-4, p. 239-251.

Hall, J.S., P. Mozley, J.M. Davis and N.D. Roy 2004. Environments of formation and controls on spatial distribution of calcite cementation in Plio-Pleistocene fluvial deposits, New Mexico, U.S.A. Journal of Sedimentary Research, v. 74, no. 5, p. 643-653.

Hallam, A. 1986. Origin of minor limestone shale cycles: climatically induced or diagenetic? Geology, v. 14, no. 7, p. 609-612.

Hallam, A. 1987. Mesozoic marine organic-rich shales. In, A.J. Fleet and J. Brooks (Eds.), Marine Petroleum Source Rocks. Geological Society, Special Publication 26, p. 251-261.

Hallam, A., P.B. Wignall, J. Yin and J.B. Riding 2000. An investigation into possible facies changes across the Triassic-Jurassic boundary in southern Tibet. Sedimentary Geology, v. 137, no. 3-4, p. 101-106.

Harris, P.M. and S.H. Frost 1984. Middle Cretaceous carbonate reservoirs, Fahud field and northwestern Oman. American Association of Petroleum Geologists Bulletin, v. 68, no. 5, p. 649-658.

Hendry, J.P. 1993. Calcite cementation during bacterial manganese, iron and sulphate reduction in Jurassic shallow marine carbonates. Sedimentology, v. 40, no. 1, p. 87-106.

Hendry, J.P. and R.M. Kalin 1997. Are oxygen and carbon isotopes of mollusc shells reliable palaeosalinity indicators in marginal marine environments? A case study from the Middle Jurassic of England. Journal of the Geological Society, v. 154, no. 2, p. 321-333.

Heydari, E. and W.J. Wade 2002. Massive recrystallization of low-Mg calcite at high temperatures in hydrocarbon source rocks: implications for organic acids as factors in diagenesis. American Association of Petroleum Geologists Bulletin, v. 86, no. 7, p. 1285-1303.

Hochuli, P.A., A.P. Menegatti, H. Weissert, A. Riva, E. Erba and I.P. Silva 1999. Episodes of high productivity and cooling in the early Aptian Alpine Tethys. Geology, v. 27, no. 7, p. 657-660.

Holail, H., K.C. Lohmann and I. Sanderson 1988. Dolomitization and dedolomitization of Upper Cretaceous carbonates: Bahariya Oasis, Egypt. In, V. Shukla and P.A. Baker (Eds.), Sedimentology and Geochemistry of Dolostones. SEPM (Society for Sedimentary Geology), Special Publication 43, p. 191-207.

Homewood, P., P. Razin, C. Grélaud, H. Droste, V. Vahrenkamp, M. Mettraux and J. Mattner 2008. Outcrop sedimentology of the Natih Formation, northern Oman: a field guide to selected outcrops in the Adam Foothills and Al Jabal Al Akhdar areas. GeoArabia, v. 13, no. 3, p. 39-120.

Hudson, J.D. 1977. Stable isotopes and limestone lithification. Journal of the Geological Society, v. 133, p. 637-660.

Hudson, J.D. and D.M. Martill 1991. The Lower Oxford Clay: production and preservation of organic matter in the Callovian (Jurassic) of central England. In, R.V. Tyson and T.H.

Pearson (Eds.), Modern and Ancient Continental Shelf Anoxia. Geological Society, Special Publication 58, p. 363-379.

Hughes Clarke, M.W. 1988. Stratigraphy and rock units nomenclature in the oil-producing area of interior Oman. Journal of Petroleum Geology, v. 11, no. 1, p. 5-60.

Irwin, H. 1980. Early diagenetic carbonate precipitation and pore-fluid migration in the Kimmeridge Clay of Dorset, England. Sedimentology, v. 27, no. 5, p. 577-591.

Katz, B.J. 2005. Controlling factors on source rock development - a review of productivity, preservation, and sedimentation rate. In, N.B. Harris (Ed.), The Deposition of Organic-Carbon-Rich Sediments: Models, Mechanisms, and Consequences. SEPM (Society for Sedimentary Geology), Special Publication 82, p. 7-16.

Katz, B.J., E.I. Dittmar and G.E. Ehret 2000. A geochemical review of carbonate source rocks in Italy. Journal of Petroleum Geology, v. 23, no. 4, p. 399-424.

Klemme, H.D. and G.F. Ulmishek 1991. Effective petroleum source rocks of the world: stratigraphic distribution and controlling depositional factors. American Association of Petroleum Geologists Bulletin, v. 75, no. 12, p. 1809-1851.

Kuhnt, W., A. Nederbragt and L. Leine 1997. Cyclicity of Cenomanian-Turonian organic-carbon-rich sediments in the Tarfaya Atlantic Coastal Basin (Morocco). Cretaceous Research, v. 18, no. 4, p. 587-601.

Lazo, D.G., M. Cichowolski, D.L. Rodriguez and M.B. Aguirre-Urreta 2005. Lithofacies, palaeoecology and palaeoenvironments of the Agrio Formation, Lower Cretaceous of the Neuquen Basin, Argentina. Geological Society Special Publications, v. 252, no. 1, p. 295-315.

Machent, P.G., K.G. Taylor, J.H.S. Macquaker and J.D. Marshall 2007. Patterns of early post-depositional and burial cementation in distal shallow-marine sandstones: Upper Cretaceous Kenilworth Member, Book Cliffs, Utah, USA. Sedimentary Geology, v. 198, no. 1-2, p. 125-145.

Machhour, L., J.P. Masse, J.L. Oudin, B. Lambert and P. Lapointe 1998. Petroleum potential of dysaerobic carbonate source rocks in an intra-shelf basin: the Lower Cretaceous of Provence, France. Petroleum Geoscience, v. 4, no. 2, p. 139-146.

Macquaker, J.H.S. and A.E. Adams 2003. Maximizing information from fine-grained sedimentary rocks: an inclusive nomenclature for mudstones. Journal of Sedimentary Research, v. 73, no. 5, p. 735-744.

Macquaker, J.H.S., S.J. Bentley and K.M. Bohacs (in press). Wave-enhanced sediment-gravity flows and mud dispersal across continental shelves: reappraising sediment transport processes operating in ancient mud-dominated successions. Geology.

Macquaker, J.H.S. and K.M. Bohacs 2007. On the accumulation of mud. Science, v. 318, no. 5857, p. 1734-1735.

Macquaker, J.H.S., R.L. Gawthorpe, K.G. Taylor and M.J. Oates 1998. Heterogeneity, stacking patterns and sequence stratigraphic interpretation in distal mudstone successions:

examples from the Kimmeridge Clay Formation, U.K. In, J. Schieber, W. Zimmerle and P. Sethi (Eds.), Shales and Mudstones, Volume I: Basin Studies, Sedimentology, and Palaeontology. E. Schweizerbart'sche Verlagsbuchhandlung, p. 163-186.

Macquaker, J.H.S. and K.G. Taylor 1996. A sequence-stratigraphic interpretation of a mudstone-dominated succession: the Lower Jurassic Cleveland Ironstone Formation, UK. Journal of the Geological Society, v. 153, no. 5, p. 759-770.

Macquaker, J.H.S., K.G. Taylor and R.L. Gawthorpe 2007. High-resolution facies analyses of mudstones: implications for palaeoenvironmental and sequence-stratigraphic interpretations of offshore ancient mud-dominated successions. Journal of Sedimentary Research, v. 77, no. 3-4, p. 324-339.

Maliva, R.G., J.A.D. Dickson and A.E. Fallick 1999. KAolin cements in limestones: potential indicators of organic-rich pore waters during diagenesis. Journal of Sedimentary Research, v. 69, no. 1, p. 158-163.

Mallon, A.J. and R.E. Swarbrick 2008. Diagenetic characteristics of low permeability, non-reservoir chalks from the Central North Sea. Marine and Petroleum Geology, v. 25, no. 10, p. 1097-1108.

Markello, J.R. and J.F. Read 1982. Upper Cambrian intrashelf basin, Nolichucky Formation, southwest Virginia Appalachians. American Association of Petroleum Geologists Bulletin, v. 66, no. 7, p. 860-878.

Marshall, J.D. and M. Ashton 1980. Isotopic and trace element evidence for submarine lithification of hardgrounds in the Jurassic of eastern England (Lincolnshire Limestone). Sedimentology, v. 27, no. 3, p. 271-289.

Marynowski, L., M. Zaton, B.R.T. Simoneit, A. Otto, M.O. Jedrysek, C. Grelowski and S. Kurkiewicz 2007. Compositions, sources and depositional environments of organic matter from the Middle Jurassic clays of Poland. Applied Geochemistry, v. 22, no. 11, p. 2456-2485.

Mazzullo, S.J. 2000. Organogenic dolomitization in peritidal to deep-sea sediments. Journal of Sedimentary Research, v. 70, no. 1, p. 10-23.

McCrea, J.M. 1950. On the isotopic chemistry of carbonates and a paleotemperature scale. The Journal of Chemical Physics, v. 18, no. 6, p. 849-857.

Meng, X., M. Ge and M.E. Tucker 1997. Sequence stratigraphy, sea-level changes and depositional systems in the Cambro-Ordovician of the North China carbonate platform. Sedimentary Geology, v. 114, no. 1-4, p. 189-222.

Molenaar, N. and J.J.P. Zijlstra 1997. Differential early diagenetic low-Mg calcite cementation and rhythmic hardground development in Campanian-Maastrichtian chalk. Sedimentary Geology, v. 109, no. 3-4, p. 261-281.

Molina, J.M., P.A. Ruiz-Ortiz and J.A. Vera 1997. Calcareous tempestites in pelagic facies (Jurassic, Betic Cordilleras, Southern Spain). Sedimentary Geology, v. 109, no. 1, p. 95-109.

Moore, C.H. 1989. Carbonate Diagenesis and Porosity. Developments in Sedimentology 46, Elsevier, 338 p.

Moss, S. and M.E. Tucker 1995. Diagenesis of Barremian-Aptian platform carbonates (the Urgonian Limestone Formation of SE France): near-surface and shallow-burial diagenesis. Sedimentology, v. 42, no. 6, p. 853-874.

Muchez, P., W. Viaene and J.D. Marshall 1991. Origin of shallow burial cements in the Late Viséan of the Campine Basin, Belgium. Sedimentary Geology, v. 73, no. 3-4, p. 257-271.

Munnecke, A., H. Westphal, J.J.G. Reijmer and C. Samtleben 1997. Microspar development during early marine burial diagenesis: a comparison of Pliocene carbonates from the Bahamas with Silurian limestones from Gotland (Sweden). Sedimentology, v. 44, no. 6, p. 977-990.

Murris, R.J. 1980. Middle East: stratigraphic evolution and oil habitat. American Association of Petroleum Geologists Bulletin, v. 64, no. 5, p. 597-618.

Myrow, P.M. and J.B. Southard 1996. Tempestite deposition. Journal of Sedimentary Research, v. 66, no. 5, p. 875-887.

Nelson, C.S. and N.P. James 2000. Marine cements in mid-Tertiary cool-water shelf limestones of New Zealand and southern Australia. Sedimentology, v. 47, no. 3, p. 609-629.

Niebuhr, B. 2005. Geochemistry and time-series analyses of orbitally forced Upper Cretaceous marl-limestone rhythmites (Lehrte West Syncline, northern Germany). Geological Magazine, v. 142, no. 1, p. 31-55.

Osleger, D. 1991. Subtidal carbonate cycles: implications for allocyclic vs. autocyclic controls. Geology, v. 19, no. 9, p. 917-920.

Osleger, D. and J.F. Read 1991. Relation of eustasy to stacking patterns of metre-scale carbonate cycles, late Cambrian, USA. Journal of Sedimentary Research, v. 61, no. 7, p. 1225-1252.

Patterson, W.P. and L.M. Walter 1994. Syndepositional diagenesis of modern platform carbonates: evidence from isotopic and minor element data. Geology, v. 22, no. 2, p. 127-130.

Philip, J., J. Borgomano and S. Al-Maskiry 1995. Cenomanian-Early Turonian carbonate platform of northern Oman: stratigraphy and palaeoenvironments. Palaeogeography, Palaeoclimatology, Palaeoecology, v. 119, p. 77-92.

Pingitore, N.E. 1982. The role of diffusion during carbonate diagenesis. Journal of Sedimentary Petrology, v. 52, no. 1, p. 27-39.

Pittet, B. and E. Mattioli 2002. The carbonate signal and calcareous nannofossil distribution in an Upper Jurassic section (Balingen-Tieringen, Late Oxfordian, southern Germany). Palaeogeography, Palaeoclimatology, Palaeoecology, v. 179, no. 1-2, p. 71-96.

Preto, N., C. Spötl and C. Guaiumi 2009. Evaluation of bulk carbonate $\delta^{13}C$ data from Triassic hemipelagites and the initial composition of carbonate mud. Sedimentology, v. 56, no. 5, p. 1329-1345.

Rachidi, M., F. Neuweiler and D. Kirkwood 2009. Diagenetic-geochemical patterns and fluid evolution history of a Lower Jurassic petroleum source rock, Middle Atlas, Morocco. Journal of Petroleum Geology, v. 32, no. 2, p. 111-128.

Raven, M.J. and T. Dickson 2007. Methanogenesis during Shu'aiba diagenesis: examples from Al Shaheen Field, Block 5, offshore Qatar. GeoArabia, v. 12, no. 1, p. 37-58.

Reid, R.P. and I.G. Macintyre 1998. Carbonate recrystallization in shallow marine environments: a widespread diagenetic process forming micritized grains. Journal of Sedimentary Research, v. 68, no. 5, p. 928-946.

Reid, R.P., I.G. Macintyre and N.P. James 1990. Internal precipitation of microcrystalline carbonate: a fundamental problem for sedimentologists. Sedimentary Geology, v. 68, no. 3, p. 163-170.

Reuning, L., J.J.G. Reijmer and E. Mattioli 2006. Aragonite cycles: diagenesis caught in the act. Sedimentology, v. 53, no. 4, p. 849-866.

Ricken, W. 1986. Diagenetic Bedding: A Model for Marl-Limestone Alternations. Lecture Notes in Earth Sciences, Springer-Verlag, 210 p.

Ricken, W. 1996. Bedding rhythms and cyclic sequences as documented in organic carbon - Carbonate patterns, Upper Cretaceous, Western Interior, U.S. Sedimentary Geology, v. 102, no. 1-2, p. 131-154.

Ricken, W. and C. Hemleben 1982. Origin of marl-limestone alternation (Oxford 2) in southwest Germany. In, G. Einsele and A. Seilacher (Eds.), Cyclic and Event Stratification. Springer-Verlag, p. 63-71.

Robertson, A.H.F. 1987. Upper Cretaceous Muti Formation: transition of a Mesozoic carbonate platform to a foreland basin in the Oman Mountains. Sedimentology, v. 34, no. 6, p. 1123-1142.

Ruffell, A.H. and G. Watch 1998. Firmgrounds - key surfaces in the recognition of parasequences in the Aptian Lower Greensand Group, Isle of Wright (southern England). Sedimentology, v. 45, no. 1, p. 91-107.

Sansone, F.J., G.W. Tribble, C.C. Andrews and J.P. Chanton 1990. Anaerobic diagenesis within Recent, Pleistocene, and Eocene marine carbonate frameworks. Sedimentology, v. 37, no. 6, p. 997-1009.

Sassen, R., C.H. Moore and F.C. Meendsen 1987. Distribution of hydrocarbon source potential in the Jurassic Smackover formation. Organic Geochemistry, v. 11, no. 5, p. 379-383.

Savrda, C.E. and D.J. Bottjer 1994. Ichnofossils and ichnofabrics in rhythmically bedded pelagic/hemi- pelagic carbonates: recognition and evaluation of benthic redox and scour cycles. Orbital forcing and cyclic sequences, p. 195-210.

Savrda, C.E., J.V. Browning, H. Krawinkel and S.P. Hesselbo 2001. Firmground ichnofabrics in deep-water sequences stratigraphy, Tertiary clinoform-toe deposits, New Jersey slope. Palaios, v. 16, no. 3, p. 294-305.

Savrda, C.E. and L.L. Nanson 2003. Ichnology of fair-weather and storm deposits in an Upper Cretaceous estuary (Eutaw Formation, western Georgia, USA). Palaeogeography, Palaeoclimatology, Palaeoecology, v. 202, no. 1-2, p. 67-83.

Scasso, R.A., M.S. Alonso, S. Lanes, H.J. Villar and G. Laffitte 2005. Geochemistry and petrology of a Middle Tithonian limestone-marl rhythmite in the Neuquen Basin, Argentina: depositional and burial history. Geological Society Special Publications, v. 252, no. 1, p. 207-229.

Schieber, J. 1994. Evidence for high-energy events and shallow-water deposition in the Chattanooga Shale, Devonian, central Tennessee, USA. Sedimentary Geology, v. 93, no. 3-4, p. 193-208.

Schieber, J. 2003. Simple gifts and buried treasures – implications of finding bioturbation and erosion surfaces in black shales. The Sedimentary Record, v. 1, no. 2, p. 4-8.

Schieber, J. 2009. Discovery of agglutinated benthic foraminifera in Devonian black shales and their relevance for the redox state of ancient seas. Palaeogeography, Palaeoclimatology, Palaeoecology, v. 271, no. 3-4, p. 292-300.

Schieber, J., J. Southard and K. Thaisen 2007. Accretion of mudstone beds from migrating floccule ripples. Science, v. 318, no. 5857, p. 1760-1763.

Schieber, J. and J.B. Southard 2009. Bedload transport of mud by floccule ripples - direct observation of ripple migration processes and their implications. Geology, v. 37, no. 6, p. 483-486.

Schneidermann, N. and P.M. Harris (Eds.) 1985. Carbonate Cements. SEPM (Society for Sedimentary Geology), Special Publication 36, 379 p.

Scholle, P.A., T. Albrechtsen and H. Tirsgaard 1998. Formation and diagenesis of bedding cycles in uppermost Cretaceous chalks of the Dan Field, Danish North Sea. Sedimentology, v. 45, no. 2, p. 223-243.

Scholle, P.A. and M.A. Arthur 1980. Carbon isotope fluctuations in Cretaceous pelagic limestones: potential stratigraphic and petroleum exploration tool. American Association of Petroleum Geologists Bulletin, v. 64, no. 1, p. 67-87.

Scholle, P.A. and D.S. Ulmer-Scholle 2003. A Color Guide to the Petrography of Carbonate Rocks: Grains, Textures, Porosity, Diagenesis. American Association of Petroleum Geologists, Memoir 77, 486 p.

Schröder-Adams, C.J., D.A. Leckie, J. Bloch, J. Craig, D.J. McIntyre and P.J. Adams 1996. Paleoenvironmental changes in the Cretaceous (Albian to Turonian) Colorado Group of western Canada: microfossil, sedimentological and geochemical evidence. Cretaceous Research, v. 17, no. 3, p. 311-365.

Schultz, L.G. 1964. Quantitative interpretation of mineralogical composition from X-ray and chemical data for the Pierre Shale. United States Geological Survey, Professional Paper, 391-C, p. 1-31.

Scott, R.W. 1990. Chronostratigraphy of Cretaceous carbonate shelf, southeastern Arabia. In, A.H.F. Robertson, M.P. Searle and A.C. Ries (Eds.), The Geology and Tectonics of the Oman Region. Geological Society, Special Publication 49, p. 89-108.

Shackleton, N.J. and J.P. Kennett 1975. Paleotemperature history of the Cenozoic and the initiation of Antarctic glaciation: oxygen and carbon isotope analyses in DSDP sites277, 279, and 281. In, J.P. Kennett and R.E. Houtz (Eds.), Initial Reports of the Deep Sea Drilling Project, v. 29, p. 743–756.

Shinn, E.A. and D.M. Robbin 1983. Mechanical and chemical compaction in fine-grained shallow-water limestones. Journal of Sedimentary Petrology, v. 53, no. 2, p. 595-618.

Steuber, T., M. Rauch, J.P. Masse, J. Graaf and M. Malkoč 2005. Low-latitude seasonality of Cretaceous temperatures in warm and cold episodes. Nature, v. 437, no. 7063, p. 1341-1344.

Summerhayes, C.P. 1987. Organic-rich Cretaceous sediments from the North Atlantic. In, A.J. Fleet and J. Brooks (Eds.), Marine Petroleum Source Rocks. Geological Society, Special Publication 26, p. 301-316.

Swart, P.K., D.L. Cantrell, H. Westphal, C.R. Handford and C.G. Kendall 2005. Origin of dolomite in the Arab-D reservoir from the Ghawar field, Saudi Arabia: evidence from petrographic and geochemical constraints. Journal of Sedimentary Research, v. 75, no. 3, p. 476-491.

Taghavi, A.A., A. Mørk and E. Kazemzadeh 2007. Flow unit classification for geological modelling of a heterogeneous carbonate reservoir: Cretaceous Sarvak Formation, Dehluran field, SW Iran. Journal of Petroleum Geology, v. 30, no. 2, p. 129-146.

Taylor, K.G. and J.H.S. Macquaker 2000a. Early diagenetic pyrite morphology in a mudstone-dominated succession: the Lower Jurassic Cleveland Ironstone Formation, eastern England. Sedimentary Geology, v. 131, no. 1-2, p. 77-86.

Taylor, K.G. and J.H.S. Macquaker 2000b. Spatial and temporal distribution of authigenic minerals in continental shelf sediments: implications for sequence stratigraphic analysis. In, C.R. Glen, L. Prévôt-Lucas and J. Lucas (Eds.), Marine Authigenesis: From Global to Microbial. SEPM (Society for Sedimentary Geology), Special Publication 66, p. 309-323.

Terken, J.M.J. 1999. The Natih petroleum system of north Oman. GeoArabia, v. 4, no. 2, p. 157-180.

Tucker, M.E., J. Gallagher and M.J. Leng 2009. Are beds in shelf carbonates millennial-scale cycles? An example from the mid-Carboniferous of northern England. Sedimentary Geology, v. 214, no. 1-4, p. 19-34.

Tucker, M.E. and V.P. Wright 1990. Carbonate Sedimentology. Blackwell Science, 482 p.

van Buchem, F.S.P., A.Y. Huc, B. Pradier and M. Stefani 2005. Stratigraphic patterns in carbonate source-rock distribution: second-order to fourth-order control and sediment flux. In, N.B. Harris (Ed.), The Deposition of Organic-Carbon-Rich Sediments: Models, Mechanisms, and Consequences. SEPM (Society for Sedimentary Geology), Special Publication 82, p. 191-223.

van Buchem, F.S.P., P. Razin, P.W. Homewood, W.H. Oterdoom and J. Philip 2002. Stratigraphic organization of carbonate ramps and organic-rich intrashelf basins: Natih Formation (middle Cretaceous) of northern Oman. American Association of Petroleum Geologists Bulletin, v. 86, no. 1, p. 21-53.

van Buchem, F.S.P., P. Razin, P.W. Homewood, J.M. Philip, G.P. Eberli, J.P. Platel, J. Roger, R. Eschard, G.M.J. Desaubliaux, T. Boisseau, J.P. Leduc, R. Labourdette and S. Cantaloube 1996. High-resolution sequence stratigraphy of the Natih Formation (Cenomanian/Turonian) in northern Oman: distribution of source rocks and reservoir facies. GeoArabia, v. 1, no. 1, p. 65-91.

Varban, B.L. and A.G. Plint 2008. Palaeoenvironments, palaeogeography, and physiography of a large, shallow, muddy ramp: Late Cenomanian-Turonian Kaskapau Formation, western Canada foreland basin. Sedimentology, v. 55, no. 1, p. 201-233.

Weedon, G.P. 1986. Hemipelagic shelf sedimentation and climatic cycles: the basal Jurassic (Blue Lias) of South Britain. Earth and Planetary Science Letters, v. 76, no. 3-4, p. 321-335.

Weedon, G.P. and H.C. Jenkyns 1999. Cyclostratigraphy and the Early Jurassic timescale: data from the Belemnite Marls, Dorset, southern England. Bulletin of the Geological Society of America, v. 111, no. 12, p. 1823-1840.

Westphal, H. 2006. Limestone-marl alternations as environmental archives and the role of early diagenesis: a critical review. International Journal of Earth Sciences, v. 95, no. 6, p. 947-961.

Westphal, H., M.J. Head and A. Munnecke 2000. Differential diagenesis of rhythmic limestone alternations supported by palynological evidence. Journal of Sedimentary Research, v. 70, no. 3, p. 715-725.

Westphal, H. and A. Munnecke 1997. Mechanical compaction versus early cementation in fine-grained limestones: differentiation by the preservation of organic microfossils. Sedimentary Geology, v. 112, no. 1-2, p. 33-42.

Westphal, H., A. Munnecke, F. Böhm and S. Bornholdt 2008. Limestone-marl alternations in epeiric sea settings - witnesses of environmental changes or diagnesis? Special Paper - Geological Association of Canada, p. 389-406.

Westphal, H., A. Munnecke, J. Pross and J.O. Herrle 2004. Multiproxy approach to understanding the origin of Cretaceous pelagic limestone-marl alternations (DSDP site 391, Blake-Bahama Basin). Sedimentology, v. 51, no. 1, p. 109-126.

Wetzel, A. and A. Uchmann 1998. Biogenic sedimentary structures in mudstones - an overview. In, J. Schieber, W. Zimmerle and P. Sethi (Eds.), Shales and Mudstones,

Volume I: Basin Studies, Sedimentology, and Palaeontology. E. Schweizerbart'sche Verlagsbuchhandlung, p. 351-369.

Chapter 6

Summary

As outlined in the Introduction Section of the thesis (Chapter 1), the purpose of this final chapter is two fold: a) to draw together the various outcomes of the study into a coherent synthesis, and b) to indicate directions for future work in this area of research.

6.1. Overall Study Conclusions and Synthesis

In Chapters 3 to 5 we discussed various aspects of the key factors controlling lithofacies variability and organic-matter enrichment within epeiric intrashelf basins, using the Upper Cretaceous Natih-B Member of North Oman as an ideal example. By combining optical and backscattered electron-optical microscopy, in addition to mineralogical (X-ray diffraction) and geochemical (total organic carbon [TOC] and stable isotope) analyses, together with the traditional but detailed core and outcrop descriptions, we investigated, in detail, the processes that operated in the Natih-B intrashelf basin and fundamentally controlled: a) organic-matter preservation, b) small- to medium-scale temporal and spatial lithofacies variability, and c) early diagenesis. This process-detailed, multi-proxy approach proved to be successful in achieving the goals of this research. Also, it significantly helped to avoid misidentifying some of the primary and diagenetic features within fine-grained, organic-carbon-rich intrashelf-basinal carbonates; for instance description of fissile thin beds as “depositional laminae” and partially-bioturbated organic-rich mudstones as “monotonous black shales”, which led many researchers to assume that organic-matter enrichment in these units was a result of high primary production, associated with the presence of persistent bottom-water anoxia and low-energy suspension-settling processes. Moreover, careful analyses, utilising these high-resolution techniques, enabled the origin of the individual components of fine-grained carbonate sediments to be determined, as it is difficult to achieve this using only core and outcrop methods. Furthermore, this approach allowed detailed correlation between the exposed stratigraphy of the Natih-B Member in the Adam Foothills to the subsurface stratigraphy in the nearby oilfields of North Oman (e.g. Natih and Fahud fields).

From this detailed investigation, nine main lithofacies were recognised in the Natih-B Member. The deposition of these lithofacies occurred in a clastic-starved intrashelf basin (40 to 60 m maximum water depth) and associated outer- and inner-ramp settings, recording marine transgression. These lithofacies are differentiated from one another on the basis of their sedimentary structures and variable proportions of biogenic, diagenetic, and clastic components, in addition to their primary carbonate textures. They are composed predominantly of calcite (as primary skeletal debris and both replacive and pore-filling spar), together with a subordinate fraction composed of organic matter (amorphous and woody), detrital quartz, detrital and authigenic clay, replacive and pore-filling pyrite and dolomite, and fish debris. The textures preserved by these units are predominantly of mudstone and wackestone, with some packstone and floatstone ("shell beds").

As discussed in the previous chapters, the abundant evidence of bioturbation (including *Thalassinoides* isp., *Planolites* isp. and *Phycosiphon* isp.) and in-place fauna (including thick-shelled bivalves and small benthic foraminifera) throughout the middle-late Cenomanian Natih-B succession, even in the most organic-carbon-rich lithofacies (up to 13.7% TOC), suggest that persistent bottom-water anoxia (or "oceanic anoxia") did not exist during the deposition of this unit and it is very likely that at the sediment/water interface conditions varied from oxic to dysoxic, but probably were never anoxic. Therefore, alternative models to explain the enhanced organic-matter preservation in this setting have to be considered.

Based on the observations of relict thin beds, partial bioturbation (predominantly flattened *Planolites* isp.), inclined lenticular laminae (enclosing organo-mineralic aggregates) and abundance of surface-water-derived components (including planktonic foraminifera, coccoliths and organic matter) in the intrashelf-basinal organic-carbon-rich mudstone-wackestone lithofacies that alternate with sparry-calcite-rich wackestone-packstone units, might suggest that short-term enhanced organic production in the water column, coupled with episodic and rapid sedimentation rates were the key factors controlling organic-matter enrichment in the Natih-B source rock. It is likely that the organic-rich pelagic sediments were delivered episodically to the sediment/water interface as phytoplankton blooms and buried rapidly, prior to being significantly mineralised in the oxic zone, during periods of high relative seal level and increase of accommodation. In contrast, the relatively lower proportions of planktonic fauna and flora and reduced organic-matter content (< 1.5%

TOC) in the sparry-calcite-rich lithofacies, which have been extensively bioturbated and contain relatively higher proportions of basin-margin-derived shell debris, indicate that organic-matter dilution by carbonate tests (autodilution) and early diagenesis (extensive bioturbation and pervasive carbonate cementation and replacement), associated with slow sedimentation rates, were the main factors reducing source potential of these units. The occasionally encrusted and bored tops of these early-lithified units are here interpreted to represent major breaks in sediment accumulation during relatively lower sea level and decrease of accommodation, associated with the development of hard-/firmgrounds (discontinuity surfaces). Therefore, these tops occur where stacking patterns change, capping shallowing-upward parasequences, which typically encompass organic-carbon-rich mudstone-wackestone overlain by sparry-calcite-rich wackestone-packstone.

Moreover, the evidence of lenticular laminae, faecal pellets, relict thin beds in the organic-carbon-rich lithofacies, and the abundance of bioclast concentrations together with the evidence of scoured bases and amalgamation of thin normally-graded beds in the sparry-calcite-rich lithofacies imply that the Natih-B intrashelf-basin was not dominated by low-energy depositional conditions, associated with suspension-settling processes. Instead, these observations indicate that the Natih-B intrashelf basin was, to different levels, energetic and dynamic, and that advective and episodic depositional processes operated, at least partially, during deposition of both alternating lithofacies. Specifically, the observations from the sparry-calcite-rich lithofacies suggest that deposition of these units was partially influenced by episodic distal storms ("tempestites") when the sea level was relatively lower.

As discussed in Chapter 4, differential early diagenesis also played a role in controlling lithofacies variability and enhancing cyclicity in the Natih-B intrashelf-basinal sediments. The uncompacted, extensively-bioturbated, sparry-calcite-rich wackestone-packstone lithofacies were pervasively cemented and replaced early, prior to compaction and burial. In contrast, the partially-bioturbated organic-carbon-rich mudstone-wackestone interbeds comprise uncemented matrix which resulted in the compacted ("fissile") nature of these units. This differential diagenesis was very likely a function of changes in sedimentation rate, related to sea-level fluctuations and accommodation availability. When sea-level is relatively high, there is more accommodation available in the basin to accumulate organic-carbon-rich sediments at the sediment/water interface and then burying them rapidly before

being significantly mineralised. On the other hand, when relative sea level is lower, there is less accommodation available, resulting in sediment starvation at the seafloor and extending the sediment residence time in the oxic zone, which caused the sediments to be significantly bioturbated and mineralised. The early sparry-calcite cements (in the uncompacted bioclast tests of both alternating lithofacies) and replacements ("microspar", in the matrix of the sparry-calcite-rich units), associated with evidence of isopachous cementation, together with stable-isotopic compositions (average +0.8‰ $\delta^{13}C$ and −4.2‰ $\delta^{18}O$ VPDB [Vienna Pee Dee Belemnite]), were predominantly derived from normal-marine (open, oxic) porewaters.

Based on the above observations and interpretations, it can be concluded that the Natih-B intrashelf basin was probably never too deep, never persistently anoxic, and never too quiescent or isolated ("silled"). Instead these data suggest that this intrashelf basin was relatively shallow (circa 50 m water maximum water depth), energetic, open and oxic to dysoxic.

Overall, this high-resolution, multi-proxy study demonstrates the complex interplay between the mechanisms that underpin organic-matter enrichment and lithofacies variability (both temporally and laterally) within the Natih-B Member intrashelf-basinal sediments and associated units. These mechanisms characterise the delicate balance between primary production (both organic and inorganic), clastic input, bottom-water oxygen concentrations and energy conditions, rates of sediment accumulation and burial, and early diagenesis. All of these factors are fundamentally related to high-frequency changes in eustatic sea-level and associated accommodation availability.

Lastly, the final outcomes of this study suggest that exiting models on intrashelf basins, which simply rely on the styles of primary production and existence of bottom-water anoxia, associated with predominantly low-energy depositional conditions, suspension-settling processes and closed-system (anoxic) diagenesis, are probably erroneous. Instead, this study, using the Upper Cretaceous Natih-B Member as an ideal example, demonstrates that deposition and diagenesis of intrashelf-basinal carbonate source rocks may occur under oxic-dysoxic, energetic conditions, associated with advective processes and predominantly open, oxic calcite precipitation, with mostly active sediment reworking and bioturbation. The Natih-B source rock is very unlikely a unique case of its own, and

similar outcomes to this study maybe reached from studying other same- and different-aged carbonate source rocks worldwide, especially if a similar multi-proxy, high-resolution, process-detail approach is being applied. Therefore, the paradigms of carbonate source-rocks deposition and diagenesis need to be considerably modified, in order to develop the residual exploration potential, and enhance hydrocarbon exploitation in outer-platform settings, especially those that occur in the Mesozoic petroleum systems of the Middle East.

6.2. Recommendations for Future Research

This PhD work revealed various areas of possible future research that could develop and enhance the research undertaken in this study. The detailed scope of this study and integration of the small-scale datasets have inevitably resulted in the exclusion of some avenues of potential interest from the regional perspective. The endeavour of this section is to provide some recommendations for future work that may further develop the results of the study. Some specific indications are outlined below:

- As mentioned above, this study shows how instrumental is the combined optical and backscattered electron-optical microscopy in obtaining detailed information from fine-grained sedimentary rocks and, thus, it should always be considered when studying such sediments, along with other techniques.

- This study has provided detailed information needed to understand the fundamental controls over temporal and small-scale (local) lateral lithofacies variability and organic-matter enrichment within the Natih-B intrashelf basin in North Oman; additional work could be done to map out and correlate the regional spatial distribution of the organic-carbon-rich, intrashelf-basinal units across the Middle East, or at leas between Oman and UAE (see Figure 1.5).

- Because this study is mainly focused on Natih-B core and outcrop sections located within the outline of the intrashelf basin (see Figure 3.1), additional work could be done on Jabal Madmar and Jabal Madar (proximal locations,

carbonate platform) to investigate how does the Natih-B succession in distal locations compare to that in proximal locations.

- Additional work is needed to confirm the adequacy of the classification scheme followed in this study for other regional and global carbonate depositional systems, associated with carbonate source rocks.

- Given that the Natih-B carbonates are bioturbated to varying degrees, a further detailed study focused on the trace fossils of these intrashelf-basinal sediments could be conducted, in order to more precisely describe and interpret the ichnofabrics. This could, for instance, provide additional information on bioturbation index of the lithofacies, styles of trace-fossil tiering, sediment retexturing by burrowers, and burrow frequency, size and infill material. These data could enhance both the palaeoenvironmental reconstructions (e.g. oxygenation, nutrition, tiering depth, sedimentation rate, hydrodynamic regime, and nature of the substrate) and sequence-stratigraphic interpretations (e.g. nature of the key stratal surfaces, genetically-related successions, and event beds).

- Additional work is needed to strengthen our understanding of the processes responsible for dolomite formation within fine-grained, argillaceous carbonates (e.g. Lithofacies 4 [LF4], Chapter 4) by trying to perform, in addition to the petrographic analyses from this study, geochemical (both isotopic [including C, O and Sr] and elemental) analyses on the these microcrystalline rhombohedral dolomites.

- Finally, in order to provide an evaluation of the fundamental controls on organic-matter preservation within intrashelf basins, which have been discussed in this thesis, other ancient settings could be investigated, especially those from neighbouring Middle-Eastern countries. In particular, it would be very useful to conduct a similar kind of research on the two other Cretaceous intrashelf basins in Oman (lower Natih-E and lower Shu'aiba intrashelf basins; see Figure 4.2) and find out how their

depositional and diagenetic models compare to those of the Natih-B intrashelf basin.